A SYSTEMATIC APPROACH FOR PREFERENTIAL CRYSTALLIZATION- THERMODYNAMICS, KINETICS, OPTIMAL OPERATION AND IN-SITU MONITORING

WANG XIUJUAN

NATIONAL UNIVERSITY OF SINGAPORE

2006

A SYSTEMATIC APPROACH FOR PREFERENTIAL CRYSTALLIZATION- THERMODYNAMICS, KINETICS, OPTIMAL OPERATION AND IN-SITU MONITORING

WANG XIUJUAN
(*B.Eng., M. Eng., Tianjin University*)

A THESIS SUBMITTED
FOR THE DEGREE OF DOCTOR OF PHILOSOPHY
DEPARTMENT OF CHEMICAL & BIOMOLECULAR ENGINEERING

NATIONAL UNIVERSITY OF SINGAPORE

2006

ACKNOWLEDGEMENT

I am full of gratitude to my supervisor, Prof Ching Chi Bun, for his invaluable guidance, encouragement and continuous supervision during my graduate study. His endless patience and understanding has allowed me to carry out this work to the best of my ability.

I would like to thank my co-supervisor Prof Hidajat Kus, for his help and kindness.

Many thanks go to Prof Ng Siu Choon for his kind assistance.

Special thanks must go to my husband, Dr Li Chuanzhao, for his continuous support, encouragement and willingness to share my anxieties and joy of my success.

Many thanks go to Ms Ang Shiou Ching who supported me whenever she could.

I wish to thank my colleagues in Prof Ching's group, especially Dr Lu Jie and Mr Wiehler Harald for their help.

I am greatly indebted to Chemical and Process Engineering Centre (CPEC, NUS) and Division of Chemical and Biomolecular Engineering, NTU, for providing research facilities.

Finally, this thesis is dedicated to my daughter Li Chen.

Probably there are some people who would also have deserved to be mentioned here, but are not. I am also grateful to them.

TABLE OF CONTENTS

SUMMARY

The application of preferential crystallization as an effective and cheap technology for the production of pure enantiomers has become increasingly important. Synthetic organic chemists have put much attention on the chemistry aspects and thermodynamic behaviours, but the understanding of the factors that govern the chiral crystallization process itself is very limited. Particularly, the existence of unstable metastable zone in chiral nucleation has been documented in several cases. It indicates that supersaturation degree should play a crucial role in the optical purity during preferential crystallization. Furthermore, the importance of supersaturation control has been widely recognized in the aspects of crystal habits and purity. Therefore, it is necessary to systematically investigate the preferential crystallization process from thermodynamics and kinetics, and apply them in supersaturation control. Such efforts have been rather rare until now.

In this dissertation, a systematic approach has been developed and applied to the preferential crystallization of 4-hydroxy-2-pyrrolidone in isopropanol by integration of system thermodynamics, crystallization kinetics, optimal operation and in-situ monitoring.

Three types of racemate crystals, namely racemic conglomerates (4-hydroxy-2-pyrrolidone and N-methylephedrine), racemic compounds (propranolol hydrochloride) and pseudoracemates (atenolol) were characterized using thermal analysis and structural characterizations. The two conglomerates and the racemic compound showed similar solubility characteristics. The metastable zone widths (MSZWs) of both conglomerates were independent of enantiomeric excess, while the MSZWs of the racemic compound were different with racemate and pure enantiomer. Their crystal lattice properties were attributed to this difference and three MSZW possibilities were discussed for racemic

compound. Furthermore, for the conglomerate 4-hydroxy-2-pyrrolidone, different orders of primary nucleation rate at different enantiomeric excess were observed, which suggests a critical supersaturation beyond which the nucleation of opposite isomer could occur. This appears to be the first detailed experimental investigation of metastable zone widths of different types of racemates in solution.

S-plane analysis was developed and applied to the crystallization kinetics estimation of (R)- and (S)-4-hydroxy-2-pyrrolidone in isopropanol and similar kinetics were obtained. With combination of thermodynamics properties and crystallization kinetics, a process modelling for batch crystallization was developed to predict the cooling profiles for the preferential crystallization of 4-hydroxy-2-pyrrolidone in isopropanol. The in-situ monitoring showed that relatively high supersaturation of the target enantiomer induced spontaneous nucleation of the undesired enantiomer, which accordingly resulted in low optical purity and poor crystal size distribution. The proposed optimal temperature trajectory to control the critical supersaturation successfully inhibited the induced nucleation of the undesired enantiomer, and hence produced almost pure crystals with good habits. Further investigations under various supersaturations indicated that there could be an optimal supersaturation which would not sacrifice optical purity. The supersaturation control was extended to the application of direct crystallization to racemic compound propranolol hydrochloride coupling with chromatography.

The metastable zone analysis and the optimal operation and monitoring results strongly suggest that it is important to control supersaturation degree in preferential crystallization and it is essential and helpful to integrate thermodynamics, crystallization kinetics and population balance modelling to establish the control strategy.

NOMENCLATURE

Abbreviations

AT	Atenolol
CMPA	Chiral mobile phase additive
CSD	Crystal size distribution
CSP	Chiral stationary phase
DSC	Differential scanning calorimetry
FBRM	Focused beam reflectance measurement
FDA	US Food and Drug Administration
FESEM	Field emission scanning electron microscopy
FT-IR	Fourier transform infrared
4-HP	4-hydroxy-2-pyrrolidone
IPA	Isopropanol
LALLS	Low angle laser light scattering
ME	N-methylephedrine
MSMPR	Mixed-suspension, mixed-product removal
MSZW	Metastable zone width
NMR	Nuclear magnetic resonance
PNCl	Propranolol hydrochloride
PVM	Particle vision measurement
P-XRD	Powder X-ray diffraction
SMB	Simulated Moving Bed (chromatography)

Symbols

B	[#/litre min]	Nucleation rate
c	[g/100ml]	Concentration (mass per volume), used in polarimetry
c	[kg/kg solvent]	Concentration (crystallization kinetics)
C^*	[kg/kg solvent]	Solubility
Δc_{max}	[kg/kg solvent]	The maximum allowable supersaturation
d	[mm]	Length of measurement cell (polarimeter)
d	[nm]	Interplanar spacing between the atoms in the crystal
D		Dextrorotatory (right, according to Fischer convention)
DL		Racemic mixture
E_b	[kJ]	Nucleation energy
E_g	[kJ]	Crystal growth energy
ee		Enantiomeric Excess
H	[J/mol]	Molar enthalpy
J	[#/m^3 s]	Primary nucleation rate
k_b		Nucleation rate constant
k_g		Crystal growth rate constant
k_n		Nucleation rate constant
k_v		Shape factor
L		Levorotary (left, according to Fischer convention)
L	[µm]	Particle size
m_j		jth moment of crystal size distribution
M_T	[kg/litre]	Suspension density

n		Nucleation constant (MSZW)
n	[#/m^4]	Population density
n^0	[#/m^4]	Nuclei population density
N	[#/m^3]	Total number of particles
q		Cooling rate
R		Rectus (right, acc. to Cahn-Ingold-Prelog convention)
R		Racemic Compound (Racemate)
R	[J/mol K]	Gas constant
s		Laplace transform variable
s	[J/mol K]	Molar entropy
S		Sinister (left, acc. to Cahn-Ingold-Prelog convention)
t	[s] or [min]	Time
τ	[s]	Residence time
T	[°C] or [K]	Temperature
ΔT_{max}	[°C] or [K]	The maximum allowable supercooling
u_k		*k*th moment of the population density
V	[m^3]	Volume
wt%	[g/g]%	Weight percentage
x	[mol/mol]	Mole fraction (in liquid or solid phase)

Greek Letters

α	[°]	Angle of rotation of plane polarized light
α		Solubility ratio of racemate to enantiomer

$[\alpha]_{\lambda}^{T}$	[°]	Specific rotation at wavelength λ and temperature T
β	[°]	Correcting angle for DSC-thermograms
θ	[°]	Bragg angle in P-XRD patterns
λ	[nm]	Wavelength
ν	[Hz]	Frequency (of radiation according to wave theory)
$\tilde{\nu}$	[cm^{-1}]	Wavenumber
ρ	[kg/m^3]	Density

Subscripts

A	Referring to one pure enantiomer (D or L)
D	"D-Line" of sodium vapour lamp λ=589.3 nm
s	Solid state
l	Liquid state
i	Component i
Op	Operating (operating temperature)
R	Racemic
S	Surface
V	Volume

Superscripts

b	Order of nucleation
f	Fusion

g	Order of growth
i	Relative kinetic order
j	Magma density dependence of nucleation rate
L	Liquid phase
Cal	Calculated data
LS	Phase transition from liquid to solid state (crystallization)
S	Solid phase
SL	Phase transition from solid to liquid state (melting)

LIST OF FIGURES

LIST OF TABLES

CHAPTER 1 INTRODUCTION

With the increasing demand of enantiomerically pure compounds, particularly in the industries of pharmaceuticals and fine chemicals, efficient strategies for preparation of enantiomers are required (Sheldon, 1993; Collins et al., 1997; Collet, 1999; Wibowo and Ng, 2000; Schroer, et al. 2001; Coquerel, 2003). There are different ways proposed to obtain pure enantiomers, such as biological resolution, asymmetric synthesis, chromatography, classical diastereomer crystallization, and immobilization and membrane technologies. From the low cost and advantages of solid product standpoints, preferential crystallization, which is also called resolution by entrainment, is very attractive and promising. It consists of alternate selective nucleation/ crystallizations (O'Dell et al., 1978) of each antipode from a supersaturated mother liquor containing a slight excess of one enantiomer, by seeding with crystals of the enantiomer that is in excess (Collet et al, 1980; Jacques et al., 1994; Lim et al., 1995; Ndzié et al., 1997; Schroer et al., 2001, 2003; Coquerel, 2003; Elsner et al., 2005).

Considerable academic efforts have been put to study the potential of preferential crystallization as an effective and cheap technology for the production of pure enantiomers in past years. Most of these emphases are often given to the chemistry aspects, conglomerate screening, and the knowledge of equilibrium phase diagrams with the purpose of identifying the concentration and temperature regions of thermodynamic stability of solid phases (Collet et al., 1980; Coquerel and Petit, 1993; Jacques et al, 1994; Miyazaki et al., 1994; Shiraiwa et al., 1994, 1997, 2003, 2005 ; Collet, 1999; Myerson, 1999; Beilles et al., 2001; Dufour et al, 2001; Gervais et al., 2002; Pallavicini et al., 2004).

From the process engineering viewpoint, the application of preferential crystallization requires the mastery of the factors that control the rate difference of crystallization between the two enantiomers (Collet et al., 1980; Jacques et al., 1994). It is therefore important to obtain the information on preferential crystallization process itself by combining studies of thermodynamic properties with kinetic measurements and therefore apply them in the control of preferential crystallization process. What is surprising, however, very few attempts have been directed towards this effort. Indeed, only several other experimental studies have been conducted on the process itself of preferential crystallization. Most of the studied preferential crystallization was conducted under isothermal conditions - cooling the solution to a certain temperature, seeding and crystallization induced with the seeds (Collet et al., 1980). Coquerel et al. found that the classical Seeded Isothermal Preferential Crystallization (SIPC) programme was not suitable for the systems where the solubility ratio of racemate to enantiomer was bigger than 2 (Collect et al., 1980; Coquerel et al., 1990). Accordingly, an Auto Seeded Programmed Polythermic Preferential Crystallization (AS3PC) was proposed and applied to the preferential crystallization (Coquerel et al., 1995; Ndzie et al., 1997; Beilles et al., 2001; Courvoisier et al., 2001, 2002; Dufour et al. 2001). AS3PC method did not require inoculation of solid to initiate the crystallization and the temperature could be programmed, but the considerations of metastable zone and crystallization kinetics were not emphasized. Other efforts include simplified mathematical description and optimal initial conditions for isothermal preferential crystallization (Elsner et al. 2005; Angelov et al., 2006). Some preliminarily satisfying agreement was shown but further model improvement and more detailed experimental works are necessary. Ng and co-workers (Berry and Ng., 1997; Berry et al., 1997; Wibowo and Ng, 2000; Schroer,et al. 2001) had

studied the synthesis of chiral crystallization processes by considering the separation steps in the flowsheet as movements on phase diagrams.

In view of thermodynamic aspects, supersaturation control is very important in preferential crystallization. It is crucial to keep the freedom of supersaturation of the undesired enantiomer in its metastable zone. On the other hand, the supersaturation of the target enantiomer should be also kept within its metastable zone. Otherwise, the spontaneous nucleation of the target enantiomer will happen, which will easily initiate the spontaneous nucleation of its isomer. Indeed, in most of the preferential crystallization processes, there is only a slight excess of the target enantiomer and the concentrations of the two enantiomers are quite close. Under this circumstance and considering the identical physical properties of the two isomers in solutions, the spontaneous nucleation is expected to occur simultaneously for both enantiomers. This is the most important issue that should be avoided in the chiral resolution by direct crystallization (Jacques et al., 1994; Collet, 1999). Although metastable zone width is very useful in understanding the crystallization process in chiral resolution, it has been rarely reported on its measurement and interpretation in enantiomeric systems.

Furthermore, it appears that the supersaturation of the target enantiomer should be controlled even lower than its spontaneous nucleation metastable zone. The effect of supersaturation degree on the optical purity was reported as early as 1950 in the system of β-phenylglyceric acid (Furberg and Hassel, 1950). In the synthesis of the agrochemical paclobutrazol where resolution of a racemic chiral ketone was involved, a similar phenomenon was observed (Black et al., 1989; Collins et al., 1997). Very low supersaturation (1 ^{o}C undercooling) was required to give the product with a high optical purity. It was suggested that if high supersaturations which are still within the metastable

zone are used, some conglomerates will form crystals that contain domains of both lattices in a single crystal, which means that the enantiomerically pure seed could nucleate the other enantiomer at its surface. In studies of the stability of the supersaturation state of DL-serine m-xylene-4-sulfonate dehydrate (Hongo et al., 1981), two metastable regions were identified. The first region was the one where the supersaturation degree was lower than a constant value and no spontaneous crystallization of the unseeded isomer was observed, while the supersaturation was stable for only a certain time in the second metastable region and spontaneous crystallization was ready to take place.

Investigations of chiral nucleation also support the existence of a critical supersaturation within the metastable zone during the preferential crystallization process. In studies of nuclei breeding from a chiral crystal seed of $NaClO_3$ (Denk and Botsaris, 1972; Kondepudi et al., 1990, 1993, 1995; McBride and Carter, 1991;Yokota and Toyokura, 1992; Qian and Botsaris, 1997, 1998), it was found that at low supersaturation all nuclei were of the same chirality. At relatively high supercooling, but still lower than the critical value for spontaneous nucleation, many nuclei with opposite chirality to that of seed were formed. Similar findings were presented in triazolylketone chiral crystallization (Davey et al.,1990). The Embryos Coagulation Secondary Nucleation (ECSN) mechanism was applied to the explanation of this phenomenon (Qian and Botsaris, 1998).

In addition, crystal size distribution (CSD) is an important factor in the production of high-quality solid products and determines the efficiency of downstream operations, such as filtration and washing. Many works have been reported to show the benefits of controlling the supersaturation in batch crystallization (Mullin and Nyvlt, 1971; Jones and Mullin 1974; Rousseau, 1987; Rohani and Bourne, 1990). These advantages include larger crystals and narrower crystal size distribution. This means product purity could be

improved in the filtration and washing process (Mersmann, 1995; Matthews and Rawlings, 1998), which is especially important for chiral purification (Courvoisier et al, 2003).

All of these perspectives, i.e. metastable zone, critical supersaturation and crystal size distribution, clearly underline the importance of controlling the supersaturation of the target enantiomer to a certain extent to inhibit the nucleation of its isomer and get high quality crystal products during preferential crystallization process. In order to get effective supersaturation control, system characterization, thermodynamic data and crystallization kinetics are required to predict the operating concentration profiles with population balance modelling (Randolph and Larson, 1988). The newly developed on-line monitoring and controlling techniques provide good tools to facilitate this kind of investigation (Barrett and Glennon, 2002; Elsner et al., 2005). For preferential crystallization, such a systematic procedure to consider all of the above issues to optimize process operation has been rarely reported in literature.

The main objective of this project is to present a systematic approach to integrate thermodynamics, crystal nucleation and growth kinetics, optimal control and in-situ monitoring to study preferential crystallization. In addition to system characterizations as solids and in solutions, the special metastable zone width characteristics of different racemates were experimentally investigated and the crystallization kinetics was measured. Accordingly, the critical supersaturation control concept and the systematic approach were illustrated by the preferential crystallization of 4-hydroxy-2-pyrrolidone to get optically pure products with good crystal habit. This application was also attempted to the direct crystallization of a racemic compound.

Chapter 2 is literature review.

In Chapter 3, all the chemicals and experimental and theoretical methods implemented in the thesis have been detailed including the principle of the technique, experimental set-up and procedures.

Chapter 4 characterizes four racemates, namely 4-hydroxy-2-pyrrolidone, N-methylephedrine, propranolol hydrochloride, and atenolol by their binary melting point phase diagrams and various spectroscopic techniques. Based on a thermodynamic cycle involving the solid and liquid phases of the enantiomers and racemic species, the melting point, enthalpy, entropy and Gibbs free energy of the racemic species were derived from the thermodynamic data. 4-hydroxy-2pyrrolidone and N-methylephedrine can be classified as racemic conglomerate forming systems. The characteristic of melting point phase diagram of propranolol hydrochloride is similar to the one of a conglomerate forming system, but the evidently negative value of the difference in the enthalpies of fusion of (R)- and (RS)- indicates it is a racemic compound favoring system. Atenolol is an ideal pseudoracemate forming system.

In Chapter 5, the solubilities, metastable zone widths and ternary phase diagrams at different enantiomeric excess (ee) for the above four racemates in the chosen solvents were measured using Lasentec FBRM and PVM. All the chosen solvents were found suitable for cooling crystallization in the studied temperature ranges.

The solubilities of the two conglomerates increase with decreased ee. The metastable zone widths of both studied conglomerates were found independent of enantiomeric excess at different cooling rates, which is consistent with classical nucleation theory and indicates the characteristic of two enantiomers forming separate crystals for a racemic conglomerate. The solubility characterization and ternary phase diagram of racemic compound propranolol hydrochloride were found similar to that of conglomerate,

but its metastable zone width was dependent on the enantiomeric excess. A solubility ratio 2 of racemate to pure enantiomer was found closely correlated with the different MSZW situations for racemic compound. This indicates that metastable zone width can be used as an additional characteristic to identify these two kinds of racemates. More importantly, the regressed primary nucleation rates of 4-hydroxy-2-pyrrolidone suggest the existence of critical supersaturation beyond which the nucleation of opposite isomer could occur. This appears to be the first experimental and theoretical investigation of metastable zone in the chiral system. The solubility, metastable zone will be the thermodynamic basis for the critical supersaturation control in the preferential crystallization process.

Chapter 6 is on the crystal nucleation and growth kinetics, which is essential for the crystallization modeling and control. Laplace transform method was successfully developed and applied to the estimation of crystallization kinetics of (R)-4-hydroxy-2-pyrrolidone and (S)-4-hydroxy-2-pyrrolidone in isopropanol. A more suitable Laplace transform variable s range was employed for current crystallization system. The size dependence of crystal growth was found negligible using modified s-plane approach. The crystal nucleation rate seems independent on the experimental temperature range. The two enantiomers show similar characteristics in crystal nucleation and growth.

In Chapter 7, based on the measured thermodynamics and crystallization kinetics, the concept of critical supersaturation control in preferential crystallization was proposed and applied to the preferential crystallization of 4-hydroxy-2-pyrrolidone in isopropanol. The orthogonal collocation method and the second momentum were combined to solve the mathematical model of batch preferential crystallization. The in-situ monitoring, product purity and crystal morphology showed that relatively high supersaturation of the target enantiomer induced spontaneous nucleation of the undesired enantiomer. This kind of

unwanted nucleation was successfully inhibited by the proposed optimal temperature trajectory to control the critical supersaturation and therefore produced almost pure crystals with good habits. Furthermore, a series of batch operations were experimentally studied under various supersaturations to seek the optimal operating strategy without loss of product optical purity. It was proven essential and useful to integrate thermodynamics, crystallization kinetics and population balance simulation in the critical supersaturation control for preferential crystallization.

Chapter 8 tried to extend the above investigations to the direct crystallization of a racemic compound coupling with semi-preparative HPLC. Direct crystallization of propranolol hydrochloride was conducted with the same initial composition as that partially resolved from HPLC. Based on the solubilities and MSZWs of (R)- and (RS)-propranolol hydrochloride, the direct crystallization progression was clearly illustrated under seeding and non-seeding processes. With the relative solubility and supersaturation control, optically pure crystal product could be obtained from the partially resolved sample within certain safe supersaturation limit.

In Chapter 9, the conclusions were drawn and some suggestions were provided for the future work.

CHAPTER 2 LITERATURE REVIEW

2.1 Overview of chirality

An object is chiral when it lacks reflectional symmetry. Molecules that are nonsuperimposable on their mirror images are called enantiomers. Most chiral molecules contain a tetrahedral carbon atom, a carbon atom attached to four different functional groups (Rosanoff, 1906). The carbon atom is then an asymmetric centre of the molecule. A racemate will consist of 1:1 mixture of enantiomers, if the compound has one chiral center (1:1:1:1, if it has two chiral centers). Unlike diastereomers and geometric isomers, which are chemically distinct and physically different entities, enantiomers have exactly the same physical and chemical properties (except for optical rotation of polarized light) in an achiral (symmetrical) environment. However, they will differ when they are exposed to a chiral environment (e.g. in the human body, because most enzymes are chiral as well.).

Most pharmaceuticals, agrochemicals (herbicides, insecticides and fungicides) but also flavours, fragrances and food stuffs are chiral molecules (Sheldon, 1993; Collins et al., 1997). Some of them even contain more than one asymmetric centre. A molecule containing two or three asymmetric centres has four or eight different stereoisomers respectively. For molecules with two asymmetric centres the term diastereomers is used. Since only two forms can be mirror images, enantiomers occur always in pairs. The importance of separating a racemic mixture (a mixture containing an equal amount of a pair of enantiomers) has been emphasised by many authors (e.g. Sheldon, 1993; Agranat and Caner, 1999; Caldwell, 2001; Caldwell and Leonard, 2001; Maier et al, 2001). Often only one enantiomer (the eutomer) shows the desired effect, the other (the distomer) is

either less effective, shows no effect at all or even worse has undesired side-effects. Probably the most well-known example is the sedative thalidomide (trade name: Contergan®) which was distributed in the 1960s as a racemate (Botting, 2002). It was not known that although the (R)-enantiomer is an effective sedative, the (S)-enantiomer is highly teratogenic (causes fetal abnormalities). Another recent example is the development of single isomer β-agonist, which plays a significant role in the treatment of asthma albuterol, a bronchodilator used to treat acute asthma, is a racemic drug that is improved without one enantiomer, as shown from recent studies (Nelson et al., 1998). The (*R*)-albuterol (a.k.a. levalbuterol, because it rotates polarize light to the left) is found to be the effective enantiomer of the racemic albuterol, whereby its counterpart (*S*)-albuterol lacks any therapeutic benefit. In fact, (*S*)-albuterol has been found to have an adverse effect of airway hyperactivity and potentially pro-inflammatory action with long-term usage. Studies have shown that by administering the pure (*R*)-albuterol to the asthmatic patients, the duration of the therapeutic efficacy was found to be longer than that of the racemic albuterol, with almost 8 times less dosage of the pure enantiomer than the racemate.

Besides these tragic cases there are many other examples for (toxic) side-effects, different therapeutic effects or different flavours or scents of two enantiomers. Some agents with their specific properties were described by Sheldon (1993).

Furthermore the US Food and Drug Administration (FDA) published a Policy Statement for the development of new stereoisomeric drugs (Anon, 1992). According to this Policy Statement the admission of a new drug is only given if adequate information on pharmacologic and toxicologic assessment, proper characterization of metabolism and distribution, clinical studies etc. are done for the pure enantiomers.

Separating a chiral drug which is distributed as a racemate at present into enantiomers may extend the patent for it, because a stereochemically pure compound derived from the available racemate will be treated as a new drug. This strategy is referred to as the "chiral switch" (sometimes also referred to as "racemic switch") (Agranat and Caner,1999). Companies now begin to separate the racemic mixtures of their drugs which patents are about to expire into its enantiomers and distribute only the eutomer. Several examples of companies specialized in chirotechnology applying for the approval of single enantiomers, either to distribute them on their own or to profit from licensing the patents back to the innovator firms or third parties are reported (Anon, 1993; van Annum, 1999; Stinson, 2001). An elaborate description with case histories is presented by (Agranat and Caner, 1999).

For agrochemicals the advantage of using pure enantiomers is that the desired effect can be achieved with a lower environmental burden (Buser et al., 2000). When the distomer is less effective, only half of the agent must be brought on the field.

According to Anon, Stinson and Rouhi (Anon, 1993; Stinson, 2001; Rouhi, 2002), the market of single enantiomers in chiral drugs and intermediates and agrochemicals as well as other sectors is expected to grow greatly in the near future.

Due to the advantages of single enantiomers and the big chiral market, production of enantiomerically pure materials using asymmetric methods, both in synthesis and separation, has become important. As the more common techniques of separation used elsewhere in chemical industry cannot be employed to racemic mixtures (due to the identical properties for the two enantiomers), research in the field of alternative resolution methods and research for a better understanding of the known resolution techniques become more and more important. Over decades, engineers and scientists have been

putting much effort to develop cost- and time-efficient techniques to produce pure enantiomers (Sheldon, et al., 1993; Collins et al., 1997).

2.2 Methods to obtain pure enantiomers

There are many different ways to obtain pure enantiomers (Crosby, 1991; Sheldon, 1993; Collins et al, 1997; McCague, 1998; Challener, 2001; Maier et al, 2001; Rekoske, 2001). Figure 2.1 gives an overview of the methods available.

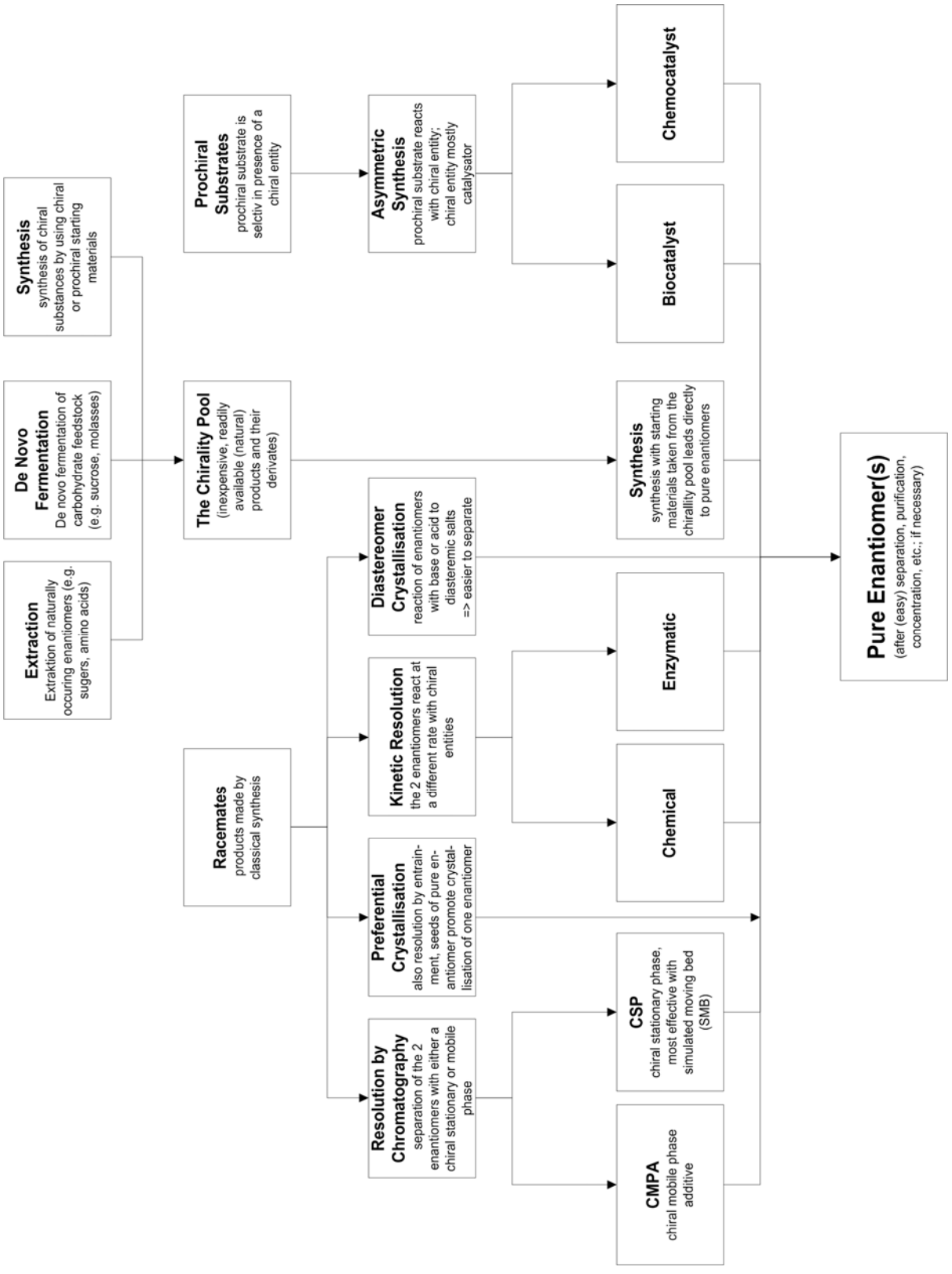

Figure 2.1 An overview of methods to obtain pure enantiomers

Basically they are divided into three classes, which are chirality pool, asymmetric synthesis and separation of racemates.

For most natural chiral substances, probably the easiest and cheapest way to obtain them as pure enantiomers is a classical extraction, because in nature often only one single enantiomer exists. Other methods using microorganisms or synthesis of pure enantiomers from chiral starting material are also frequently used. All chiral molecules which are available from nature or are obtained by classical synthesis of chiral or prochiral starting materials are referred to as the "chirality pool" (Sheldon,1993, 1996). Therefore all chiral molecules belonging to the chirality pool are readily available in large amounts. Using the chirality pool whenever possible is the first choice to obtain pure enantiomers because technical effort and process costs are low.

The invention of asymmetric synthesis dates back Monsanto's original work on the synthesis of l-dopa (Reinhold et al, 1968), and it has gained much progress and scope in the development of pure enantiomers during the last decade. Various methods of asymmetric synthesis have been developed and used to obtain high enantiomeric excess materials. Most of known asymmetric reactions are substrate-controlled, auxiliary-controlled, reagent-controlled and catalyst-controlled (Lin et al, 2001). However, in most cases, they are quite complicated and the product is highly diluted and its recovery is expensive. Even by asymmetric synthesis, a totally pure enantiomer cannot be yielded. A product of 90% enantiomeric excess is normally considered to be a satisfying result. Although extensive research has been conducted on the laboratory-scale, against the totality of examples of the manufacture of optically active materials, at the industrial level, asymmetric syntheses are still relatively scarce. Hence, alternatives have to be sought to solve this problem.

The third main branch is the separation of a racemic mixture. A racemic mixture can be separated with chromatography using either a chiral mobile phase additive (CMPA) or a chiral stationary phase (CSP). For large-scale application, only the latter has been approved. The simulated moving bed (SMB) chromatography developed in the late 1960s is the most widely used technique. There is much literature about employing SMB for separation of chiral systems (Routhven and Ching, 1989; Juza et al., 2000; Wang and Ching, 2005). This technique, however, employs a substantial amount of solvent and requires significant capital investment in the form of expensive chiral stationary phase and high-pressure equipment. In addition, the product stream is obtained from the process in extremely dilute form, and thus a further expensive concentration step is required to recover the desired compound.

Another approach for separating chiral molecules is a method called kinetic resolution (Noyori et al., 1995). One of the enantiomers of a racemate is more readily converted to product than the other. As it is easy to see, this method cannot be employed if both enantiomers are valuable products.

Diastereoisomer crystallization, which uses a resolving agent to form a pair of diastereomeric salts, is also widely used. The resulting salts can be separated easier, because they have distinct properties. Wilen et al.(1977) have provided guidelines which permit a rational approach with a high probability of success. The methodology, principles of the technique and criteria for good resolving agents have been well described in many literatures (Jacques et al., 1994). Advancements in the use of computer aided molecular modelling have provided some assistance to researchers in the rational design and selection of resolving agents. Many types of pharmaceuticals have been prepared utilizing crystallization of diastereoisomeric salts as a means of obtaining optically pure

intermediates, for example, Ampicillin, Ethambutol, Choramphenicol, Fosfomycin, Thiampenicol, Naproxen, and Diltiazem etc (Sheldon, 1993; Collins et al., 1997; Collet, 1998).

Despite the effectiveness and wide applicability of this method, a limitation of this procedure is that only enantiomers with appropriate functionality can form diastereomeric salts of acids or bases. Thus simple hydrocarbons and other unfunctionalized compounds cannot be derivatized and then separated in this manner. Other difficulties such as recovery of the resolving agent and racemization of the unwanted isomer are also troublesome.

One of the most attractive methods of resolution is separation of enantiomers by preferential crystallization (Secor, 1963; Collet et al, 1980; Coquerel et al, 1988, 1990; Sheldon, 1993; Jacques et al., 1994; Coquerel, 2003). In this method, no derivatization or reaction of the starting material is required. It is regarded as an effective and cheap technology to produce pure enantiomers at different scales. The progress of preferential crystallization will be reviewed in detail in Section 2.5.

2.3 Characterization of racemic species

A racemic species can exist as racemic conglomerates, racemic compounds or pseudoracemates. In order to choose the suitable resolution method, it is essential to determine the type to which the crystalline racemate belongs (Collet et al., 1980; Jacques et al., 1994; Li et al, 1999). There are mainly two different kinds of techniques used to identify the racemic species, namely thermal analysis and structural studies by spectroscopy.

The binary melting point phase diagram or ternary phase diagram with solvent is widely used to determine the characteristic of racemic species. The first to characterize racemic species by their phase diagrams was Roozeboom (1899). Roozeboom identified the three fundamental types of the binary melting point phase diagrams: a racemic conglomerate, a racemic compound and a pseudoracemate. Subsequently, various thermal analysis techniques have been applied to construct binary melting point phase diagram, but Differential Scanning Calorimetry (DSC) and Differential Thermal Analysis (DTA) are the most popular instruments used today (Collet et al., 1980; Jacques et al., 1994; Li et al., 1999; Lorenze et al., 2002). Coquerel (2000) had a comprehensive review on binary phase diagrams of chiral systems considering also reversible transitions which may occur between condensed phases such as polymorphism, reversible decomposition of racemate.

Based on the Schroder-Van Laar or Prigogine-Defay equations (Prigogine and Defay, 1954), all the required features of binary phase diagrams of conglomerates and of true racemates, or even of diastereomer mixtures exhibiting eutectics, can be calculated out. This has been known for long time but not much applied because of the difficulty of measuring heats of fusion, especially on small samples (Wilen et al., 1977). The introduction of DSC has changed this situation. To calculate the differences in the thermodynamic quantities between a racemic compound and its corresponding racemic conglomerate, Jacques et al. (Collet et al, 1980; Jacques et al., 1994) developed a thermodynamic approach by using thermodynamic cycles. Li et al. (1999) modified this approach and applied to circa 25 chiral pharmaceuticals. These differences were even considered as ways to reveal the driving force for the formation of racemic compound versus a racemic conglomerate or a pseudoracemate.

On the other hand, it is not unusual that the racemic species exist as a metastable racemic compound or as a racemic conglomerate (Collet et al., 1980; Brock et al., 1991; Li and Grant, 1997; Houllemare-Druot and Coquerel, 1998). Sometimes the reversible transitions may occur between condensed phases such as polymorphism, reversible decomposition of racemate (Coquerel, 2000; Dufour et al., 2004). In this case, examination of binary phase diagram alone is not adequate to identify them. Comparison of solid state spectra of pure enantiomer and its racemate is necessary to identify or prove the solid nature of racemic species. These structural differences usually come from X-ray diffraction patterns or from spectroscopic techniques such as infrared (IR), Raman and solid-state NMR (Collet et al., 1980; Jacques et al., 1994; Li et al., 1999). All properties of conglomerate crystals are independent of chirality, which means that their densities, specific heats, refractive index etc. are identical for the enantiomers and the racemic mixture; while this identity does not exist with racemic compounds and pseudoracemates. Therefore, the comparison of IR/Raman or XRD spectra of enantiomers and of the corresponding racemate in the solid state will provide an excellent test to identify the nature of the racemic species (Jacques et al., 1994). The spectra of enantiomers are identical to that of a racemic conglomerate but different from that of a racemic compound.

The X-ray diffraction of a powdered sample is analyzed to determine the long range order of the crystal lattice (the distance between two adjacent planes within a crystal lattice can be determined). A spectroscopic technique such as solid-state infrared or Raman spectroscopy is used to determine differences in the short range order of the samples (due to different relative arrangement of the molecules within the lattice different vibration modes are caused). Solid-state ^{13}C nuclear magnetic resonance spectroscopy is

also used to diagnose the difference in the arrangement of pure enantiomer molecules in the crystal lattice for different racemic species (Jacques et al, 1994; Li et al., 1999).

The above mentioned techniques have been extensively used to characterize racemic species (Collet et al., 1980; Bettinetti et al, 1990; Dwivedi et al, 1992; Coquerel and Petit, 1993; Neau et al, 1993; Jacques et al., 1994; Miyazaki et al., 1994; Prankerd and Elsabee, 1995; Kommuru et al, 1998; Pena et al, 1998; Gervais and Coquerel, 2002; Lorenz and Seidel-Morgenstern, 2002; Shiraiwa et al., 1992, 1994, 1996, 1997, 1998, 2002, 2003, 2005). Coquerel's group also has shown that the family of 5-alkyl-5-arylhydantonins exhibits a very high frequency of conglomerates (Coquerel and Petit, 1993; Gervais and Coquerel, 2002).

Another approach for studying enantiomeric interactions in the solid state is molecular modelling. A molecular modelling study with lattice energy calculation was explored to look for the factors of chiral discrimination in the crystalline state (Li et al., 2001). The results might explain that why salt forms favour the formation of racemic conglomerate (Collet et al., 1980, Jacques et al., 1994). Leusen et al. (1993; 2003) and Gervais (Gervais and Coquerel, 2002) also tried crystal structure prediction of diastereomeric salts which could be a step toward rationalization of racemate resolution.

2.4 Solubility and metastable zone

2.4.1 Solubility of enantiomers

Solubility data (solid-liquid equilibrium) is the prerequisite for crystallization from solution. The knowledge and use of solubility properties of enantiomer mixtures is not only a matter of theoretical interest, but also allows one to carry out resolutions in a more rational manner than usually obtainable (Jacques et al., 1994).

For a conglomerate, Meyerhoffer (1904) first rationalized the "double solubility" rule which means that a conglomerate has a solubility equal to the sum of the solubilities of the corresponding enantiomers. The non-ideal (dissociation/association) effects were analyzed and a good agreement was obtained between the experimental data and the foregoing theoretical considerations (Collet et al., 1980). They also derived the favourable conditions for preferential crystallization from ternary phase diagram (Collet et al.,1980; Jacques et al., 1994). If the solubility ratio α of racemic mixture to enantiomer is less than 2, the resolution process is more favourable. A similar conclusion was drawn by Watanabe and Noyori (1969) with the industrial-scale resolution of glutamic acid. The ternary phase diagram was also used widely to describe preferential crystallization process (Collet et al., 1980; Elsner et al., 2005). Unlike conglomerate, no matter whether solvation is present or not, the solubility of the racemic compound is not related to that of the enantiomers. The solubility can be either higher or lower (Jacques et al., 1994). There have been only few literatures reported on the influence of solvent and the interactions in solution between enantiomers (Druot et al., 1996; Profir and Rasmuson, 2004).

2.4.2 Metastable zone width

The metastable zone width (MSZW) is a critical parameter in the crystallisation process as it allows an insight into the nucleation behaviour of the system (Mullin, 2001; Teja and Rousseau, 2004). It was Ostwald that first proposed the terms "labile" (unstable) and "metastable" supersaturation, referring to supersaturated solutions in which spontaneous deposition of solid phase, in the absence of solid nuclei, will or will not occur, respectively (Ostwald, 1897). The metastable zone was later divided into the first and the second areas (Ting and McCabe, 1934).

A number of factors influence the value of MSZW including the rate of cooling, agitation, the presence of foreign particles and impurities (Young and Van Sicklen, 1913; Nyvlt et al, 1985). Many efforts have been reported to express the metastable zone width with certain parameters as semiempirical relationships (Nyvlt et al., 1970; Sohnel and Nyvlt, 1975; Kim and Ryu,1997, Ulrich and Strege,2002). Polythermal method is widely used to measure MSZW (Nyvlt, 1968; Nyvlt et al., 1970; Sohnel and Nyvlt, 1975; Mullin and Jancic,1979; Kim and Ryu, 1997, Mullin, 2001). Experimental values of the metastable zone width for a given system depend very strongly on the method of determination. The onset of nucleation can be detected visually or instrumentally. Various instrumental techniques have been employed to detect the onset of nucleation, e.g. electrozone sensing, optical turbidity, laser diffraction or scattering etc (Mullin and Jancic, 1979; Gerson et al, 1991; Barrett and Glennon, 2002; Barrett et al, 2005). Among these methods, Focused Beam Reflectance Measurement (FBRM) is a recently available technique. The advantage of FBRM method is that it does not depend on the presence of a threshold nuclei concentration before a nucleation event is detected (Sparks and Dobbs, 1993; Tadayyon and Rohani, 1998; Barrett and Glennon, 1999, 2002; Barrett et al, 2005). A simplified model based on integral growing of nucleus in nucleation was introduced to predict the metastable zone width (Mersmann and Bartosch, 1997; Kim and Mersmann, 2001).

Although metastable zone width is very useful in understanding the crystallization process in chiral resolution, not much attention has been paid on the measurement and interpretation of MSZW in the enantiomeric systems. Hongo et al. (1981) identified the metastable region into two areas where the second one was more unstable. The dependence of MSZW on the enantiomeric excess was reported in the compounds of

mandelic acid (Perlberg A et al., 2002, 2003). Metastable zone widths were measured for establishing a basis for growth kinetics investigations via isothermal seeded batch experiments in the chiral system mandelic acid/water (Perlberg et al., 2005). Ching's group recently started a series of characterization of MSZW of both conglomerate and racemic compound systems (Wang et al., 2002, 2003, 2004, 2006; Lu and Ching, 2006).

2.5 Enantiomeric resolution by direct crystallization

As introduced before, the classical resolution via diastereoisomer crystallization is making use of the solubility difference of the diastereoisomers. If the racemate is a conglomerate, although the solubilities are almost the same for the two isomers, it is still possible to separate the two enantiomers by direct crystallization from their mixtures. Separation of enantiomers via direct crystallization is the more attractive option as no derivatization or reaction of the starting material is required. There are basically two kinds of resolution methods, namely simultaneous crystallization and preferential crystallization. Collet et. al (1980,1994) had a great review on this subject.

2.5.1 Simultaneous crystallization

This method makes use of the advantages of the spontaneous resolution of the two enantiomers for a racemic conglomerate. Louis Pasteur (1848) was apparently the first person to pioneer this area in 1848. He successfully separated the dextrorotatory and levorotatory crystals constituting the racemic double salt sodium ammonium tartrate by manual sorting (Pasteur, 1848; Kauffman and Myers, 1975). This laborious technique is now only occasionally used to collect the first crystals of enantiomer required to apply the technique of resolution by entrainment. Other variants of this technique include

localization of crystallization of individual enantiomers on suitably disposed seeds in a supersaturated racemic solution (Zaugg, 1955), fluidized bed system (Sato, et al., 1969; Brugidou et al., 1974; Dolling et al.,1978). Dowling (1959) reported an ingenious resolution procedure through seeding of a racemic supersaturated solution with relatively large seeds of one enantiomer in the purification of glutamic acid salts and this procedure was later applied to acetylglutamic acid (Watanabe and Noyori, 1969). This method has been used in the preparation of α-methyl-L-dopa and for the C_3-synthon glycidyl-3-nitrobenzenesulfonate etc (Merck, 1965; Challener, 2001).

2.5.2 Preferential crystallization

Preferential crystallization is also called resolution by entrainment. It is mainly dependent on the differences in the rates of crystallization of the enantiomers in a solution supersaturated with respect to the racemate.

The first example to show the way of resolution by entrainment was reported by Gernez (Collet et al., 1980) who got only dextrorotatory crystals when he seeded the supersaturated solution of the double salt sodium ammonium racemate with a particle of dextrorotatory salt. Jungfleisch (Collet et al., 1980) confirmed the similar observations, but this method was ignored for a long time until 1914 that Werner (1914) rediscovered the same phenomenon in the cobalt bromide system. Surprisingly, this discovery was again forgotten for almost two decades until 1934 that Duschinsky showed the efficiency of resolution by preferential crystallization of histidine monohydrochloride (Duschinsky, 1934). From then onwards, this technique began to get attention of chemists and especially those in industry.

The process of enantiomer separation by preferential crystallization is visualized

best in the ternary phase diagram of the two enantiomers (D and L) and solvent (S).

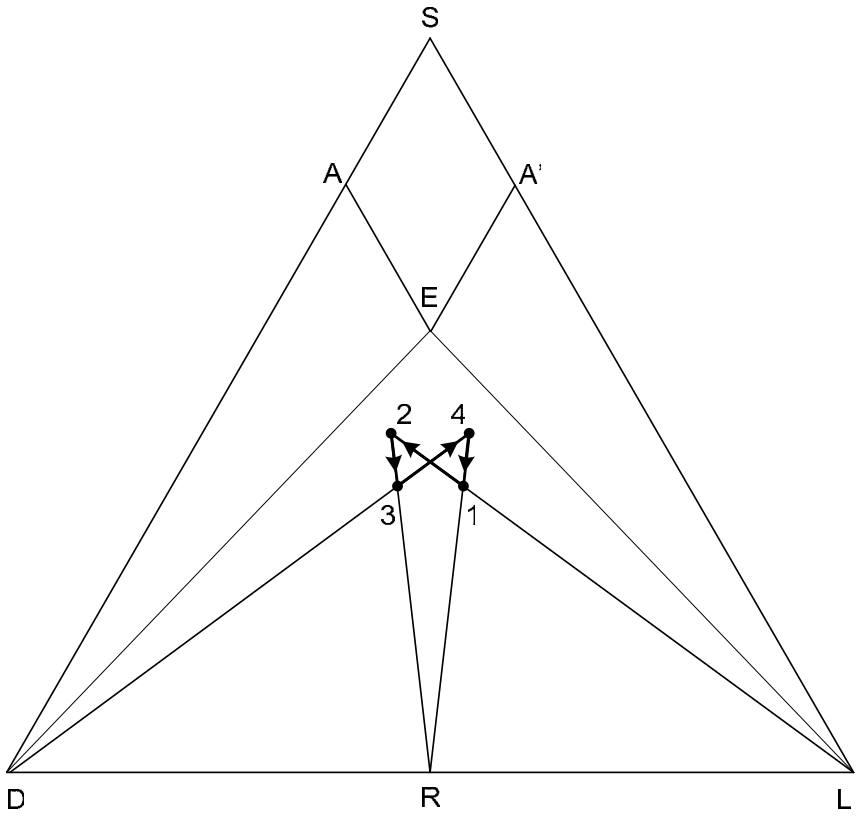

Figure 2.2 Preferential crystallization in the ternary phase diagram (Jacques et al., 1994)

As shown in Figure 2.2, the solubility of the enantiomer mixture in the solvent is given by the line A'EA. For starting the process a racemic solution is enriched artificially by adding a pure enantiomer or a partially resolved solution obtained by a different method. The solution is cooled until it is slightly supersaturated (1). Subsequently pure seed crystals of the more abundant enantiomer (L in this case) are added, as a result the L-enantiomer starts to crystallize. Crystallization of the other enantiomer does not take place if the seed crystals show a selective effect (no suitable nuclei inducing crystallization of the opposite enantiomer is present in the solution and the degree of supersaturation is not sufficient for nucleation to take place). The concentration of the more abundant

enantiomer (L) in solution decreases (1→2). Crystals are collected from the solution when the enrichment by the opposite enantiomer (D in this case) has reached the same value as in the initial solution (2). The same amount of crystalline racemate as collected as crystals is added to the solution. Subsequently the temperature is increased to dissolve the additional racemate (not shown in Figure 2.2). After cooling to the operation temperature seed crystals (pure D-enantiomer) are added to the (slightly supersaturated) solution (3). Crystallization (3→4) yields pure D-enantiomer and a solution enriched by the L-enantiomer (4). Dissolving of racemate and cooling to the operation temperature the initial solution (1) is attained and the process can be repeated.

The first preferential crystallization process was commercialized by Merck (1965) to produce α-methyldopa. It has been used in the synthesis of chloramphenicol and intermediates for benzothiazepines (Collins et al., 1997; Challener, 2001). In some cases, direct crystallization occurs simultaneously with spontaneous in-situ racemization of the enantiomer that remains in excess in the solution, for example, the preferential crystallization of 1,4-benzodiazepene derivatives. This crystallization occurs with spontaneous racemization in solution at room temperature and one enantiomer crystallizes in 75% yield (Hongo et al., 1983; Murakami et al, 1992, 1993; Sheldon, 1993). In spite of the limitations of this method, the preferential crystallization process still has great potential and real economic importance in both the pharmaceutical and chemical industries. It is not only applied to resolution of racemic conglomerates but also possible to purification of partially resolved racemic compounds which are prepared by other methods (Lim et al, 1995; Lorenz et al., 2001; Wibowo and O'Young, 2005).

By 1980s, circa 250 conglomerates had been identified (Jacques et al., 1994). So far about 5-10% of chiral compounds have been reported as conglomerates (Jacques et al.,

1994; Collet, 1999). To date, a lot of efforts are still being put in the inventory of enantiomer mixtures that exist as conglomerates and the preferential crystallization are applied in the resolution. Among these, Shiraiwa's group has extensively screened for racemic amino acids and other compounds (Shiraiwa et al., 1992, 1994, 1996, 1997, 1998, 2002, 2003, 2005;Miyazaki et al., 1994). Coquerel's group also has shown that the family of 5-alkyl-5-arylhydantonins exhibits a very high frequency of conglomerates (Coquerel and Petit, 1993; Gervais et al., 2002).

2.5.3 Mechanism of preferential crystallization

As mentioned by Jacques et al. (1980, 1994), the application of preferential crystallization requires the mastery of the factors that control the rate of crystallization. These factors include the properties of the ternary phase diagram itself and the experimental character such as stirring and seeding etc. Duschinsky (1934) first investigated the resolution mechanism using histidine monohydrochloride. A more systematic search was later conducted by Amiard's group (Velluz and Amiard, 1953;Velluz et al., 1953; Amiard, 1956; Amiard, 1959) on the resolution of threonine and thero-p-nitrophenyl-2-amino-1,3-propanediaol and accordingly the concept of *residual supersaturation* and the definition of *entrainment* of crystallization was introduced.

As mentioned before, the solubility ratio α of racemate to enantiomer in solutions is crucial for the preferential crystallization process (Watanae and Noyori,1969; Collet et al.,1980). A smaller solubility ratio α of racemate to enantiomer will result in a more favourable preferential crystallization operation. This has led to systematic search of dissociable derivatives by combining substrates to be resolved with a variety of achiral reagents (Yamada et al., 1973, 1975) as it is more possible to find a ratio α that is less than

2 in salts than organic compounds. In the optical resolution of (±)-N-acylnorfenfluramine derivatives, the preferential crystallization under isothermal conditions failed primarily due to unfavourable solubility ratio α (Coquerel et al., 1990). A molecular modelling study based on lattice energy calculations was explored later to explain this phenomenon (Li et al., 2001). Leusen et al (1993, 2003) also tried crystal structure prediction of diastereomeric salts which could be a step toward rationalization of racemate resolution.

Factors such as metastable supersaturation, seeding and stirring etc. were also discussed by Collet et al.(1980). A good example is the industrial-scale resolution of glutamic acid hydrochloride with ultrasonic irradiation to produce large number of optically pure microcrystalline seeds (Merck, 1965).

From the processes and phenomenon of purity decrease during the optical resolution of DL-threonine by preferential crystallization, it was found that onset of the purity decrease was strongly related to the consumption of the supersaturation of the crystallizing enantiomer (L-threonine) and to the surface morphology changes of the seed crystals (Matsuoka et al., 1990,1997; Profir and Matsuoka, 2000).

Perez-Garcia and Amabilino (2002) had a detailed review on the spontaneous resolution under supramolecular control. The non-covalent interactions were discussed in explaining the transfer of chirality from molecule to bulk and in particular the spontaneous resolution of enantiomers. The mechanism of an unusual enantiomeric resolution phenomenon caused by polymorphic transition during crystallization of mixed crystals composed of two enantiomers were studied and a mechanism of preferential enrichment was proposed based on the unique polymorphism of the compounds , their metastable and stable crystal structures, the association mode and the aspects of polymorphic transition etc. (Tamura et al., 2002).

The effect of unstable racemic compound on the performance of preferential crystallization of α-methylbenzylamine chloroacetate was investigated and various routine tests were recommended to avoid derivatives which may possibly give the unstable racemic compound (Houllemare-Druot and Coquerel, 1998). A later study by the same group showed the similar impact on the resolution of chiral acids and bases (Dufour et al., 2001). The limited entrainment effect observed with Pasteur salt was found consistent with the presence of a metastable racemic compound (Petit and Coquerel, 2003). In the preferential crystallization of (±)-ephedrine and (±)-mandelic acid, not only this kind of unstable compound was found, a new polymorphic form was also reported to contribute to the limited entrainment effect (Dufour et al., 2004). A rare temperature-dependent racemic compound-conglomerate crystallization of 2,3:6,7-dibenzobicyclo[3.3.1]nona-2,6-diene-4,8-dione was studied in detail and it was found that higher temperature induced the formation of conglomerate (Levkin et al.,2003).

The combined effect of polymorphism and process on preferential crystallization with (+/-)-5(4'-methylphenyl)-5-methylhydantoin was investigated and the genuine impact of polymorphism was highlighted (Courvoisier et al., 2003). The AS3PC programme, stable polymorph and pre-treatment of the solid particles were recommended to achieve the best results in terms of robustness, yield and scale-up. Effect of the polymorphic form of the seeds on the preferential crystallization was also discussed with 5(4'-methylphenyl)-5-methyl-hydantoin (Courvoisier et al., 2001).

2.5.4 Preferential crystallization process

In the application of preferential crystallization process, the conventional method is conducted under isothermal condition (Jacques et al., 1994). The saturated solution is

cooled to the target temperature, seed is added in the supersaturated solution, keep the solution for a time period and finally the crystals are filtrated out. This approach is called as Classical Seeded Isothermal Preferential Crystallization (SIPC) programme by Coquerel's group (Coquerel et al., 1995). As mentioned before, it was found that such isothermal method was not suitable for the preferential crystallization where solubility ratio α is bigger than 2 (Coquerel et al., 1990). Subsequently, an Auto Seeded Programmed Polythermic Preferential Crystallization (AS3PC) was proposed and applied to the preferential crystallization (Coquerel et al., 1995; Ndzie et al., 1997; Beilles et al., 2001; Courvoisier et al., 2001, 2002; Dufour et al. 2001; Wermester et al., 2005). The influence of the process on the mechanisms and the performances of the preferential crystallization were investigated with (+/-)-5-(4-bromophenyl)-5-methylhydantoin (Courvoisier L et al., 2001). More than 25 different molecules have been tested by using this programme. AS3PC process was found more efficient than SIPC process for purity, yield, scale-up and filtration.

More recently, Elsner et al. (2005) presented an interesting investigation of preferential crystallization with focus on aspects of quantification and application using simplified mathematical description. The optimal initial conditions for isothermal preferential crystallization were also tried in this group (Angelov, et al., 2006). The amino acid threonine was used as model system to analyze the isothermal single step crystallization experiments. Some preliminarily satisfying agreement was shown but further model improvement and more detailed experimental works are necessary. An optical resolution technique by natural cooling crystallization combined with pulse heating was proposed, in which a "tailor-made" additive was used as a separation agent in the purification of asparagine to improve the optical purity (Doki et al., 2004). On-line

polarimetry (Rodrigo et al., 2004) in combination with measurements of an on-line density meter was attempted to monitor the resolution process.

From the system engineering perspective, Ng et al. (Berry and Ng., 1997; Wibowo and Ng, 2000; Schroer, et al. 2001) had studied the synthesis of chiral crystallization processes by considering the separation steps in the flowsheet as movements on phase diagrams. Ching's group (Lim et al., 1995) attempted the recovery of praziquantel from racemic mixture by continuous chromatography and crystallization. A systematic procedure has been recently presented for the synthesis of chromatography-crystallization hybrid separation processes (Fung et al., 2005). An approach that couples equilibrium phase behavior and kinetics was proposed for the design of chiral crystallization processes. A generic model that accounts for reaction, as well as crystal nucleation, growth, and dissolution kinetics was developed (Schroer and Ng, 2003).

2.6 Chiral nucleation

Preferential crystallization is normally conducted with seeding. In the seeded crystallizer, secondary nucleation plays an important role and the mechanism has been well studied by experiments with single crystal seeds (Clontz and McCabe, 1971; Denk and Botsaris, 1972; Rousseau et al., 1975, 1976) and in suspension crystallizers (Evans et al., 1974; Qian et al., 1987, 1989; Randolph and Larson, 1988). An embryo-coagulation secondary nucleation (ECSN) mechanism was also proposed to explain some unusual observations and phenomenon (Qian and Botsaris, 1996, 1997). In the nucleation experiments conducted with chiral $NaClO_3$, at low supercoolings, almost all the nucleated crystals had the same chirality as the seed. Above a certain supercooling, however, crystals of both chiralities were obtained (Denk and Botsaris, 1972; Kondepudi et al.,

1990, 1993, 1995, 1998; McBride and Carte, 1991; Yokota and Toyokura, 1992; Qian and Botsaris, 1997, 1998). Davey et al. (1990) also showed the similar findings in triazolylketone chiral crystallization. This transition was thought consistent with the ECSN mechanism (Qian and Botsaris, 1998). It was argued that the origin of the nuclei was the solution layer next to the crystal and the van der Waals forces, which brought the embryos close to the seed were non-discriminating. Therefore, embryos of both chiralities were thought attracted by and concentrated around the seed and their coagulation could produce nuclei of either chirality.

In a later study, it was also found that this phenomenon could be related with the way that the seed crystals were prepared (Qian and Botsaris, 2004). The primary nucleation was also investigated by the same group with the same system (Botsaris et al., 1999). Their experiments with spontaneous crystallization by air bubbling supported the idea of a single progenitor in cases of spontaneous nucleation by cooling. It was also pointed out that in many processes that are perceived as cases of primary nucleation, only one crystal is actually generated primarily and all the others are bred from it by secondary nucleation.

Kondepudi et al. (1990, 1993, 1995, 1998) have outlined an explanation for the production of one-chirality crystals based on the physical nucleation model. They introduced the idea that a parent crystal can breed secondary nuclei only when it reaches a minimum size. The stirring effects on this phenomenon were also discussed (Mcbride and Carter, 1991).

The effect of supersaturation degree on the optical purity was reported as early as 1950 in the system of β-phenylglyceric acid (Furberg and Hassel, 1950). Very low supersaturation was required to get high purity. Another typical example is in the

synthesis of agrochemical paclobutrazol where resolution of a racemic chiral ketone is involved (Black et al., 1989; Collins et al., 1997). Only when very low supersaturation (1 ^{o}C undercooling) was used, did the effects of nucleating the unwanted isomer disappear to give the product with a high optical purity. It was suggested that if high supersaturations within the metastable zone are used, some conglomerates will form crystals that contain domains of both lattices in a single crystal, which means that the enantiomerically pure seed could nucleate the other enantiomer at its surface.

The stability of supersaturation in the preferential crystallization process was first quantitatively described in the optical resolution of DL-serine-4-sulfonate dehydrate in the early 1980s (Hongo et al., 1981). The metastable region was divided into the first and the second metastable regions. The first region was the one where the supersaturation degree was lower than a constant value and no spontaneous crystallization of the unseeded isomer was observed. The second metastable region was the one where the supersaturation was stable for only a certain time and spontaneous crystallization was ready to take place. Consequently, the waiting time for the spontaneous crystallization of the unseeded isomer was predicted by a conventional calculation method (Hongo et al., 1981).

For the effects of additives in the chiral nucleation, Weissbuch et al. (2003) had a good review. The delicate interplay between stereochemical control, monitoring at the subnanometer level, and an understanding of crystal nucleation were probed. The effects of chiral additive and wetting agent in the preferential crystallization of (+/-)-5-ethyl-5-methylhydantoin were experimentally studied in Conquerel's group (Ndzie et al., 1999; Beilles et al., 2001). Some salts have been used to stabilize the supersaturated solution in the optical resolution (Soichiro, 1983; Harada et al., 1986).

2.7 Crystallization kinetics

Crystal growth and nucleation kinetics are the basis of modelling, design and operation of a crystallizer. There are two basic categories of techniques to evaluate crystallization kinetics, namely, steady state method and dynamic method. For the former one, the most famous is the classical continuous method proposed by Randolph and Larson (1988) with mixed-suspension, mixed-product-removal (MSMPR) crystallizer.

Dynamic method is an alternative approach for the estimation of kinetics using unsteady-state data from batch experiments. Various dynamic techniques have been reported with batch crystallizations. These include thermal response technique (Omran and King, 1974) and mass balance approach (Garside et al., 1982; Halfon and Kaliaguine, 1976). But most of the proposed methods using batch crystallization process are based on crystal size distribution (CSD) analysis (Garside and Jancic, 1976; Way, 1985; Tavare and Garside, 1986; Nyvlt, 1989; Witkowski et al., 1990; Qiu and Rasmuson, 1991, 1994; Farrell and Tsai, 1994; Yokota et al., 2000; Garside et al., 2002; Zhang and Rohani, 2003; Hu et al., 2004). These include moment method (Tavare and Garside, 1986), nonlinear optimization algorithm (Nyvlt, 1989; Witkowski et al., 1990; Qiu and Rasmuson, 1991, 1994; Farrell and Tsai, 1994; Yokota et al., 2000; Zhang and Rohani, 2003; Hu et al., 2004) and *s*-plane analysis (Tavare and Garside, 1986). The details will be discussed in Chapter 6.

For chiral crystallization, only Elsner et al. (2005) recently attempted to use moment method to determine crystallization kinetics of L-/D-threonine in water with difficulty in nucleation rate prediction.

2.8 Optimal operation of batch crystallization

Many works have been reported to show the benefits of controlling the supersaturation in batch crystallization (Mullin and Nyvlt, 1971; Jones and Mullin 1974; Rohani and Bourne, 1990). These benefits include larger crystals and narrower crystal size distribution. This means product purity could be improved in the filtration and washing process (Mersmann, 1995; Matthews and Rawlings, 1998), which is especially important for chiral purification (Courvoisier et al, 2003).

Numerous efforts have been put on optimal operation of batch crystallizer. Mullin and Nyvlt (1971), Jones (1974), and Jones and Mullin (1974) did the pioneer work both theoretically and experimentally. Mayrhofer and Nyvlt (1988) dealt with a general derivation of a theoretical cooling curve of a batch crystallizer. Rohani and Bourne (1990) derived a simplified optimal cooling curve by assuming constant nucleation and supersaturation. Various objectives have been chosen to optimize batch crystallization, such as mean crystal size and coefficient of variation (Chianese et al., 1984; Choong and Smith, 2004; Costa and Maciel Filho, 2005), seed ratio (Bohlin and Rasmuson, 1992; Mathews and Rawlings, 1998; Chung et al., 1999) and even shape (Ma et al., 2002). The newly developed on-line monitoring and controlling techniques greatly facilitate these investigations (Barrett and Glennon, 2002; Elsner et al., 2005).

2.9 Summary

The application of direct crystallization, particularly preferential crystallization, in the enantiomeric separation of pharmaceuticals and fine chemicals has become increasingly important from both practical (clinical/environmental etc.) as well as economic (cost/efficiency etc.) viewpoint. However, most of the past studies are focused on the chemistry aspects and the thermodynamic behaviours of solid phases. Little

attention has been given to the crystallization process itself from the system engineering perspective. Both the previous studies on chiral nucleation and unstable metastable zone and the implications of crystal habits control suggest that supersaturation plays a crucial role in preferential crystallization process. The philosophy of the present work was to develop a systematic engineering approach to study preferential crystallization, especially on the metastable zone measurement and interpretation, and application of critical supersaturation control in the optical resolution. Accordingly, the preferential crystallization was investigated from system characterization and thermodynamics, to metastable zone and chiral nucleation analysis and crystallization kinetics determination, and finally to the process modelling, optimal operation and in-situ monitoring.

CHAPTER 3 EXPERIMENTAL SET-UP AND METHODOLOGY

3.1 The studied chiral systems

The (R)- and (S)-4-hydroxy-2-pyrrolidone, (+)- and (–)-N-methylephedrine, (R)-, (S)- and (RS)-propranolol hydrochloride and (R)-, (S)- and (RS)-atenolol were purchased from Sigma-Aldrich Pte Ltd (Singapore) and were used as received. All enantiomers were stored in a refrigerator at about 5 °C to reduce the risk of decomposition. In the following Figures 3.1-3.4 show their chemical structures of all enantiomers and their physical properties and specifications are listed in Tables 3.1-3.4.

4-hydroxy-2-pyrrolidone:

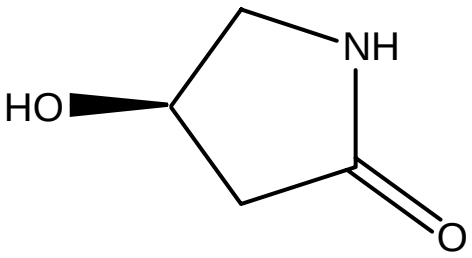

(R)-4-Hydroxy-2-Pyrrolidone

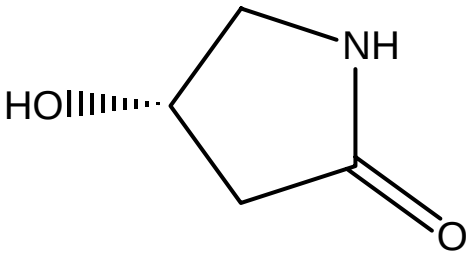

(S)-4-Hydroxy-2-Pyrrolidone

Figure 3.1 Chemical structure of (R)- and (S)-4-hydroxy-2-pyrrolidone

Table 3.1 Properties and specifications of 4-hydroxy-2-pyrrolidone

Name	(R)-4-Hydroxy-2-Pyrrolidone	(S)-4-Hydroxy-2-Pyrrolidone
Synonyms	(R)-β-Hydroxy-γ-butyrolactam	(S)-β-Hydroxy-γ-butyrolactam
Molecular Formula	$C_4H_7NO_2$	$C_4H_7NO_2$
Molecular Weight	101.1 g/mol	101.1 g/mol
Melting Point	156-160 °C	156-160 °C
Purity	Puriss. ≥ 99.0% (GC, sum of enantiomers)	Puriss. ≥ 99.0% (GC, sum of enantiomers)
Optical rotation	$[\alpha]_D^{20}$=+41±3° (c=1 in EtOH)	$[\alpha]_D^{20}$=-41±3° (c=1 in EtOH)
Optical rotation	$[\alpha]_{546}^{20}$=+50±3° (c=1 in EtOH)	$[\alpha]_{546}^{20}$=-50±3° (c=1 in EtOH)

4-hydroxy-2-pyrrolidone is a versatile chiral intermediate for the synthesis of many biological active compounds. Examples are the drugs (R)-γ-amino-β-hydroxybutyric acid (GABOB), which is an antiepileptic agent (Aubé et al., 1991), (R)-carnitine (vitamin B_T) and 4-hydroxy-2-pyrrolidone acetamide (oxiracetam), which is a nootropic (acting selectively on the cerebral cortex) agent used in the treatment of amnesic condition (Di Silvestro et al., 1993; Huang et al., 1999). One of the enantiomers could be isolated from the European fly agaric (Amanita muscaria (L. ex. Fr.)), but the amount contained in the mushroom is very low (Matsumoto et al., 1969).

N-methylephedrine:

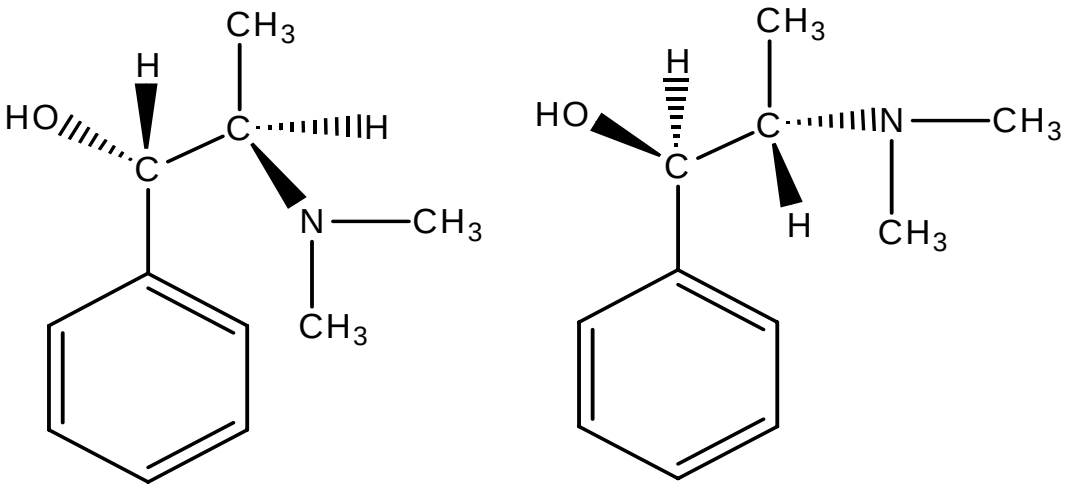

(1S,2R)-(+)-N-Methylephedrine (1R,2S)-(-)-N-Methylephedrine

Figure 3.2 Chemical structure of (+)- and (-)-N-methylephedrine

N-methylephedrine contains two asymmetrical centres; therefore four stereoisomers of this substance exist. The two forms (1S, 2R)-(+)-N-methylephedrine and (1R, 2S)-(-)-N-methylephedrine are the erythro pair of the diastereomers, the corresponding threo pair consists of (1R, 2R)-(-)-N-methylpseudoephedrine and (1S, 2S)-(+)-N-methylpseudoephedrine (Kawasuji et al., 1996; Herráez-Hernández and Campíns-Falcó, 2001).

N-methylephedrine belongs to the class of ephedrines, which are potential central nervous stimulant drugs (Herráez-Hernández and Campíns-Falcó, 2001). The substances belonging to the class of ephedrines are very similar; the chemical structure of the different forms differentiates only in the two groups which are attached to the nitrogen atom.

Methylephedrine is an antitussive, which is contained in many over-the-counter cough and cold mediations, often mixed with other drugs (Inoue and Suzuki, 1990; Ishigooka et al., 1991; Kunsman et al., 1998).

Table 3.2 Properties and specifications of N-methylephedrine

Name	(1S,2R)-(+)-N-Methylephedrine	(1R,2S)-(-)-N-Methylephedrine
Synonyms	(+)-(1S,2R)-2-Dimethylamino-1-phenylpropanol	(-)-(1R,2S)-2-Dimethylamino-1-phenylpropanol
Molecular Formula	$C_{11}H_{17}NO$	$C_{11}H_{17}NO$
Molecular Weight	179.3 g/mol	179.3 g/mol
Melting Point	87-90 °C	86-88 °C
Purity	99%	99%
Optical rotation	$[\alpha]_D^{20}$=+29° (c=5 in CH_3OH)	$[\alpha]_D^{21}$=-29.2° (c=5 in CH_3OH)

Propranolol hydrochloride:

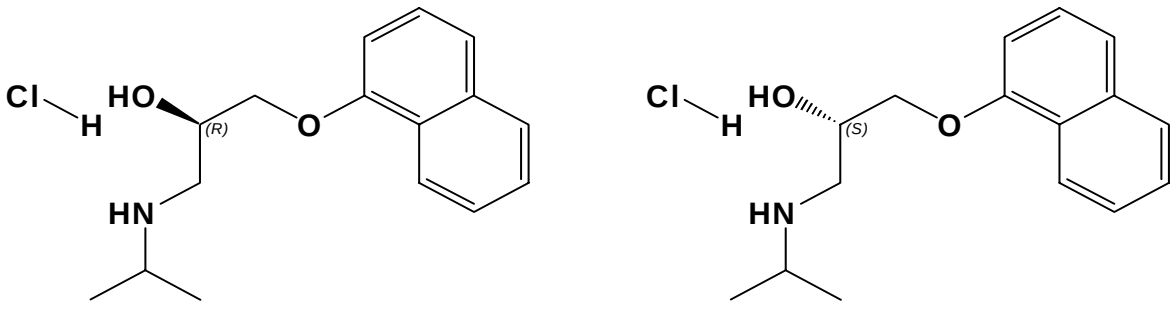

R-propranolol hydrochloride **S-propranolol hydrochloride**

Figure 3.3 Chemical structure of (R)- and (S)-propranolol hydrochloride

Table 3.3 Properties and specifications of propranolol hydrochloride

Name	(R)-Propranolol Hydrochloride	(S)-Propranolol Hydrochloride
Molecular Formula	$C_{16}H_{21}NO_2 \cdot HCl$	$C_{16}H_{21}NO_2 \cdot HCl$
Molecular Weight	295.81 g/mol	295.81 g/mol
Melting Point	193-195 °C	193-195 °C
Purity	Puriss. ≥ 99.0% (HPLC, sum of enantiomers)	Puriss. ≥ 99.0% (HPLC, sum of enantiomers)
Optical rotation	$[\alpha]_D^{20}$=+26±1° (c=1 in EtOH)	$[\alpha]_D^{20}$=-26±1° (c=1 in EtOH)

Propranolol hydrochloride is a synthetic beta-adrenergic receptor blocking agent widely used in the treatment of hypertension and cardiac arrhythmias (Neau et al., 1993).

Atenolol:

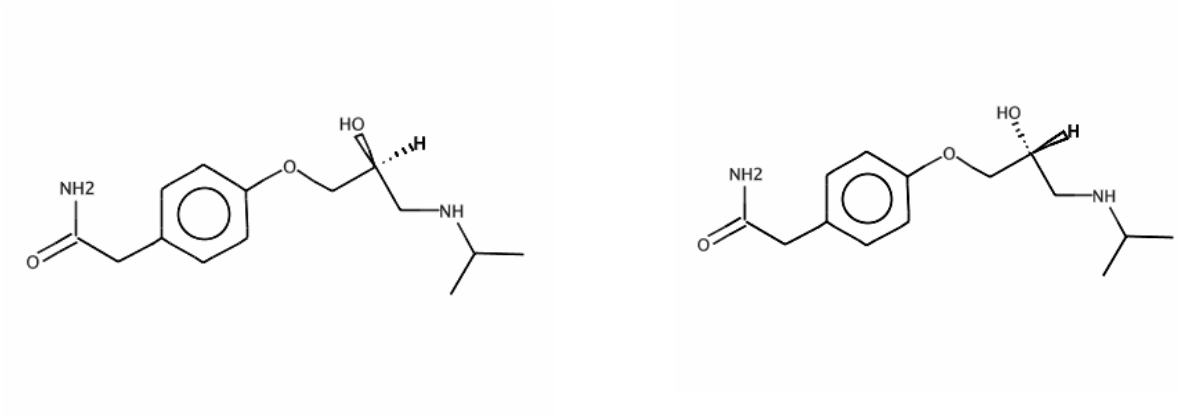

(R)-Atenolol (S)-Atenolol

Figure 3.4 Chemical structure of (R)- and (S)-atenolol

Table 3.4 Properties and specifications of atenolol

Name	(R)-Atenolol	(S)-Atenolol
Molecular Formula	$C_{14}H_{22}N_2O_3$	$C_{14}H_{22}N_2O_3$
Molecular Weight	266.34 g/mol	266.34 g/mol
Melting Point	148-152 °C	148-152 °C
Purity	Puriss. ≥ 99.0%	Puriss. ≥ 99.0%
Optical rotation	$[\alpha]^{25}$=+16° (c=1 in 1N HCl)	$[\alpha]^{25}$=-16° (c=1 in 1N HCl)

Atenolol is a drug belonging to the group of beta blockers, a class of drugs used primarily in cardiovascular diseases. Introduced in 1976, atenolol was developed as a replacement for propanolol in the treatment of hypertension.

Other chemicals:

Analytical and HPLC grade isopropanol, methanol, acetone and hexane were purchased from Aik Moh Paints & Chemicals Pte Ltd (Singapore) and were used as received. The ultra pure deionized water was obtained through a Millipore ultrapure water system (Milli-Q Gradient A10 System).

3.2 Characterization and analysis methods

3.2.1 Differential scanning calorimetry (DSC)

In this work, all differential scanning calorimetry measurements were performed using a Mettler Toledo DSC822^e Module (heat flux DSC), together with the STAR^e–software. Samples of 2-7 mg are prepared in standard 40 µl aluminium crucibles using a

Mettler Toledo XS205 microbalance. The crucibles were sealed with a perforated cover. The flow rate of purging gas nitrogen was 40 mL/min. Preceding investigation of samples, the DSC apparatus was calibrated using a pure indium sample.

3.2.1.1 Analysing the thermogram

Two routines are available for converting the set of DSC experiments (the experiments for different compositions of the binary mixture) to the binary melting point diagram. They are the enthalpy/liquid fraction routine (DIN 51004, 1994; Di Silvestro et al., 1993) and the more commonly used routine where beginning and end of fusion are determined from the thermogram by means of some characteristic points (Jacques et al., 1994; Lorenz and Seidel-Morgenstern, 2002).

In this work, determination by characteristic points of the thermogram was used to evaluate the melting points. A pure substance (e.g. a single enantiomer) was examined first. Due to the fact that a pure substance melts at a definite temperature, the peak is narrow and the melting point is determined as the point of intersection of the tangent on the leading edge of the fusion peak with the baseline. The angle between the leading edge and the straight line passing through the maximum peak point was recorded as the correcting angle. If the phase diagram shows a eutectic, two peaks appear in the thermogram. The first peak marks the beginning of fusion (and therefore the solidus line), where the first liquid-phase (of eutectic composition) is formed. This peak is followed by a second one, which is most often diffuse. The same correcting angle as determined for the pure enantiomer was employed to the peaks of the thermograms for the other compositions. Therefore, the beginning and end of fusion, which represents the solidus and liquidus line, respectively, are obtained directly from the thermogram.

3.2.2 Powder X-ray diffraction (PXRD)

The wavelength of X-ray lies between 10^{-12} and 10^{-8} m, which is the same magnitude as the distance of two adjacent planes within a crystal lattice. The phenomenon of diffraction occurs whenever the wavelength of electromagnetic radiation and a characteristic dimension of interfering matter are of the same magnitude. From the diffraction pattern the distance of two adjacent planes within the crystal can be determined if the frequency of the X-ray radiation is known using Bragg's law (Atkins and dePaula, 2002). Even if a large crystal without inclusions or other imperfections is available, measurement of all different crystal faces is difficult, that is why most often a powder is examined (Powder X-ray diffraction, PXRD). In a powder the number of particles is big enough, that even with small samples all different orientations are exposed to the X-ray beam simultaneously. Due to the small size of particles no orientation will be preferred when the powder is attached to an inert carrier such as paper. The distances between adjacent planes of different orientation are unique for each substance and even for different polymorphs of the same substance. That is why a racemic conglomerate should have the same diffraction pattern as a pure enantiomer, but a different diffraction pattern than a racemic compound. The depiction of Ewing (1985) provides information on the instrumentation.

$$d = \lambda / (2\sin\theta) \tag{3.1}$$

where θ is the diffraction angle.

In this work, the PXRD patterns of both the racemates and pure enantiomers were determined at room temperature using a Bruker D8 Advance diffractometer with Cu-Kα

radiation at 40 mA, 40kV. The samples were packed into an aluminum holder and scanned with the diffraction angle 2θ increasing from 5-70^{o}, with a step size of 0.02^{o} for 1 sec.

3.2.3 Fourier transform infrared spectroscopy (FT-IR)

In this work, the FT-IR spectra of both the racemates and pure enantiomers were obtained in the range of 400-4000 cm^{-1} with a Bio-Rad FTS 135 FTIR spectrometer using the KBr disk method. The scans were performed with a resolution of 4 cm^{-1} and the number of scans was 40. All spectra were collected at ambient temperature.

3.2.4 Raman spectroscopy

Infrared (IR) and Raman spectroscopy both measure the vibrational energies of molecules. Raman spectroscopy is based on the Raman effect, which is the inelastic scattering of photons by molecules. Raman spectroscopy complements IR spectroscopy. For a vibrational motion to be IR active, the dipole moment of the molecule must change. But for a vibration to be Raman active, the polarizability of the molecule must change with the vibrational motion. The spectra are plotted with intensity vs. Raman shift in cm^{-1}.

In this work, a Renishaw's inVia Raman microscope was used. It is with Renishaw's WiRE™ 2.0 software and RenCam CCD detector. A 785 nm laser was used to measure the Raman spectra in the range of 0-2000 cm^{-1}.

3.2.5 Nuclear magnetic resonance (NMR)

Solid state NMR has many potential applications in the characterization of solids that are largely intractable by other means. ^{13}C spectra show chemical shifts that are more sensitive to the details of structure than are proton shifts. Differences between structural

and stereoisomers can easily be seen. In a powdered crystalline material, all orientations are present, and the signal observed is a distribution of resonances, hence a relatively wide peak is seen, whereas the fluidity of a liquid solution ensures that only a single peak is observable.

In this work, ^{13}C SS-NMR spectra were acquired at 100.613 MHz, using a CAMPAS DRX 400 spectrometer. Spinning speeds were 8-10 kHz.

3.3 Solubility and metastable zone width measurement

The limit of the metastable zone is also referred to as supersolubility. The difference in concentration (for constant temperature) or the difference in temperature (for constant concentration) between a saturated solution and a solution on the limit of the metastable zone is called metastable zone width or maximal allowed temperature of supercooling.

Polythermal method was used to measure the solubility and metastable zone width, using 25 - 500 ml jacketed crystallizers equipped with a magnetic stirrer bar (for small volume) or an overhead stirrer (for large volume) and a Julabo programmable circulator FP25-ME (for small volume) or FP88-HL (for large volume). A Lasentec S400A FBRM (Focused Beam Reflectance Measurement) was used to detect the onset of nucleation and dissolution. A Lasentec 700 PVM (Particle Vision and Measurement) system was also integrated into the experiments. The image has a field of view of 860 x 645 um, with resolution down to approximately 5 um and capturing speed up to 10 images per second.

FBRM and PVM have recently emerged as a widely used technique for the in situ characterization of particulate slurries.

FBRM instrumentation is composed of three parts: a probe which can be installed directly in the crystallizer without the need for sample dilution or manipulation, the electronic measurement unit and a computer for data acquisition and analysis (as shown in Figures 3.5 and 3.6).

FBRM measures a chord length distribution (CLD), which is a function of the number, size, and shape of particles under investigation. FBRM uses a focused beam of laser light, which scans in a circular path. As this light scans across a particle or particle structure passing in front of the probe window, light is scattered in all directions. The light scattered back towards the probe is used to measure a chord length of the given particle. Typically, many thousands of chords are measured per second, providing a robust measurement that is sensitive to the change in the size or number of particles under investigation. Unlike, for example, optical turbidity or laser diffraction, FBRM does not depend on the presence of a threshold nuclei concentration before a nucleation event is detected. This is especially for the current studied chiral system, where the suspension density is normally very low. A more detailed description of the operation of the FBRM probe is provided in the literature (Barrett and Glennon, 1999, 2002; Worlitschek and Mazzotti, 2003; Barret et al., 2005).

FBRM is a useful tool for detecting crystal behaviour during crystallization processes. It can accurately detect a nucleation event and characterize the metastable zone width. However, there are a variety of parameters that affect the particle chord length and count measurements. Some researchers have tried to interpret the FBRM chord length distribution with respect to an actual particle size distribution (Ruf et al, 2000; Heath et al., 2002; Worlitschek et al., 2005; Kougoulos et al., 2005; Barthe and Rousseau, 2006;

Pons et al., 2006). There is still no generally applicable model to convert chord length distribution to particle size distribution.

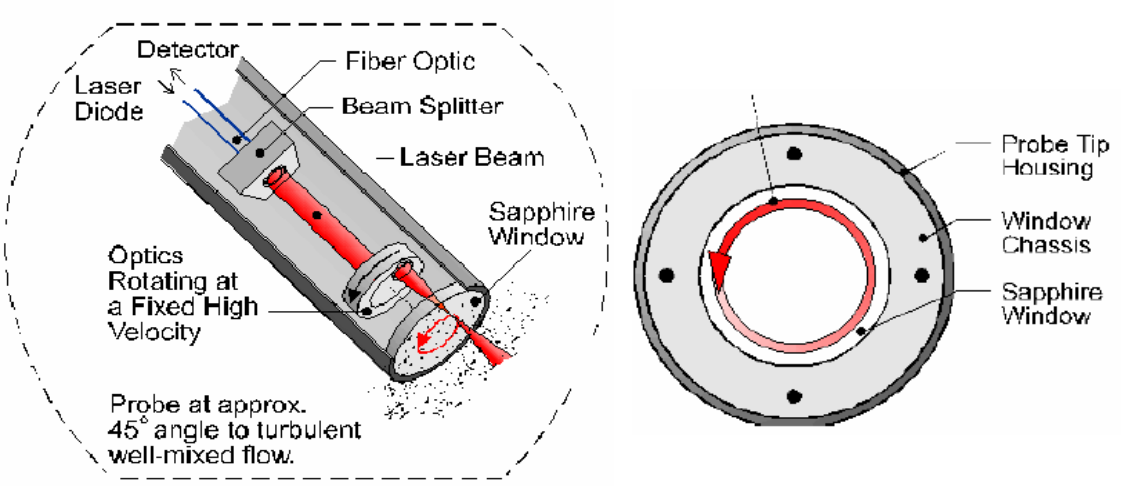

Figure 3.5 FBRM probe

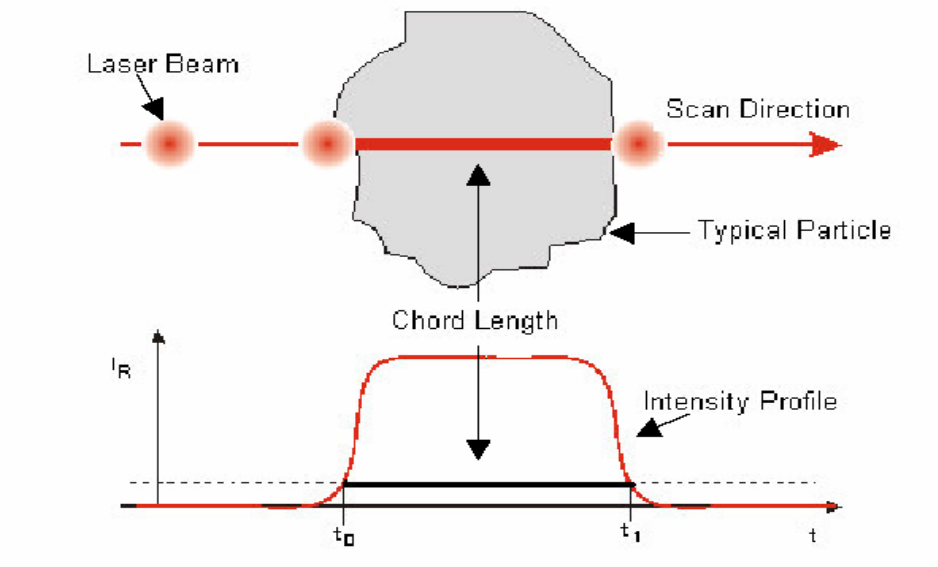

Figure 3.6 FBRM chord length measurement

3.4 Direct crystallization experimental set-up

Direct cooling crystallizations were carried out in an automated apparatus. A Mettler Toledo LabMax Automatic Laboratory Reactor system was used to control and monitor crystallizer operation. As shown in Figure 3.7, it was equipped with a 1-litre jacketed curved-bottom glass crystallizer, a downward glass propeller stirrer driven by a heavy duty motor, a temperature sensor, a solenoid diaphragm dosing pump and a balance. It performed temperature control and monitoring, solvent addition and stirring speed in an automated and highly accurate mode. The temperature of the crystallizer was measured at 2 s intervals throughout a crystallization run. A Lasentec S400A FBRM and a Lasentec 700 PVM were used for in-situ crystal monitoring.

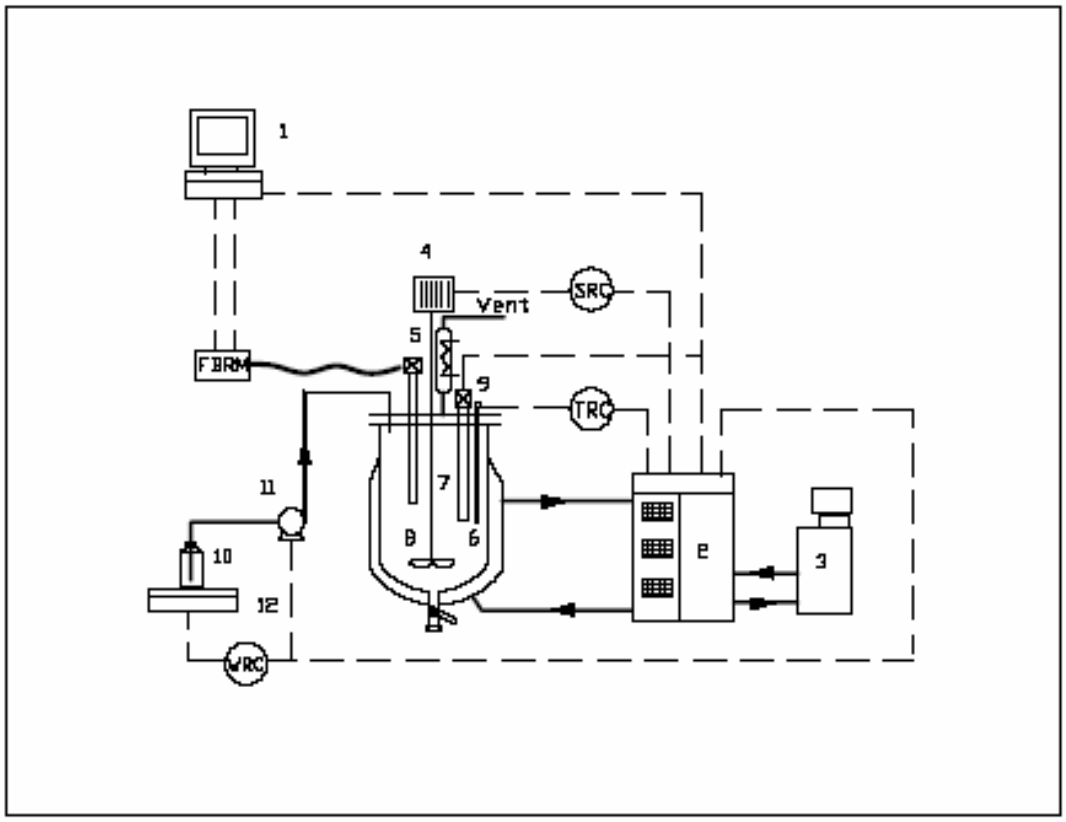

Figure 3.7 Experimental set-up: 1– Computer; 2- LabMax; 3- Julabo cooling/heating refrigerator; 4- Heavy duty stirrer; 5- Condenser; 6- Temperature sensor; 7- 600ml double-wall crystallizer; 8- FBRM; 9- PVM; 10- Solvent bottle; 11- Dosing pump;12-Balance

3.5 Crystal analysis and monitoring

3.5.1 Principle of optical rotation and polarimetry

Many molecules with a lack of symmetry (e.g. chiral molecules) rotate the plane of plane-polarized radiation. The extent of optical rotation caused by optical active molecules in a solution depends on the concentration of the solution, the solvent used, the path length of the measurement cell, the temperature and the wavelength of radiation used. The optical

rotation caused by the two enantiomeric forms of a racemic specie is of the same magnitude but of contrary direction, therefore a racemic mixture is optical inactive and the optical rotation of any enriched solution is in addition to the factors described above dependent on the enantiomeric excess (ee) of the solution (Ewing, 1985).

For specified solvent, temperature and wavelength, it is common to report not the actual measured optical rotation α, but the specific rotation $[\alpha]_\lambda^T$. The specific rotation is defined as

$$[\alpha]_\lambda^T = \frac{\alpha}{dc} 10000 \tag{3.2}$$

where d is the path length of the measurement cell and c is the concentration of optical active solute in solution.

In this work, the optical rotations were measured at 589.3 nm using a JASCO P-1030 digital polarimeter equipped with a quartz cell of 50 mm path length at ambient temperature in a solution of isopropanol.

3.5.2 Particle size analysis

Several methods based on different measurement principles exist to determine a particle size distribution. An elaborate description of the different techniques with their advantages and disadvantages is presented in the monograph of Allen (1997). A shorter overview is given by Rawle (2006). The most important methods are: image analysis (e.g. with an optical microscope or electron microscope), sieving, sedimentation, electrozone sensing (Coulter Counter) and laser diffraction.

The method of laser diffraction or more precisely Low Angle Laser Light Scattering (LALLS) is widely used for determining particle size distributions with many applications in quality control and research. Advantages are the fast obtained results and the coverage of a wide range of particle sizes ranging from 0.1 to 2000 μm. The method, applicable for most particles of interest (dry powders, suspensions, emulsions, aerosols, sprays, etc.) is volume-based, which means a volume or weight distribution is obtained directly. The principle of a low angle laser light scattering instrument is shown in Figure 3.8. To obtain a representative size distribution measurement time should not be too short (typically measurements last 10-20 seconds) and data sampling should be as fast as possible. This ensures that the measured population is large enough to be representative for the investigated sample. The stirring speed should be high enough to ensure a good dispersion of the particles present in the sample; additionally the bath should be ultrasonically agitated if the particles tend to agglomerate.

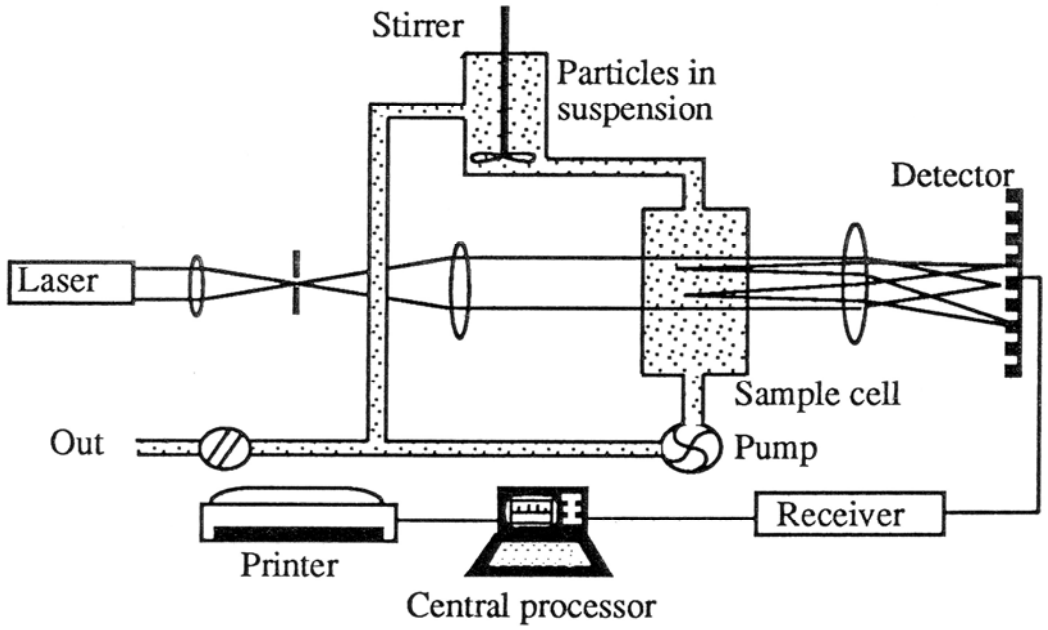

Figure 3.8 Principle of LALLS instruments (Allen, 1997)

In this work, a Malvern Mastersizer 2000 (laser diffraction) was used to measure crystal size distribution. In the meantime, a Lasentec S400A FBRM and a Lasentec Particle Vision and Measurement (PVM) 700 were also used to in-situ monitor the crystallization process.

3.5.3 Field emission scanning electron microscope (FESEM)

There are two classes of emission source: thermionic emitter and field emitter. Emitter type is the main difference between the SEM and FESEM. FESEM produces a cleaner and higher resolution topographical image.

In this work, the crystal morphology was investigated using a Jeol JSM-6700F Field Emission SEM. A small amount of samples were scattered on double-sided adhesive carbon tabs mounted on SEM stubs, and were coated with Au/Pd in a Cressington 208 sputter coater.

CHAPTER 4 CHARACTERIZATION OF RACEMIC SPECIES

4.1 Introduction

The basis for any enantiomer separation, but especially for a separation approach via crystallization, is the knowledge about the solid-state characteristic of the racemate. Racemate crystals can be divided into three types: racemic conglomerates, racemic compounds or pseudoracemates (Roozeboom, 1899; Collet et al., 1980; Jacques et al, 1994; Li and Grant, 1997; Li et al, 1999; Lorenz and Seidel-Morgenstern, 2002). The three fundamental types of racemic species are shown in Figure 4.1.

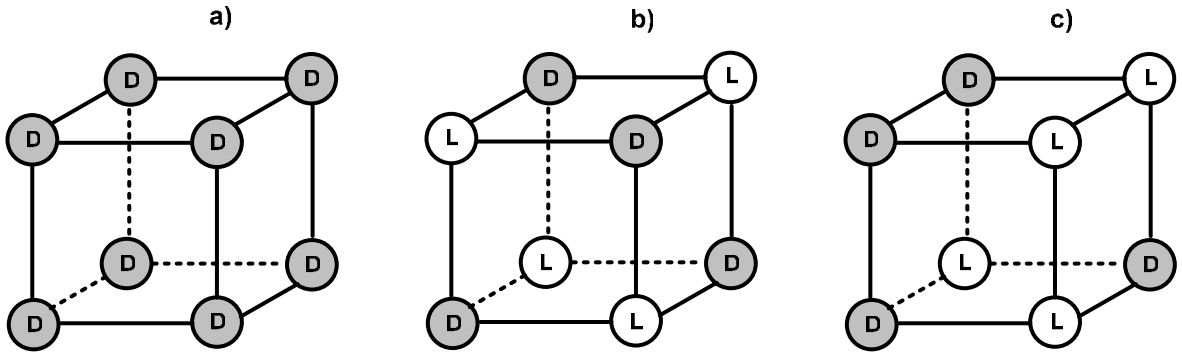

Figure 4.1 Crystal lattices of the three fundamental types of racemates:
a) a conglomerate; b) a racemic compound; c) a pseudoracemate

The crystal lattice of a conglomerate is built up by the same enantiomer molecules as shown in Figure 4.1a. A racemate is a mechanical mixture of crystals containing the corresponding enantiomers. In a racemic compound, the two corresponding enantiomers

are present in equal quantities in a well-defined arrangement within the crystal lattice as shown in Figure 4.1b. For a pseudoracemate, two enantiomer molecules coexist in the crystal lattice in a random manner as shown in Figure 4.1c.

The aim of this chapter is to identify and characterize the solid-state nature of different racemic mixture with various techniques. First the characterization of racemic species by their binary melting point phase diagram was discussed. Based on a thermodynamic cycle involving the solid and liquid phases of the enantiomers and racemic species, the melting point, enthalpy, entropy and Gibbs free energy of the racemic species were derived from the thermodynamic data. Furthermore, racemic species are possible to exist as a metastable racemic compound or as a racemic conglomerate (Collet et al., 1980; Li and Grant, 1997; Houllemare-Druot and Coquerel, 1998). Sometimes the reversible transitions may occur between condensed phases such as polymorphism, reversible decomposition of racemate (Coquerel, 2000; Dufour et al., 2004). As such, examination of binary phase diagram alone is not adequate to identify them. Additional spectroscopic techniques were employed to compare the solid state spectra of pure enantiomer and its racemate to identify or prove the solid nature of racemic species.

4.2 Methods for characterization of racemic species

4.2.1 Characterization by the binary phase diagram

The binary phase diagram (melting point diagram) is considered to be the most important tool for determining the solid-state characteristic. The first to characterize racemic species by their phase diagram was Roozeboom (Roozeboom, 1899). The three types of racemates are readily distinguished by reference to their melting point diagrams as shown in Figure 4.2. A racemic conglomerate is shown in Figure 4.2 a), a racemic

compound in Figure 4.2 b) and the case of pseudoracemate in Figure 4.2 c). Pseudoracemates are further differentiated in ideal pseudoracemates as shown in Figure 4.2 c1) and pseudoracemates showing a maximum Figure 4.2 c2) or minimum Figure 4.2 c3), respectively.

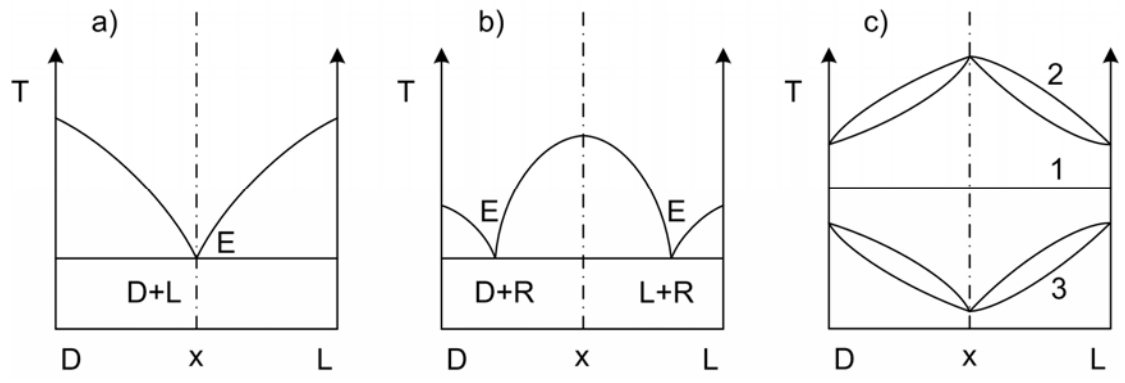

Figure 4.2 Typical binary phase diagrams of various racemic species; a) racemic conglomerate, b) racemic compound, c) pseudoracemate : 1, ideal; 2, with a maximum; or 3, with a minimum. R, D and L indicate the racemic compound, pure dextrorotatory enantiomer and pure levorotatory enantiomer, respectively. E indicates the eutectic point.

There are a number of reasons why a binary phase diagram should be determined first. The sample mass required to determine the binary phase diagram is small, measurements require short time and additional information such as the enthalpy of fusion can be determined by employing thermal analysis (DTA, DSC) to predict the phase diagram.

In this work, a heat flux DSC apparatus (Mettler Toledo DSC822^e) was employed to measure the binary melting point phase diagram and enthalpy of fusion.

4.2.2 Characterization of racemic species by analytical spectroscopic techniques

As a matter of fact many organic substances show polymorphism, that means different crystalline arrangements in the solid state are observed dependent most often on temperature. That is why today the phase diagram alone is not considered to be sufficient for an unambiguous characterization of racemic species. Experimentalists have agreed on employing additional analytical techniques to ensure a definite recognition of the solid-state behavior. The X-ray diffraction of a powdered sample is analyzed to determine the long range order of the crystal lattice (the distance between two adjacent planes within a crystal lattice can be determined). A spectroscopic technique such as solid-state Infrared or Raman spectroscopy is used to determine differences in the short range order of the samples (due to different relative arrangement of the molecules within the lattice, different vibration modes are caused). Solid-state ^{13}C nuclear magnetic resonance spectroscopy is also used to diagnose the difference in the arrangement of pure enantiomers molecules in the crystal lattice for different racemic species (Jacques et al, 1994; Li and Grant, 1997).

The spectra of enantiomers are identical to that of a racemic conglomerate but different from that of a racemic compound.

4.3 Results and discussion

4.3.1 Characterization by the binary phase diagram

For the characterization of the studied chiral systems by their binary phase diagrams, samples of different compositions (different enantiomeric excess) were prepared and measured in a differential scanning calorimetry apparatus as described in Chapter 3. The resulting thermograms were evaluated and the resulting binary phase diagrams are shown and discussed in the following sections.

4.3.1.1 Melting point phase diagram of 4-hydroxy-2-pyrrolidone

The theoretical background about evaluating the thermograms has been explained in Chapter 3 already. Because formation of a solvate (with different melting point) was reported by Di Silvestro et al (1993), DSC runs of samples prepared by different methods were investigated for the binary phase diagram. DSC runs of samples prepared by mixing the two enantiomers directly in the crucible were evaluated. Samples prepared with crystals recovered from solvent (isopropanol) were also checked on different melting points.

No differences in the thermograms were observed for the different methods of preparing the samples. The determined temperature of fusion was only dependent on the composition. The unfavourable formation of a stable solvate of 4-hydroxy-2-pyrrolidone recovered from a solution containing isopropanol (Di Silvestro et al, 1993) could not be confirmed. For dried crystals (dried for four hours at 60 °C under vacuum) recovered from a solution in isopropanol, neither a different melting point compared to the untreated crystals in DSC measurements nor different FT-IR spectra were obtained. It can be concluded that, even if a solvate with different melting point was formed by crystallization from isopropanol, it was transformed to unsolvated crystals during drying.

For 4-hydroxy-2-pyrrolidone, the graphic procedure of determining the temperatures of fusion is shown in the following figure (Figure 4.3) for the pure R-enantiomer and for one exemplary mixture (composition R:S = 82%:18%).

For thermograms of 4-hydroxy-2-pyrrolidone measured with a heating rate of 2, 5, and 10 ^{o}C/min, the corresponding angle which was employed to every peak was $\beta = 5.2^{o}$, 6.7^{o} and 7.2^{o}, respectively.

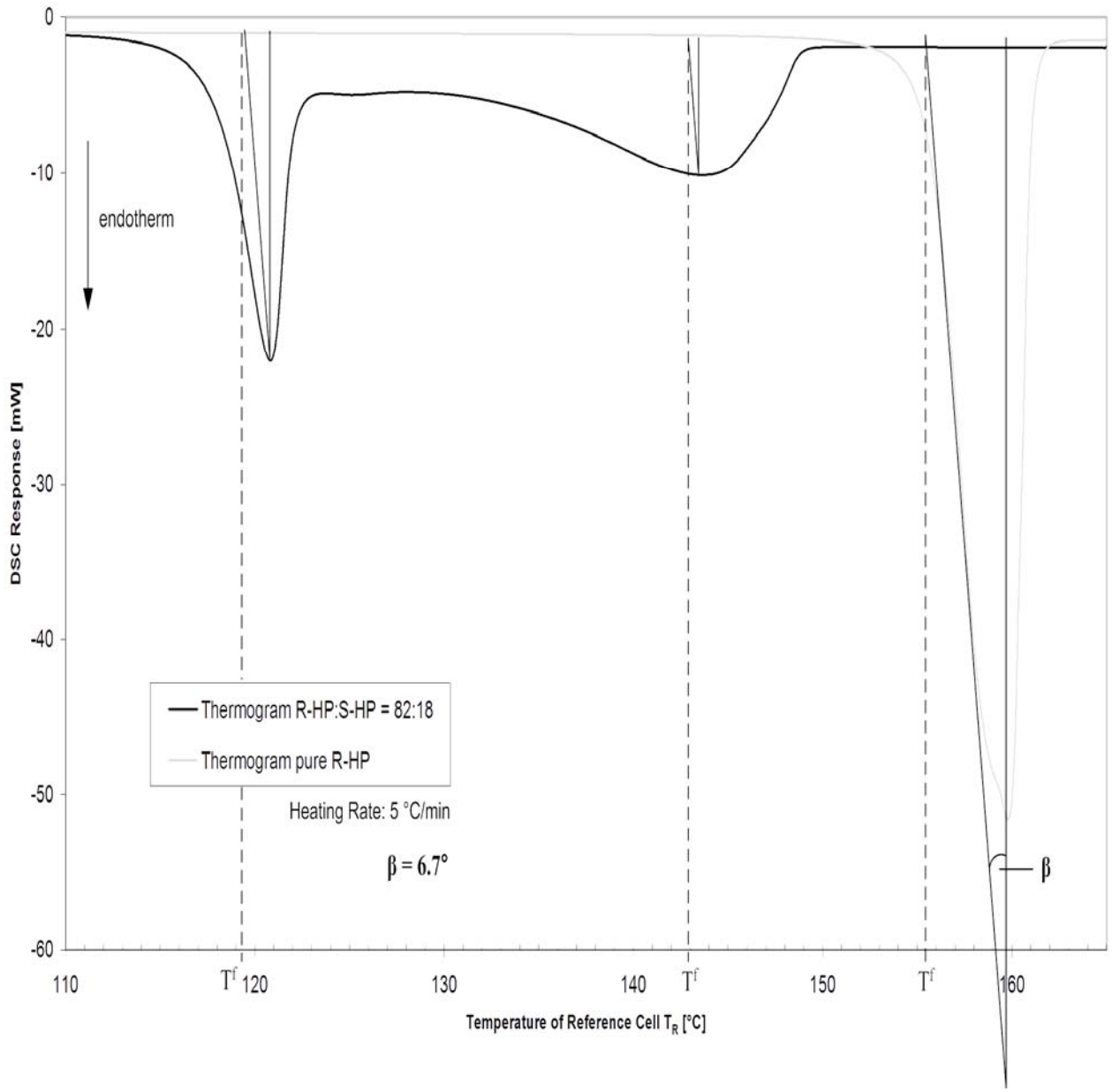

Figure 4.3 Determination of temperatures of fusion (T^f) for 4-hydroxy-2-pyrrolidone

In the case of 4-hydroxy-2-pyrrolidone, the peaks in the thermogram were well separated and easy to evaluate. According to the above evaluation method, the temperatures of fusion of different compositions were obtained, which are given in Table 4.1. Based on the determined temperatures of fusion, the binary melting point phase

diagram of (R)- and (S)-4-hydroxy-2-pyrrolidone is given in Figure 4.5. For consecutive runs and for heating rates of 2 and 5 ^{o}C/min, the data are consistent. For heating rate of 10 ^{o}C/min, the data are also close to the above values. Therefore, in Figure 4.4, only the data for the heating rate of 5 ^{o}C/min are shown.

From the binary phase diagram of 4-hydroxy-2-pyrrolidone, we can find its eutectic composition is the racemic composition (R:S = 50%:50%). This indicates that (RS)-4-hydroxy-2-pyrrolidone possesses the important characteristic of a racemic conglomerate forming system.

Table 4.1. Temperature of fusion of 4-hydroxy-2-pyrrolidone determined with differential scanning calorimetry (DSC)

X	T^f [^{o}C]	X	T^f [^{o}C]	X	T^f [^{o}C]	X	T^{Cal} [K]	T^{Cal} [^{o}C]
100.0	155.3	100.0	155.3	100.0	155.4	100.0	428.48	155.33
95.0	153.0	95.0	153.0	95.0	153.6	95.0	425.46	152.31
92.8	151.5	92.8	151.5	92.8	151.8	92.8	424.10	150.95
90.0	150.0	90.0	150.0	90.0	150.1	90.0	422.33	149.18
87.0	148.2	87.0	148.2	87.0	149.2	87.0	420.38	147.23
85.0	145.4	85.0	145.4	85.0	145.7	85.0	419.06	145.91
82.0	142.8	82.0	142.8	82.0	143.3	82.0	417.03	143.88
80.0	142.0	80.0	142.0	80.0	142.4	80.0	415.65	142.50
75.9	139.5	75.9	139.5	75.9	140.1	75.9	412.74	139.59
75.0	138.0	75.0	138.0	75.0	138.7	75.0	412.08	138.93
70.0	134.6	70.0	134.6	70.0	134.8	70.0	408.34	135.19
68.5	134.0	68.5	134.0	68.5	133.8	68.5	407.17	134.02
65.0	130.0	65.0	130.0	65.0	130.5	65.0	404.39	131.24
60.0	126.3	60.0	126.3	60.0	126.9	60.0	400.20	127.05
59.2	125.0	59.2	125.0	59.2	126.2	59.2	399.51	126.36
55.0	120.0	55.0	120.0	55.0	121.8	55.0	395.76	122.61
50.0	117.0	50.0	117.0	50.0	118.8	50.0	390.10	117.84
Heating Rate = 2 ^{o}C/min		Heating Rate = 5 ^{o}C/min		Heating Rate = 10 ^{o}C/min			Simplified Schröder-Van Laar Eq	

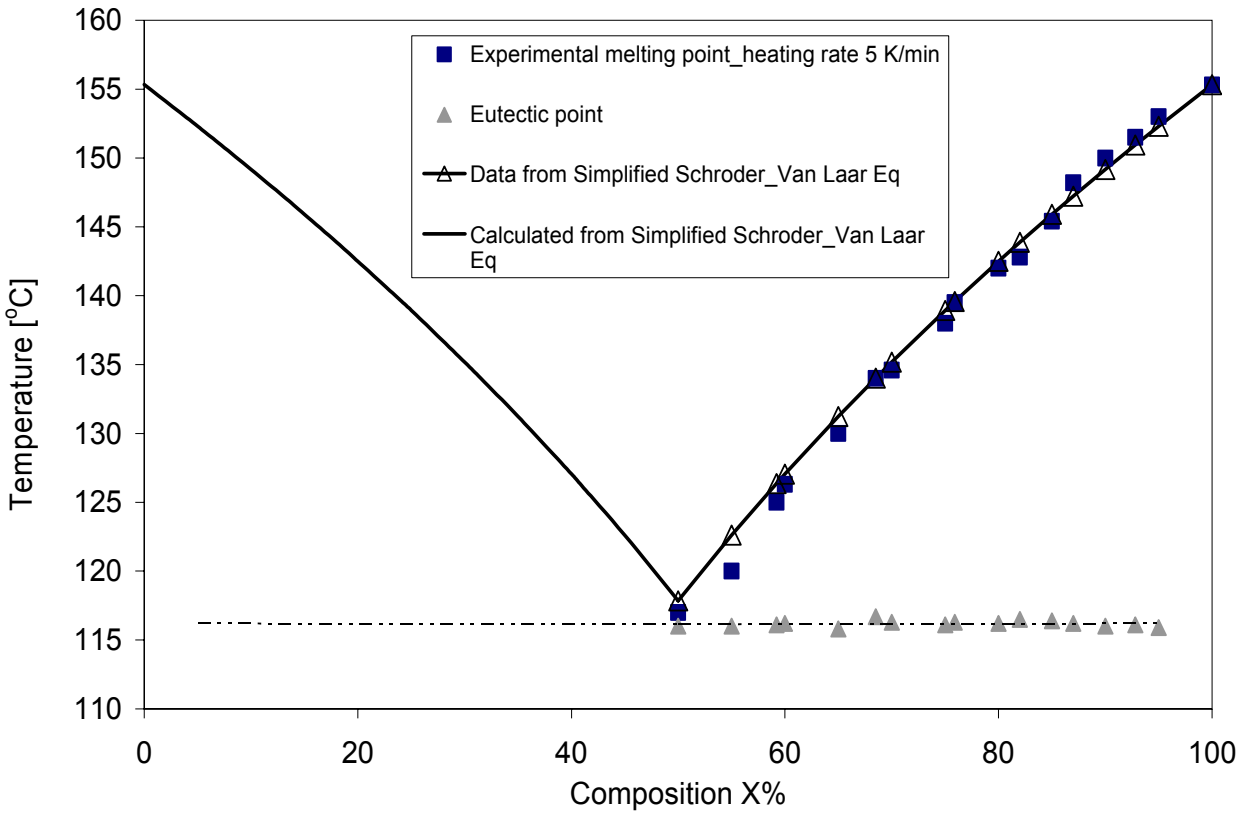

Figure 4.4 Binary phase diagram (melting point diagram) of 4-hydroxy-2-pyrrolidone: ■, Experimental data: heating rate 5 °C/min; ▲, Eutectic temperature; Δ, Calculated data from Simplified Schröder-Van Laar Equation; ─, Curve from Simplified Schröder-Van Laar Equation.

The enthalpies of fusion of the pure (R)- and (RS)-4-hydroxy-2pyrrolidone were determined by integrating the melting peaks with the DSC software. The enthalpies of fusion and the temperatures of fusion of the pure (R)- and (RS)-4-hydroxy-2-pyrrolidone are listed in Table 4.2.

Based on the above data, the corresponding temperatures of fusion for the different compositions were also calculated using the simplified Schröder-Van Laar Equation (Eq. 4.1).

$$\ln x = \frac{25217}{8.314}\left(\frac{1}{428.45} - \frac{1}{T^f}\right) \tag{4.1}$$

As indicated in Table 4.1 and Figure 4.4, the experimental results are in substantial agreement with the theoretically calculated values.

Besides construction and prediction of the binary phase diagram from the DSC measurements, the changes in the thermodynamic quantities (such as enthalpies and entropies) were also calculated using the thermodynamic approach. The thermodynamic cycle was applied to a recemic conglomerate system as follows (Jacques et al., 1994):

$$D_s + L_s \xrightarrow{\Delta H_A^f} D_l + L_l \xrightarrow{\Delta H_l^m} DL_l \qquad (\text{at } T_A^f)$$

$$C^s(T_A^f - T_R^f) \uparrow \qquad\qquad \downarrow C^l(T_R^f - T_A^f)$$

$$D_s + L_s \xleftarrow[-\Delta H_s^m]{} DL_s \xleftarrow[-\Delta H_R^f]{} DL_l \qquad (\text{at } T_R^f)$$

Figure 4.5 Thermodynamic cycle for calculation of enthalpies for a racemic conglomerate system

In this cycle, *D* and *L* represent the pure enantiomers, and *DL* represents the racemic mixture. C^s and C^l represent the heat capacities of the solids and liquids,

respectively. T_A^f and T_R^f represent the fusion points of the pure enantiomer and the racemic mixture, respectively. ΔH_A^f and ΔH_R^f represent the enthalpies of fusion of the pure enantiomer and the racemic mixture, respectively. ΔH_l^m and ΔH_s^m represent the enthalpies of mixing of the enantiomers in the liquid and solid states, respectively.

If the enantiomers are perfectly immiscible in the solid state and if their mixture is ideal in the liquid state, then ΔH_s^m and ΔH_l^m equal zero. We may then write

$$\Delta H_s^m = 0 = C^s (T_A^f - T_R^f) + \Delta H_A^f + C^l (T_R^f - T_A^f) - \Delta H_R^f \qquad (4.2)$$

$$\Delta H_A^f - \Delta H_R^f = (C^l - C^s)(T_A^f - T_R^f) \qquad (4.3)$$

Since $C^l > C^s$ and $T_A^f > T_R^f$, it follows that $\Delta H_A^f > \Delta H_R^f$. Typically the difference in the enthalpies of fusion of the pure enantiomer and the racemic mixture lies between (1600 and 5100) J mol^{-1} for a conglomerate forming system (Jacques et al., 1994). This is in fact what is observed in Table 4.2.

Likewise, the changes in entropy can be determined with the thermodynamic cycle shown below:

$$D_s + L_s \xrightarrow{\Delta S_A^f} D_l + L_l \xrightarrow{\Delta S_l^m} DL_l \qquad (\text{at } T_A^f)$$

$$C^s \ln\frac{T_A^f}{T_R^f} \uparrow \qquad\qquad \downarrow C^l \ln\frac{T_R^f}{T_A^f}$$

$$D_s + L_s \xleftarrow[-\Delta S_s^m]{} DL_s \xleftarrow[-\Delta S_R^f]{} DL_l \qquad (\text{at } T_R^f)$$

Figure 4.6 Thermodynamic cycle for calculation of entropies for a racemic conglomerate system

In this cycle, ΔS_A^f and ΔS_R^f represent the entropies of fusion of the pure enantiomer and the racemic mixture, respectively. ΔS_l^m and ΔS_s^m represent the entropies of mixing of the enantiomers in the liquid and solid states, respectively. For a conglomerate, DL_s exists in the form of two separate phases, D_s and L_s, which are present as a mechanical mixture. Consequently, ΔS_s^m=0 and $\Delta S_l^m = R\ln 2 = 5.77 J\ mol^{-1}\ K^{-1}$ if the system behaves ideally. We may then write

$$\Delta S_s^m = 0 = C^s \ln\frac{T_A^f}{T_R^f} + \Delta S_A^f + \Delta S_l^m + C^l \ln\frac{T_R^f}{T_A^f} - \Delta S_R^f \tag{4.4}$$

$$-\Delta S_l^m = \frac{\Delta H_A^f}{T_A^f} - \frac{\Delta H_R^f}{T_R^f} - \frac{\Delta H_A^f - \Delta H_R^f}{T_A^f - T_R^f}\ln\frac{T_A^f}{T_R^f} \tag{4.5}$$

The value of ΔS_l^m calculated with Equation (4.5) is shown in Table 4.2. It is close to the value expected from theory, which indicates that (RS)-4-hydroxy-2-pyrrolidone is a conglomerate. The agreement with the data published by Li et al. (1999) is satisfying.

Table 4.2. Melting points and enthalpies of fusion of (R)-4-hydroxy-2-pyrrolidone and (RS)-4-hydroxy-2-pyrrolidone; entropy of mixing of (R)- and (S)-4-hydroxy-2-pyrrolidone in the liquid state

T_R^f [K]	T_A^f [K]	$(T_A^f - T_R^f)$ [K]	ΔH_R^f [J mol^{-1}]	ΔH_A^f (J mol^{-1})	$(\Delta H_A^f - \Delta H_R^f)$ [J mol^{-1}]	ΔS_l^m [J mol^{-1} K^{-1}]
391.95	428.45	36.5	23413	25217	1804	5.28

4.3.1.2 Melting point phase diagram of N-methylephedrine

For N-methylephedrine, the graphic procedure of determining the melting point is shown in Figure 4.7 for the pure (+)-enantiomer and for one exemplary mixture (composition (+):(-) = 90%:10%).

For thermograms of N-methylephedrine collected with a heating rate of 5 °C/min, the correcting angle which was employed to every peak was β = 6.4 °C (HR = 2 °C/min, β = 5.1 °; HR = 10 °C/min, β = 7.3 °). Only samples with high enantiomeric excess could be evaluated. For samples closer to the racemic mixture (low ee), no clear second peak was obtained in the thermograms. As example the thermogram of a sample with lower enantiomeric excess ((+):(–)=77%:23%), for which an evaluation was not possible, is also shown in Figure 4.7.

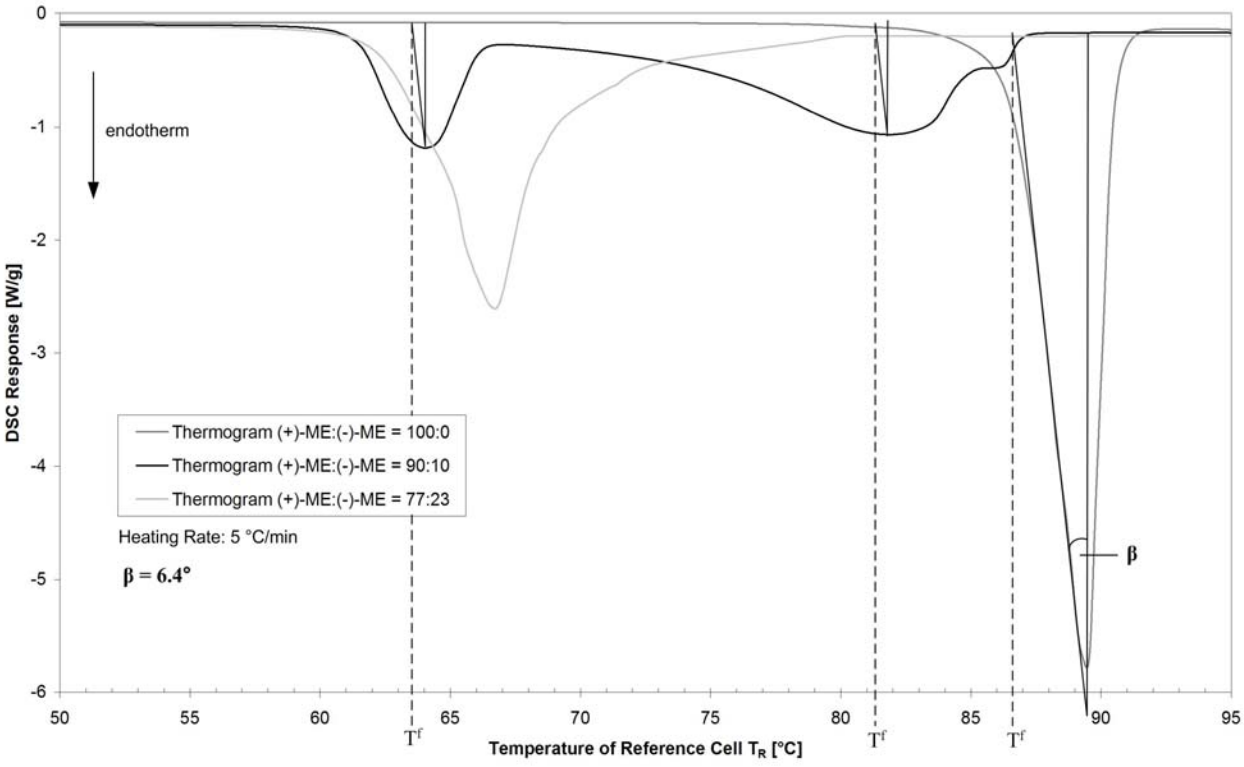

Figure 4.7 Determination of temperatures of fusion (T^f) for N-methylephedrine

It should be noted that some difficulties were encountered in preparing samples of N-methylephedrine for the DSC measurements. For N-methylephedrine, samples can be molten only once, because heating for the second or third time, peaks representing melting of the racemic mixture were observed at temperatures approximately 5 °C lower than those upon the first melting. The endothermic peaks were accompanied by preceding exothermic peaks. This behaviour was only observed for the mixtures of two enantiomers. For both pure enantiomers, the reproducible peaks were obtained for repeatedly melting. Therefore decomposition due to thermal stress can be excluded for this behaviour, but no unambiguous explanation can be given. A possible explanation is the formation of a different polymorphic phase. For example a different polymorph (e.g. a racemic compound) can be obtained upon recrystallization if the crystallization is very slow for the stable phase. Then a different polymorph even when thermodynamically not stable can be formed if the rate of crystallization is faster. This phenomenon is frequently observed in crystallization and known as "law of successive reactions" or "Ostwald's rule of stages" (Jacques et al, 1994; Mullin, 2001). Sometimes the metastable polymorph can be transformed into the stable form by heating to a transition temperature. In some cases the solid-solid transformation is extremely slow and therefore the metastable form is virtually stable. The appearance of the thermograms for N-methylephedrine was akin to the cases of polymorphism in binary systems discussed by Jacques et al (1994), but no definite explanation can be given from the thermograms alone. As stated in the same monograph, it is difficult to determine polymorphism in a binary system. However, also a comparison of the IR-spectra of the once molten and recrystallized sample revealed no differences to the pure enantiomers or the racemic mixture before being molten.

Preparing samples of crystals recovered from solvent was also not applicable. The

melting point of the racemic mixture was about 63 °C. Therefore drying at ambient pressure was ineffective due to the limited temperature. Attempts to dry the crystals under vacuum resulted in partially sublimation of the sample. Due to the fact that the vapour is always racemic as long as both enantiomers are present in the sample (Jacques et al, 1994), the actual sample composition is no longer known.

The mixture attained by preparing the samples with the mortar method was sufficient to evaluate the peaks obtained during the first run of the DSC program (peaks obtained from poorly mixed samples were not smooth and broader than those where good mixing was achieved). For samples with low enantiomeric excess the liquidus temperature can not be determined, because the two peaks representing melting of the racemic mixture and subsequently melting of the enantiomer in excess were overlapping too much. That is why additional to the heating rate of 5 °C/min, heating rates of 2 and 10 °C/min were applied with the aim of better separated peaks for the lower heating rate and larger peaks in the case of the higher heating rate. The desired effects were observed, but due to the drawbacks of very small peaks (lower heating rate) or even more overlapping of peaks (higher heating rate), those runs were not advantageous for evaluating the temperatures of fusion.

The second peak for N-methylephedrine was not as distinct as that for 4-hydroxy-2-pyrrolidone. The reason might be the lower heat of fusion ($\Delta h_{ME}^{SL} = 164.5\, J/g$, $\Delta h_{HP}^{SL} = 249.4\, J/g$), resulting in overall smaller peaks. Furthermore a slow dissolution was observed in the solubility experiments. If this is also true for dissolution in the melt, the peaks would be more diffusive and therefore more overlapping. Probably a combination of both effects caused the poorly separated peaks in the thermogram.

In the case of N-methylephedrine, only the compositions with high enantiomeric excess can be evaluated and no consecutive runs were possible, but reproducible thermograms were obtained analysing samples of constant composition. The temperatures of fusion of different compositions and binary melting point phase diagram of (+)- and (-)-N-methylephedrine are given in Table 4.3 and Figure 4.8, respectively.

From the binary phase diagram of N-methylephedrine, we can find its eutectic composition is the racemic composition. This indicates that (±)-N-methylephedrine exhibits the dominant characteristic of a conglomerate forming system.

Similarly, using the thermodynamic cycles (Figures 4.5 and 4.6) the difference in the enthalpies of fusion for pure (+)- and (±)-N-methylephedrine as well as the entropy of mixing of the enantiomers in the liquid state was calculated and shown in Table 4.4.

The temperatures of fusion for the corresponding compositions were also calculated using the simplified Schröder-Van Laar Equation (Eq.4.6).

$$\ln x = \frac{30531}{8.314}\left(\frac{1}{359.75} - \frac{1}{T^f}\right) \qquad (4.6)$$

For sufficiently separated peaks (obtained for samples with high enantiomeric excess) the data attained are scattered around the values predicted by the simplified Schröder-Van Laar equation. The agreement of the experimentally determined liquidus line data with the theoretical values predicted by the Schröder-Van Laar equation is not so good as for 4-hydroxy-2-pyrrolidone, nevertheless no experimental point does differ more than ±2 °C from the predicted value.

Table 4.3. Temperature of fusion of N-methylephedrine determined with differential scanning calorimetry (DSC)

X%	T^f [^{o}C]	X%	T^f [^{o}C]	X%	T^f [^{o}C]	X%	T^{Cal} [K]	T^{Cal} [^{o}C]
100	86.8	100	86.6	100	87	100	357.22	84.07
87.5	82.3	91.0	81.1	84.8	78.5	90	356.07	82.92
78.6	79.4	84.2	80.7	74.4	77.4	80	352.05	78.90
50	63	83.4	78.4			70	347.60	74.45
		50	63.5			50	336.87	63.72
Heating Rate = 2 ^{o}C/min		Heating Rate = 5 ^{o}C/min		Heating Rate = 10 ^{o}C/min		Simplified Schröder-Van Laar Eq		

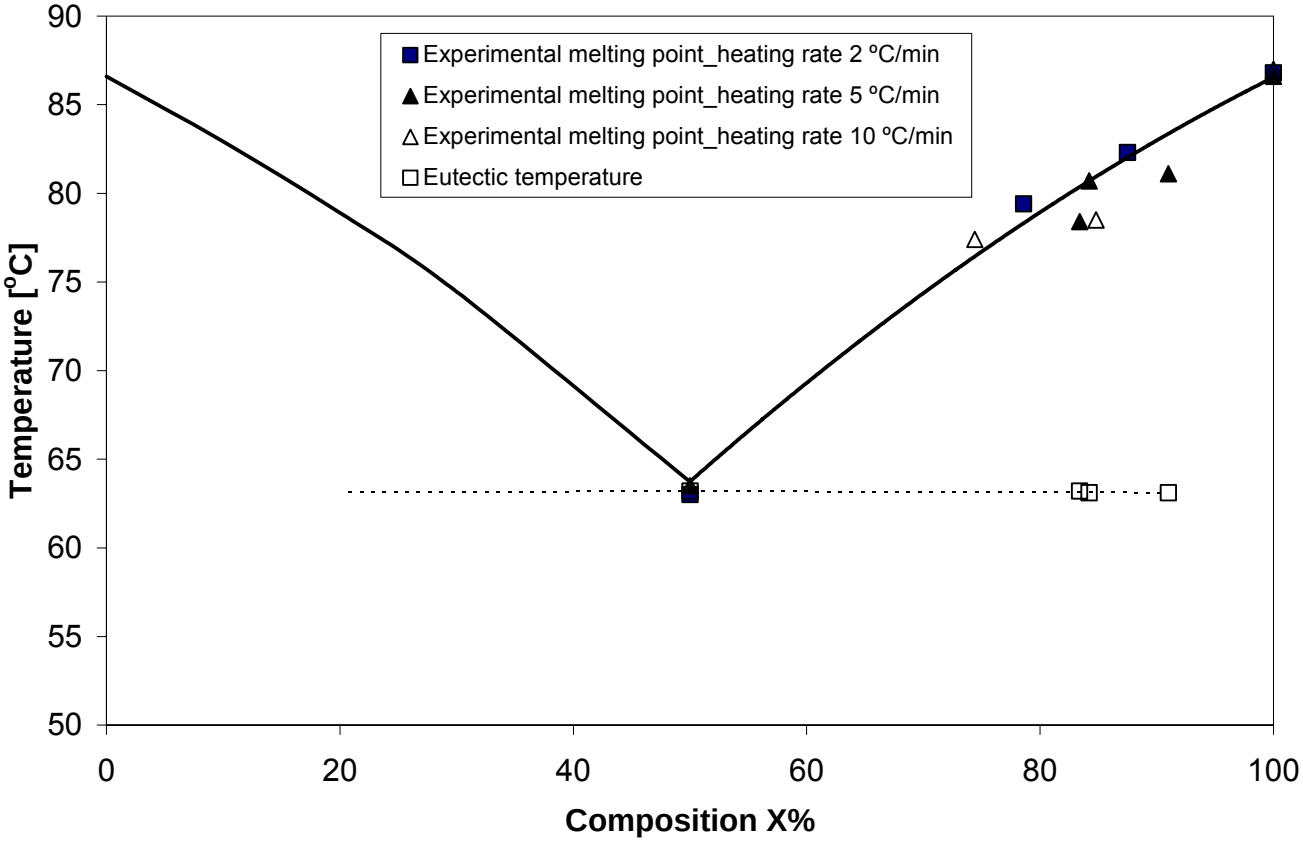

Figure 4.8 Binary phase diagram (melting point diagram) of N-methylephedrine: ■, Experimental data: heating rate 2 °C/min; ▲, Experimental data: heating rate 5 °C/min; Δ, Experimental data: heating rate 10 °C/min; □, Eutectic temperature; ▬, Curve from Simplified Schröder-Van Laar Equation.

Table 4.4. Melting points and enthalpies of fusion of (+)-N-methylephedrine and (±)-N-methylephedrine; entropy of mixing of (+)- and (-)-N-methylephedrine in the liquid state

T_R^f [K]	T_A^f [K]	$(T_A^f - T_R^f)$ [K]	ΔH_R^f [J mol^{-1}]	ΔH_A^f [J mol^{-1}]	$(\Delta H_A^f - \Delta H_R^f)$ [J mol^{-1}]	ΔS_l^m [J mol^{-1} K^{-1}]
336.65	359.75	23.10	26576	30531	3955	5.44

The values of ($\Delta H_A^f - \Delta H_R^f$) and ΔS_l^m are closed to the values expected from theory, which indicates that (±)-N-methylephedrine is a conglomerate (Li et al., 1999).

The binary phase diagram is considered to be the most important evidence for classification of racemic species. Both 4-hydroxy-2-pyrrolidone and N-methylephedrine show the typical binary phase diagram of a conglomerate forming system. In the case of N-methylephedrine, the liquidus line data for intermediate compositions can not be determined and therefore also a classification as a racemic compound came into consideration. Though, due to the distinct melting peak observed for the racemic composition, which occurs at the lowest temperature in the system, the typical binary phase diagram of a racemic compound (Figure 4.2b) may not be possible, to ensure the classification of both racemic species as racemic conglomerates, the results of three additional techniques (IR, Raman-spectroscopy and powder X-ray diffraction) would be presented in the later sections (4.3.2 – 4.3.4).

4.3.1.3 Melting point phase diagram of propranolol hydrochloride

For propranolol hydrochloride, the graphic procedure of determining the melting point is shown in Figure 4.9 for the pure (S)-enantiomer and for one exemplary mixture (composition R:S = 90%:10%).

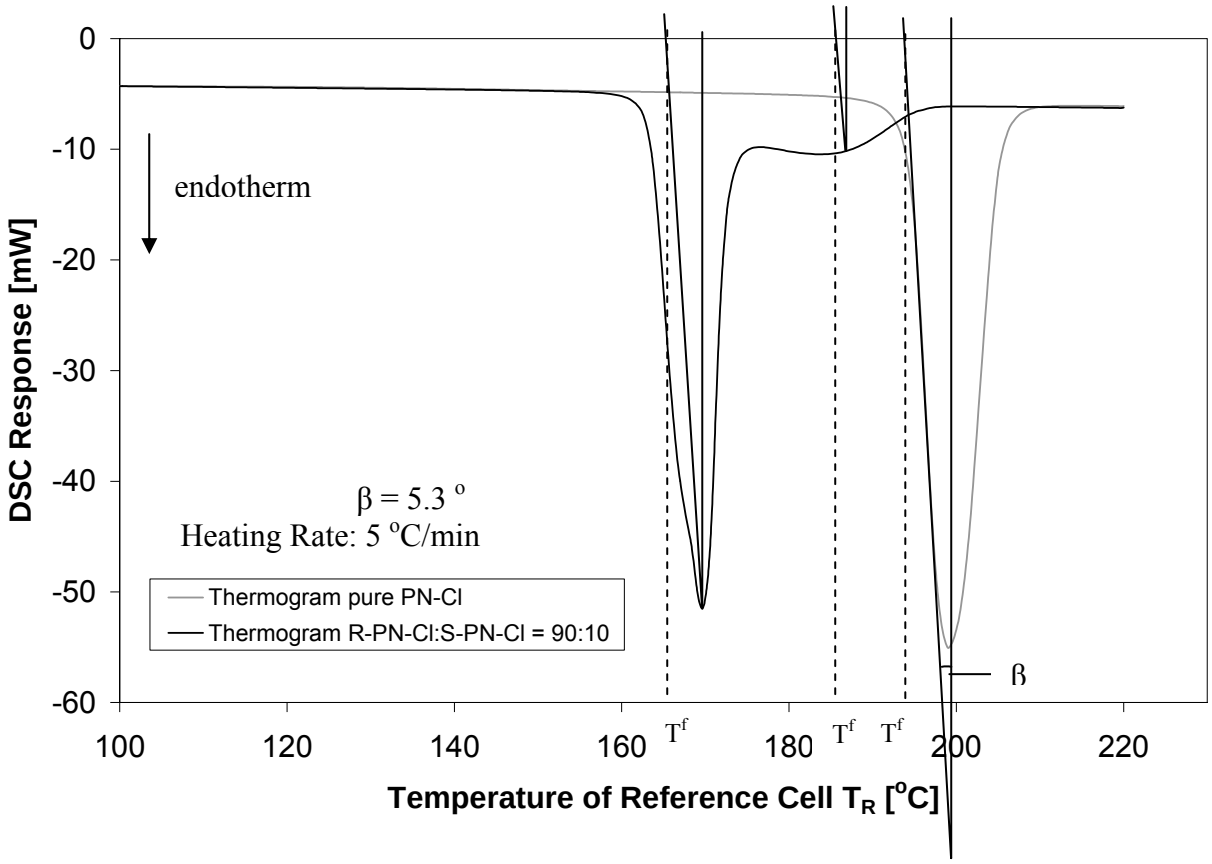

Figure 4.9 Determination of temperatures of fusion (T^f) for propranolol hydrochloride

For thermograms of propranolol hydrochloride collected with a heating rate of 5 °C/min, the correcting angle which was employed to every peak was β = 5.3 ° (HR = 2 °C/min, β = 5.3 °; HR = 10 °C/min, β = 6.1 °).

The temperatures of fusion of different compositions and binary melting point phase diagram of (R)- and (S)-propranolol hydrochloride are given in Table 4.5 and Figure 4.10, respectively.

Table 4.5. Temperature of fusion of propranolol hydrochloride determined with differential scanning calorimetry (DSC)

X%	T^f [^{o}C]	X%	T^f [^{o}C]	X%	T^f [^{o}C]
100	197.9	100	197.9	100	197.9
95	195.1	95	195.1	95	195.1
90	192.6	90	192.6	90	192.6
85	190.7	85	190.7	85	190.7
80	188.9	80	188.9	80	188.9
75	187.1	75	187.1	75	187.1
70	184.8	70	184.8	70	184.8
65	181.7	65	181.7	65	181.7
60	177.3	60	177.3	60	177.3
55	173.4	55	173.4	55	173.4
50	167.2	50	167.2	50	167.2
Heating Rate = 2 ^{o}C/min		Heating Rate = 5 ^{o}C/min		Heating Rate = 10 ^{o}C/min	

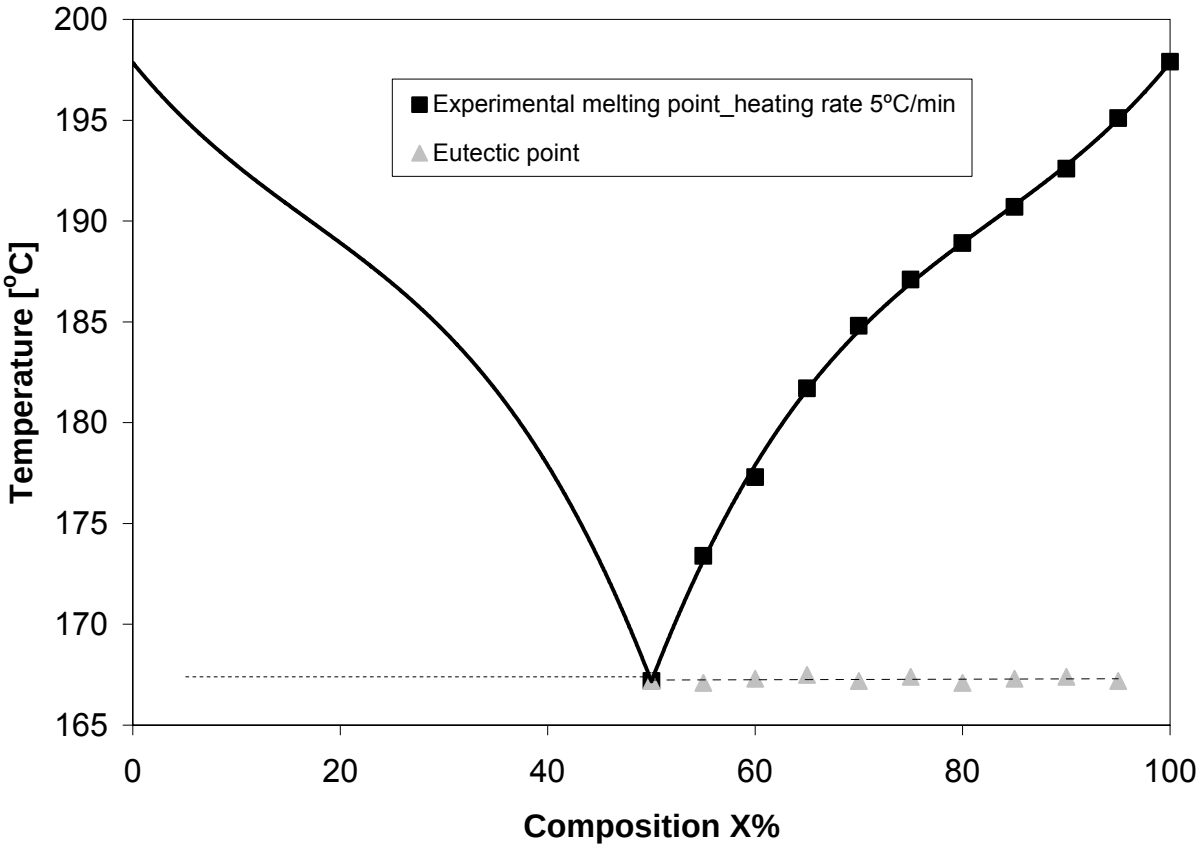

Figure 4.10 Binary phase diagram (melting point diagram) of propranolol hydrochloride: ■, Experimental data: heating rate 5 °C/min; ▲, Eutectic temperature.

From Figure 4.10, it can be seen that the eutectic composition of propranolol hydrochloride is the one of racemate. It seems to have the same characteristics as a conglomerate.

If the thermodynamic cycles (Figures 4.5 and 4.6) which are applicable for a racemic conglomerate were used to calculate and verify the characteristic of propranolol hydrochloride, the results of the difference in the enthalpies of fusion of (S)-propranolol

hydrochloride and (RS)-propranolol hydrochloride as well as the entropy of mixing of (R)- and (S)-propranolol hydrochloride in the liquid state are given in Table 4.6.

Table 4.6. Melting points and enthalpies of fusion of (S)-propranolol hydrochloride and (RS)-propranolol hydrochloride; entropy of mixing of (S)- and (R)-propranolol hydrochloride in the liquid state

T_R^f [K]	T_A^f [K]	$(T_A^f - T_R^f)$ [K]	ΔH_R^f [J mol^{-1}]	ΔH_A^f [J mol^{-1})	$(\Delta H_A^f - \Delta H_R^f)$ [J mol^{-1}]	ΔS_l^m [J mol^{-1} K^{-1}]
440.35	471.05	30.7	35271	32725	-2546	5.04

It is noticed that the value of ($\Delta H_A^f - \Delta H_R^f$) is negative. A negative value of ($\Delta H_A^f - \Delta H_R^f$) may reveal the probability of formation of a racemic compound, which is enthalpically favorable. This is consistent with the conclusion that the racemic compound has greater stabilization energy than the individual enantiomers. There were some arguments on the solid nature of propranolol hydrochloride as a racemic conglomerate or a racemic compound (Barrans and Cotrait, 1973; Ammon et al, 1977; Roberts and Rowe, 1994; Shankland and Knight, 1996; Li et al, 1999; Wang et al, 2002; Bredikhin et al, 2003, 2004). In order to get the unambiguous chiral discrimination of propranolol hydrochloride, the solid-state IR spectra, Raman spectra, Powder XRD spectra and solid-state NMR spectra of (R)- and (RS)-propranolol hydrochloride were further examined to identify the characteristic of propranolol hydrochloride in the later sections (4.3.2 - 4.3.5).

Chapter 5 will also show that the metastable zone width measurements could be used as an additional characteristic to identify racemic compound from conglomerate.

4.3.1.4 Melting point phase diagram of atenolol

For atenolol, the melting points of different compositions were measured using the DSC under different cooling rates of 2 ^{o}C/min, 5 ^{o}C/min and 10 ^{o}C/min. It was found that the melting peaks were almost superimposable for the same sample under the different cooling rates, and only one distinct peak was obtained for any prepared sample regardless composition. The thermograms (heating rate = 5 ^{o}C/min) are given in Figure 4.11.

The graphic procedure of determining the melting point of atenolol is shown in Figure 4.12 for the pure (R)-enantiomer.

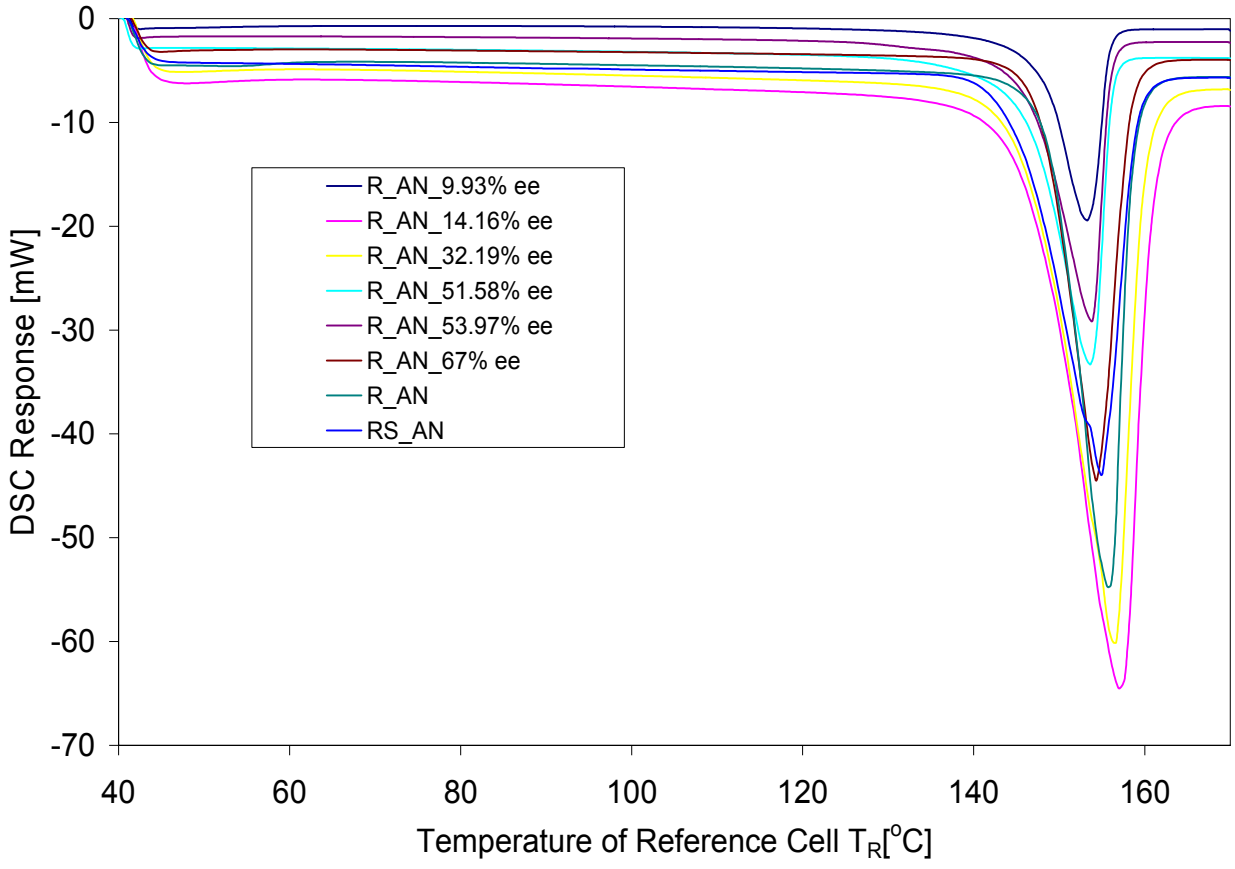

Figure 4.11 DSC thermograms of atenolol with different enantiomeric compositions

From the DSC thermograms, we can find the temperatures of the melting peaks of different compositions are approximately identical (Table 4.7 and Figure 4.13). This indicates that atenolol is an ideal pseudoracemate. This was also observed in Burger et al's work (Burger et al, 1999),while a very small difference (3 ^{o}C) was reported elsewhere (Li et al., 1999).

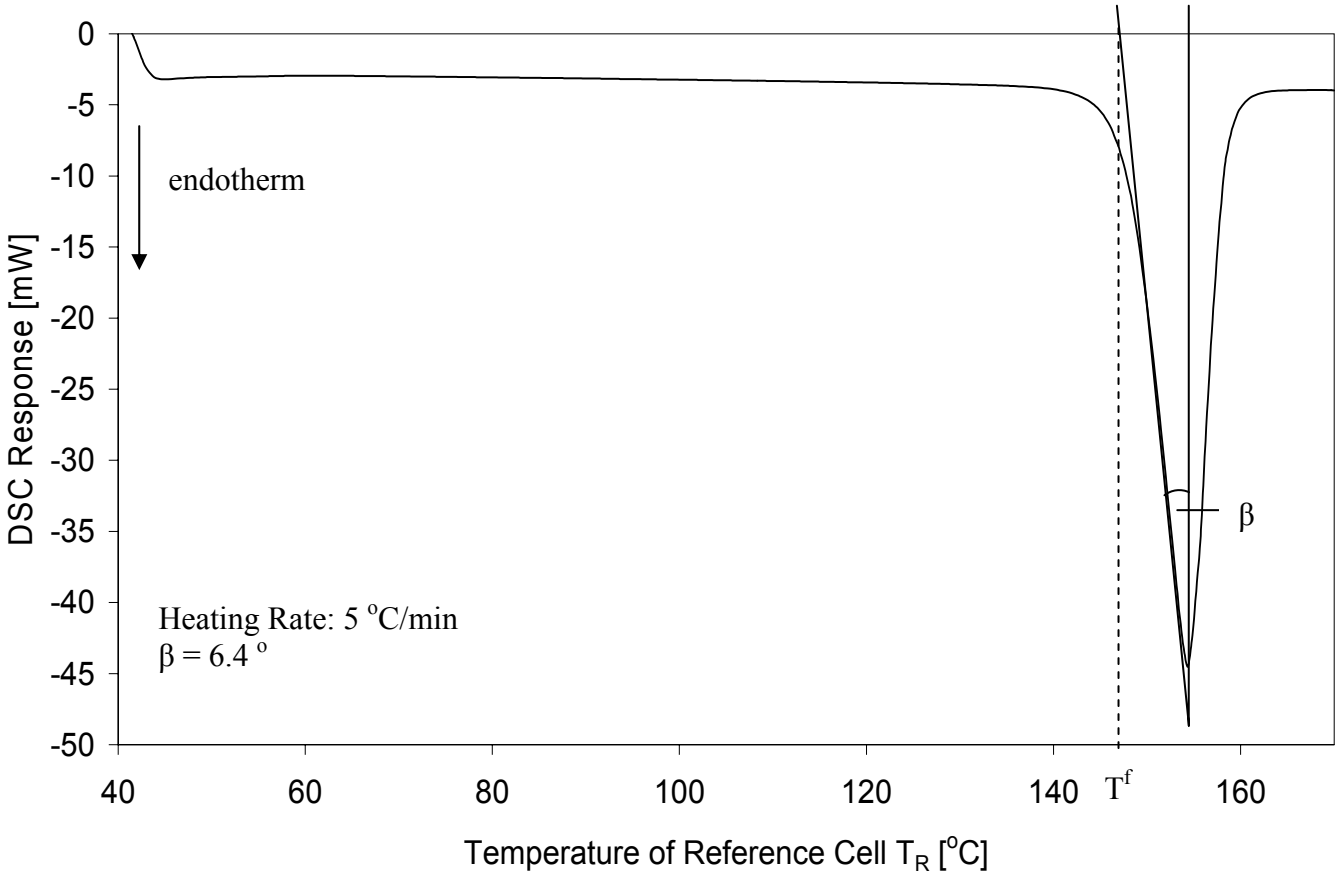

Figure 4.12 Determination of temperatures of fusion (T^f) for atenolol

Table 4.7. Temperature of fusion of atenolol determined with differential scanning calorimetry (DSC)

X%	T^f [^{o}C]	X%	T^f [^{o}C]	X%	T^f [^{o}C]
100	148.0	100	148.0	100	148.0
83.50	148.0	83.50	148.0	83.50	148.0
76.99	148.0	76.99	148.0	76.99	148.0
75.79	147.8	75.79	147.8	75.79	147.8
66.10	148.2	66.10	148.2	66.10	148.2
57.08	148.3	57.08	148.3	57.08	148.3
54.97	148.0	54.97	148.0	54.97	148.0
50	148.0	50	148.0	50	148.0
Heating Rate = 2 ^{o}C/min		Heating Rate = 5 ^{o}C/min		Heating Rate = 10 ^{o}C/min	

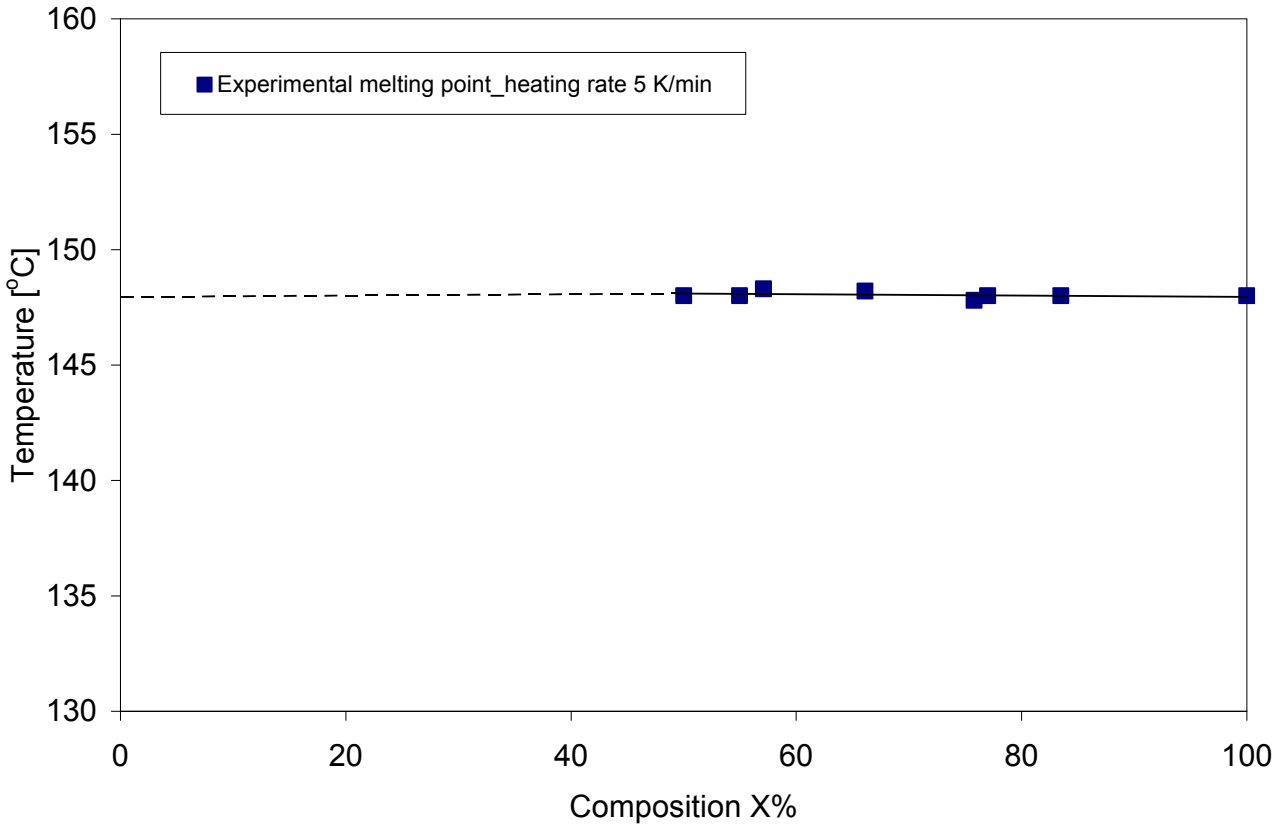

Figure 4.13 Binary phase diagram (melting point diagram) of atenolol: ■, Experimental data: heating rate 5 °C/min.

The results of difference in the enthalpies of fusion of (R)- and (RS)-atenolol as well as the entropy of mixing of (R)- and (S)-atenolol in the liquid state are given in Table 4.8. The negative value of ΔS_l^m also indicates the evident difference from a racemic conglomerate or racemic compound.

Table 4.8. Melting points and enthalpies of fusion of (R)-atenolol and (RS)-atenolol; entropy of mixing of (S)- and (R)-atenolol in the liquid state

T_R^f (K)	T_A^f (K)	$(T_A^f - T_R^f)$ (K)	ΔH_R^f (J mol^{-1})	ΔH_A^f (J mol^{-1})	$(\Delta H_A^f - \Delta H_R^f)$ (J mol^{-1})	ΔS_l^m (J mol^{-1} K^{-1})
421.15	421.15	0	34623	36533	1910	-4.54

4.3.2 Characterization by powder X-ray diffraction spectra (PXRD)

4.3.2.1 Powder X-ray diffraction spectra of 4-hydroxy-2-pyrrolidone

In Figure 4.14, the X-ray diffraction patterns of (R)- and (RS)-4-hydroxy-2-pyrrolidone are presented. For easier comparison only the region where most of the characteristic peaks appeared (glancing angles (2θ) 10 to 35°) is shown. The intensity (counts) is plotted versus the glancing angle.

All patterns were collected under the same experimental conditions and equipment settings. Only a small difference between patterns of the pure enantiomer and the racemate was observed. The most important information of the patterns is the position of the peaks (at which glancing angel does a peak occur). The peak position is the same for the pure and racemic samples, so that no difference in the crystal lattice could be revealed leading to the conclusion that all samples contained crystals constituted from one enantiomer only.

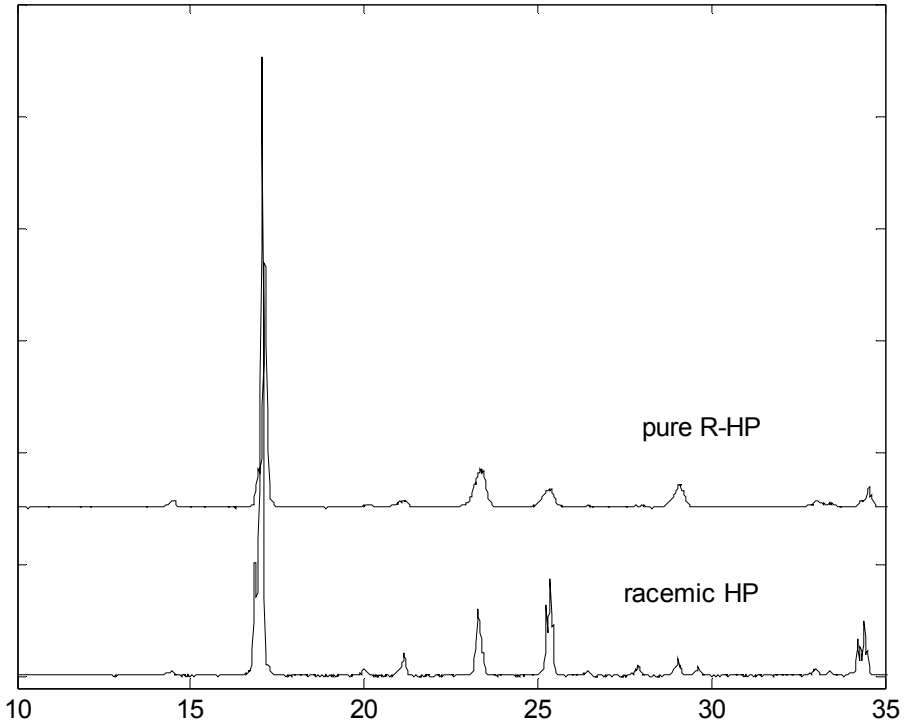

Figure 4.14 Powder X-ray diffraction patterns of (R) and (RS)-4-hydroxy-2-pyrrolidone (glancing angles $2\theta = 10 - 35^{o}$)

4.3.2.2 Powder X-ray diffraction spectra of N-methylephedrine

The PXRD patterns of pure enantiomer and racemic mixture of N-methylephedrine are shown in Figure 4.15. The peak positions in the recorded PXRD patterns are almost the same for the racemic mixture and the pure enantiomer. The difference in peak intensity may be from the preferred orientation (Li et al., 1999).

This would be the case if the two separate enantiomers are present as a mechanical mixture, which confirms that (±)-N-methylephedrine is a racemic conglomerate.

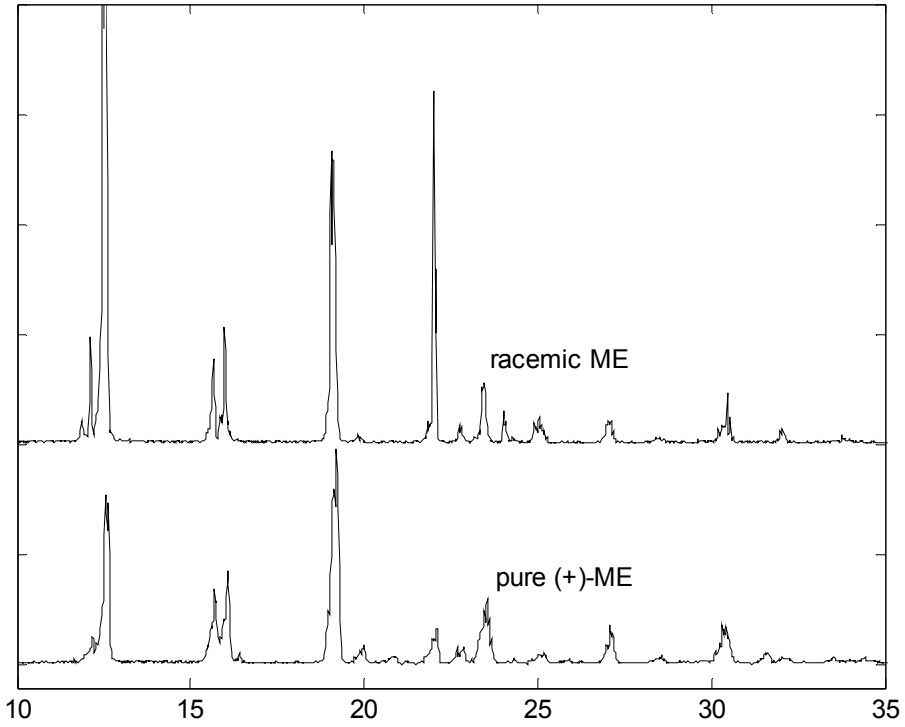

Figure 4.15 Powder X-ray diffraction patterns of (+) and (±)-N-methylephedrine (glancing angles $2\theta = 10 - 35^{o}$)

4.3.2.3 Powder X-ray diffraction spectra of propranolol hydrochloride

The PXRD patterns of pure enantiomer and racemic mixture of propranolol hydrochloride are shown in Figure 4.16. The PXRD patterns show that most of the peak positions and intensities differ significantly between (S)- and (RS)-propranolol hydrochloride which means different crystal lattice structures. It may indicate that the racemic mixture of propranolol hydrochloride is a racemic compound.

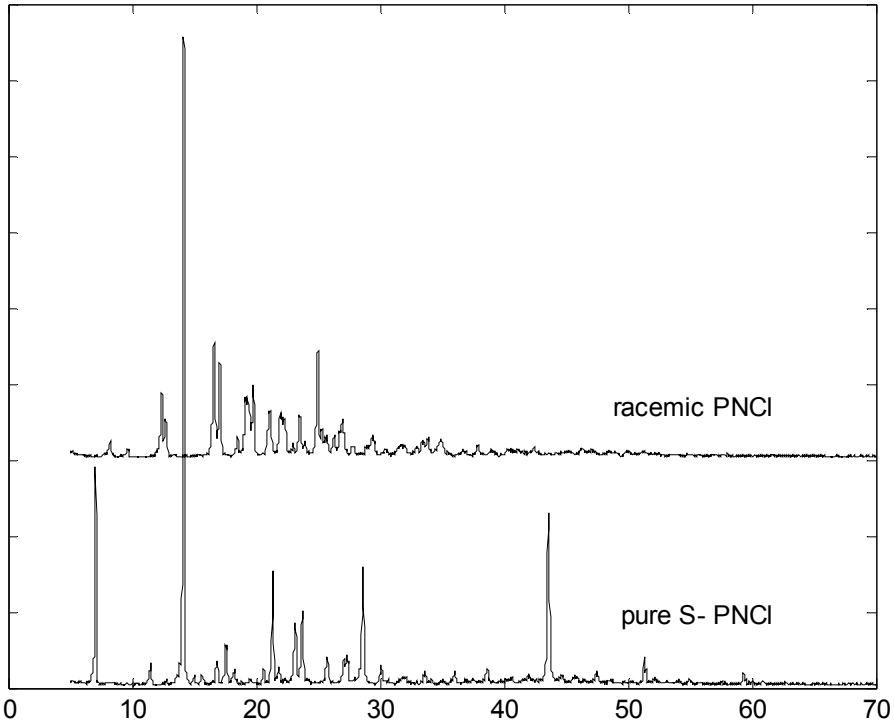

Figure 4.16 Powder X-ray diffraction patterns of (S) and (RS)-propranolol hydrochloride (glancing angles $2\theta = 5 - 70^{o}$)

4.3.3 Characterization by solid state fourier transform infrared spectra (FT-IR)

4.3.3.1 FT-IR spectra of 4-hydroxy-2-pyrrolidone

The solid state FT-IR spectra of (R)- and (RS)-4-hydroxy-2-pyrrolidone are shown in Figure 4.17. As common practice in FT-IR spectroscopy, the spectra are plotted as transmittance versus wavenumber.

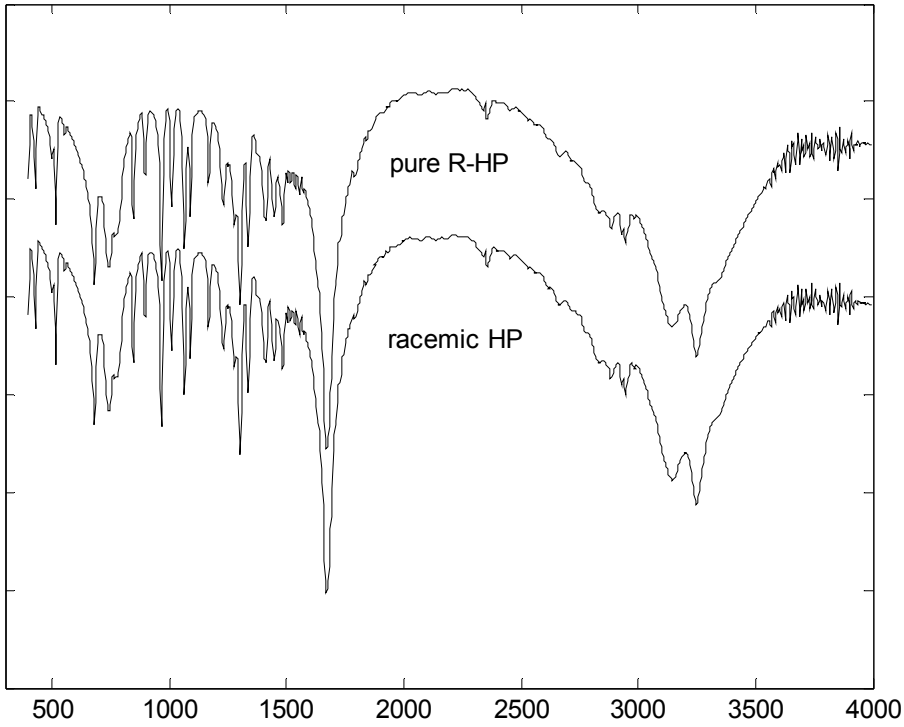

Figure 4.17 FT-IR spectra of (R)- and (RS)-4-hydroxy-2-pyrrolidone

All spectra were collected under the same experimental conditions and equipment settings. Two factors varying from run to run were affecting the appearance of the spectra: the thickness of the analysed pellet and the concentration of the studied substance in the potassium bromide carrier. That is why the absolute transmittance was not the same for each sample, but more important than the absolute transmittance is the position of the peaks along the abscissas (at which wavenumber radiation is absorbed) and their relative amplitude (intensity of absorption).

Comparing the different spectra, the position and the relative peak intensity are almost the same for pure enantiomer and racemic mixture, which lead to the conclusion

that all samples contained crystals constituted from one enantiomer only. The FT-IR spectra reveal no hints for the formation of a racemic compound.

4.3.3.2 FT-IR spectra of N-methylephedrine

The solid state FT-IR spectra of (+)- and (±)-N-Methylephedrine are shown in Figures 4.18.

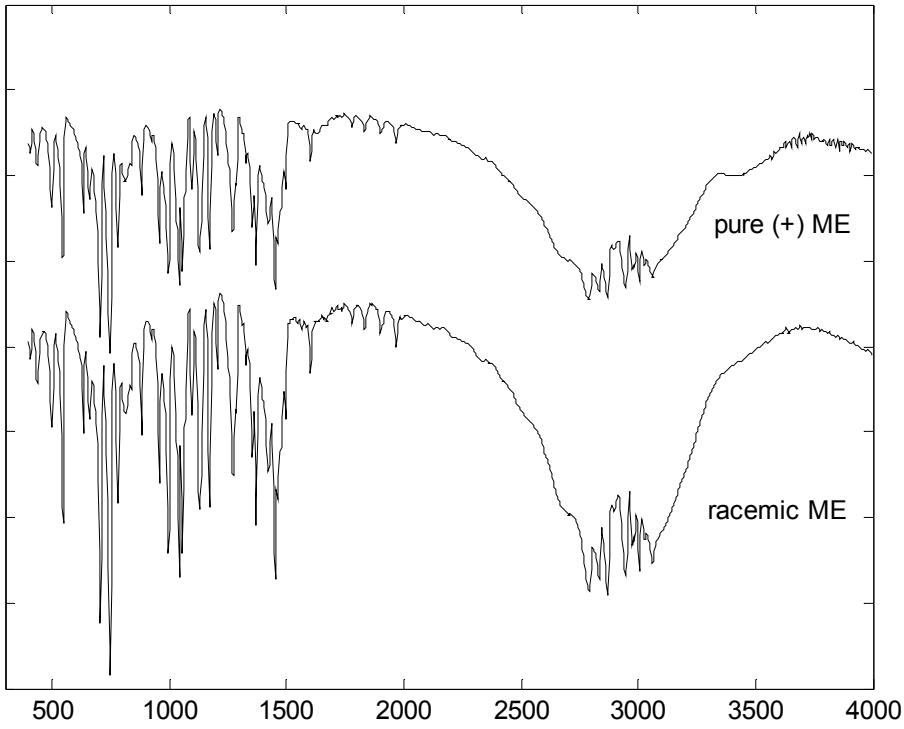

Figure 4.18 FT-IR spectra of (+) and (±)-N-methylephedrine

Again, comparing the different spectra, the positions and the relative peak intensities are almost the same for pure enantiomer and racemic mixture, which lead to the conclusion that all samples contained crystals constituted from one enantiomer only. The FT-IR spectra reveal no hints for the formation of a racemic compound.

4.3.3.3 FT-IR spectra of propranolol hydrochloride

The solid state FT-IR spectra of (S)- and (RS)-propranolol hydrochloride are shown in Figure 4.19.

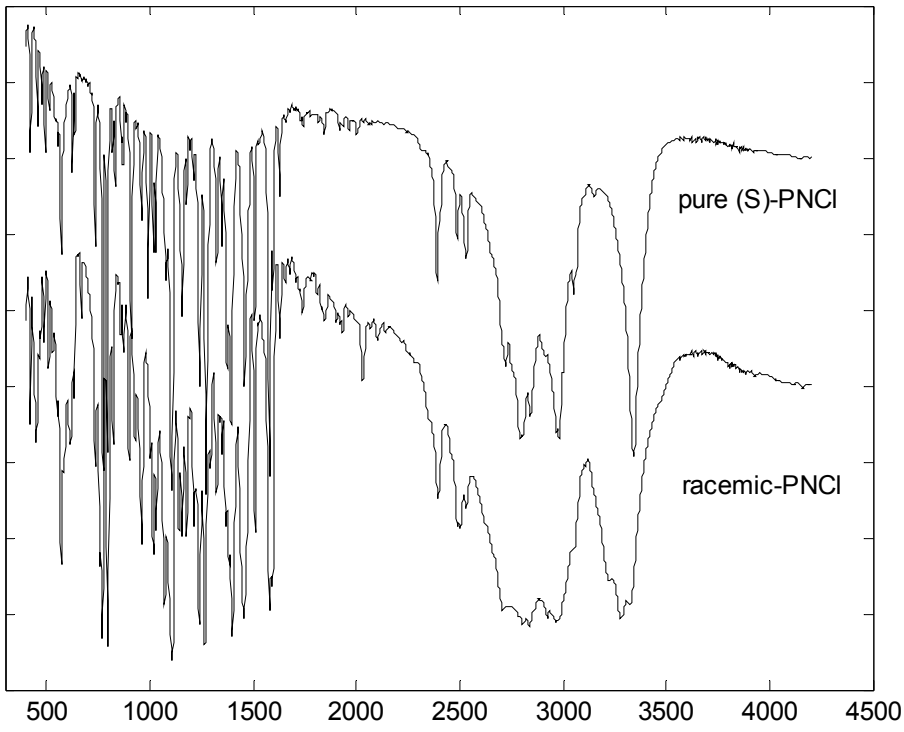

Figure 4.19 FT-IR spectra of (S) and (RS)-propranolol hydrochloride

The FT-IR spectra show that most of the peak positions and intensities in the range of 1700-3500 cm^{-1} differ obviously between (S)- and (RS)-propranolol hydrochloride. It may imply that the racemic mixture of propranolol hydrochloride is a racemic compound. This is due to the fact that the crystals of the enantiomers and of the racemic compounds possess different organizations, such as lattice symmetry and relative arrangement of the molecules. These differences will give rise to the differences in their frequencies and intensities with vibration modes (Jacques et al., 1994).

4.3.4 Characterization by solid state Raman spectra

4.3.4.1 Raman spectra of 4-hydroxy-2-pyrrolidone

The solid state Raman spectra of (R) and (RS)-4-hydroxy-2-pyrrolidone are shown in Figure 4.20.

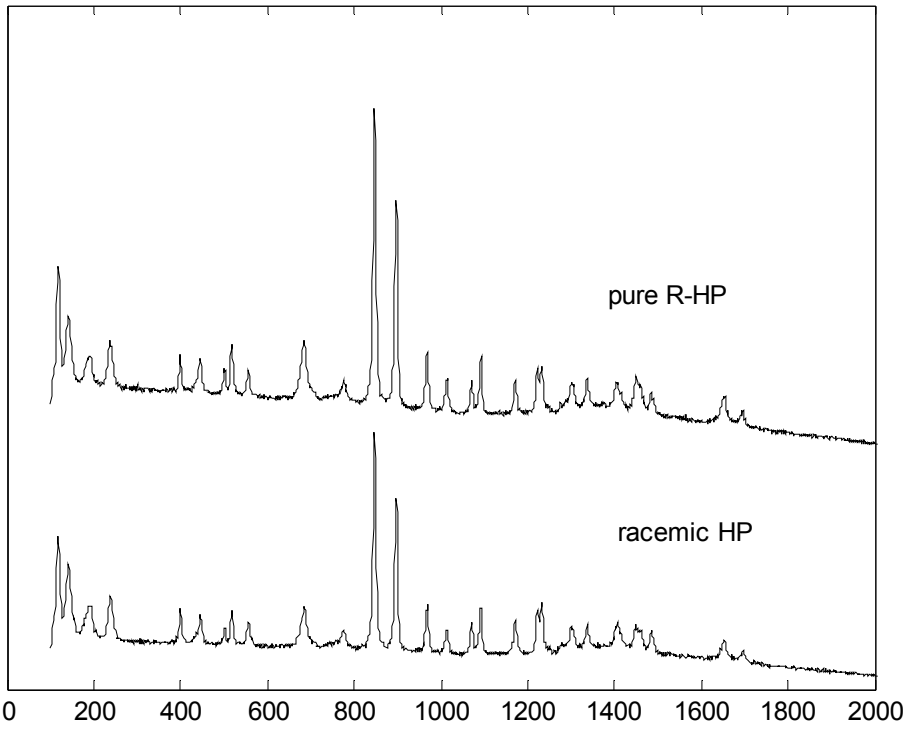

Figure 4.20 Raman spectra of (R) and (RS)-4-hydroxy-2-pyrrolidone

Comparing the different spectra, the positions and the relative peak intensities are almost same for the pure enantiomer and racemic mixture, which is again consistent with the conclusion that all samples contained crystals constituted from one enantiomer only. The Raman spectra confirm the formation of a racemic conglomerate for 4-hydroxy-2-pyrrolidone.

4.3.4.2 Raman spectra of N-methylephedrine

The solid state Raman spectra of (+) and (±)-N-methylephedrine are shown in Figure 4.21.

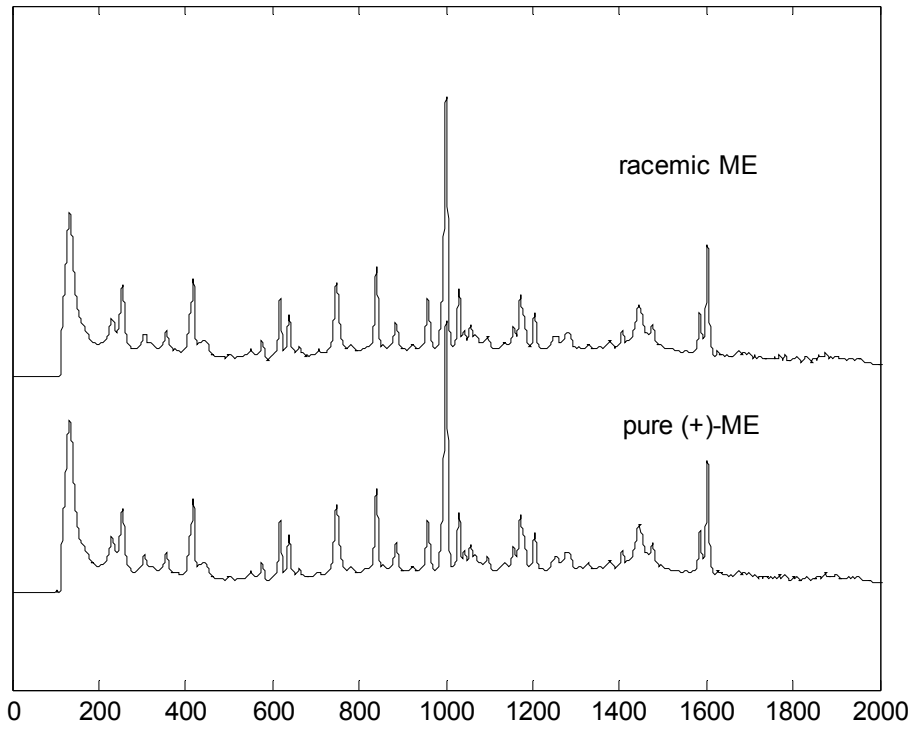

Figure 4.21 Raman spectra of (+) and (±)-N-methylephedrine

From the Raman spectra, it can be seen the positions and the relative peak intensities are almost same for the pure enantiomer and racemic mixture. It also indicates that all samples contained crystals constituted from one enantiomer only. The Raman spectra confirm the formation of a racemic conglomerate for N-methylephedrine.

4.3.4.3 Raman spectra of propranolol hydrochloride

The solid state Raman spectra of (S) and (RS)-propranolol hydrochloride are shown in Figure 4.22.

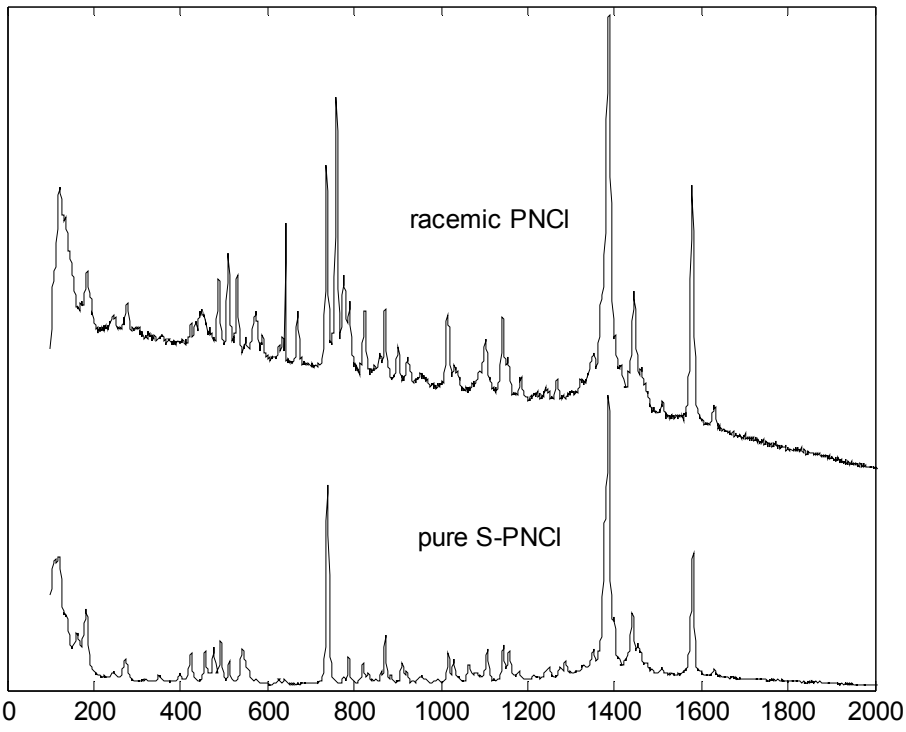

Figure 4.22 Raman spectra of (S)- and (RS)-propranolol hydrochloride

The Raman spectra show that most of the peak positions and intensities in the range of 400-1200 cm^{-1} differ significantly between (S)- and (RS)-propranolol hydrochloride. This is consistent with the IR observations. It indicates that the racemic mixture of propranolol hydrochloride is a racemic compound.

4.3.5 Characterization by solid state nuclear magnetic resonance (NMR)

In order to obtain an unambiguous characterization of racemic species for propranolol hydrochloride, which is a more complex case, the solid state NMR spectra of (S)- and (RS)-propranolol hydrochloride were also examined, as shown in Figure 4.23.

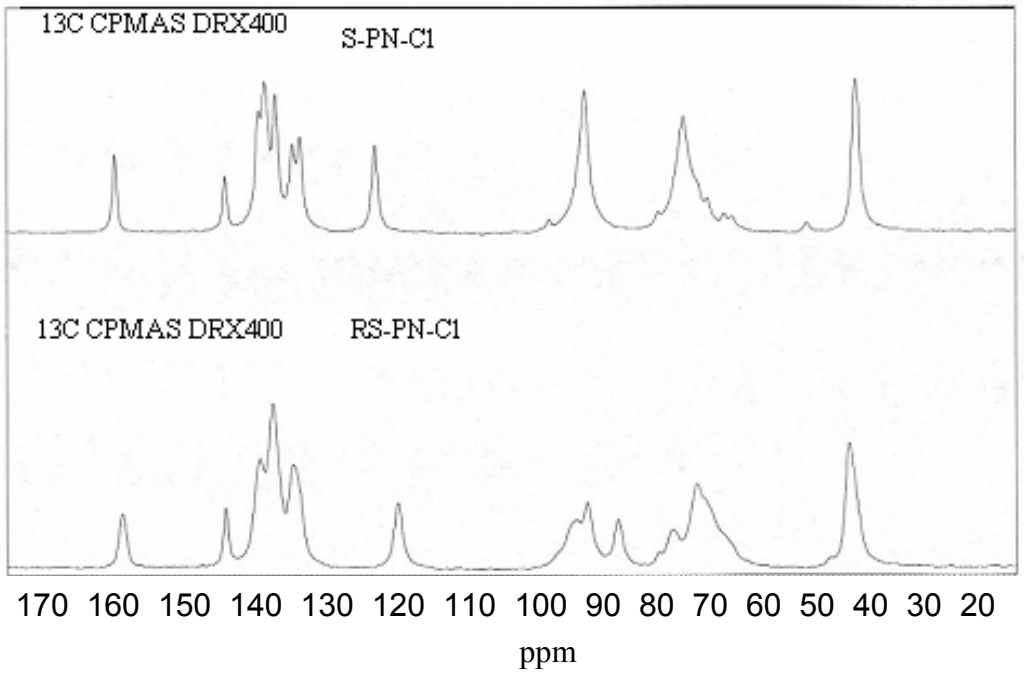

Figure 4.23 ^{13}C Solid state NMR spectra of (S)- and (RS)-propranolol hydrochloride

The solid state NMR spectra also differ significantly between (S)- and (RS)-propranolol hydrochloride. Like the PXRD, the ^{13}C chemical shifts for the pure enantiomer and the racemic mixture are quite different, which means the asymmetric unit contains two molecules with different molecule conformations which are crystallographically nonequivalent (Maciel et al., 1988). This again confirms that the racemic mixture of propranolol hydrochloride is a racemic compound.

4.4 Summary

Four racemic species, namely 4-hydroxy-2pyrrolidone, N-methylephedrine, propranolol hydrochloride and atenolol were characterized with thermal analysis, thermodynamic calculation and various spectroscopic techniques.

From the melting point phase diagrams, 4-hydroxy-2pyrrolidone and N-methylephedrine can be classified as racemic conglomerate forming systems with a eutectic composition of a racemic mixture (R:S =50%:50%). Based on the thermodynamic quantities calculated from thermodynamic cycles, the positive values of the difference in the enthalpies of fusion of pure-enantiomer and racemic mixture lie between 1600 and 5100 J mol^{-1}; the values of entropies of mixing of the enantiomers in the liquid states are close to Rln2. This is consistent with a typical conglomerate forming system. The close match of the FTIR, Raman spectra and the PXRD patterns of pure-enantiomer and of its corresponding racemic mixture further confirms that 4-hydroxy-2-pyrrolidone and N-methylephedrine are racemic conglomerates.

In the case of propranolol hydrochloride, although the characteristic of the melting point phase diagram is similar to the one of a conglomerate forming system, the evidently negative value of the difference in the enthalpies of fusion of (S)- and (RS)-propranolol hydrochloride indicates propranolol hydrochloride is a racemic compound favoring system. The significant difference of the FT-IR, Raman spectra, PXRD patterns and NMR spectra of pure-enantiomer and of its corresponding racemate again confirms that propranolol hydrochloride is a racemic compound.

The obviously identical melting temperatures for atenolol with different compositions undoubtedly indicate that atenolol is an ideal pseudoracemate forming system.

The corresponding properties in solutions would be investigated in the following Chapters.

Part of the results in this Chapter have been reported on Journal of Chemical and Engineering Data, 48, pp.1092-1098. 2003, Chirality, 14, pp. 318-324, 2002 and Chirality, 16, pp.220-227. 2004.

CHAPTER 5 CRYSTALLIZATION THERMODYNAMICS: SOLUBILITY AND METASTABLE ZONE

5.1 Introduction

In Chapter 4, four racemates, namely 4-hydroxy-2-pyrrolidone, N-methylephedrine, propranolol hydrochloride, and atenolol were characterized into three different types of racemic species using various techniques. It was shown that the binary phase diagram allowed a first characterization of the racemic species of interest. For solution crystallization, solvent is normally needed. Hence, it is the ternary phase diagram that is essential for design and optimization of a reasonable separation process. The prerequisite for direct crystallization from solution is the knowledge of the solid-liquid equilibrium of the two enantiomers in a solvent. The introduction of a new third substance (the solvent) increases the degree of the system. Therefore the measurement and presentation of data are more complicated than those in the case of the binary phase diagram.

Crystallization process can only take place in the supersaturated phase. The rates of crystal nucleation and growth, as well as the crystal size distribution, are affected by the degree of supersaturation (Mullin, 2001). Therefore, it is required to determine the solubility (saturation limit) and supersolubility (supersaturation limit) diagram. The difference in concentration (for constant temperature) or the difference in temperature (for constant concentration) between solubility and supersolubility is called metastable zone

width (Ostwald, 1897; Ting et al., 1934; Nyvlt, 1968; Nyvlt et al., 1970; Sohnel and Nyvlt, 1975; Mullin and Jancic, 1979; Kim and Ryu, 1997).

For preferential crystallization process, it is essential to keep the freedom of supersaturation of the undesired enantiomer within its metastable zone to avoid its spontaneous nucleation (Jacques et al., 1994; Collet, 1999). More importantly, the metastable zone of the target enantiomer could be also closely related with the nucleation of the unwanted isomer (Hongo et al., 1976, 1981; Black et al., 1989; Collins et al., 1997). Therefore, to measure and interpret the metastable zone of both enantiomers in solution should be very useful in understanding the preferential crystallization process, which has been rarely reported.

The saturation curve (solubility) can be well-defined. For a given system (solute – solvent) the saturation concentration is only dependent on temperature and pressure (of which the latter can be neglected, unless very high pressure is considered). However, the limit of the metastable zone (metastable zone width) is affected considerably by a variety of process parameters including saturation temperature, rate of supersaturation generation, impurity level, mixing, and solution history etc. It is therefore important to characterize the metastable zone width under a specific set of operating conditions, which relate closely to the conditions of the final scale crystallization. There are many methods available to measure the metastable zone width. The polythermal technique is perhaps the most widely used technique for determining the metastable zone width (Nyvlt, 1968; Nyvlt et al., 1970; Sohnel and Nyvlt, 1975; Mullin and Jancic, 1979; Kim and Ryu, 1997). This methodology involves cooling a saturated solution at a fixed rate until nucleation occurs.

In practice, the value of metastable zone width strongly depends on the method of detecting the onset of nucleation and dissolution. A wide variety of measurement techniques can be applied to the detecting, such as visualization, electrozone sensing, laser scattering and optical turbidity etc. In this work, the newly developed Lasentec Focused Beam Reflectance Measurement (FBRM) (as described in Chapter 3) was used to determine the nucleation and dissolution properties of the materials. The four characterized racemates, namely 4-hydroxy-2-pyrrolidone, N-methylephedrine, propranolol hydrochloride, and atenolol, were measured to obtain their solubility and metastable zone data.

5.2 Experimental

5.2.1 Solvent selection

The selection of the suitable solvent for an effective crystallization operation is crucial. Many factors must be considered. The solute to be crystallized should be readily soluble in the solvent. It should also be easily deposited from the solution in the desired crystalline form after cooling, evaporation or salting-out with an additive. Furthermore a favorable dependency of solubility on temperature is desired if a cooling crystallization process is considered. For easy controllability of the crystallization process and low loss of solvent due to evaporation, a solvent with low vapor pressure is desired. In addition to this, the solvent should be relatively cheap and easily available, not hazardous, stable under all process conditions, and show a low viscosity etc. A mixture of two or more solvents is sometimes found to possess the best properties for a particular crystallization purpose (Nass, 1994; Mullin, 2001). This is especially important for the expensive pure

enantiomers of chiral systems. Therefore, some initial experiments were first conducted in a 25 ml jacketed glass crystallizer with magnetic stirrer to screen the potential solvents.

5.2.2 Characterizing the metastable zone width and solubility curve using Lasentec FBRM and PVM

The experimental set up (Figure 3.7) has been described in Chapter 3. Recently, crystallization practitioners have become increasingly interested in the Focused Beam Reflectance Method (FBRM), which allows on-line and in-situ measurements even in systems with high solids concentrations. The principle of the FBRM measurement is illustrated in Figure 3.6 (Barrett and Glennon, 1999; Worlitschek, 2003). The FBRM is implemented using a cylindrical probe which can easily be located within the suspension to be characterized. An infrared laser beam rotates at high velocity, propagating into the suspension through a sapphire window on the probe tip. When the beam hits a particle, it is reflected and propagated back through the probe window. This optical signal is then processed by the device electronics and the corresponding chord length s is calculated as the product of the measured crossing time Δt and the beam velocity v_b. Chord length counts are summed up in a finite number of chord length intervals (channels in the Lasentec jargon), thus yielding the chord length distribution (CLD). Several research groups have used the FBRM method and proven its reliability to determine the MSZW and monitor crystal size distributions on-line (Tadayyon and Rohani, 1998; Barrett and Glennon, 1999, 2002; Ruf et al, 2000; Heath et al, 2002; Worlitschek and Mazzotti, 2003; Barthe and Rousseau, 2006).

In this work, the metastable zone width, i.e. the difference between the properties of onset of nucleation and dissolution was determined based on the measurements

sensitive to the changes in the solid phase with FBRM. These measurements were also validated by the crystal images following nucleation and during dissolution by PVM probe.

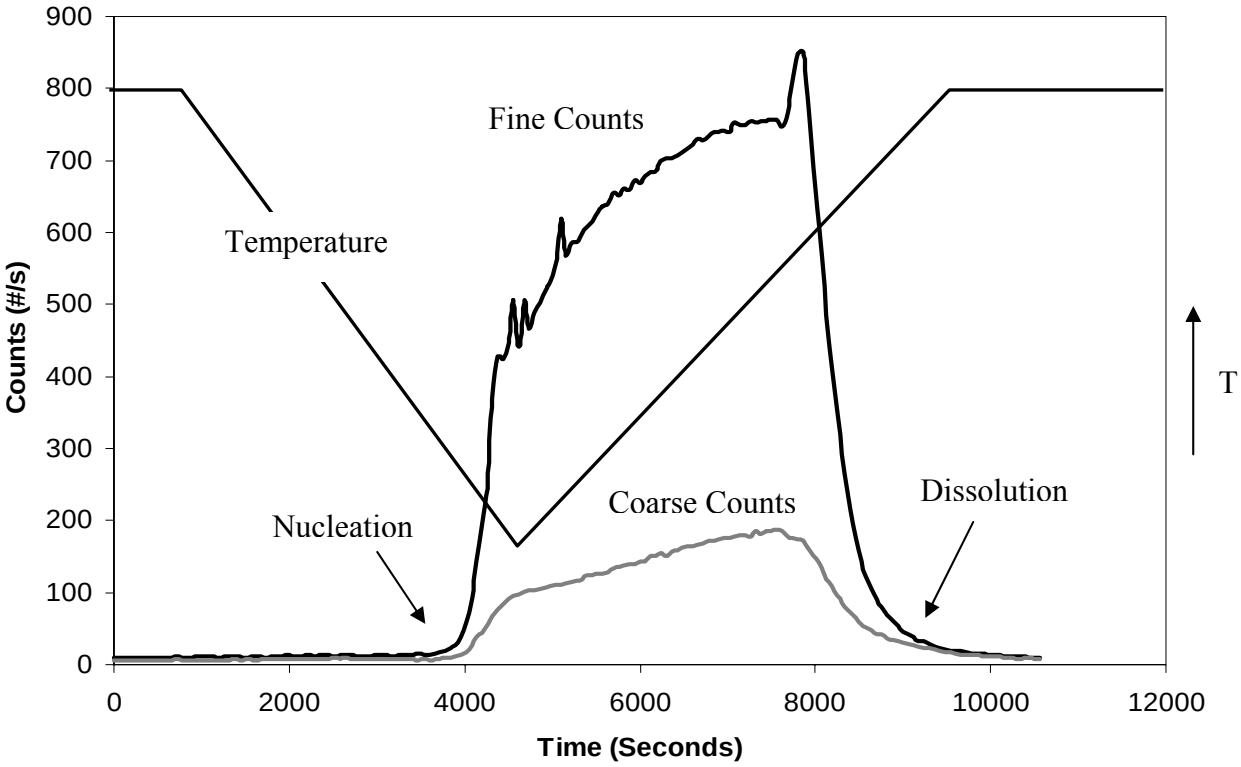

Figure 5.1 FBRM data and temperature profile for a typical batch

Figure 5.2 A typical PVM imagine when nucleation occurred

A typical procedure for measuring solubility and metastable zone data is as follows. A certain amount of sample of known enantiomeric composition was added to a certain amount of solvent in a 500 ml cylindrical jacketed glass vessel with diameter of 75mm. The solution was continuously stirred with an electronic overhead stirrer, which was equipped with a 4-bladed propeller stirrer of diameter 50 mm, at 300 rpm. The temperature of solution was controlled using a programmable Julabo FP88-HL heating/cooling circulator. Temperature data were recorded on PC via a PT-100 probe which was in the crystallizer and connected to the Julabo heating/cooling system. The onset of nucleation and dissolution was detected using FBRM probe as shown in Figure 5.1, and a typical PVM image is shown in Figure 5.2.

First, relatively fast heat up the mixture of solute and solvent until clear solution was attained, and then fast cool down the clear solution until nucleation occurred. After that, carefully heat up the suspension solution until the clear solution was attained. The temperature of the beginning of dissolution is the saturation temperature (T_{sat}). After that, further heat up the solution to 3 ^{o}C above the saturation temperature (T_{sat}) and keep for 10 mins, and then cool the solution carefully under the selected cooling rate until nucleation occurred. The temperature of the beginning of nucleation is the supersaturation temperature ($T_{supersat}$). The metastable zone width of the solution was determined under different cooling rates 1, 5 and 10 ^{o}C/h. The values of solubilities and metastable zone widths were repeated three times to check the reproducibility.

5.3 Results and discussion

5.3.1 Solubility and metastable zone width of 4-hydroxy-2-pyrrolidone in isopropanol

5.3.1.1 Solubility

For determination of solubilities and metastable zone widths of 4-hydroxy-2-pyrrolidone with different compositions with respect to the two enantiomers in isoprapanol, the well-known polythermal method was applied. The solubilities of 4-hydroxy-2-pyrrolidone with composition (R) 20% ee, 25% ee, 40% ee, 50% ee, 75% ee, pure (R)- and (RS)- in isopropanol are listed in Table 5.1 and shown in Figure 5.3, respectively.

Table 5.1. Solubility of 4-hydroxy-2-pyrrolidone in isopropanol

ee%	T [^{o}C]	C [g solute/100g IPA]
Pure R_4_HP	40.0	2.56
	35.0	2.21
	34.7	2.04
	33.2	2.04
	30.0	1.81
	27.5	1.76
	27.0	1.63
	25.0	1.53
	22.8	1.46
	20.5	1.34
	20.0	1.31
	16.4	1.16
	15.0	1.08
	10.0	1.04
	5.0	0.74
	0.0	0.73
RS_4_HP	34.5	5.13
	32.5	4.74
	30	4.28
	27	3.81
	23.5	3.39
	20	3.12
	15	2.45
	10	2.06
	5	1.48
20% ee_R_4_HP	40.0	4.55
	35.0	3.89
	31.5	3.42
	27.3	2.85
	23.0	2.44
	19.6	2.15
	15.0	1.77
	10.0	1.44
	5.0	1.19

25% ee_R_4_HP	35.0	3.78
	25.0	2.57
	20.0	2.14
	15.0	1.85
	10.0	1.68
	5.0	1.63
40% ee_R_4_HP	40.0	3.80
	35.0	3.22
	30.0	2.71
	25.0	2.29
	20.0	1.93
	15.0	1.65
	10.0	1.45
	5.0	1.18
50% ee_R_4_HP	35.0	3.18
	25.0	2.23
	20.0	1.89
	15.0	1.68
	10.0	1.56
	5.0	1.54
75% ee_R_4_HP	35.0	2.59
	25.0	1.91
	20.0	1.68
	15.0	1.45
	10.0	1.30
	5.0	1.19

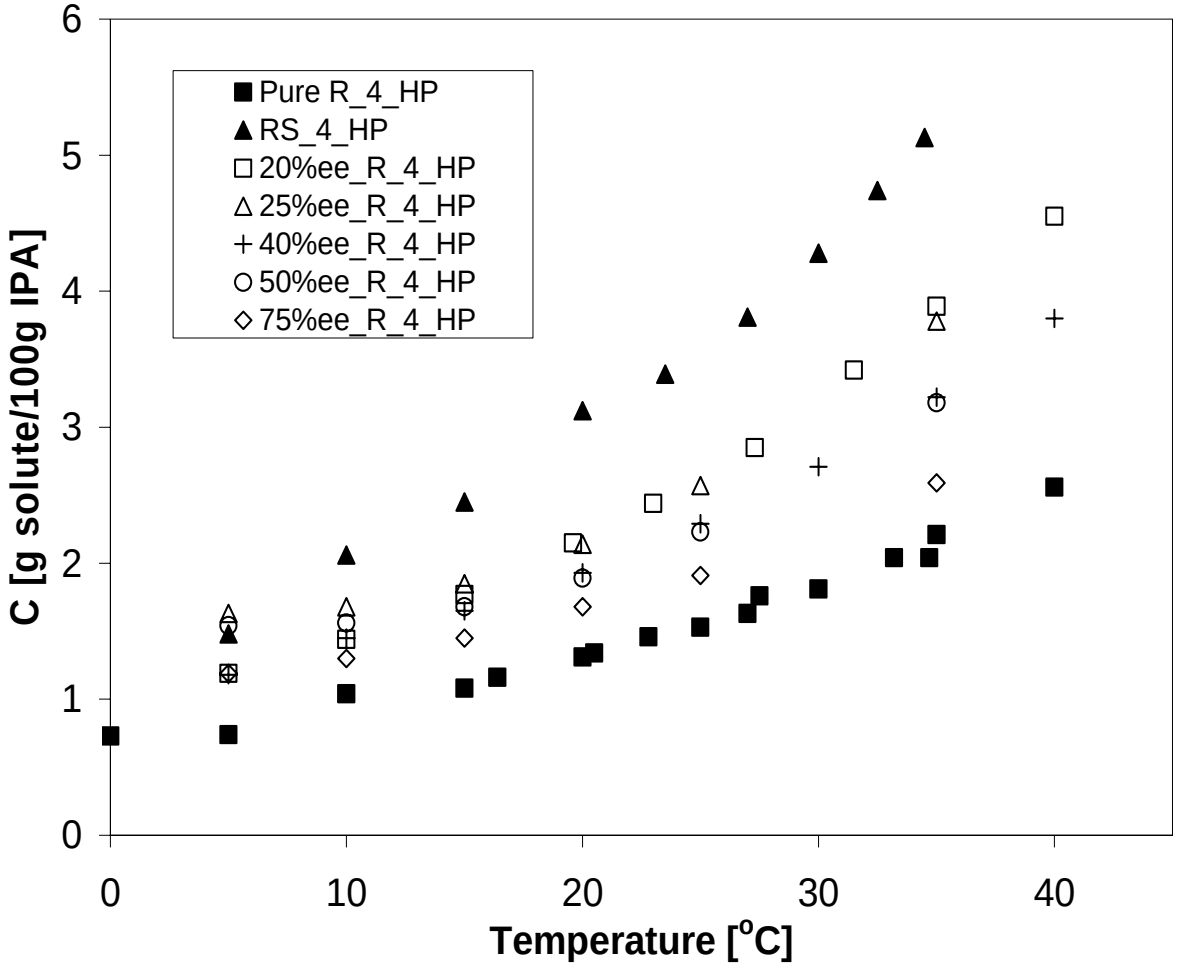

Figure 5.3 Solubility of 4-hydroxy-2-pyrrolidone with different enantiomeric excess in isopropanol

The solubility curves can be regressed to obtain the following solubility equations.

Pure R_4_HP: $C = 0.0008T^2 + 0.0139T + 0.7227$ (5.1)

RS_4_HP: $C = 0.0015T^2 + 0.0603T + 1.2167$ (5.2)

20% ee R_4_HP: $C = 0.0016T^2 + 0.0259T + 1.0201$ (5.3)

25% ee R_4_HP: $C = 0.0025T^2 - 0.0275T + 1.7016$ (5.4)

40% ee R_4_HP: $C = 0.0015T^2 + 0.0025T + 1.2751$ (5.5)

50% ee R_4_HP: $C = 0.0021T^2 - 0.0275T + 1.6271$ (5.6)

75% ee R_4_HP: $C = 0.0010T^2 + 0.0066T + 1.1320$ (5.7)

As shown in Figure 5.3, the solubilities of (R)-, (RS)-, 20% ee, 25% ee, 40% ee, 50% ee, and 75% ee (R)-4-hydroxy-2-pyrrolidone in isopropanol all properly increase with temperature over the range of 0 – 40 ^{o}C. The chosen solvent isopropanol is suitable for cooling crystallization operation.

Figure 5.3 also shows that the solubilities decrease with increased ee. This is in agreement with the general findings in conglomerate system that the racemate is more soluble than the constituent enantiomers (Jacques et al., 1994). Actually, the solubility ratio α of RS to R is circa 2.0-2.5 in the temperature range of 0 – 40 ^{o}C. This is quite close to the old empirical "double solubility" rule proposed by Meyerhofer (1904). The current system of 4-hydroxy-2-pyrrolidone in isopropanol appears to be close to ideal solution. But the dissociation/association among the dissolved molecules of the enantiomers in solution can be still observed as indicated by the ratio α of 2.5.

The range of the solubility ratio α of RS to R is more than 2, which suggests the resolution of this system is not easy to carry out by direct crystallization. It was suggested that the classical isothermal preferential crystallization process was not suitable for such kind of case (Coquerel et al., 1990). In the case of α less than 2, the degree of supersaturation of the undesired enantiomer will decrease during the crystallization and therefore it is easy to obtain pure crystals with large extent of resolution. On the contrary, when α is bigger than 2, the degree of supersaturation of the undesired enantiomer will increase during the crystallization of its isomer and spontaneous nucleation could happen.

This is the major case for most of organic compounds (Collet et al., 1980; Jacques et al., 1994).

It is also interesting to note that the solubility ratio of RS to R decreases from circa 2.5 at 35 ^{o}C to circa 2.0 at 5 ^{o}C. This suggests that the preferential crystallization of 4-hydroxy-2-pyrrolidone in the chosen solvent is more favorable as temperature decreases. As illustrated by Jacques et al. (1994), the decreased solubility ratio of RS- to R-4-hydroxy-2-pyrrolidone means that the solution tends to decreasingly destabilize during the course of the resolution process, with the consequence that the risk of spontaneous nucleation of the undesired enantiomer is slowly increased. Therefore, special attention should be paid to the supersaturation control for this case during the preferential crystallization of this conglomerate. This will be elaborated in Chapter 7.

For studies on preferential crystallization, the ternary phase diagram of the two enantiomers and solvent is helpful. The purpose of the ternary diagram is the visualization of the whole preferential crystallization process as shown in Chapter 2 (Figure 2.2). Furthermore it is especially helpful for layout of the crystallization step. More importantly, it also assists to identify the racemic species besides the binary phase diagram. Tables 5.2 – 5.9 are the solubilities of 4-hydroxy-2-pyrrolidone in isopropanol with different ee at different temperatures.

Table 5.2. Solubility of 4-hydroxy-2-pyrrolidone in isopropanol at 40 ^{o}C

	R (wt%)	S (wt%)	IPA (wt%)
100ee	2.50	0	97.50
75ee	2.55	0.36	97.09
50ee	2.52	0.84	96.64
40ee	2.56	1.10	96.34
20ee	2.61	1.74	95.65
RS (0ee)	2.85	2.85	94.30

Table 5.3. Solubility of 4-hydroxy-2-pyrrolidone in isopropanol at 35 ^{o}C

	R (wt%)	S (wt%)	IPA (wt%)
100ee	2.16	0	97.84
75ee	2.21	0.32	97.47
50ee	2.31	0.77	96.92
40ee	2.18	0.94	96.88
20ee	2.25	1.50	96.25
RS (0ee)	2.46	2.46	95.08

Table 5.4. Solubility of 4-hydroxy-2-pyrrolidone in isopropanol at 30 ^{o}C

	R (wt%)	S (wt%)	IPA (wt%)
100ee	1.78	0	98.22
75ee	1.95	0.27	97.78
50ee	1.96	0.65	97.39
40ee	1.85	0.79	97.36
20ee	1.88	1.26	96.86
RS (0ee)	2.05	2.05	95.90

Table 5.5. Solubility of 4-hydroxy-2-pyrrolidone in isopropanol at 25 ^{o}C

	R (wt%)	S (wt%)	IPA (wt%)
100ee	1.51	0	98.49
75ee	1.64	0.23	98.13
50ee	1.64	0.55	97.81
40ee	1.57	0.67	97.76
20ee	1.56	1.04	97.40
RS (0ee)	1.77	1.77	96.46

Table 5.6. Solubility of 4-hydroxy-2-pyrrolidone in isopropanol at 20 ^{o}C

	R (wt%)	S (wt%)	IPA (wt%)
100ee	1.29	0	98.71
75ee	1.45	0.21	98.34
50ee	1.40	0.46	98.14
40ee	1.33	0.57	98.10
20ee	1.28	0.85	97.87
RS (0ee)	1.52	1.52	96.96

Table 5.7. Solubility of 4-hydroxy-2-pyrrolidone in isopropanol at 15 ^{o}C

	R (wt%)	S (wt%)	IPA (wt%)
100ee	1.07	0	98.93
75ee	1.25	0.18	98.57
50ee	1.24	0.41	98.35
40ee	1.14	0.49	98.37
20ee	1.04	0.70	98.26
RS (0ee)	1.20	1.20	97.60

Table 5.8. Solubility of 4-hydroxy-2-pyrrolidone in isopropanol at 10 ^{o}C

	R (wt%)	S (wt%)	IPA (wt%)
100ee	1.03	0	98.97
75ee	1.10	0.16	98.74
50ee	1.15	0.38	98.47
40ee	1.00	0.43	98.57
20ee	0.85	0.57	98.58
RS (0ee)	1.01	1.01	97.98

Table 5.9. Solubility of 4-hydroxy-2-pyrrolidone in isopropanol at 5 ^{o}C

	R (wt%)	S (wt%)	IPA (wt%)
100ee	0.73	0	99.27
75ee	1.03	0.15	98.82
50ee	1.14	0.38	98.48
40ee	0.82	0.35	98.83
20ee	0.71	0.47	98.82
RS (0ee)	0.73	0.73	98.54

The ternary phase diagram was plotted using the above solubility data as shown in Figure 5.5. It is confirmed that 4-hydroxy-2-pyrrolidone exists as a conglomerate during the studied temperature range 5 - 40 ^{o}C as the shape of the ternary phase diagram keeps unchanged with the characteristic of a conglomerate forming system. The transformation

of conglomerate to racemic compound is not uncommon (Collet et al., 1980; Houllemare-Druot and Coquerel, 1998).

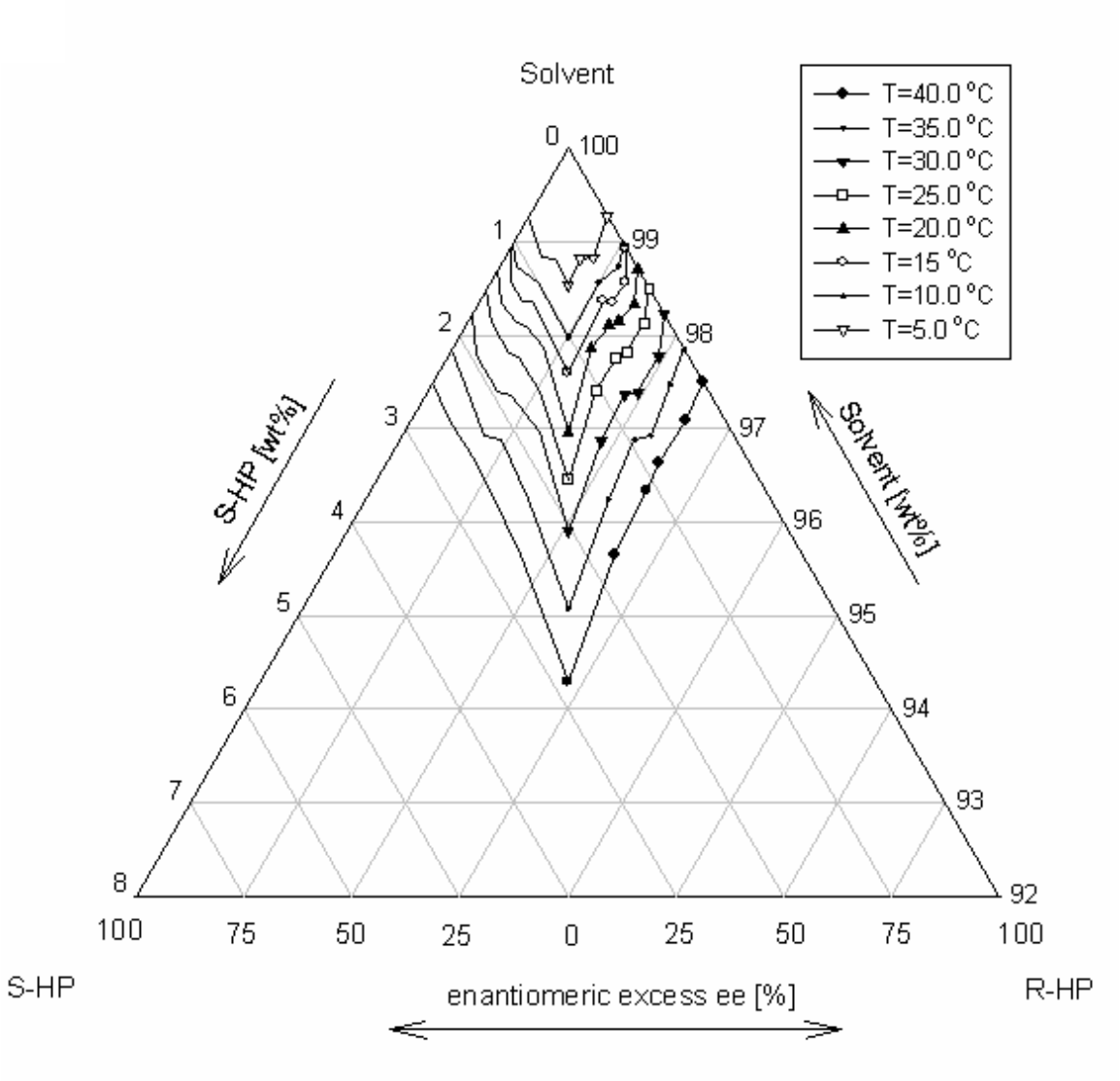

Figure 5.4 Ternary phase diagram of 4-hydroxy-2-pyrrolidone in isopropanol

5.3.1.2 Metastable zone width (MSZW)

The corresponding metastable zone widths of different enantiomeric compositions (R-, RS-, 20%ee, 25%ee, 40%ee, 50%ee and 75%ee) under different cooling rates 1, 5, and 10 ^{o}C/h are given in Figures (5.5 – 5.11). The metastable zone widths were determined using FBRM and validated by PVM images. The maximum allowable supersaturation was expressed in terms of the maximum allowable undercooling ($T_{dissolution} - T_{nucleation}$).

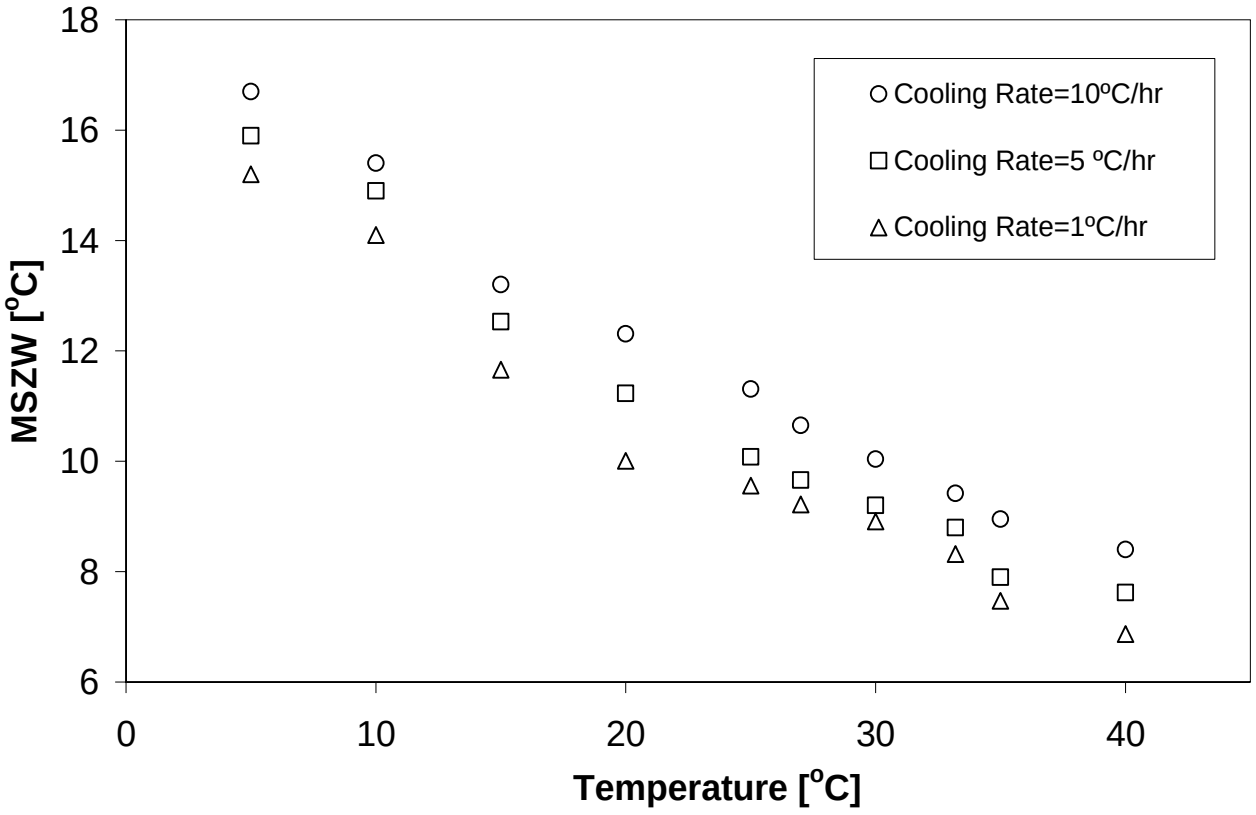

Figure 5.5 Experimental metastable zone widths of pure R-4-hydroxy-2-pyrrolidone in IPA for different cooling rates

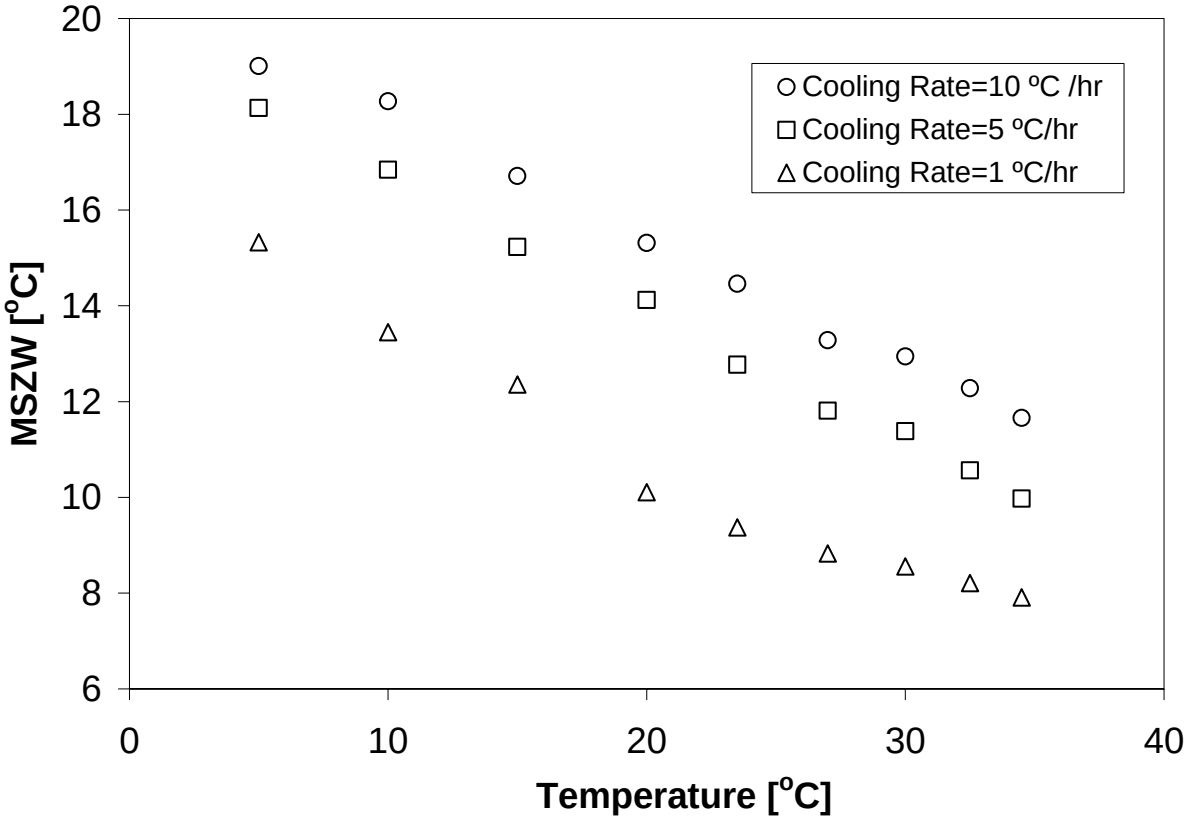

Figure 5.6 Experimental metastable zone widths of RS-4-hydroxy-2-pyrrolidone in IPA for different cooling rates

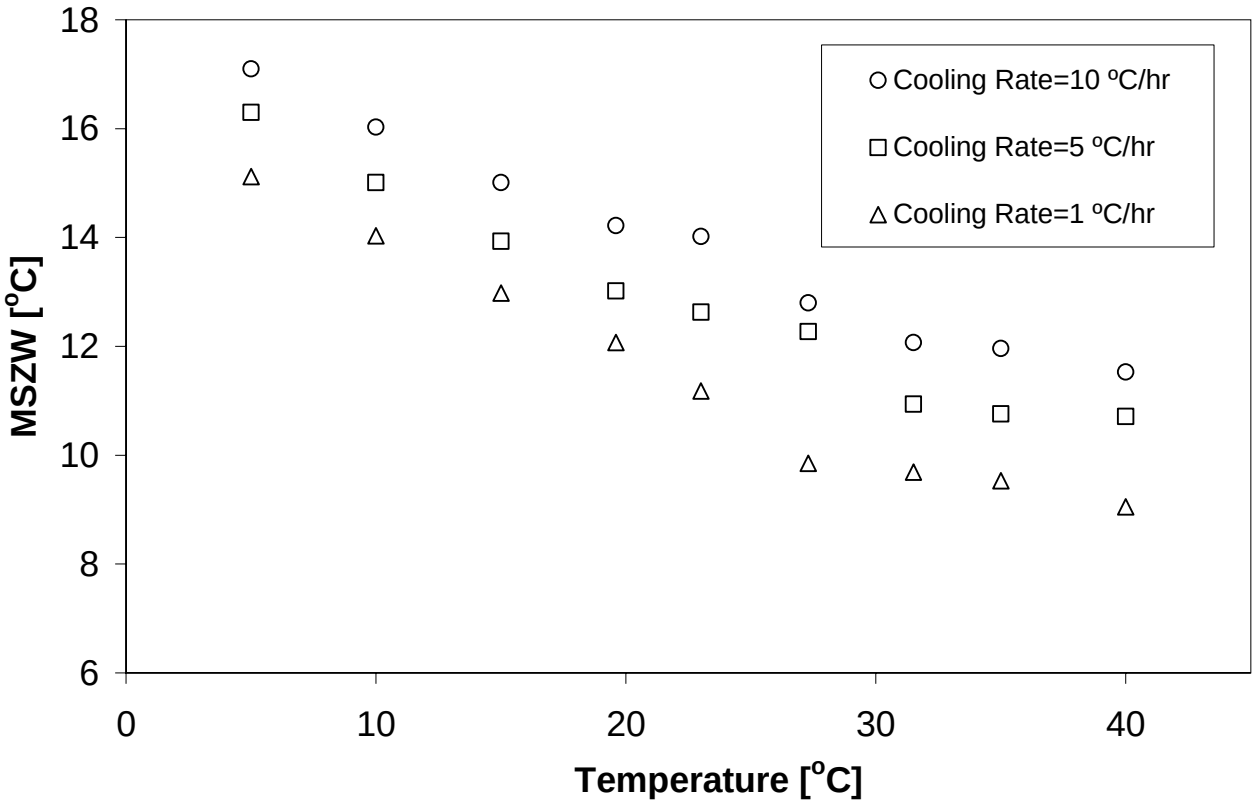

Figure 5.7 Experimental metastable zone widths of R-20%ee-4-hydroxy-2-pyrrolidone in IPA for different cooling rates

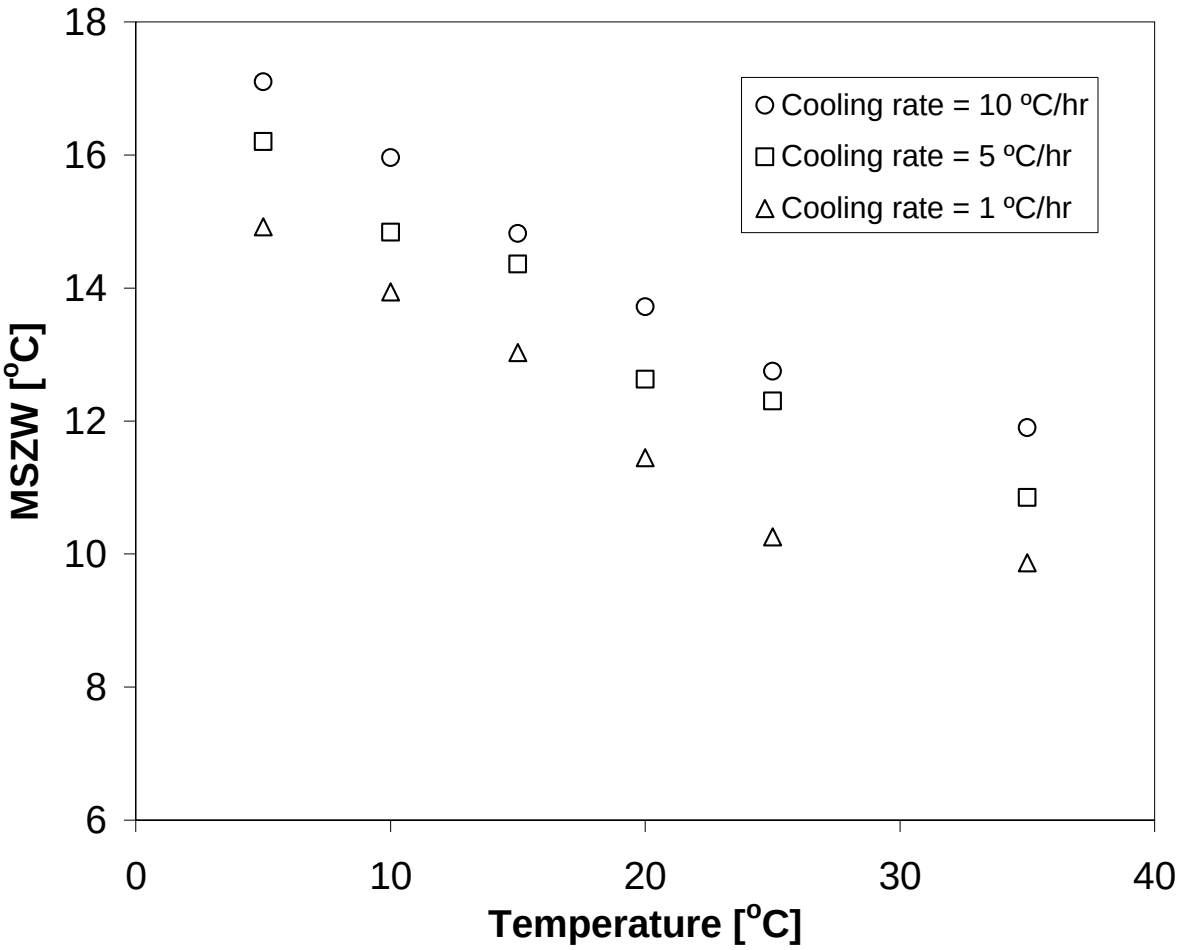

Figure 5.8 Experimental metastable zone widths of R-25%ee-4-hydroxy-2-pyrrolidone in IPA for different cooling rates

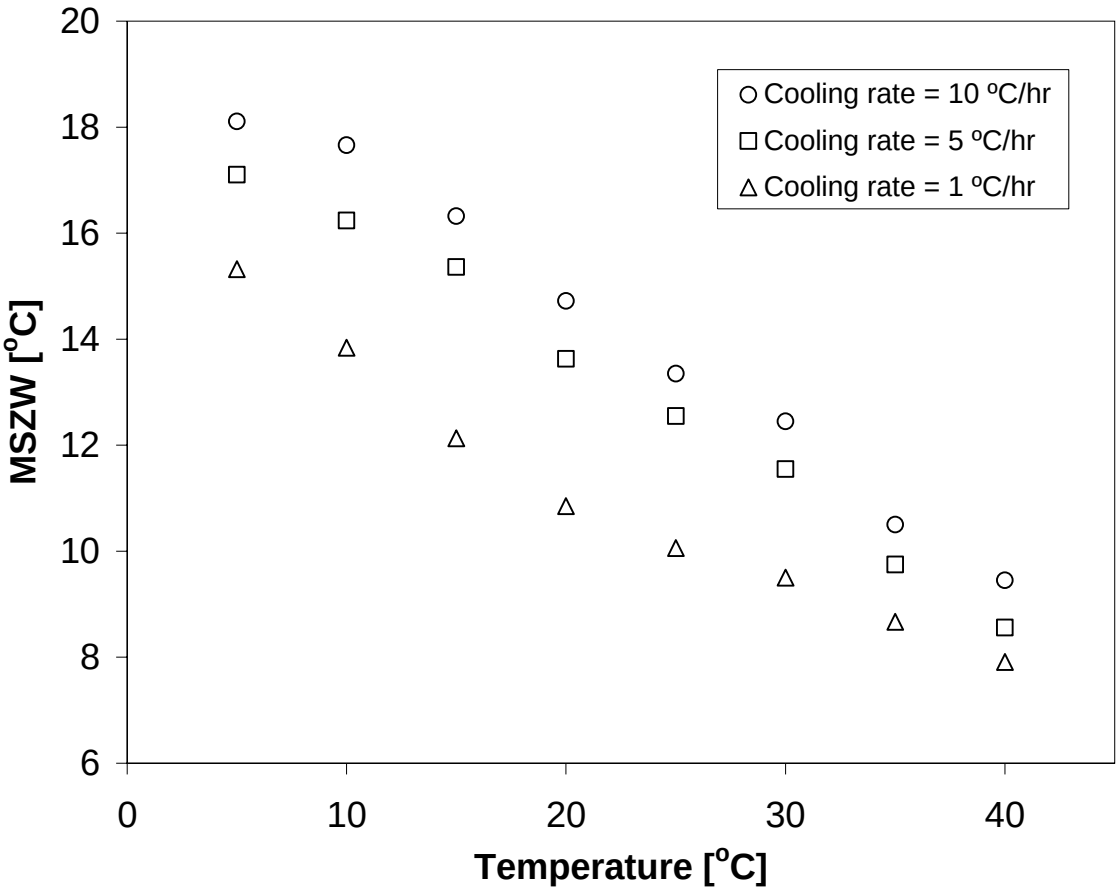

Figure 5.9 Experimental metastable zone widths of R-40%ee-4-hydroxy-2-pyrrolidone in IPA for different cooling rates

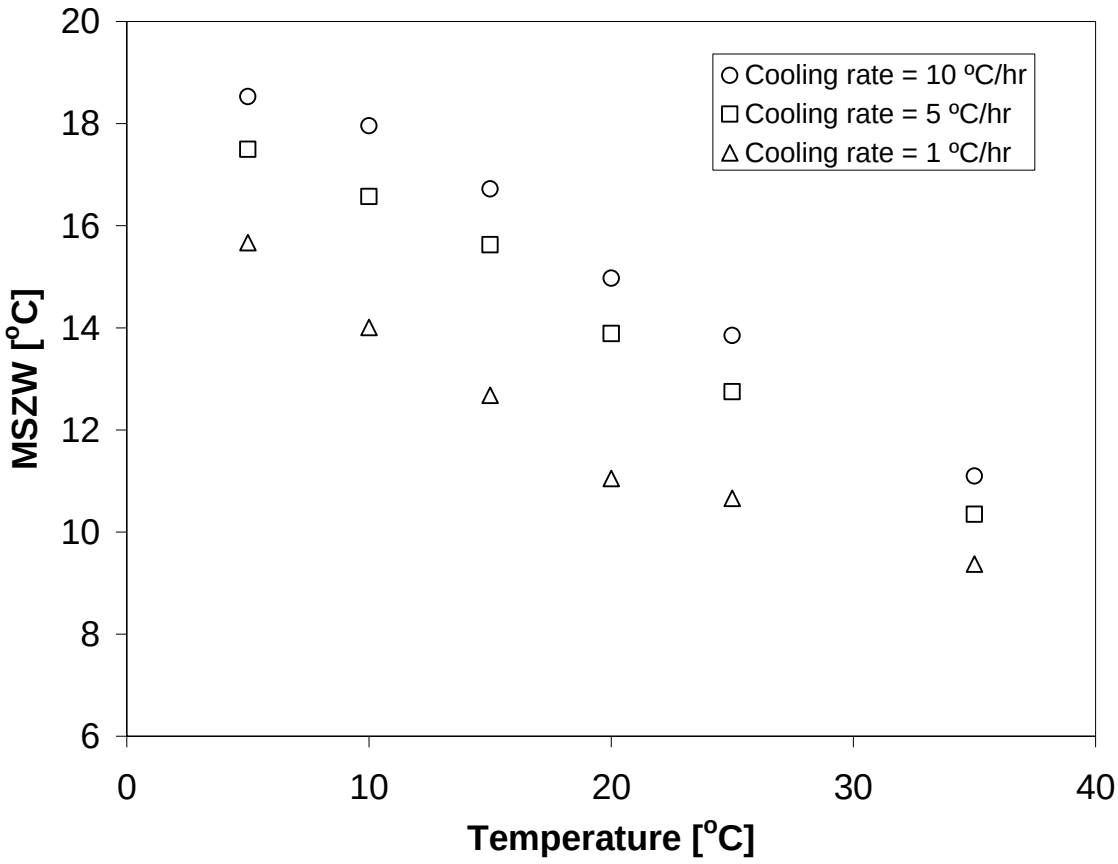

Figure 5.10 Experimental metastable zone widths of R-50%ee-4-hydroxy-2-pyrrolidone in IPA for different cooling rates

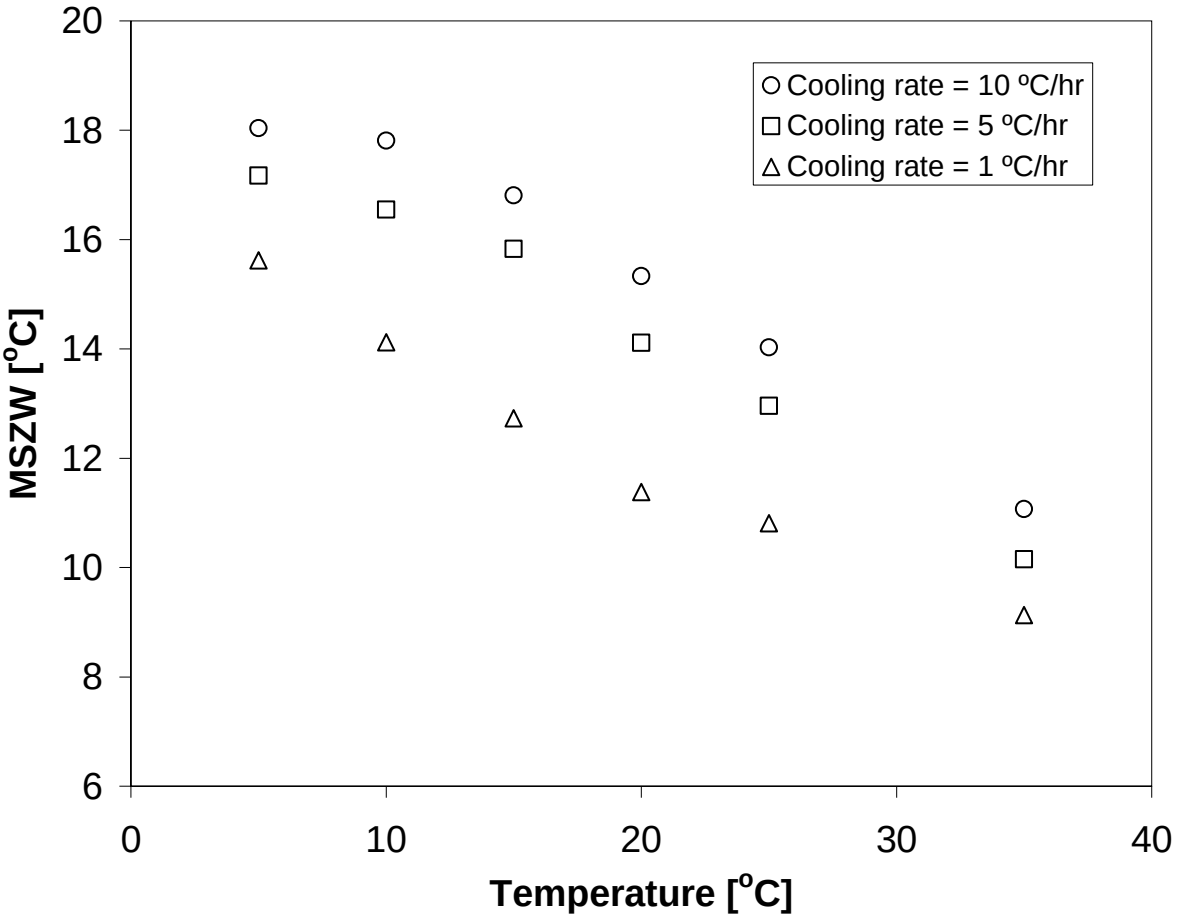

Figure 5.11 Experimental metastable zone widths of R-75%ee-4-hydroxy-2-pyrrolidone in IPA for different cooling rates

Figures (5.5 – 5.11) show that a range of 7 - 18 ^{o}C metastable zone widths could be used if direct crystallization is applied to 4-hydroxy-2-pyrrolidone in isopropanol. These values are big enough to be of great practical relevance. It is clear that the maximum allowable undercoolings greatly depend on the saturation temperatures as well as the cooling rates. When the cooling rate was constant, the metastable zone widths became narrower at higher saturation temperatures. This is consistent with the classical nucleation theory (Mullin, 2001). At higher temperature, the saturated solute concentration is higher.

Therefore, there would be more molecules and more chances for molecule additions to the critical cluster which would result in faster nucleation and subsequent growth of the observable nucleus.

However, it is most interesting to notice that there was no significant difference of MSZWs under the similar operating conditions when the enantiomeric excess changed from 0 (RS) to 100% (pure R) and the corresponding solubility decreased almost 50%. This could be one of the characteristics of a conglomerate forming system. In solution, although the physical properties of both R and S are the same, the two enantiomers respond separately to form crystal nucleus, which means that the MSZW will be dependent on only concentration of isolated enantiomer. The following relationship of MSZWs with cooling rates will give some further quantitative analysis.

As discussed by Mullin (2001), the empirical power law is widely used to describe the primary nucleation in industrial crystallizer.

$$J = k_n \Delta c_{\max}^n \tag{5.8}$$

where J is the primary nucleation rate, k_n is the nucleation rate constant and Δc_{max} is the maximum allowable supersaturation (MSZW).

In the mean time, the nucleation rate can be derived from classical nucleation relationship (Nyvlt, 1968) in terms of cooling rate q.

$$J = q\frac{dC^*}{dT} \tag{5.9}$$

The relationship of Δc_{max} and ΔT_{max} can be expressed as

$$\Delta c_{\max} = \Delta T_{\max} \frac{dC^*}{dT} \tag{5.10}$$

The above Equations (5.8 – 5.10) can be combined to get

$$\log q = n \log \Delta T_{\max} + (n-1) \log \frac{dC^*}{dT} + \log k_n \tag{5.11}$$

This equation indicates that log q is linearly dependent on log ΔT_{max} with a straight line of slope *n*.

Figures 5.12 and 5.13 present the relationship of log ΔT_{max} with log q for RS and 20ee% respectively. Good linearity can be observed for most of the data points. Indeed, the regressed *n* for RS is in the range of 5.3 - 7.4. A slope of circa 7-19 could cover most of the other data sets, namely for pure R (n=11-19), 20%ee(R) (n=10-19), 25%ee(R) (n=10-18), 40%ee(R) (n=7-14), 50%ee(R) (n=7-14) and 75%ee(R) (8-16). This is again consistent with the previous observations that MSZW is independent of enantiomeric excess.

It is obvious that the apparent primary nucleation order of RS is generally smaller than those of other cases, especially pure R, 20%ee and 25%ee. As discussed in Chapter 4, for conglomerate system, the two isomers respond separately to form crystal nucleus. Therefore, for solutions of pure R or with certain R enantiomeric excess, it is expected only R form nucleus at least during the very initial period and ΔT_{max} is only related with supersaturation of R. But for RS, two isomers should form nucleus at the same time and the contribution to the apparent nucleation rate is the addition of both R and S isomers. If the observable nucleation rate is assumed to be constant, Equation 5.8 can be rewritten as

$$n = \frac{\log J / k_n}{\log \Delta c_{\max}} \tag{5.12}$$

The nucleation rate constant k_n can be considered the same for both R and S enantiomers. Therefore, the above equation indicates the apparent primary nucleation order n for pure R or with certain ee% should be smaller than that of RS solution, which is what was exactly observed.

It is also very interesting to note that small apparent primary nucleation order *n* (circa 7-8) was also observed in several cases for (R) 40 ee% -75ee%. This could be due to some extent of nucleation of S, which could initiate itself or could be induced by spontaneous nucleation of R when the supersaturation surpasses a critical level.

Actually, when high supersaturations within the metastable zone are used, some conglomerates will form crystals that contain domains of both lattices in a single crystal, which means that the enantiomerically pure seed could nucleate the other enantiomer at its surface. One typical example is in the synthesis of agrochemical paclobutrazol where resolution of a racemic chiral ketone is involved (Black et al., 1989; Collins et al., 1997). Only when very low supersaturation (1 ^{o}C undercooling) was used, did the effects of nucleating the unwanted isomer disappear to give the product with a high optical purity. This phenomenon at higher supersaturation was also observed on β-phenylglyceric acid (Furberg and Hassel, 1950).

Hongo et.al. (1981) showed the stability of supersaturated DL-serine m-xylene-4-sulfonate dehydrate and identified two metastable regions where the supersaturation was relatively unstable in the second region. In the studies of nuclei breeding from a chiral crystal seed of $NaClO_3$ (Denk and Botsaris, 1972; Kondepudi et al., 1990, 1993, 1995; McBride and Carte, 1991; Yokota and Toyokura, 1992; Qian and Botsaris, 1997, 1998), it

was found that at low supersaturation all nuclei were of the same chirality. At relatively high supercooling, but still lower than the critical value for spontaneous nucleation, many nuclei with opposite chirality to that of seed were formed. The similar findings were reported by Davey et al. (1990) in triazolylketone chiral crystallization. The current experimental findings and those found in the literature, all of these suggest that even within the metastable zone, the supersaturation of target enantiomer is tightly associated with nucleation of its opposite enantiomer. This kind of nucleation is unwanted and should be inhibited in the preferential crystallization application. Chapter 7 will discuss the strategy to control the supersaturation within a critical range to prevent this undesired nucleation.

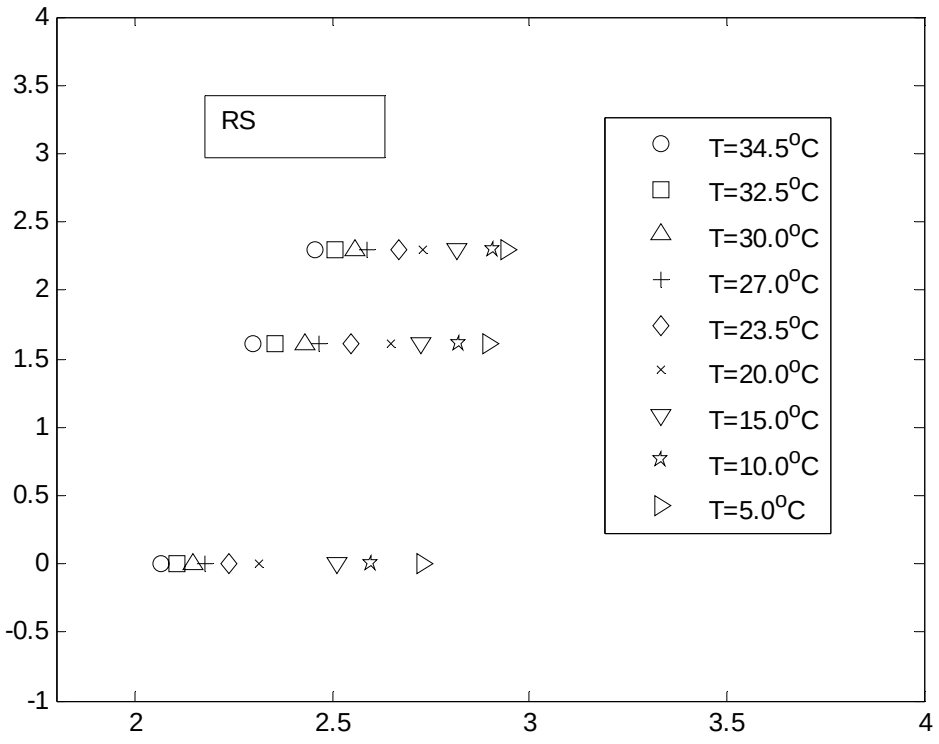

Figure 5.12 Relationship of log MSZW (log ΔT_{max}) with cooling rate (log q) for RS-4-hydroxy-2-pyrrolidone

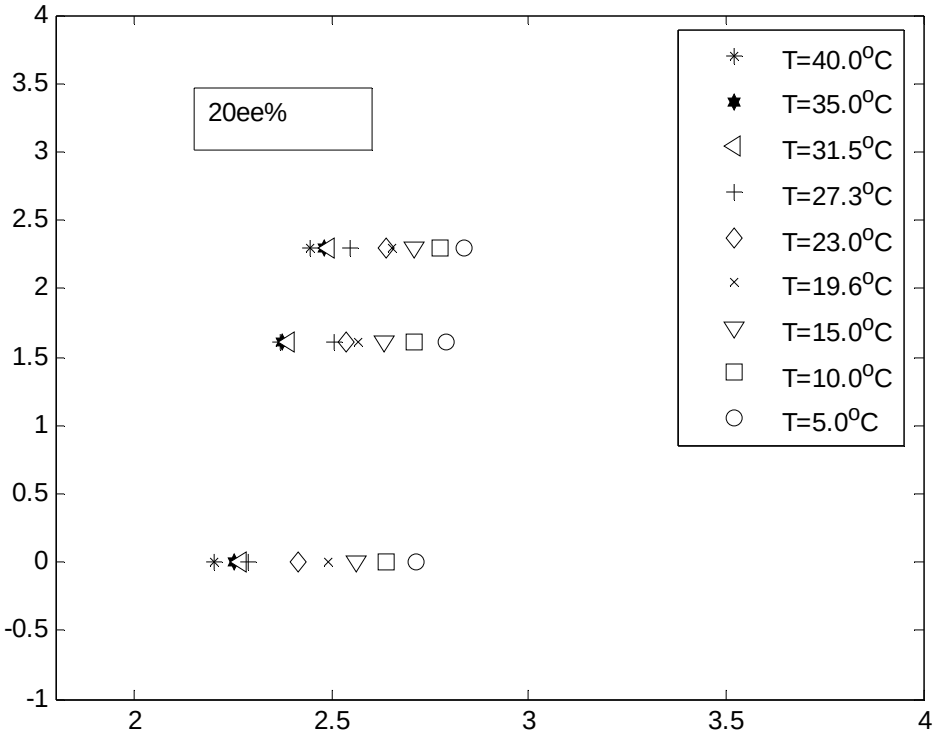

Figure 5.13 Relationship of log MSZW (log ΔT_{max}) with cooling rate (log q) for 20% ee-R-4-hydroxy-2-pyrrolidone

5.3.2 Solubility and metastable zone width of N-methylephedrine in the mixture of isopropanol and water (Vol 1:3)

5.3.2.1 Solubility

The solubilities of N-methylephedrine with composition (+) 25% ee, 50% ee, 75% ee, pure (+)- and (±)-ME in the mixture of isopropanol and water (Vol = 1:3) are listed in Table 5.10 and shown in Figure 5.14, respectively.

Table 5.10. Solubility of N-methylephedrine in the mixture of isopropanol and water (Vol = 1:3)

ee%	T [^{o}C]	C [g solute/100g solvent]
Pure (+)_ME	30	2.26
	25	1.76
	20	1.39
	15	1.14
(±)_ME	30	6.96
	25	5.28
	20	3.75
	15	2.88
25% ee_(+)_ME	30	4.45
	25	3.25
	20	2.42
	15	1.97
50% ee_(+)_ME	30	3.37
	25	2.55
	20	2.00
	15	1.63
75% ee_(+)_ME	30	2.68
	25	2.03
	20	1.63
	15	1.34

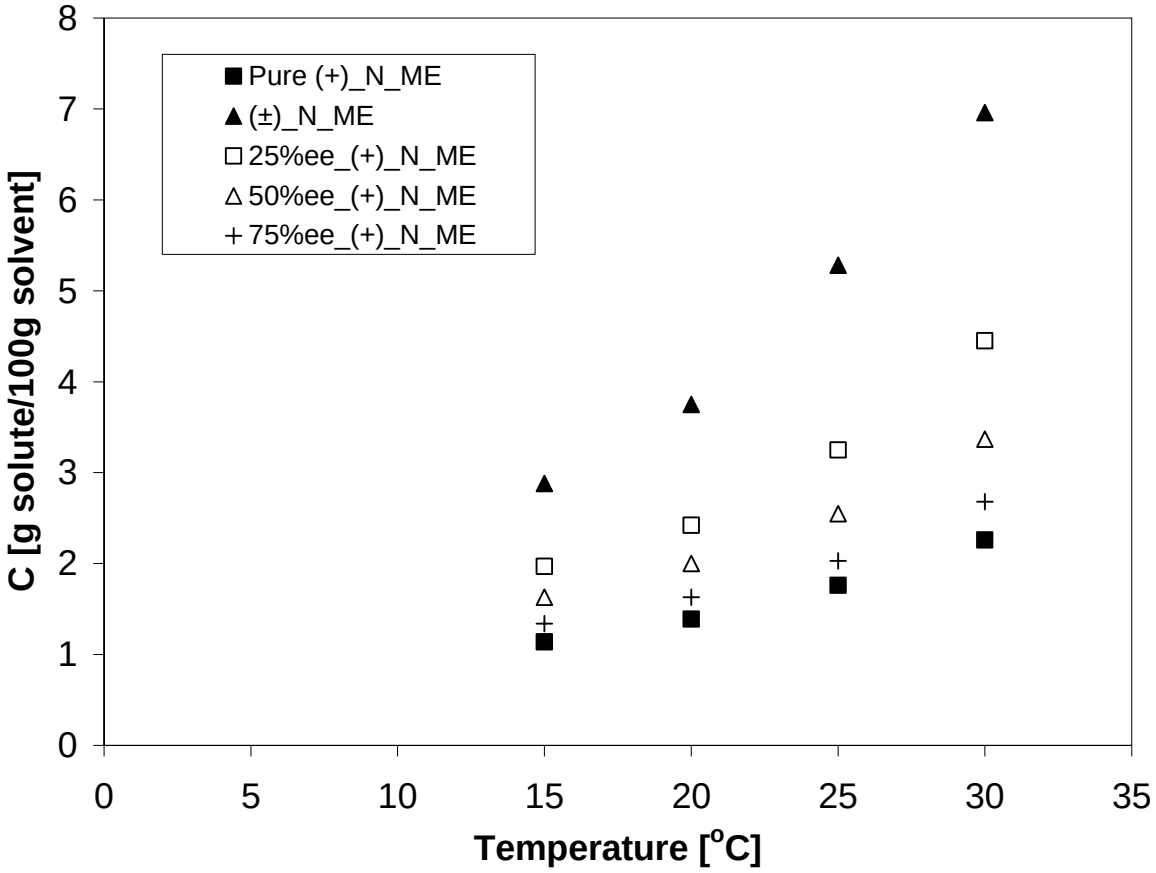

Figure 5.14 Solubility of N-methylephedrine with different enantiomeric excess in the mixture of isopropanol and water (Vol 1:3)

The solubility curves can be regressed to obtain the following solubility equations.

Pure_(+)_N_ME:	$C = 0.0025T^2 - 0.0379T + 1.1465$	(5.13)
(±)_N_ME:	$C = 0.0081T^2 - 0.0891T + 2.3685$	(5.14)
25%ee_(+)_N_ME:	$C = 0.0075T^2 - 0.1721T + 2.8635$	(5.15)
50%ee_(+)_N_ME:	$C = 0.0045T^2 - 0.0871T + 1.9285$	(5.16)
75%ee_(+)_N_ME:	$C = 0.0036T^2 - 0.0736T + 1.641$	(5.17)

The solubilities of (+)-, (±)-, 25% ee, 50% ee, and 75% ee (+)- N-methylephedrine in isopropanol and water properly increase with temperature over the range of 15 – 30 ^{o}C. The solubility ratio of (±)- to (+)-ME is between 2.5 and 3.1 in the current temperature range. It is bigger than that of 4-hydroxy-2-pyrrolidone. Although the solubility ratio of (±)- to (+)-ME also decreases from high temperature to low one, this system appears more difficult to purify using preferential crystallization technique than 4-hydroxy-2-pyrrolidone system as the solubility ratio of (±)- to (+)-ME is higher (Jacques et al., 1994).

Figure 5.15 shows the ternary phase diagram. Like 4-hydroxy-2-pyrrolidone in isopropanol, N-methylephedrine exists as a conglomerate in the chosen solvent during the studied temperature range 15-30 ^{o}C because the shape of its ternary phase diagram possesses the characteristic of a conglomerate system.

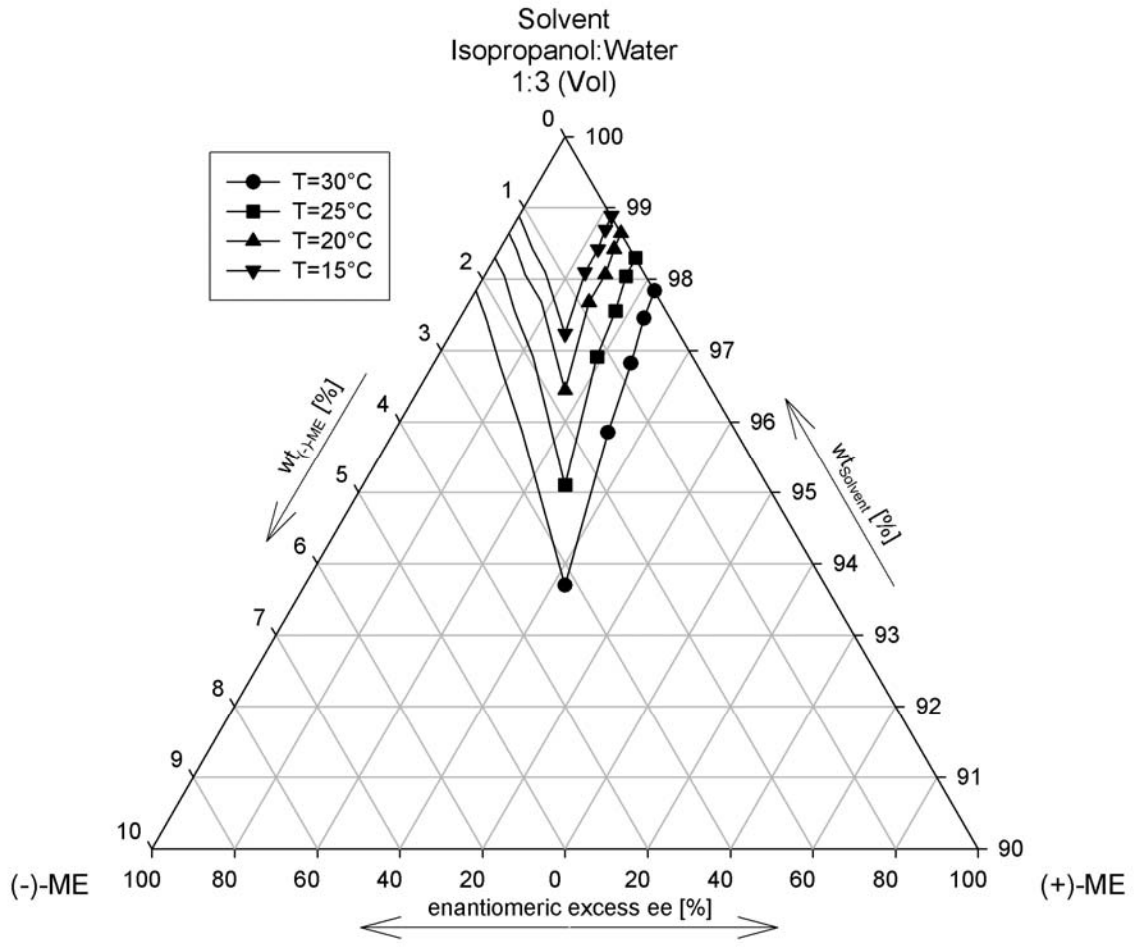

Figure 5.15 Ternary phase diagram of N-methylephedrine in the mixture of isopropanol and water (Vol 1:3)

5.3.2.2 Metastable zone width (MSZW)

The corresponding metastable zone widths measurements are given in Figure 5.16. The metastable zone widths were determined using FBRM and PVM. The maximum allowable supersaturation was expressed in terms of the maximum allowable undercooling ($T_{dissolution} - T_{nucleation}$). When the cooling rate was constant, the metastable zone widths became narrower at higher saturation temperatures.

Similar to that of 4-hydroxy-2-pyrrolidone system, the MSZW of N-methylephedrine in water and isopropanol is also independent of enantiomer excess. This is again one of the characteristics for a conglomerate.

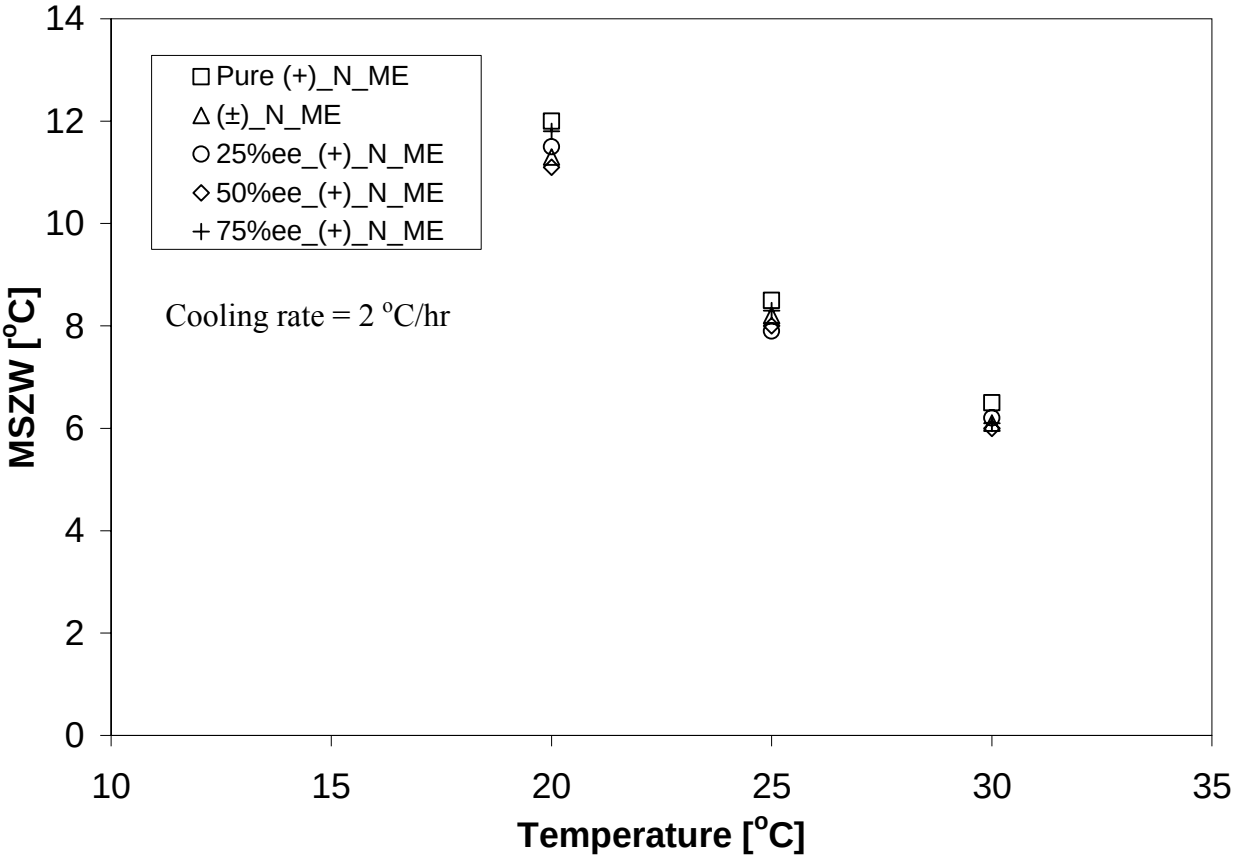

Figure 5.16 Experimental metastable zone widths of N-methylephedrine in the mixture of IPA and water (Vol = 1:3) for different enantiomeric excess

5.3.3 Solubility and metastable zone width of propranolol hydrochloride in the mixture of methanol and isopropanol (Vol 1:5)

5.3.3.1 Solubility

The solubilities of propranolol hydrochloride with composition (R) 30% ee, 50%ee, 70% ee, pure R- and RS- in the mixture of methanol and isopropanol (Vol=1:5) are listed in Table 5.11 and shown in Figure 5.17, respectively.

Table 5.11. Solubility of propranolol hydrochloride in the mixture of methanol and isopropanol (Vol = 1:5)

ee%	T [^{o}C]	C [g solute/100g solvent]
Pure (R)_PN_Cl	35	1.21
	30.6	1.10
	28.6	1.00
	23	0.86
	19	0.75
	16	0.69
	12	0.64
(RS)_PN_Cl	35	1.81
	30.6	1.67
	28.6	1.48
	23	1.21
	19	1.03
	16	0.95
	12	0.86
30% ee_(R)_PN_Cl	35	1.56
	30.6	1.45
	23	1.07
	19	0.93
	16	0.86
50% ee_(R)_PN_Cl	35	1.45
	30.6	1.34
	23	1.01
	19	0.88
	16	0.81
70% ee_(R)_PN_Cl	35	1.34
	30.6	1.22
	23	0.94
	19	0.82
	16	0.76

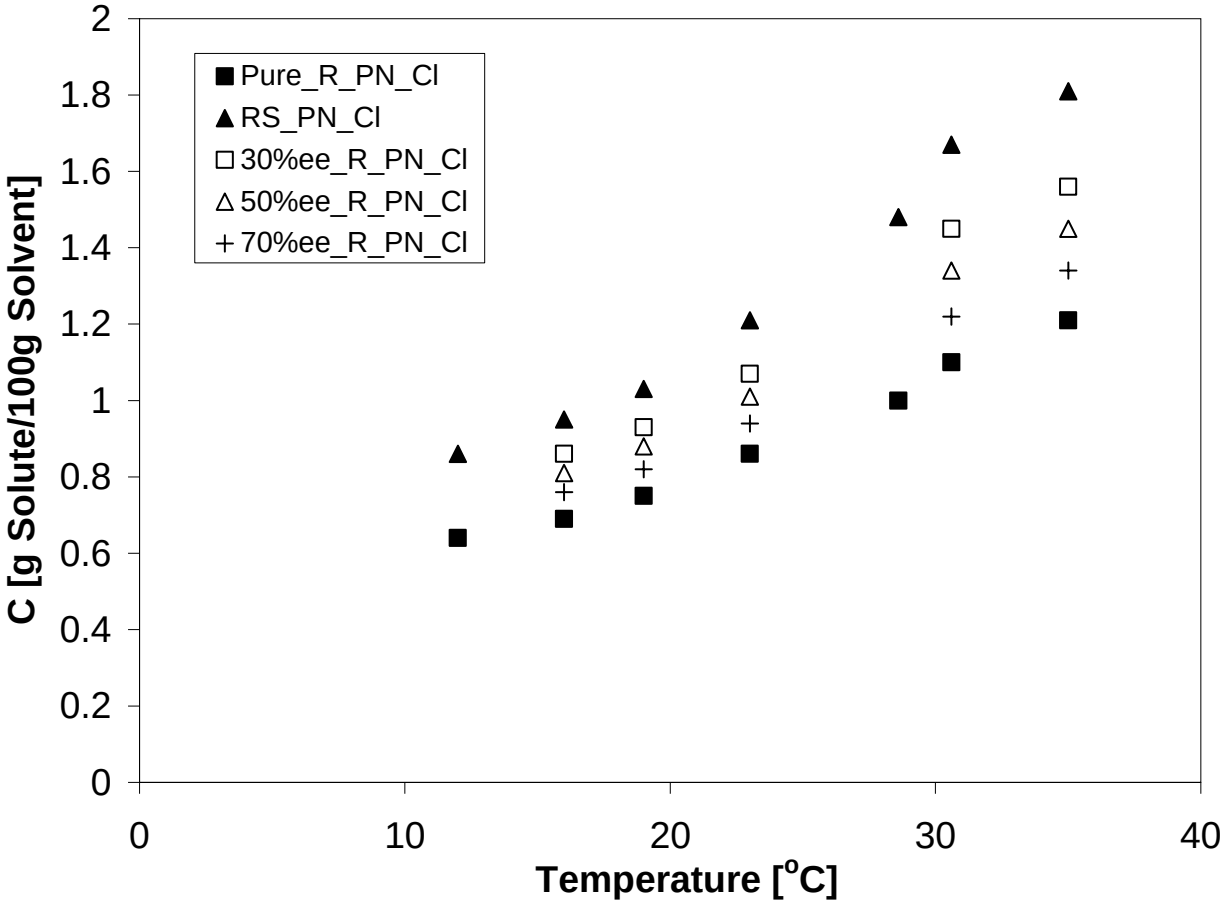

Figure 5.17 Solubility of propranolol hydrochloride with different enantiomeric excess in the mixture of methanol and isopropanol (Vol 1:5)

The solubility curves can be regressed to obtain the following solubility equations.

Pure_R_PN_Cl:	$C = 0.0004T^2 + 0.0047T + 0.5092$	(5.18)
RS_PN_Cl:	$C = 0.0008T^2 + 0.0077T + 0.636$	(5.19)
30%ee_R_PN_Cl:	$C = 0.0002T^2 + 0.0296T + 0.3166$	(5.20)
50%ee_R_PN_Cl:	$C = 0.0001T^2 + 0.0281T + 0.3078$	(5.21)

$$70\%ee\_R\_PN\_Cl: \qquad C = 0.0002T^2 + 0.0196T + 0.3731 \qquad (5.22)$$

As shown in Figure 5.17, the solubilities of (R)-, (RS)-, 30% ee, 50% ee, and 70% ee propranolol hydrochloride in the mixture of methanol and isopropanol all properly increase with temperature over the range of 12 – 35 ^{o}C. The chosen solvent is suitable for crystallization operation. The mixture of methanol and acetone also gave good solubility curves, however, it was found that propranolol hydrochloride was easily decomposed in the presence of acetone at ambient temperature (Wang et al, 2002).

Figure 5.17 also shows that the solubilities increase with decreasing ee. The excess enantiomer could be therefore separated by direct crystallization. This is especially meaningful to get pure enantiomer if partially resolved solutions can be supplied by other purification processes such as asymmetric synthesis, simulated moving bed (SMB) chromatography and diastereomeric crystallization etc. Chapter 8 will elaborate this issue.

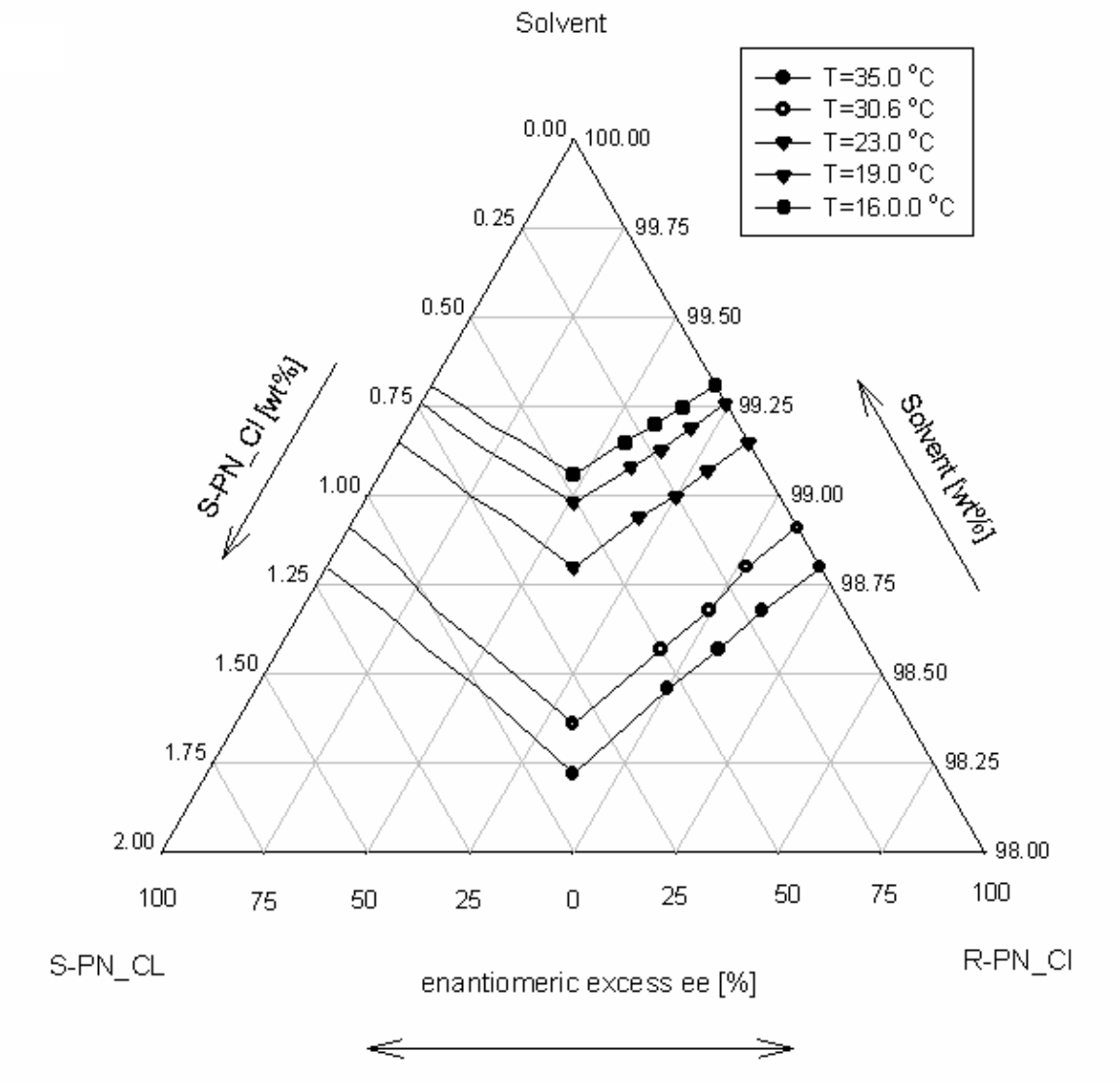

Figure 5.18 The ternary phase diagram of propranolol hydrochloride in the mixture of methanol and isopropanol (Vol = 1:5)

The ternary phase diagram is shown in Figure 5.18. It keeps as a simple eutectic system consisting of two single saturation curves in the studied temperature range. This is consistent with the binary melting phase diagram in Chapter 4 as well as that reported by Neau et al. (1993). Compared to normal racemic compound systems, it is a special case,

which has the most favorable characteristics of ternary solubility diagram to conduct direct crystallization. This will be discussed in detail in Chapter 8.

5.3.3.2 Metastable zone

Figure 5.19 shows the measured metastable zone widths of (R)- and (RS)-propranolol hydrochloride in the mixture of methanol and isopropanol (Vol = 1:5). The general trend of narrower MSZW with higher temperature is again observed here.

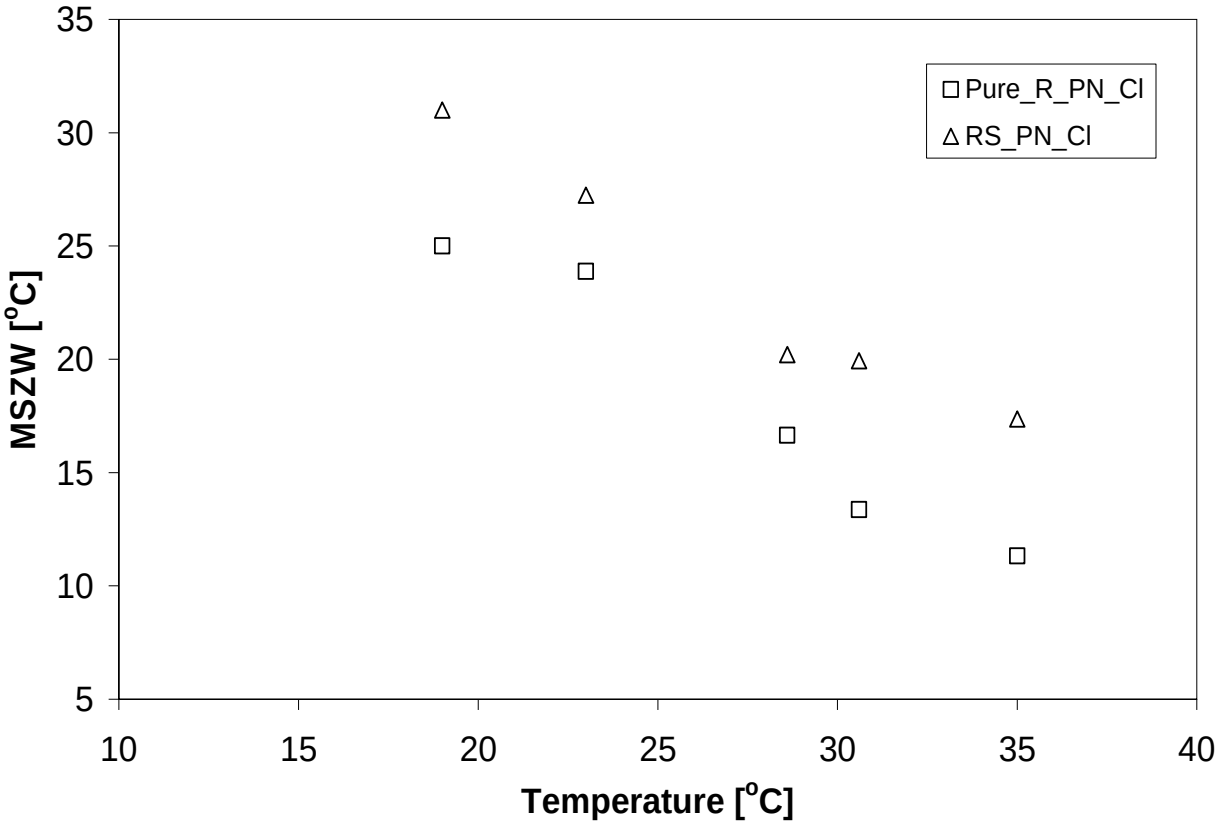

Figure 5.19 Experimental metastable zone widths of R- and RS-propranolol hydrochloride in the mixture of methanol and isopropanol (Vol = 1:5).

However, unlike the conglomerates of 4-hydroxy-2-pyrrolidone and N-methylephedrine, which have similar MSZWs for the pure enantiomer and its

corresponding racemic mixture, the metastable zone widths of pure (R)- and (RS)-propranolol hydrochloride are quite different. Under the same saturated temperature, (RS)-gave a wider MSZW than that of pure (R)-enantiomer, although the solubilities of RS were larger than R. This interesting phenomenon could be explained from the arrangement of two enantiomer molecules in the crystal lattice for a racemic compound and classical nucleation theory.

As for a racemic compound, the two enantiomers co-crystallize to form a mixed crystal containing both enantiomers in a well-defined arrangement within the crystal lattice in equal proportions (Figure 4.1b). According to the classical nucleation theory, the MSZW of RS will be dependent on the concentrations of both enantiomers. Since the solubility of RS is not definitely related to that of pure enantiomers and it can be either greater or smaller than that of pure-enantiomer (Jacques et al., 1994), three cases could arise.

(i) The solubility ratio α of racemate to pure enantiomer is smaller than 1 ($\alpha < 1$). Because the solubility of racemate is smaller than that of pure enantiomer, it is readily to expect that the MSZW of racemate is wider than that of pure enantiomer as less solute molecules are in the solution to undergo collision to form embryos and develop into nuclei. This case is widely observed in many racemic compound systems such as ketoprofen (Lu and Ching, 2006).

(ii) The solubility of racemate is bigger than that of pure enantiomer, but the ratio is smaller than 2 ($1 < \alpha < 2$). In this case, although more molecules are in the solution, the R-molecules and S-molecules are required to arrange in equal quantities to form RS racemate. Therefore, the effective concentration to form nuclei is actually only half the total concentration. Since $\alpha < 2$, the effective R concentration (R:S = 0.5:0.5) is smaller

than that of pure enantiomer. Therefore, the MSZW of racemate should be bigger than that of pure enantiomer. This is true for current studied racemic compound propranolol hydrochloride, where the solubility ratio of RS to R is bigger than 1 but less than 2 (Table 5.11 and Figure 5.17). The similar phenomenon was also observed in the mandelic acid system ((Perlberg et al., 2002, 2003). The solubility of (DL)-mandelic acid is smaller than twice that of the (D)-mandelic acid approximately at certain temperature ranges of (0-25 and 37-60 ^{o}C). The corresponding MSZW of (DL)-mandelic acid is bigger than that of (D)-mandelic acid. This is unlike the above conglomerate systems where two enantiomers are not associated in solution and the MSZW is independent of enantiomeric excess.

(iii) The solubility of racemate is bigger than twice that of pure enantiomer ($\alpha > 2$). As mentioned above, the effective R concentration is bigger than that of pure enantiomer. In this case, the MSZW of racemate should be smaller than that of pure enantiomer. This was also observed in the mandelic acid system (Perlberg et al., 2002, 2003). The solubilities of (DL)-mandelic acid are bigger than twice that of the (D)-mandelic acid approximately at certain temperature range of 23-36 ^{o}C. The corresponding MSZW of (DL)-mandelic acid is smaller than that of (D)-mandelic acid.

The above analysis indicates a cut value of 2 of α is apparently related to the MSZW in racemic compound systems. This could be used as a new additional criterion to determine whether a racemate crystallizes as a racemic compound or conglomerate crystal. It might be particularly helpful when such a special racemic compound is met which shows quite similar other properties (for example, binary/ternary phase diagram of propranolol hydrochloride is similar to that of a conglomerate).

5.3.4 Solubility and metastable zone width of atenolol in acetone

The solubility and metastable zone width of atenolol in acetone were measured in a 25 ml jacketed crystallizer with magnetic stirring. A solubility of 0.5 (wt%) was always obtained at 33 ^{o}C for different ee. Figure 5.20 presents its ternary phase diagram and the metastable zone widths are listed in Table 5.12. MSZWs of (R)- are approximately equal to those of (RS)-atenolol at the same saturated temperature. All of these are consistent with the characteristics of an ideal pseudoracemate.

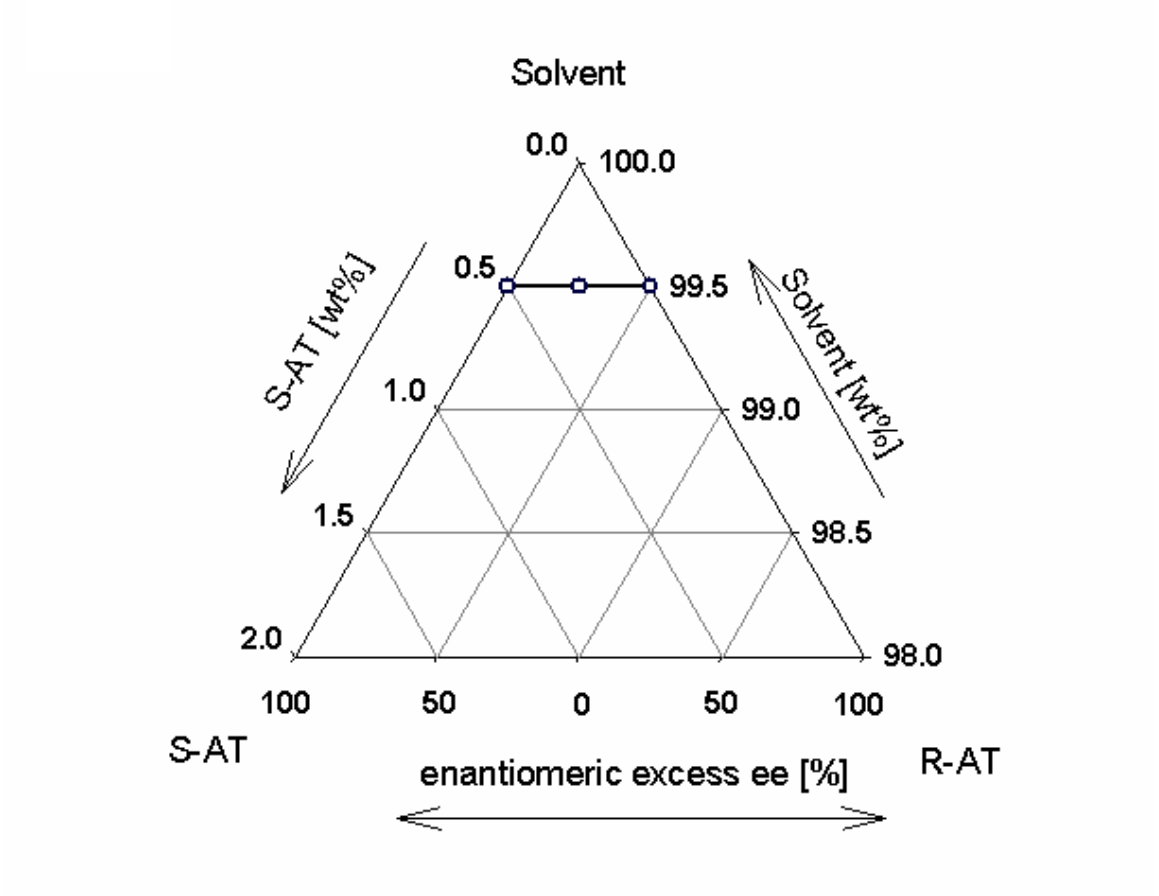

Figure 5.20 The ternary phase diagram of atenolol in acetone

Table 5.12 Experimental metastable zone widths (MSZW) of R- and RS-atenolol in acetone

Saturated Temperature, T [^{o}C]	R_MSZW, ΔT [^{o}C]	RS_MSZW, ΔT [^{o}C]
33	27.4	27.6
30	28.3	28.3
27	30.8	30.7

5.4 Summary

The solubilities, metastable zone widths and ternary phase diagrams at different enantiomer excess (ee) for four racemates, namely 4-hydroxy-2-pyrrolidone in isopropanol , N-methylephedrine in the mixture of isopropanol and water (Vol 1:3), propranolol hydrochloride in the mixture of methanol and isopropanol (Vol = 1:5), and atenolol in acetone were measured by integrating Lasentec FBRM and PVM. All the chosen solvents were found good for cooling crystallization in the studied temperature ranges.

4-hydroxy-2-pyrrolidone and N-methylephedrine show the similar characteristics of solubility as conglomerate systems, i.e., the solubilities decrease with increased ee. But the solubility ratio α of (RS)- to (R)-4-hydroxy-2-pyrrolidone is closer than that of N-methylephedrine to the theoretical value 2 for an ideal conglomerate solution. The metastable zone widths of both studied conglomerates were found independent of enantiomer excess and the data at different cooling rates were in good agreement with

classical nucleation theory. That is consistent with the characteristic of two enantiomers forming separate crystals for a racemic conglomerate. The different orders of primary nucleation rate at different enantiomeric excess indicate there may exist critical supersaturation beyond which the nucleation of opposite isomer could occur. This appears to be the first detailed experimental investigation of metastable zone in conglomerate system and its implications of supersaturation control of preferential crystallization process.

For the racemic compound propranolol hydrochloride, its solubility characteristics and ternary phase diagram are quite similar to that of a conglomerate, but its metastable zone width was obviously dependent on the enantiomer excess. A cut value 2 of solubility ratio α was found to be correlated with the MSZW differences between racemate and pure enantiomers. This reflects the properties of the evenly distributed molecules in the crystal lattice of a racemic compound. It suggests that metastable zone width can be used as an additional characteristic to identify these two kinds of racemates.

The solubility curve, ternary phase diagram and metastable zone of atenolol show the unique properties of an ideal pseudoracemate.

Part of the results in this Chapter have been reported on Journal of Chemical and Engineering Data, 48, pp.1092-1098. 2003, Chirality, 14, pp.318-324, 2002 and Chirality, 16, pp.220-227. 2004.

CHAPTER 6 CRYSTALLIZATION KINETICS OF 4-HYDROXY-2-PYRROLIDONE IN ISOPROPANOL

6.1 Introduction

As discussed in Chapter 1, the supersaturation of the target enantiomer should be carefully controlled to inhibit the spontaneous nucleation of the undesired isomer. In designing operation conditions for the preferential crystallization, the kinetic data such as crystal growth rate G, and nucleation rate B, are necessary. In this Chapter, the batch dynamic method was employed and developed to measure the crystallization kinetics of 4-hydroxy-2-pyrrolidone in isopropanol.

6.2 Characterization of crystallization kinetics

6.2.1 Steady state method

There are two basic categories of techniques to evaluate crystallization kinetics, namely, steady state method and dynamic method. For the former one, the most famous is the classical continuous method proposed by Randolph and Larson (1962, 1988) with mixed-suspension, mixed-product-removal (MSMPR) crystallizer.

In a MSMPR crystallizer,

$$n = n^o \exp(-L / G\tau) \tag{6.1}$$

$$\ln n = \ln n^o - L / G\tau \tag{6.2}$$

$$B = n^o G \tag{6.3}$$

In a semilog plot, the crystal population density ln n can be plotted with L to obtain the intercept n^o and slope $-1/G\tau$ (τ is the residence time). Therefore, the crystal growth rate G and nucleation rate B are readily to get. However, this steady state methodology is laborious and time consuming. For expensive pharmaceuticals and fine chemicals, it is not practical to use a large amount of chemicals required for this continuous scale experimental set up. Moreover, there is experimental evidence to show that the steady-state kinetic parameters do not correctly describe unsteady-state operations partly due to the underlying assumptions such as the size-independent growth rates (Tadayyon et al., 2002).

6.2.2 Dynamic method

Dynamic method is an alternative approach for the estimation of kinetics using unsteady-state data from batch experiments. Batch crystallizer is easier to operate and less time-consuming. More importantly, it is obvious that many variables such as temperature, CSD, concentration, and crystal suspension density are all changing with time in one batch crystallization operation. A single batch run will provide rich information over a wide range of operating conditions. However, as all the variables in the batch crystallizers are changing with time and crystal size, leading to hyperbolic partial differential equations (PDEs), these significantly increase the computational complexity of dynamic methods. These equations either need to be solved by transformation to an ordinary differential equations ODE or by use of an appropriate numerical technique.

Various dynamic techniques have been reported with batch crystallizations. These include thermal response technique (Omran and King, 1974) and mass balance approach (Halfon and Kaliaguine, 1976; Garside et al., 1982). But most of the proposed methods using batch crystallization process are based on crystal size distribution (CSD) analysis (Garside and Jancic, 1976; Way, 1985; Tavare and Garside, 1986; Nyvlt, 1989; Witkowski et al., 1990; Qiu and Rasmuson, 1991, 1994; Farrell and Tsai,1994; Yokota et al., 2000; Garside et al., 2002; Zhang and Rohani, 2003; Hu et al., 2004).

The moment method converts the population balance to a set of ODEs. The *k*th moment of the population density distribution is

$$u_k = \int_0^\infty nL^k dL \tag{6.4}$$

The kinetic parameters can be expressed in terms of moments with respect to size at an average time interval,

$$B = \frac{\Delta u_0}{\Delta t} \tag{6.5}$$

$$G = \frac{\Delta u_1}{\bar{u}_o \Delta t} \tag{6.6}$$

or

$$G = \frac{\Delta u_2}{2\bar{u}_1 \Delta t} \tag{6.7}$$

It was shown (Tavare and Garside, 1986) that a large scatter of the parameter estimates resulting from moment analysis, compared to actual values, was identified with

tail effects. The errors in the measurement of experimental responses toward the tail ends have significant influence on the moment evaluations and hence the parameter estimates.

In principle, the most accurate approach for the estimation of kinetic parameters is accomplished by using a nonlinear optimization algorithm, a full mathematical description of a batch crystallizer, and reliable experimental data. A lot of efforts have been put in this area (Nyvlt, 1989; Witkowski et al., 1990; Qiu and Rasmuson, 1991, 1994; Farrell and Tsai, 1994; Yokota et al., 2000; Zhang and Rohani, 2003; Hu et al., 2004). A major advantage of this method is that the estimation of growth and nucleation rates and their kinetic parameters in the mathematical method is performed simultaneously. The kinetic constants in the mathematical model are adjusted by the optimization algorithm to minimize an objective function.

Another method available is the so called *s*-plane analysis (Tavare and Garside, 1986). This method is based on population balances for discrete parts of the crystal size distribution. The change in number of crystals in discrete parts of the particle size distribution for consecutive samples can give an estimate of the growth rate of the crystals in this size range.

The crystallization kinetics measurements in preferential crystallization process are rarely reported. Elsner et al (2003, 2005) recently attempted to use moment method to determine crystallization kinetics of L-/D-threonine in water but found it was difficult to predict nucleation rate.

6.3 s-Plane analysis

The s-plane analysis proposed by Tavare and Garside is a simple and yet reliable method of extracting both crystal nucleation and growth kinetics from the population

curves obtained during batch crystallization (Tavare and Garside, 1986; Tavare, 1995; Jacobsen et al., 1998; Myerson and Ginde, 2002). This method is based on population balances for discrete parts of the crystal size distribution. We used this technique to estimate crystal nucleation and growth kinetics. For batch crystallization, assuming the crystal growth is size independent, and since the crystal suspension density used is less than 5% and the solution is well mixed, it is acceptable to assume that no crystal breakage or agglomeration occurs, therefore the population balance equation is

$$\frac{\partial n}{\partial t} + G\frac{\partial (n)}{\partial L} = 0 \tag{6.8}$$

The boundary conditions for the nuclei population density can be represented by the relation

$$B = n^o G \tag{6.9}$$

The experimentally measured population density *n(t,L)* can be converted into Laplace transformed response with respect to size *L* as

$$\bar{n}(t,s) = \int_0^\infty n(t,L)\exp(-sL)dL \tag{6.10}$$

Taking the Laplace transforms of the population balance equation with respect to size gives

$$\frac{d\bar{n}(t,s)}{dt} + G[s\bar{n}(t,s) - n(t,0)] = 0 \tag{6.11}$$

In the above equation 6.11, the crystal growth rate G and the initial population density $n(0)$ are functions of time. However, in a small time interval Δt, they can be assumed to be constant and therefore the resulting parameters will have an average value over this interval. In this case, using initial boundary conditions, the population balance equation can be transformed to

$$\frac{d\bar{n}(t,s)}{dt} + \bar{G}s\bar{n}(t,s) - \bar{B} = 0 \tag{6.12}$$

This equation can be transformed into a differential format as

$$\frac{\Delta\bar{n}(s,t)}{\Delta t} = -\bar{G}s\overline{\bar{n}(t,s)} + \bar{B} \tag{6.13}$$

where

$$\Delta t = t_2 - t_1 \tag{6.14}$$

$$\Delta\bar{n}(s,t) = \bar{n}(t_2,s) - \bar{n}(t_1,s) \tag{6.15}$$

$$\overline{\bar{n}(t,s)} = [\bar{n}(t_2,s) + \bar{n}(t_1,s)]/2 \tag{6.16}$$

Over an optimal range of the Laplace transform variable, a plot of $\Delta\bar{n}(s,t)/\Delta t$ versus $s\overline{\bar{n}(t,s)}$ should give a straight line with slope equal to - $\bar{G}$ and an intercept $\bar{B}$. Therefore, the above equation can be used to determine the crystal nucleation and growth rates from a pair of population density curves at two times Δt interval.

The estimated nucleation B and growth rate G can then be correlated with the degree of supersaturation Δc and slurry density M_T using the widely used power law expressions in conventional crystallization (Randolph and Larson, 1988; Tavare, 1995; Mullin, 2001).

$$G = k_g \exp(-E_g / RT)\Delta c^g \tag{6.17}$$

$$B = k_b \exp(-E_b / RT)G^i {M_T}^j \tag{6.18}$$

6.4 Size-dependent growth

In the previous deduction procedure, it was assumed that all crystals grow at the same rate. However, there is some evidence that crystals of different sizes may grow at different rates even though they are under the same driving force (supersaturation). This is called size-dependent crystal growth (Zumstein and Rousseau, 1987, 1989; Randolph and Larson, 1988). This phenomenon of growth dispersion could be due to various reasons. The growth rate of large crystals could be increased because of an increase in their fluid settling velocity, but this can not explain some observed large differences of growth rate among crystals of different sizes in the same suspension. Berglund and Larson (1982) showed that larger crystals had an inherent higher growth rate. Garside et al. (2002) suggested that growth rate appears to depend on the origin of nuclei. In particular, it is not unusual that many organic crystals growth rates are size dependent (Kougoulos et al., 2005).

Abegg et al.(1968) had shown that the following form can be used to fit most data for the case of size-dependent crystal growth, where G_0 is size- independent crystal growth rate and α is experimentally determined constants (O'Dell and Rousseau,1978).

$$G = G_0(1 + \alpha L) \tag{6.19}$$

The population balance equation is re-written as

$$\frac{\partial n}{\partial t} + G_0\left(\frac{\partial n}{\partial L} + \alpha \frac{\partial (nL)}{\partial L}\right) = 0 \tag{6.20}$$

Therefore, two kinds of Laplace transformations can be applied to the above equation

$$\bar{n}_1(t,s) = \int_0^\infty n(t,L)\exp(-sL)dL \tag{6.21}$$

$$\bar{n}_2(t,s) = \int_0^\infty n(t,L)L\exp(-sL)dL \tag{6.22}$$

Similarly, over a small time interval Δt, G_0 and $n(0)$ can be assumed to be constant and therefore the resulting parameters will have an average value over this time interval. Using initial boundary conditions, the population balance equation can be transformed to a series of multiple-variable linear equations. These equations can be solved to get $\overline{G_0}$, $\alpha\overline{G_0}$ and $\bar{B}$ over the small time interval Δt.

$$\frac{\Delta\bar{n}_1(s,t)}{\Delta t} = -\overline{G_0}s\overline{n_1}(t,s) - \alpha\overline{G_0}s\overline{n_2}(t,s)) + \bar{B} \tag{6.23}$$

6.5 Experimental

A total of eight batch experiments were carried out to measure the crystallization kinetics with 4-hydroxy-2-pyrrolidone in isopropanol using the experimental set-up

described in Chapter 3 (Figure 3.9). Four batch experiments were for R-4-hydroxy-2-pyrrolidone and another four batch experiments were for S-4-hydroxy-2-pyrrolidone. Typical loads of crystallizer were 13.89 g R-4-hydroxy-2-pyrrolidone and 800 ml isopropanol. The operation temperature range was 5-36 ^{o}C. Circa 8-15 ml samples were taken every 15-83 minutes for crystal size distribution, crystal slurry concentration, and solute concentration analyses. The solution concentrations were calculated using mass balance. The crystal size distribution was measured using a Malvern Mastersizer 2000 with a Hydro 2000μP dispersion cell unit. Analytical n-hexane, in which 4-hydroxy-2-pyrrolidone is almost insoluble, was used as the liquid dispersion medium.

6.6 Results: Crystal nucleation and growth kinetics

6.6.1 Crystal suspension density and supersaturation

Four batches of experiment were performed to measure the crystal nucleation and growth kinetics of R-4-hydroxy-2-pyrrolidone. As mentioned in the experimental section, in each run, a series of samples were taken from the crystallizer to analyze the crystal suspension density M_T, the solute concentration c and the crystal size distribution. The obtained M_T and c are listed in Table 6.1 to Table 6.4. The solubility data c* of 4-hydroxy-2-pyrrolidone at each temperature have been measured in Chapter 5. Accordingly, the supersaturation Δc were calculated and listed in the tables. The corresponding concentration profiles of crystal suspension density M_T, solute concentration c and supersaturation Δc are shown in Figure 6.1 to Figure 6.4. In all of the four batch runs, the solute concentration c decreased smoothly and the crystal suspension density M_T increased accordingly. The change of supersaturation Δc was moderate and this supports the constant assumption over a small time interval Δt. Moreover, the

measured crystal suspension density M_T and solute concentration c held a good mass balance for the batch crystallization system.

Table 6.1 Crystallization kinetics measurement (Run1)

Δt (min)	M_T(g/ml)	c (g/g solvent)	T(^oC)	c*(g/g solvent)	Δc (g/g solvent)
0	0.00228	0.0176	19.7	0.011610	0.004790
36	0.00347	0.0161	16.8	0.010548	0.004452
20	0.00472	0.0139	10.7	0.009713	0.004187
18	0.00511	0.0134	9.2	0.009284	0.004116
17	0.00624	0.0120	8.1	0.008983	0.003017
29	0.00673	0.0114	5.8	0.008389	0.003011
28	0.00708	0.0109	4.4	0.008050	0.002850
18	0.00799	0.00975	2.7	0.007659	0.002091

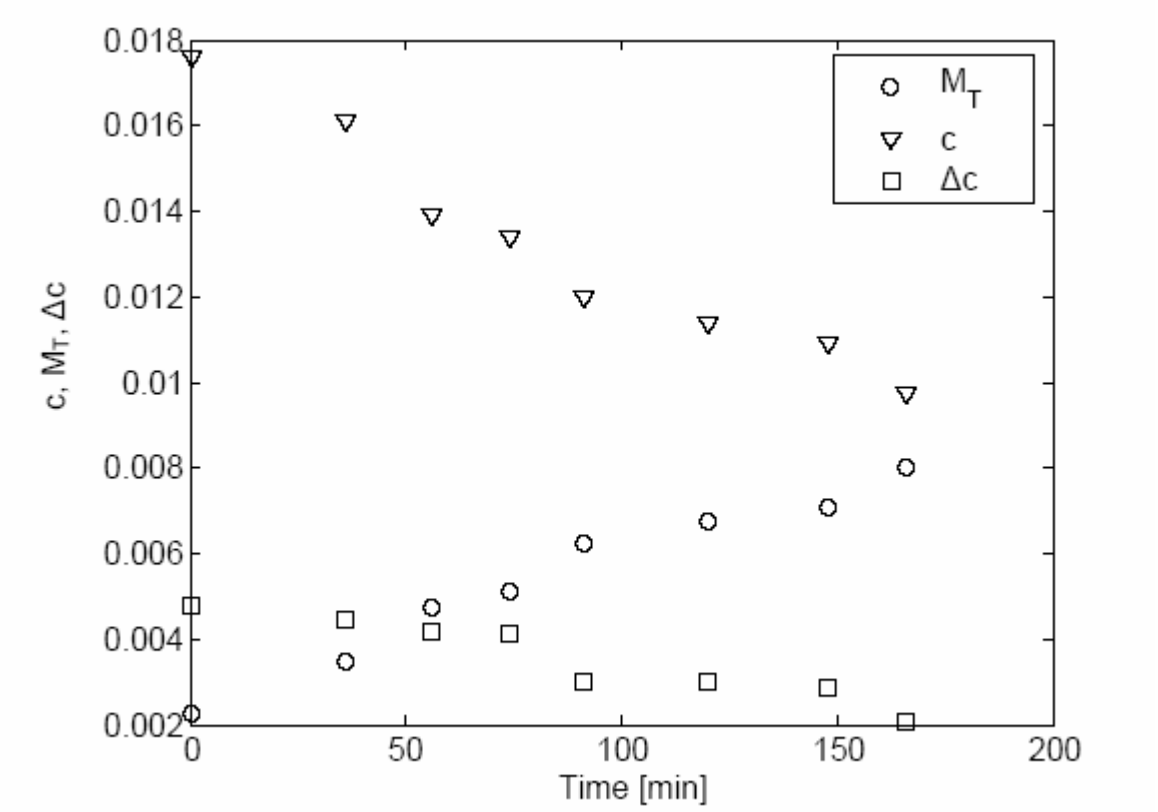

Figure 6.1 Concentration profiles of crystal suspension density M_T, solute concentration c and supersaturation Δc in Run1

Table 6.2 Crystallization kinetics measurement (Run2)

Δt(min)	M_T(g/ml)	C (g/g solvent)	T(^oC)	C*(g/g solvent)	ΔC (g/g solvent)
0	0.00177	0.0183	22.5	0.014031	0.004269
21	0.00223	0.0177	20.8	0.013293	0.004407
33	0.00392	0.0156	18.2	0.012245	0.003355
33	0.00502	0.0142	15.5	0.011254	0.002946
46	0.00737	0.0112	11.8	0.010044	0.001156

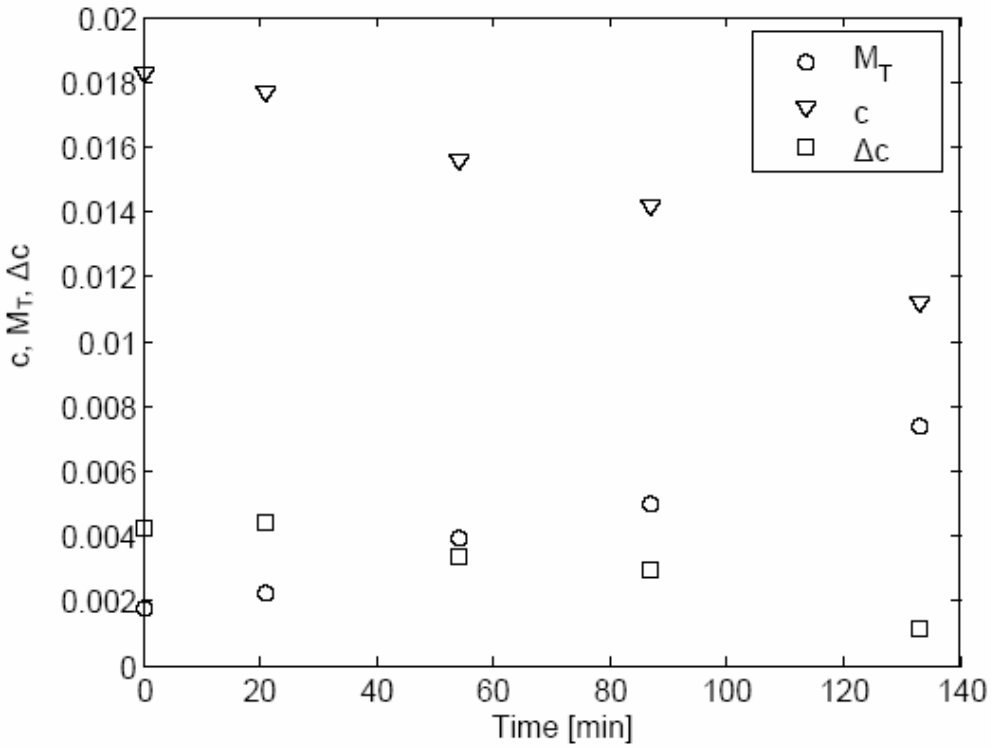

Figure 6.2 Concentration profiles of crystal suspension density M_T, solute concentration c and supersaturation Δc in Run2

Table 6.3 Crystallization kinetics measurement (Run3)

Δt(min)	M_T(g/ml)	C (g/g solvent)	T(^{o}C)	C*(g/g solvent)	ΔC (g/g solvent)
0	0.00230	0.017	20.1	0.013001	0.003999
55	0.00320	0.0158	18.2	0.012245	0.003555
39	0.0041	0.0147	16.9	0.011756	0.002944
42	0.00534	0.0131	15.5	0.011254	0.001846
83	0.00612	0.0121	12.8	0.010355	0.001745

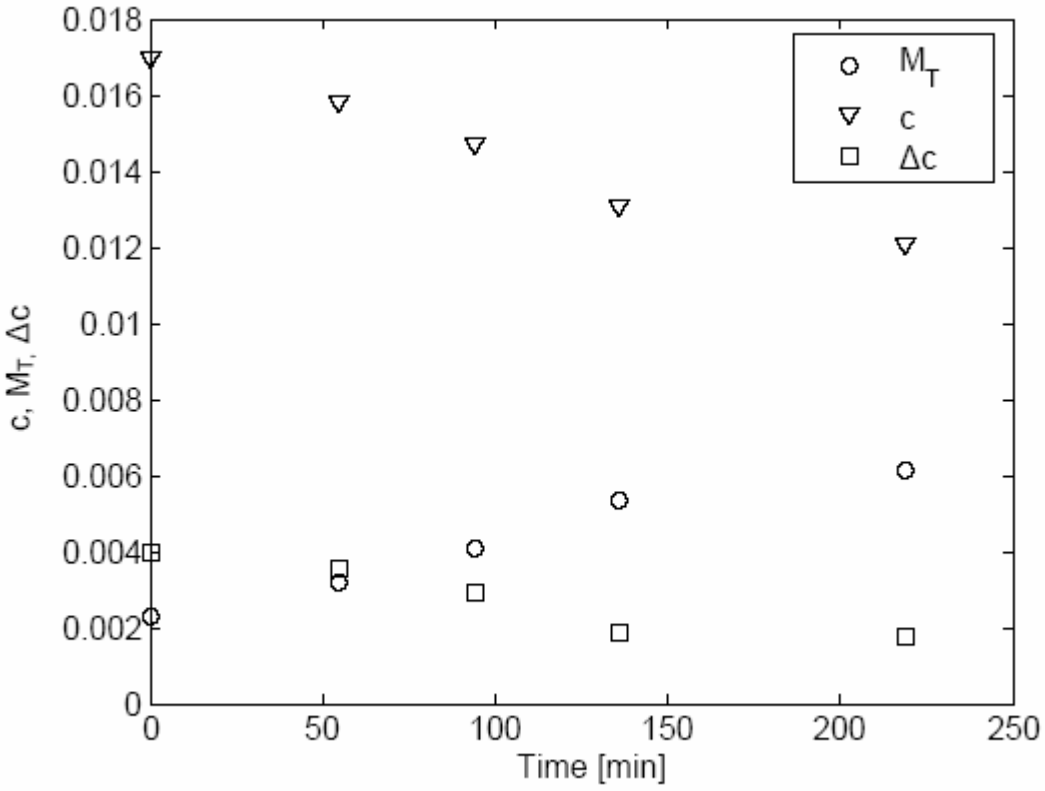

Figure 6.3 Concentration profiles of crystal suspension density M_T, solute concentration c and supersaturation Δc in Run3

Table 6.4 Crystallization kinetics measurement (Run4)

Δt(min)	M_T(g/ml)	C (g/g solvent)	T(^oC)	C*(g/g solvent)	ΔC (g/g solvent)
0	0.00234	0.0169	22.1	0.013853	0.003047
54	0.00319	0.0159	20.1	0.013001	0.002899
61	0.00384	0.0150	13.4	0.010548	0.004452
67	0.00472	0.0139	10.7	0.009713	0.004187

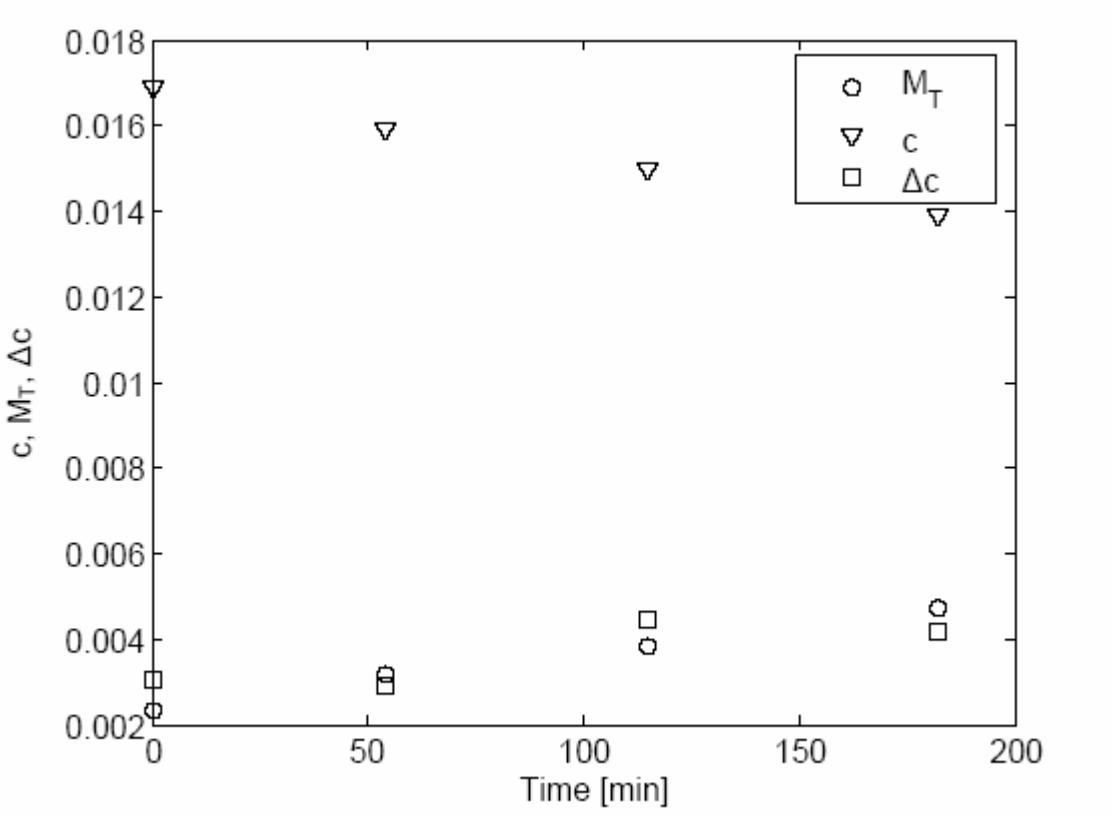

Figure 6. 4 Concentration profiles of crystal suspension density M_T, solute concentration c and supersaturation Δc in Run4

6.6.2 Crystal size distribution (CSD)

The crystal size distribution was measured using a Malvern Mastersizer 2000 with a Hydro 2000μP dispersion cell unit. Fig 6.5 shows typical crystal distribution of two samples collected at two different time in Run 2. The crystal growth can be observed as the volume percentage distribution shifts to the right side of larger size.

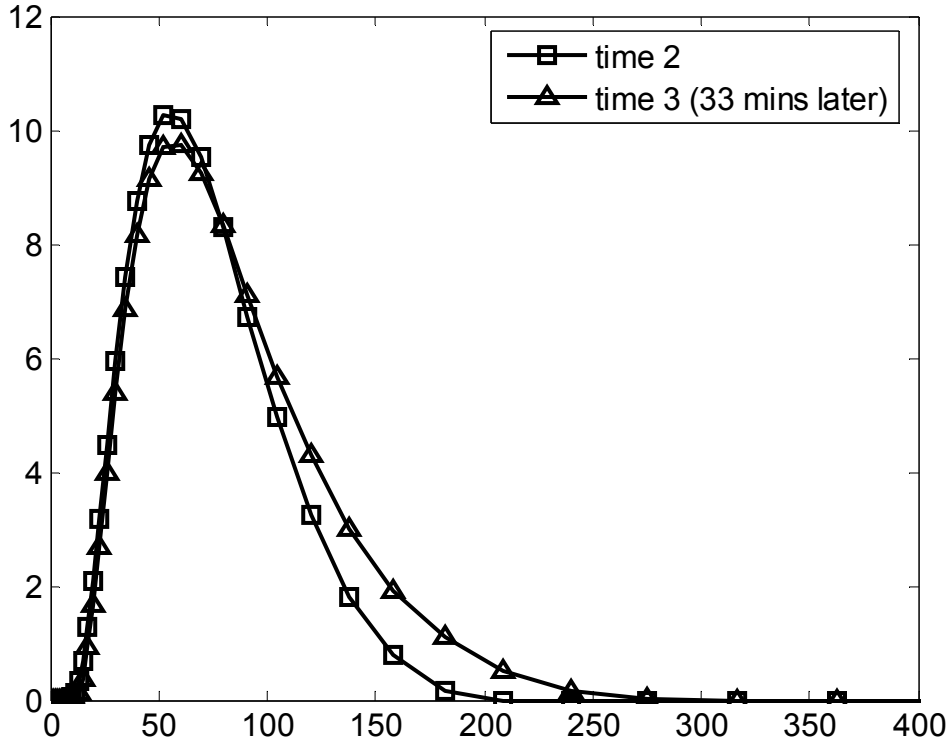

Figure 6.5 Typical crystal size distribution in kinetic measurement

Using the definition of population density *n* (Eq 6.24), Eq 6.26 can be obtained to calculate the population density n with volume percentage data.

$$n = \frac{dN}{dL} \tag{6.24}$$

The number of crystals in the size range is calculated from the mass and shape factor k_V.

$$\Delta N_i = \frac{\Delta M_i}{\rho k_V L_i^3} = \frac{\Delta V_i M_T}{\rho k_V L_i^3} \tag{6.25}$$

Thus the population density is calculated as

$$n = \frac{\Delta N_i}{\Delta L_i} = \frac{\Delta V_i M_T}{\rho k_V \overline{L}_i^3 \Delta L_i} \tag{6.26}$$

where $\overline{L}_i$ is the average crystal size in the given range.

Figure 6.6 shows the typical population density functions versus particle size calculated from crystal size distribution data shown in Figure 6.5. This figure illustrates the characteristic appearance of CSD from a batch crystallizer (Tarvare, 1995). They are quite different from those shown in continuous MSMPR crystallizer, which are normally straight lines on semi-log plot.

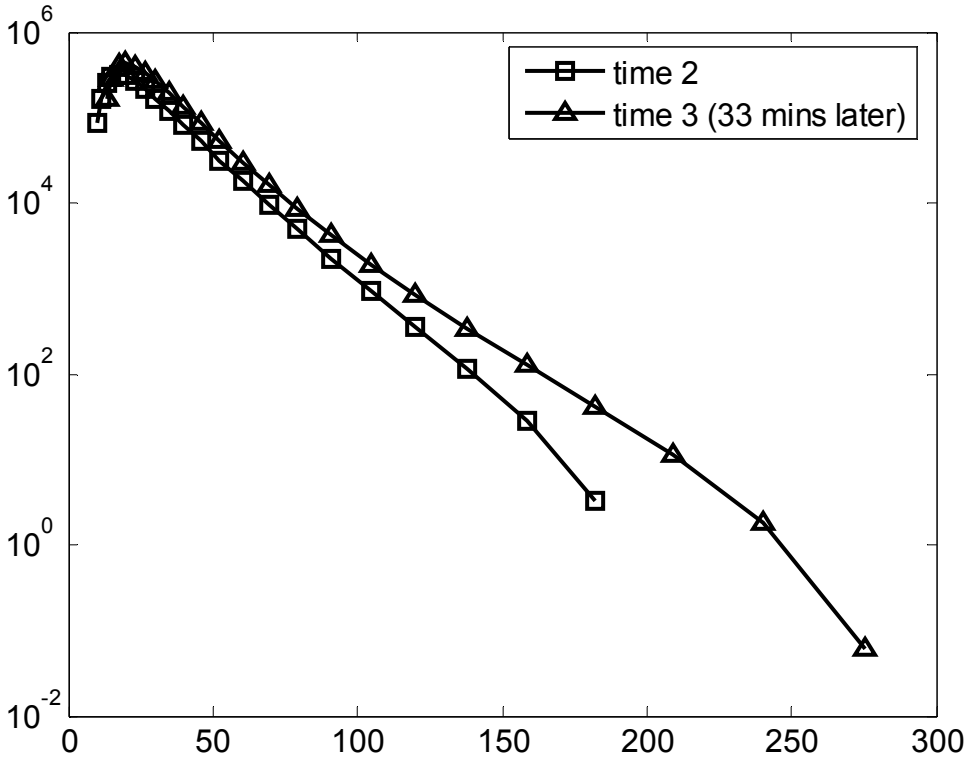

Figure 6.6 Typical crystal population density distribution

6.6.3 s-Plane analysis on the measured data

The Laplace s-plane method described in section 6.3 was used here to estimate the crystal nucleation rate *B* and growth rate *G*. The advantage of Laplace method is to estimate model parameters in the Laplace transform domain rather than in the time domain. From Eq 6.10, it is clear that a suitable value of the Laplace transform variable *s* must be chosen to reduce the sensitivity to experimental errors. As indicated by Tarvare (1995), if *s* is too small, the tail of the response will be heavily weighted. On the other hand, if *s* is too big, too much emphasis will be given to the front portion of the response. In either case, a poor estimate of the weighted moments will result. There should be an optimum value of *s*, which lies between these two limits. The s-plane analysis described

by Tavare and Garside (1986) and Tavare (1995) showed that the limits on the Laplace transform parameter s used should be considered by $s_f L_2 \approx$ 1-2, where L_2 is the population average size at time t_2.

Once s is decided, a fix number of points are chosen over this range s at regular intervals. Here 50 points were used. No further improvement can be obtained with more data points. For each value of s, the Laplace transformed population densities can be calculated as

$$\bar{n}(t_1, s) = \int_0^\infty n(t_1, L)\exp(-sL)dL = \sum n(t_1, L)\exp(-sL)\Delta L \tag{6.26}$$

$$\bar{n}(t_2, s) = \int_0^\infty n(t_2, L)\exp(-sL)dL = \sum n(t_2, L)\exp(-sL)\Delta L \tag{6.27}$$

The s-plane analysis was performed for 50 equally spaced s-values. The results of analysis of two typical sets of data from Run2 and Run3 are shown in Figure 6.7 to Figure 6.10.

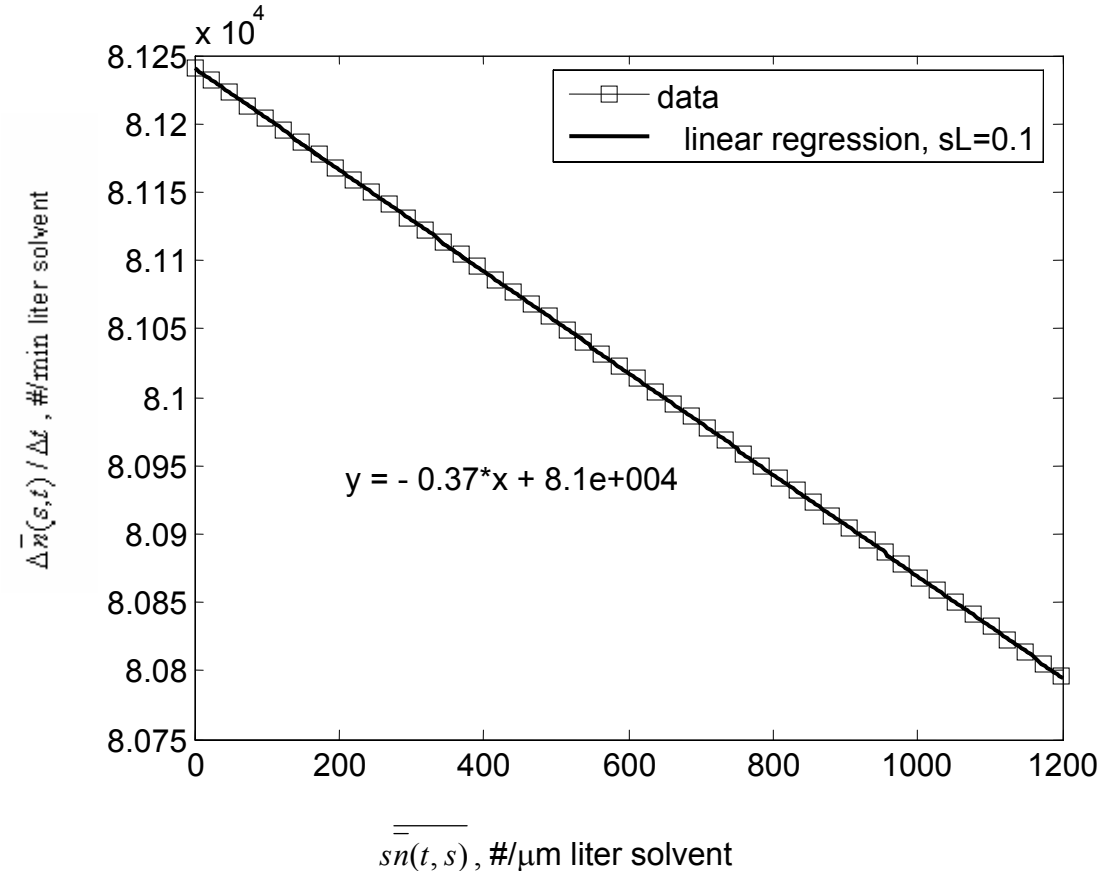

Figure 6.7 s-plane analysis of data in Fig 6.6.
sL=0.1, G=0.37 μm/min, B=8.1×10^4 #/min liter solvent

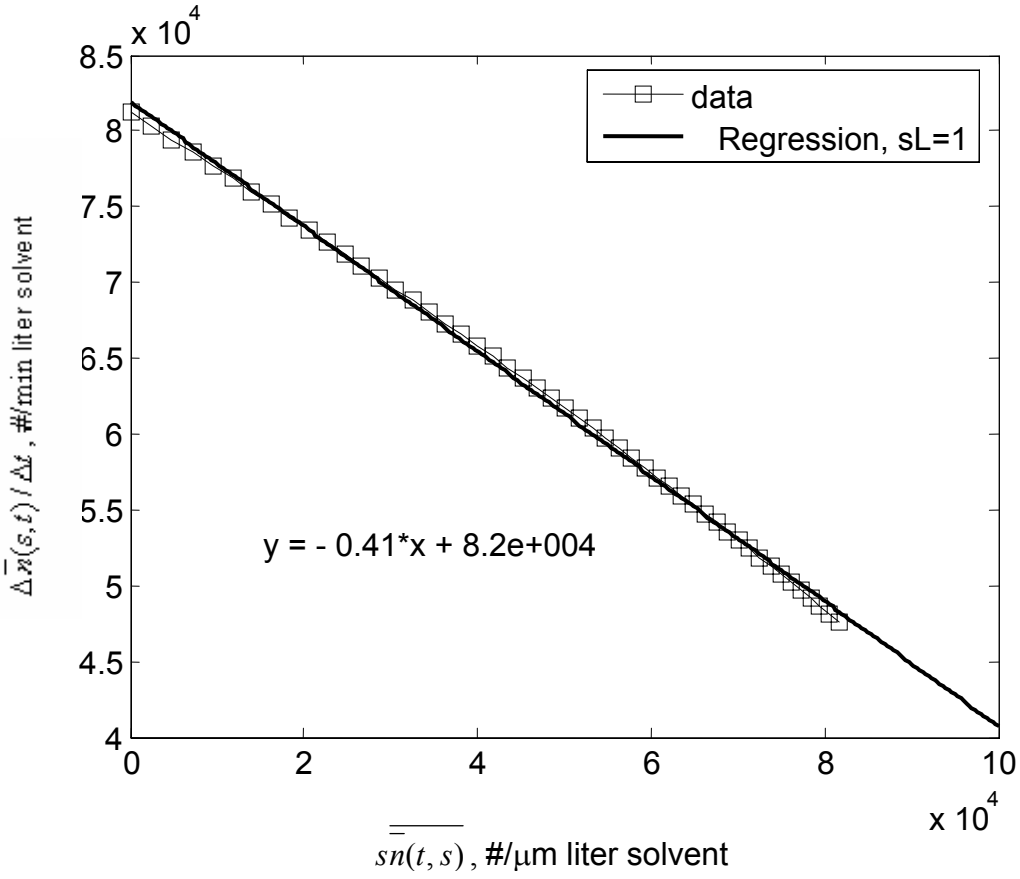

Figure 6.8 s-plane analysis of data in Fig 6.6,
sL=1, G=0.41 μm/min, B=8.2×10^4 #/min liter solvent

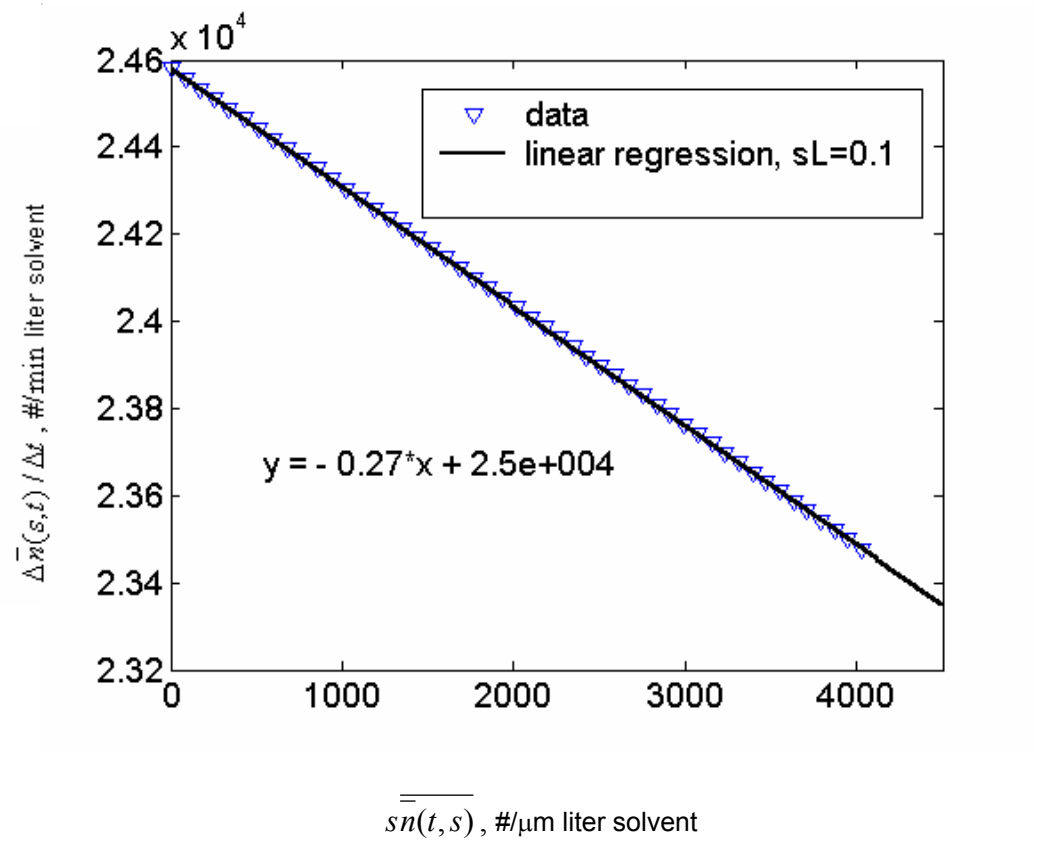

Figure 6.9 Typical s plane analysis to estimate crystal nucleation and growth rates in Run3. sL=0.1, G=0.27 μm/min, B=2.5×10^4 #/min liter solvent

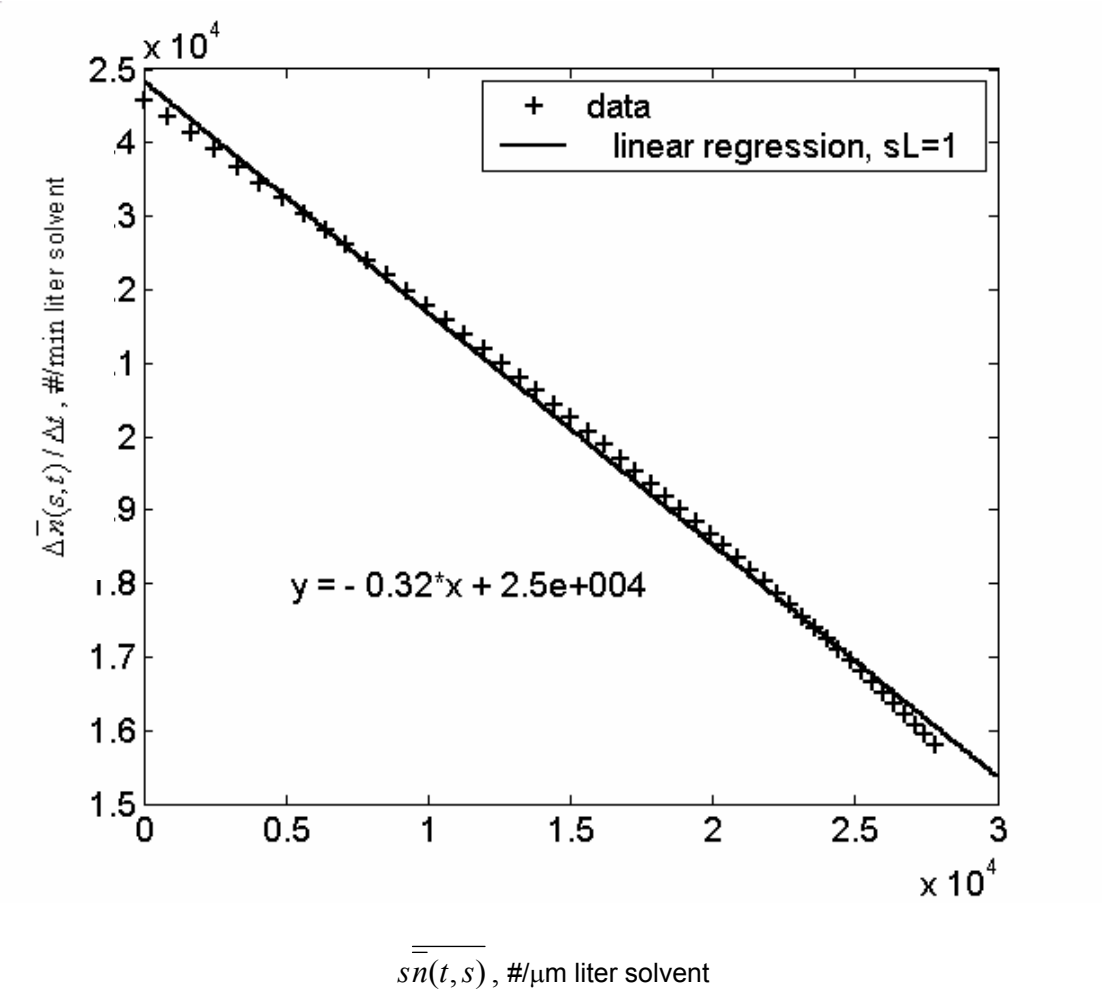

Figure 6.10. s plane analysis to estimate crystal nucleation and growth rates in Run3. sL=1, G=0.32 μm/min, B=2.5×10^4 #/min liter solvent

Our analysis showed that $s_f L_2 \approx 0.05$-0.1 was most suitable, which gave better linear regression with growth rates similar to the independent moment method. This is consistent with the later findings from Garside's group (Jacobsen et al., 1998).

From linear regression, *G* and *B* can be obtained from the slope and intercept respectively. Table 6.5 lists the estimated crystal nucleation rate *B* and growth rate *G* from the four kinetic experiments.

Table 6.5 Estimated crystal nucleation rate B and growth rate G with s plane analysis from the four kinetic experiments.

	G, μm/min	B , #/min·liter solvent	Δc, kg/kg solvent	M_T, kg/liter	T K
Run1	0.18	1.20E+04	0.004572	0.00288	291.3
	0.47	7.70E+04	0.004152	0.00492	282.9
	0.45	6.50E+04	0.003014	0.00649	279.9
	0.11	1.60E+04	0.002471	0.00754	276.6
Run2	0.40	5.70E+04	0.004338	0.00200	294.6
	0.37	8.10E+04	0.003881	0.00308	292.5
	0.16	1.70E+03	0.002051	0.00620	286.6
Run3	0.51	3.70E+04	0.003777	0.00275	292.2
	0.27	2.50E+04	0.003250	0.00365	290.6
	0.10	1.40E+04	0.002045	0.00573	287.2
Run 4	0.26	9.90E+03	0.002108	0.00406	292.2
	0.26	3.00E+05	0.004320	0.00428	285.0

Regression of the data in Table 6.5 with linear least squares provided the following kinetic expressions for the crystal growth and nucleation of R- 4-hydroxy-2-pyrrolidone.

$$B = 3.4 \times 10^6 \times G^{1.9} \times M_T{}^{0.47} \tag{6.28}$$

$$G = 4.4 \times 10^5 \times \exp(-15000/RT) \times \Delta c^{1.35} \tag{6.29}$$

The observed nucleation power dependency 0.47 on the suspended crystal density is lower than those found in industrial inorganic crystallization process. This could be due to the relatively low crystal mass concentration used here. Another possibility is that the primary nucleation occurred especially in the case that the supersaturation was under

somewhat arbitrary control in the kinetic measurement experiments. The power dependency 1.9 on crystal growth rate is comparable to those found in literature (Tavare, 1995; Garside et al., 2002). It appears that the nucleation rate dependency on the temperature could be ignored under present experimental conditions.

The order of the growth rate with respect to supersaturation 1.35 is consistent to those reported. However, the relatively low activation energy 15 kJ/mol indicates that the crystal growth could be more likely to be diffusion controlled (Garside et al, 2002).

The method proposed in Section 6.4 for size-dependent growth considerations (Equation 6.23) was applied to the experimental data. The obtained values α were very small (circa 0.00036) or even negative. The crystal growth size dependency could be therefore negligible here.

6.6.4. Crystallization kinetics of S-4-hydroxy-2-pyrrolidone in isopropanol

The same methodology has been used to estimate the crystal nucleation and growth kinetics of S-4-hydroxy-2-pyrrolidone in isopropanol. Table 6.6 lists the measured crystal growth rates and nucleation rates at different operation conditions.

Table 6.6 Estimated crystal nucleation rate *B* and growth rate *G* for S-4-hydroxy-2-pyrrolidone

	G, μm/min	B , #/min·liter solvent	Δc, kg/kg solvent	M_T, kg/liter	T K
Run1	0.86	1.20E+05	0.007790	0.00167	286.3
	0.78	7.00E+04	0.006965	0.00302	283.9
	0.41	4.10E+04	0.006291	0.00407	281.7
Run2	0.57	1.60E+04	0.007623	0.00120	280.2
	0.41	4.10E+04	0.005131	0.00416	274.8
	0.54	6.00E+04	0.004587	0.00480	273.6
Run3	0.53	5.80E+04	0.005311	0.00134	283.2
	0.28	8.00E+03	0.004700	0.00169	282.4
Run 4	0.2	6.00E+03	0.003885	0.00166	280.6
	0.1	2.00E+03	0.002841	0.00227	278.6

Regression of the data in Table 6.6 with linear least squares provided the following kinetic expressions for the crystal growth and nucleation of S- 4-hydroxy-2-pyrrolidone. It is not surprising to see that the results are in good agreement with that of its isomer. This is again consistent with the identical physical properties of two enantiomers (Collet et al., 1980; Jacques et al., 1994).

$$B = 4.4 \times 10^6 \times G^{1.85} \times M_T{}^{0.57} \tag{6.30}$$

$$G = 5.7 \times 10^5 \times \exp(-19000 / RT) \times \Delta c^{1.1} \tag{6.31}$$

6.7 Summary

Eight batches of crystallization kinetics measurements have been performed to determine the crystal nucleation and growth kinetics of R- 4-hydroxy-2-pyrrolidone and S-4-hydroxy-2-pyrrolidone in isopropanol. The two enantiomers show similar characteristics in crystal nucleation and growth. The Laplace transform method was successfully developed and applied to the estimation of crystallization kinetics. A more suitable Laplace transform variable *s* range was employed for current crystallization system. The size dependence of crystal growth was found negligible with using modified *s*-plane approach. The crystal nucleation rate seems independent on the experimental temperature range. These crystallization kinetics data will be used to guide the supersaturation control in the preferential crystallization of 4-hydroxy-2-pyrrolidone in isopropanol.

Part of results in this chapter has been reported on Chemical Engineering Science (Vol 61, pp.2406-2417. 2006)

CHAPTER 7 OPTIMAL OPERATION OF PREFERENTIAL CRYSTALLIZATION OF 4-HYDROXY-2-PYRROLIDONE IN ISOPROPANOL

7.1 Introduction

In Chapter 4 and Chapter 5, the thermodynamics properties of 4-hydroxy-2-pyrrolidone in isopropanol have been studied. The crystal nucleation and growth kinetics have been measured in Chapter 6. With the mastery of these factors that control the rate difference of crystallization between the two enantiomers, this chapter combined and applied them in the optimal control and in-situ monitoring of preferential crystallization.

From the thermodynamics issue, in order to avoid spontaneous nucleation of the undesired enantiomer, its upper limit of supersaturation is within its metastable zone. In this aspect, the solubility diagrams and supersaturation data are the thermodynamic basis for preferential crystallization for the racemic conglomerates (Jacques et al., 1994; Collet, 1999).

As mentioned in Chapter 1, it is also important to control the supersaturation of the target enantiomer. This can be elaborated in the following three aspects. (i) Firstly, this supersaturation should be kept at least within its metastable zone to prevent spontaneous nucleation of the target enantiomer. Most of the preferential crystallization processes are run with only a slight excess of the target enantiomer and the concentrations of the two

enantiomers are quite close. Considering the identical physical properties of the two isomers in solutions, the spontaneous nucleation is expected to occur simultaneously for both enantiomers, which implies that the spontaneous nucleation of the target enantiomer could initiate the nucleation of the unwanted isomer. This is the most important issue that should be avoided in the chiral resolution by direct crystallization (Jacques et al., 1994; Collet, 1999).

(ii) Secondly, the supersaturation of the target product should be kept further lower than its spontaneous nucleation metastable zone. In Chapter 5, the metastable zone width measurement and nucleation analysis indicate that there exists a critical supersaturation level beyond which the nucleation of unwanted isomer could occur. In fact, if high supersaturations within the metastable zone are used, some conglomerates will form crystals that contain domains of both lattices in a single crystal, which means that the enantiomerically pure seed could nucleate the other enantiomer at its surface. One typical example is in the resolution of a racemic chiral ketone (Black et al., 1989; Collins et al., 1997), where the nucleation of the unwanted isomer disappeared only under very low supersaturation (1 ^{o}C undercooling). This phenomenon at higher supersaturation was also observed on β-phenylglyceric acid (Furberg and Hassel, 1950). In the studies of the stability of the supersaturation state of DL-serine m-xylene-4-sulfonate dehydrate (Hongo et al., 1981), two metastable regions were identified where the supersaturation was relatively unstable in the second region. In the studies of nuclei breeding from a chiral crystal seed of $NaClO_3$ (Denk and Botsaris, 1972; Kondepudi et al., 1990, 1993, 1995; Yokota and Toyokura, 1992; Qian and Botsaris, 1997, 1998; McBride and Carter, 1991), it was found that at low supersaturation all nuclei were of the same chirality. At relatively high supercooling, but still lower than the critical value for spontaneous nucleation, many

nuclei with opposite chirality to that of seed were formed. Davey et al. (1990) also showed the similar findings in triazolylketone chiral crystallization. The Embryos Coagulation Secondary Nucleation (ECSN) mechanism was applied to explanation of the phenomenon (Qian and Botsaris, 1998). Both the second metastable zone and critical supersaturation indicate the importance of controlling the supersaturation to a critical extent to inhibit the nucleation of the undesired enantiomer during preferential crystallization.

(iii) Finally, the crystal size distribution (CSD) is an important factor not only for the production of high-quality products, but also for determining the efficiency of downstream operations, such as filtration and washing. The advantages of controlling the supersaturation in batch crystallization have been extensively shown (Mullin and Nyvlt, 1971; Jones and Mullin 1974; Rohani and Bourne, 1990). With good control of the supersaturation, larger crystals with narrower crystal size distribution can be obtained, which means product purity could be improved in the downstream filtration and washing process (Mersmann, 1995; Matthews and Rawlings, 1998; Rodriguez-Hornedo and Murphy, 1999). This is especially important for chiral purification (Courvoisier et al., 2002, 2003). Reflecting upon the above considerations, it is important to control the supersaturation of the target enantiomer in preferential crystallization process.

Numerous efforts have been reported on optimal operation of batch crystallizer. Mullin and Nyvlt (1971), Jones(1974), and Jones and Mullin (1974) did the pioneer work both theoretically and experimentally. Mayrhofer and Nyvlt (1988) dealt with a general derivation of a theoretical cooling curve of a batch crystallizer. Rohani and Bourne (1990) derived a simplified optimal cooling curve by assuming constant nucleation and supersaturation. Various objectives have been chosen to optimize batch crystallization, such as mean crystal size and coefficient of variation (Chianese et al., 1984; Choong and

Smith, 2004; Costa and Maciel Filho, 2005), seed ratio (Bohlin and Rasmuson, 1992; Matthews and Rawlings, 1998; Chung et al., 1999), and even shape (Ma et al., 2002).

In order to control the supersaturation, with the thermodynamics data, crystal nucleation and growth kinetics, the population balance model is needed to predict the concentration profiles (Randolph and Larson, 1988). The newly developed on-line monitoring techniques such as FBRM greatly facilitate these investigations (Barrett and Glennon, 2002; Elsner et al., 2005).

7.2 Mathematic model in batch crystallization

7.2.1 Population balance equation

The classical population balance equation (Randolph and Larson, 1988) is normally employed to describe the complex crystallization process. For a batch crystallizer, some general assumptions are made in order to simplify the mathematical model.

i. The crystallization process proceeds in a batch crystallizer without input or output.

ii. Crystal agglomeration and breakage are negligible.

iii. The crystals in the crystallizer are well suspended without accumulation of crystals.

iv. Crystal nuclei have negligible size.

With the above assumptions, the population balance is

$$\frac{\partial n(L,t)}{\partial t} + \frac{\partial [G(L,t)n(L,t)]}{\partial L} = 0 \tag{7.1}$$

where n is the population density of crystals and G is the crystal growth rate .

The boundary condition for this partial differential equation is

$$n(L_0 = 0, t) = \frac{B^o}{G\big|_{L=0}} \tag{7.2}$$

where B^o is the rate of formation of new crystals (nucleation rate) at size of L_0=0.

7.2.2 Crystallization kinetics

From the population balance equation, it is known that crystal nucleation and growth kinetics appear as the boundary condition. As mentioned in Chapter 6, empirical correlations of crystallization kinetics are often expressed using power laws.

$$B(t) = k_b \exp[-G_b / RT(t)] G(L,t)^i M_T{}^j \tag{7.3}$$

$$G(L,t) = k_g \exp[-G_g / RT(t)] \Delta c(t)^g \tag{7.4}$$

where M_T is the crystal suspension density and the supersateration Δc is the difference of the real concentration c(t) and the solubility c* at temperature $T(t)$

$$\Delta c(t) = c(t) - c^*(T(t)) \tag{7.5}$$

7.2.3 Mass balance equation

Since the crystal growth and nucleation rate are dependent on solute concentration and temperature, mass and energy balances are required to complete the description of crystallization process.

For a batch crystallizer, the mass balance can be made based on the solute.

$$c(t)V(t) + M_T(t)V(t) = c_0V_0 \tag{7.6}$$

where c is the solute concentration and V is the volume of slurry.

Under the assumption that the slurry volume remains constant during crystallization, the mass balance is re-written as

$$\frac{dc(t)}{dt} = -\frac{dM_T(t)}{dt} \tag{7.7}$$

If m_3 is defined as the 3rd moment of crystal size distribution,

$$m_3 = \int_0^\infty nL^3 dL \tag{7.8}$$

then the crystal suspension density M_T can be replaced as

$$M_T = \rho k_V m_3 \tag{7.9}$$

where ρ is the crystal density and k_V is its shape factor.

Therefore, the mass balance equation can be re-written as

$$\frac{dc(t)}{dt} = -\rho k_V \frac{dm_3(t)}{dt} \tag{7.10}$$

The necessary initial conditions are

$$c(0) = c_0 \tag{7.11}$$

$$m_3(0) = m_0 \tag{7.12}$$

7.2.4 Energy balance

If the shaft work is assumed negligible, the rate of change of the enthalpy of the crystallizer magma *h(t)* is given by

$$\frac{dh(t)}{dt} = -q + k_V W(-\Delta H)\frac{dm_3(t)}{dt} \tag{7.13}$$

The first term on the right-hand side is the rate of cooling, while the second term is the enthalpy rate change due to the heat of crystallization. The second term is often negligible compared to the rate of cooling.

All the equations given above form a set of nonlinear integro-differential equations for a batch crystallizer. Analytical solutions do not exist. Numerical methods are required to solve the problems.

7.3 Model solution

7.3.1 Moment method

The moment transformation approach is the most common method used to replace the partial differential equations by a set of ordinary differential equations, which simplifies the simulation and optimization of the batch crystallizer. Multiplying Equation 7.1 by L^j, integrating over L, and placing on a per-mass-of-solvent basis (Hulburt and Katz, 1964), the moment equations can be derived as

$$\frac{dm_0}{dt} = B \tag{7.14}$$

If the crystal growth is size independent,

$$\frac{dm_j}{dt} = jGm_{j-1} + BL_0{}^j \tag{7.15}$$

If the crystal growth rate is dependent on crystal size and the expression proposed by Randolph and Larson (1988) is used as

$$G = G_0(1 + \alpha L) \tag{7.16}$$

where α is a model parameter. Then the moment equations are given in following format

$$\frac{dm_j}{dt} = jG(m_{j-1} + \alpha m_j) + BL_0{}^j \tag{7.17}$$

Various numerical methods have been proposed to solve specific models on a case-by-case basis. Rawlings et al. (1993) had a good review on this aspect. It was also indicated that the recovery of the crystal size distribution (CSD) from the quantities resulting from this transformation was difficult and accordingly the use of second moment of the distribution for mass and energy balances were suggested.

In a special case for moment transformations, Mayrhofer and Nylt (1988) presented a good analysis of the programmed cooling batch crystallizers, starting with the solution of the momentum equations of the population balance.

In a batch crystallizer, it is assumed (i) crystal growth rate *G* is constant and (ii) crystal nucleation rate *B* is constant. The assumption (i) is useful for mathematical simplification, which results in a moderate supersaturation rise with the temperature

falling. Crystal growth rate generally diminishes with falling temperature but this drop could be compensated by the supersaturation rise. A similar consideration also holds for nucleation rate.

Under these considerations, the moment transformation equations can be rewritten as

$$\frac{dN_c}{dt} = B \tag{7.18}$$

$$\frac{dL_c}{dt} = N_c G \tag{7.19}$$

$$\frac{dA_c}{dt} = 2\beta L_c G \tag{7.20}$$

$$\frac{dM_c}{dt} = 3k_V \rho A_c G / \beta \tag{7.21}$$

where N_c is the crystal numbers, A_c is the surface area of the crystals, and β is the surface factor.

The momentum equations 7.18 –7.21 can be solved and combined with mass balance equation to get the temperature profile at constant supersaturation for the time $0 \leq t \leq t_c$, where N_0 is the initial seed numbers and the solubility is linearly dependent on temperature.

$$(T_0 - T)/(T_0 - T_f) = (t/t_c)^3[1 - K(1 - t/t_c)] \tag{7.22}$$

$$K = [1 + 4N_0/(Bt_c)]^{-1} \tag{7.23}$$

If the nucleation is negligible compared to seeding, which means K→0, then the above Equation 7.22 simplifies to a similar equation reported by Nyvlt and Vaclavu (1964).

$$(T_0 - T)/(T_0 - T_f) = (t/t_c)^3 \tag{7.24}$$

On the other hand, if nucleation is prevailing (no seeding) in the process, which means K→1, the following equation is readily obtained.

$$(T_0 - T)/(T_0 - T_f) = (t/t_c)^4 \tag{7.25}$$

This relationship has been discussed earlier (Nyvlt, et al., 1973; Nyvlt, 1983).This model determines the optimum cooling curve for a batch crystallizer with an arbitrary seeding and nucleation ratio. Indeed, as shown in Figure 7.1, for different K values, there is no significant difference in the cooling trend. Choong and Smith (2004) showed that the optional cooling profiles were normally convex curves in batch crystallizers.

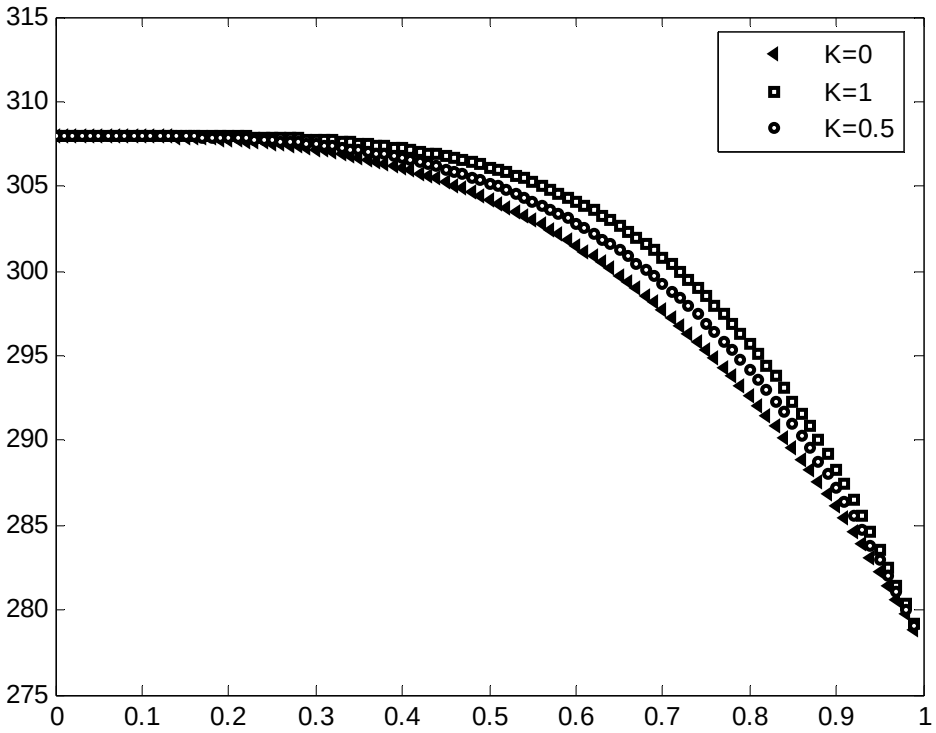

Figure 7.1 Typical convex cooling curves from Equation 7.22

7.3.2 Orthogonal collocation method

The orthogonal collocation method is very efficient for solving differential equations (Villadsen and Michelsen,1978). Miller (1993) discussed the application of orthogonal collocation with Lagrange polynomials in solving population balance equations. Hu et al. (2004) used the orthogonal collocation method to discrete the population density along the size for batch crystallization and successfully applied it in nonlinear kinetic parameter estimation from batch cooling seeded crystallization.

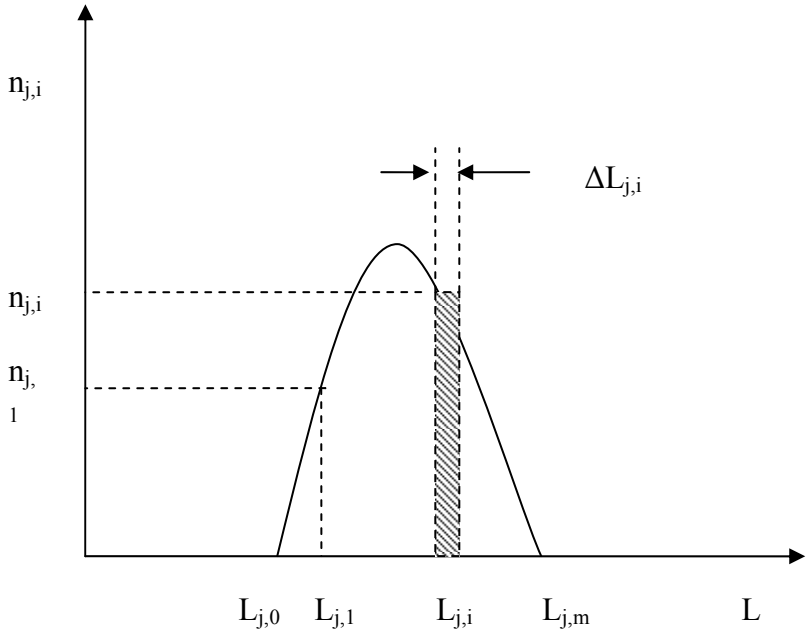

Figure 7.2 Population density discretization

As shown in Fig 7.2, the batch time period is divided into k time steps, each with length of Δt. At the time $t=j\,\Delta t$, m+1 points are chosen to calculate the population density for the time $t= (j+1)\Delta t$, with the size $L_{j,0}, L_{j,1}, \ldots, L_{j,m}$ and population densities $n_{j,0}, n_{j,1}, \ldots, n_{j,m}$. The first index (j=0,1,…,k) denotes the time interval number and the second index indicates the series number of points of the crystal size distribution.

In the case that crystal breakage and agglomeration are neglected, for seeded crystals, it was shown by Hu et al.(2004) that

$$\widetilde{n}_{j+1,i} = \frac{\widetilde{n}_{j,i}}{1+\left.\dfrac{\partial G(L,t)}{\partial L}\right|_{L=L_{j,i},\,t=j\Delta t}\Delta t} \tag{7.26}$$

It was thus proved that the solution of the above finite-difference analog converges to the solution of the population balance equation if Δt approaches to zero.

Crystal size L can be expressed as

$$L_{j+1,i} \approx G(L_{j,i}, j)\Delta t + L_{j,i} \tag{7.27}$$

Since the seed size distribution is known, $n_{0,i}$ and $L_{0,i}$ are available. Therefore, $n_{j+1,i}$ and $L_{j+1,i}$ for j=0,1,…,k-1 and i=0,1,…,m-1, can be solved iteratively by the above equations 7.26 and 7.27.

For the newly formed crystals, it is assumed that the secondary nuclei have the same growth behavior as that of seed crystals. The similar approach can be applied to obtain

$$n_{j+1,i} = \frac{n_{j,i-1}}{1 + \left.\frac{\partial G(L,t)}{\partial L}\right|_{L=L_{j,i-1},t=j\Delta t} \Delta t} \tag{7.28}$$

for j=0,1,…,k-1 and i=0,1,…,j+1, with the boundary conditions of Equation 7.2 and $L_{j,0}$=0.

7.4 Optimal operation profile of 4-hydroxy-2-pyrrolidone preferential crystallization in isopropanol

As highlighted in the introduction, it is paramount to control supersaturation within a critical value in preferential crystallization process to avoid spontaneous nucleation of both enantiomers, to inhibit possible secondary initiated nucleation of undesired isomer when the supersaturation surpasses a critical range, and to obtain good crystal size distribution. Several works have mentioned supersaturation effects in preferential crystallization process (Hongo et al., 1981; Ndzié et al., 1997; Collins et al., 1997; Beilles

et al., 2001; Courvoisier et al., 2003), but no effort has been reported to control the critical supersaturation in preferential crystallization.

7.4.1 Methodology

As discussed in Section 7.3, the orthogonal collocation method is very efficient for solving differential equations. It was developed and used here to predict the cooling profile to control the supersaturation in preferential crystallization of 4-hydroxy-2-pyrrolidone in isopropanol.

For seed crystals,

$$\tilde{n}_{j+1,i} = \frac{\tilde{n}_{j,i}}{1 + \left.\frac{\partial G(L,t)}{\partial L}\right|_{L=L_{j,i},t=j\Delta t} \Delta t} \tag{7.29}$$

For newly formed crystals,

$$n_{j+1,i} = \frac{n_{j,i-1}}{1 + \left.\frac{\partial G(L,t)}{\partial L}\right|_{L=L_{j,i-1},t=j\Delta t} \Delta t} \tag{7.30}$$

Crystal size L can be expressed as

$$L_{j+1,i} \approx G(L_{j,i}, j)\Delta t + L_{j,i} \tag{7.31}$$

The boundary condition is

$$n(L_0 = 0, t) = \frac{B^o}{G\big|L = 0} \tag{7.32}$$

Crystallization kinetics

$$B = 3.4 \times 10^6 \times G^{1.9} \times M_T{}^{0.47} \tag{7.33}$$

$$G = 4.4 \times 10^5 \times \exp(-15000 / RT) \times \Delta c^{1.35} \tag{7.34}$$

$$\Delta c(t) = c(t) - c^*(T(t)) \tag{7.35}$$

It was known that the recovery of the crystal size distribution (CSD) from the quantities resulting from this transformation was difficult (Rawlings et al., 1993). Therefore, here the second moment of the distribution was used for mass balances, where h is a conversion factor equal to the volume of slurry per mass of solvent.

$$\frac{dc(t)}{dt} = -3\rho k_V hGm_2 \tag{7.36}$$

Solubility equation was obtained in Chapter 5,

$$c^*(T) = 0.007227 + 0.000139(T - 273) + 8 \times 10^{-6}(T - 273)^2 \tag{7.37}$$

The above equations are combined together to obtain temperature profile for a given supersaturation Δc.

7.4.2 Thermodynamics considerations

A saturated solution of 20%ee R-enantiomer was used as the starting point to illustrate how to apply the above equations to control the supersaturation during the preferential crystallization by using the thermodynamics data and crystallization kinetics.

From the solubility data (Chapter 5, Figure 5.3), the starting temperature T_0 is circa 35 ^oC. After seeding with R-enantiomer crystals, the solution can be cooled down until circa 18 ^oC where the solution tends to be racemic RS (0% ee). In this region, only R-enantiomer is supersaturated. Based on the MSZW data (Chapter 5, Figures 5.5-5.11), the supersaturation should be kept within circa 7 ^oC to avoid spontaneous nucleation. Figure 5.7 indicates that the applicable supersaturation for S-enantiomer is 7-18 ^oC. Therefore it is acceptable to set the final targeted temperature at circa 5 ^oC.

It should be noted that MSZW were measured under homogenous condition and they should be narrower in the real world as large amount of crystals existed in the seeded preferential crystallization. More importantly, as discussed before, at relatively high supercooling, but still lower than the critical value for spontaneous nucleation supercooling, many nuclei with opposite chirality to that of seed could form. Hongo et al. (1981) also pointed out that the supersaturated solution was unstable in a relatively higher second metastable region. Therefore, the supersaturation should be kept even low.

7.4.3 Optimal cooling profile

As all the above factors are taken into considerations, a critical range of 2-3 ^oC (the corresponding Δc= 0.001-0.0015 kg/kg solvent) was first chosen as the control objective. The time interval used is 12 s. The simulation process showed that the orthogonal collocation method combined with the second moment approach is good enough for this batch cooling crystallization process.

Fig 7.3 shows the calculated temperature profile with respect to time when Δc= 0.0015 kg/kg solvent was used. It is a typical cooling curve for batch crystallizer and is comparable to the cooling profiles in other systems (Rohani and Bourne, 1990; Matthews

and Rawlings, 1998). The initial temperature decreases very slowly to prohibit unwanted nucleation while the temperature decreasing trend accelerates with time.

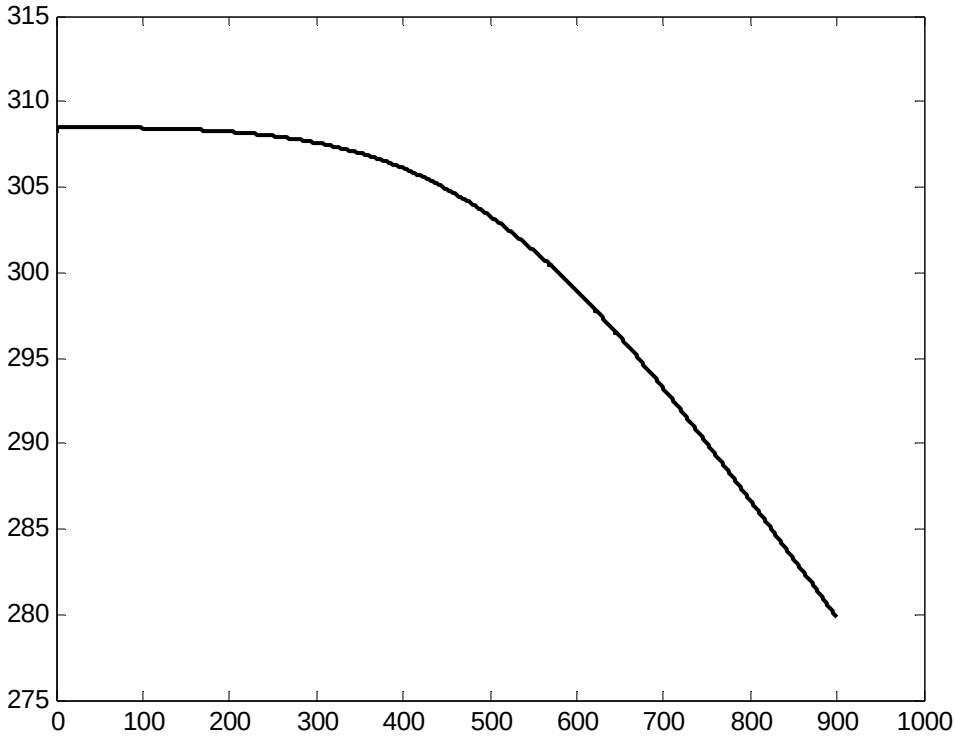

Figure 7.3 The simulated optimal cooling profile for Δc= 0.0015 kg/kg solvent

The calculated crystal population density distribution is shown in Figure 7.4. As mentioned in Chapter 6, the crystal growth rate for this system is size independent. Therefore, the seed distribution does not change the shape and it simply moves forward along the crystal size. The newly formed crystals from nucleation are also clearly shown in Figure 7.4. Accordingly, the simulated crystal size distribution at the final time is presented in Figure 7.5, where it clearly indicates the final product is composed of seeded crystals and newly formed crystals. The simulated results are comparable to other system

with similar method (Hu et al., 2005). The variations of solute concentration and crystal suspension density are reflected in Figure 7.6 and Figure 7.7, respectively.

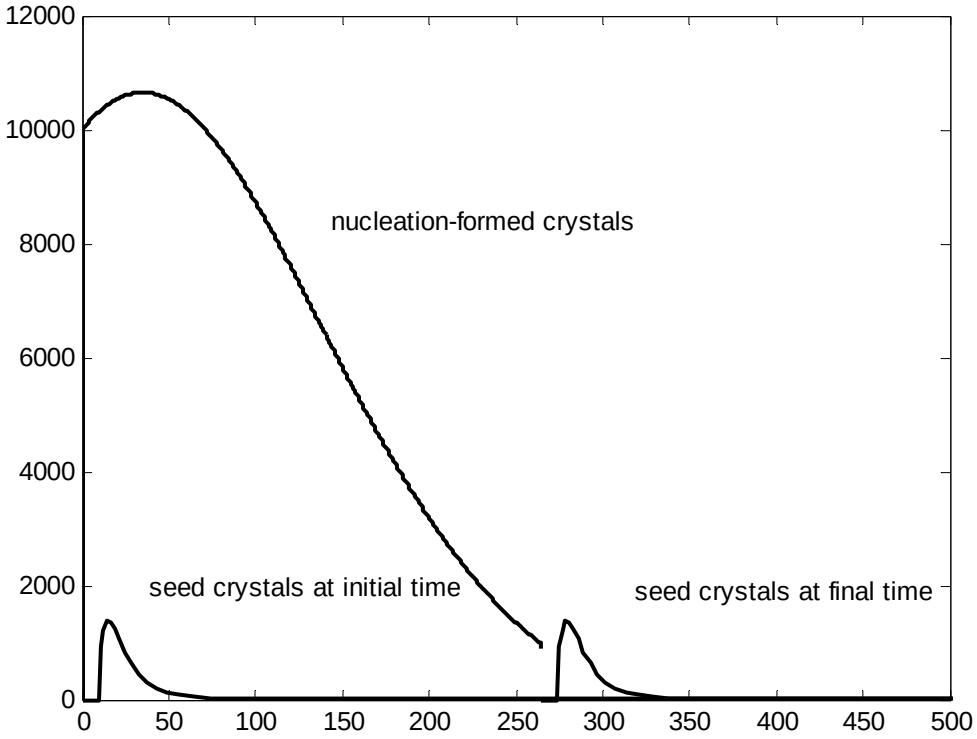

Figure 7.4 Simulated crystal population density distribution, $\Delta c = 0.0015$ kg/kg solvent

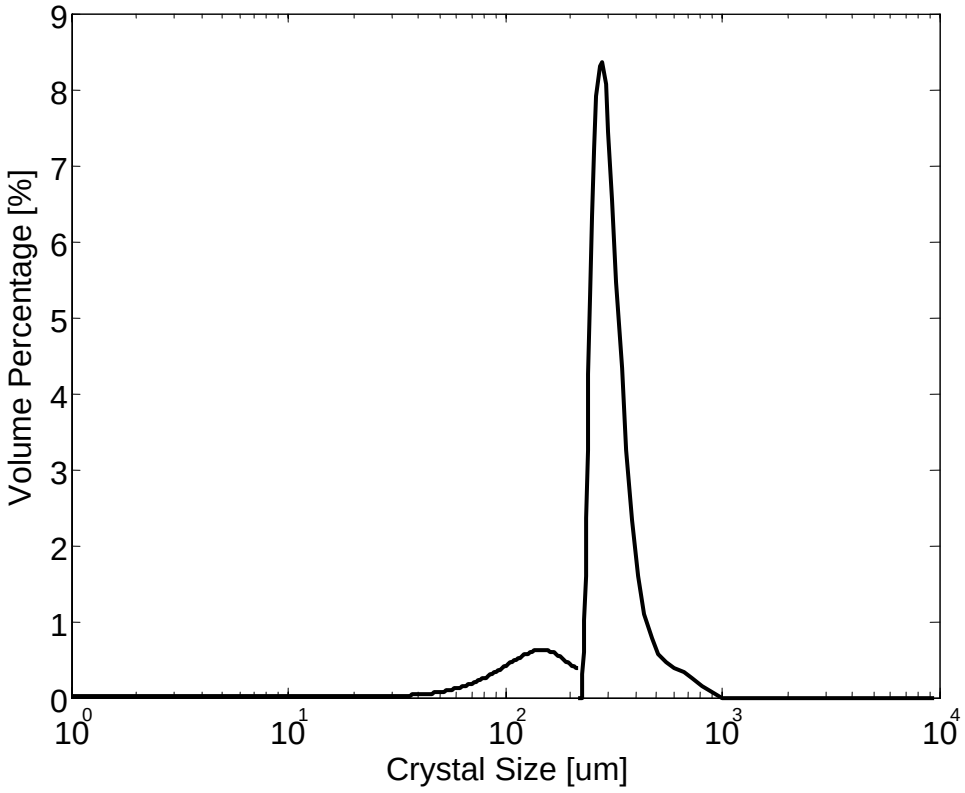

Figure 7.5 Simulated final crystal size distribution, $\Delta c = 0.0015$ kg/kg solvent

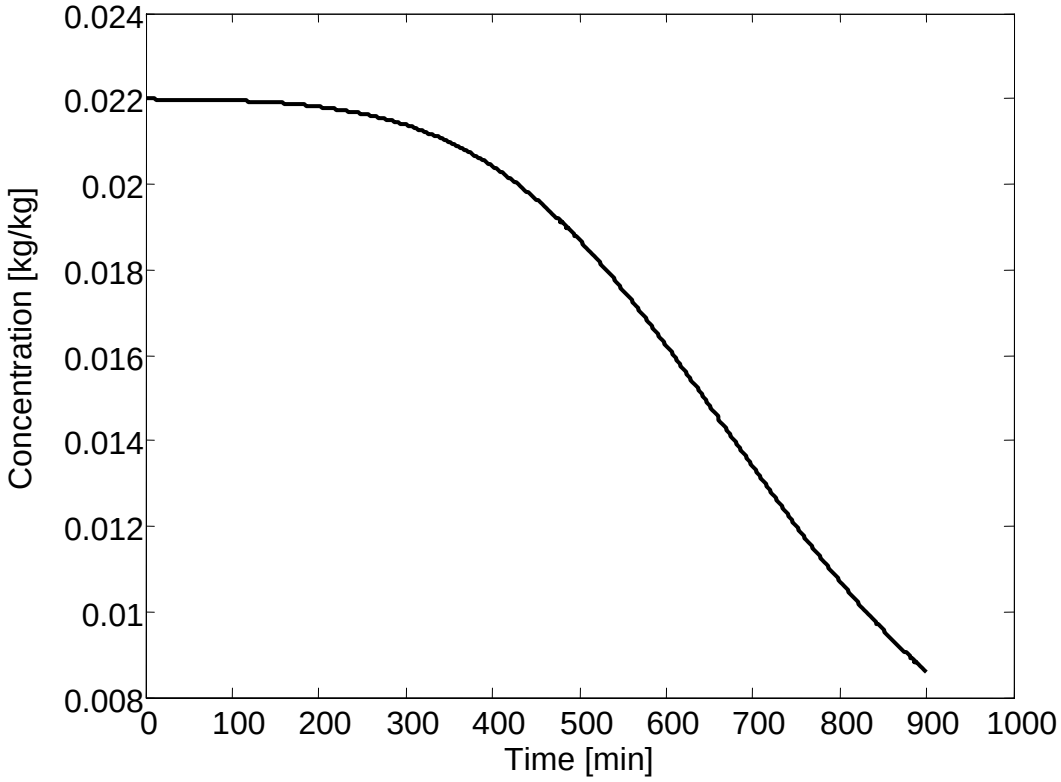

Figure 7.6 Concentration with time, Δc= 0.0015 kg/kg solvent

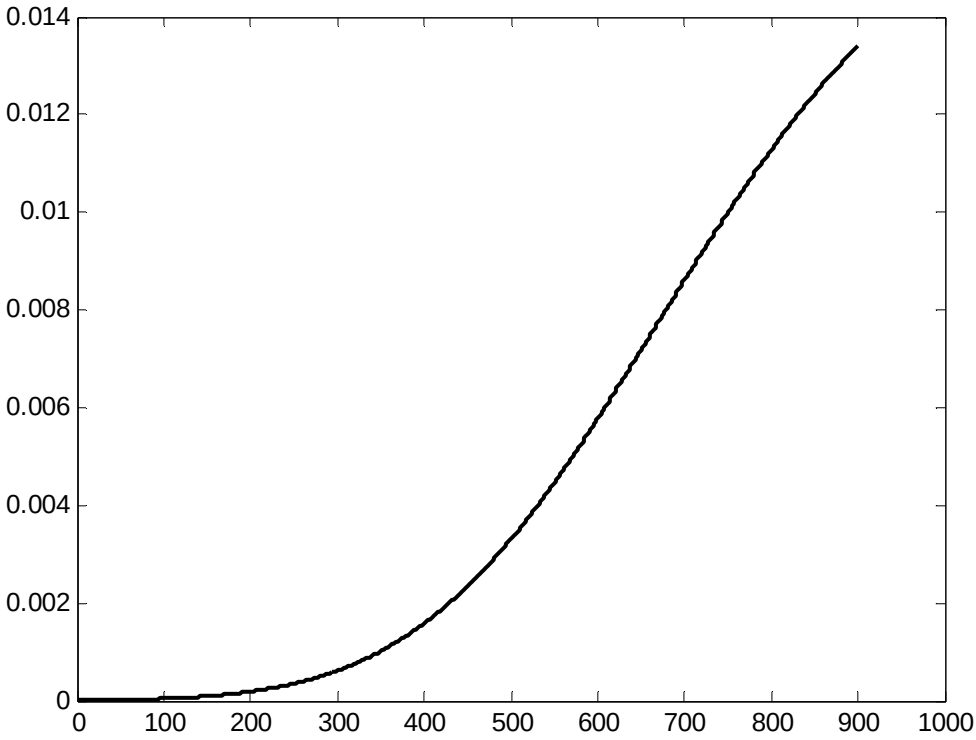

Figure 7.7 Crystal slurry suspension density with time

For the supersaturation control in preferential crystallization of 4-hydroxy-2-pyrrolidone, the simplified approach proposed by Mayrhofer and Nyvlt (1988) is also of particular interest. It determines the optimal cooling curve for a batch crystallizer with an arbitrary seeding and nucleation ratio. This is very meaningful and useful for preferential crystallization as seeding is always needed.

According to the crystal growth kinetics (Equation 7.22), if Δc=0.001 kg/kg solvent at 35 ^{o}C, G=0.11 μm/min, while G=0.10 μm/min at 5 ^{o}C with Δc=0.0015 kg/kg solvent. This suggests that it is quite acceptable to assume constant *G* during the operation while the supersaturation is still well controlled within a safe region 2-3 ^{o}C. The crystal nucleation rate expression (Equation 7.33) indicates a low dependency on the crystal

suspension density M_T. A low M_T was used in this work. Therefore, it is also reasonable to assume constant *B* in the process. The solubility dependency on temperature can be approximately assumed linear. In this case, the Equation 7.22 can be directly applied to control the supersaturation in the preferential crystallization of 4-hydroxy-2-pyrrolidone. As the mean size of seed is circa 140 μm, for a target product of 230 μm mean size, the operation time is t_c = (230-140)/0.11=818 min=13.6 hour. Figure 7.8 shows the obtained cooling profile. It is comparable to that obtained by orthogonal collocation method (Figure 7.3).

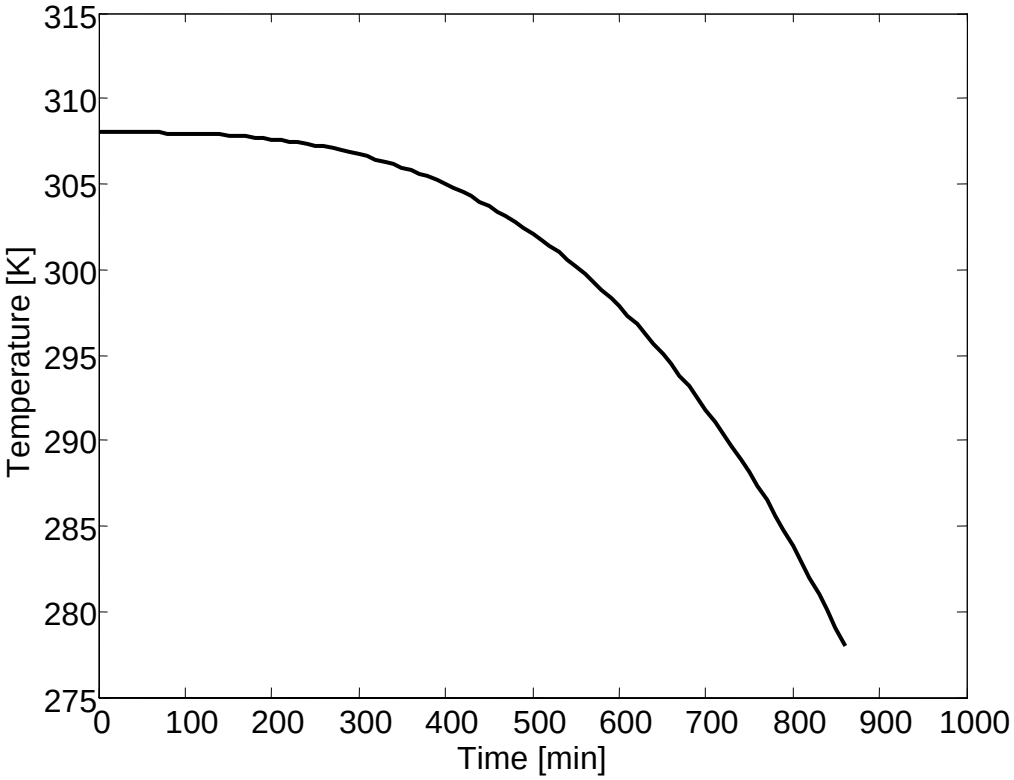

Figure 7.8 The calculated optimal cooling profile from Equation 7.22

7.5 Preferential crystallization operation

The batch preferential crystallization experiments were carried out using the experimental set up shown in Figure 3.9 (Chapter 3). Two types of cooling profiles, namely optimal cooling and forced cooling (natural cooling), were used respectively. First, 20%ee R-enantiomer saturated solutions were prepared at circa 36 ^{o}C. After slightly supersaturated, that is to say, at 35 ^{o}C, pure R-enantiomer seeds were added into the solutions and cooled down from 35 ^{o}C to 5 ^{o}C according to the specified cooling profiles. The seeds were prepared by fast evaporating the solution of certain amount of pure R-enantiomer in isopropanol. Seed preparation and seeding program is another important factor in crystallization (Girolami and Rousseau, 1986; Beilles et al., 2001; Dufour et al. 2001; Ndzié et al., 1997; Qian and Botsaris, 2004). A typical seed CSD is shown in Figure 7.9.

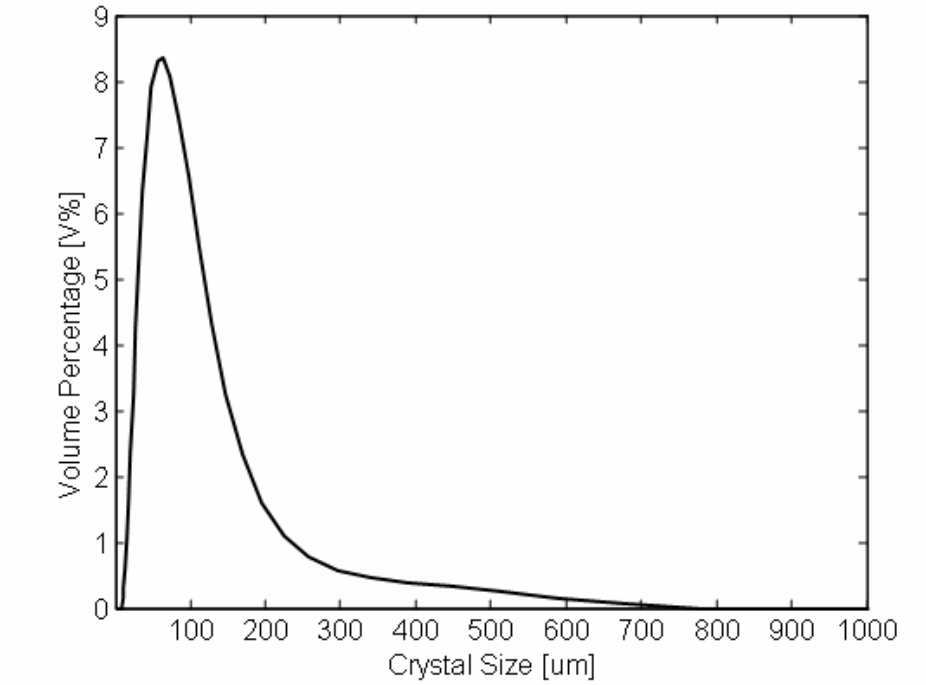

Figure 7.9 A typical seed CSD

The optical purity of crystal products were measured using a Mettler Toledo DSC 822^e Module (heat flux DSC), together with the STAR^e software. Samples of 6-10 mg were prepared in standard 40 μl aluminum crucibles. The crucibles were sealed with a perforated cover. The optical purity was also verified using a JASCO P-1020 digital polarimeter, which was equipped with a sodium vapor lamp emitting light with a wavelength of λ = 589.3 nm and a quartz cell of 50 mm path length. The crystal size distribution was also measured using a Malvern Mastersizer 2000 with a Hydro 2000μP dispersion cell unit with n-hexane as the liquid dispersion medium.

The crystal morphology was investigated using a Jeol JSM-6700F Field Emission SEM. A small amount of samples were scattered on double-sided adhesive carbon taps mounted on SEM stubs, and were coated with Au/Pd in a Cressington 208 sputter coater.

7.6 Results and discussion

7.6.1 Operation and in-situ monitoring

The temperature of the solutions inside the crystallizer was controlled by the LabMax system and the corresponding real temperature was recorded. It is shown in Figure 7.10. For comparison, a forced cooling profile was applied. The LabMax system can precisely track and control the proposed temperature profile very well. Indeed, the proposed temperature curves and the controlled curves are almost the same. The chord length distribution over the whole crystallization process was recorded using FBRM as shown in Figure 7.11. The number of fine counts in the range of 1 – 5 μm was used as the indication of nucleation.

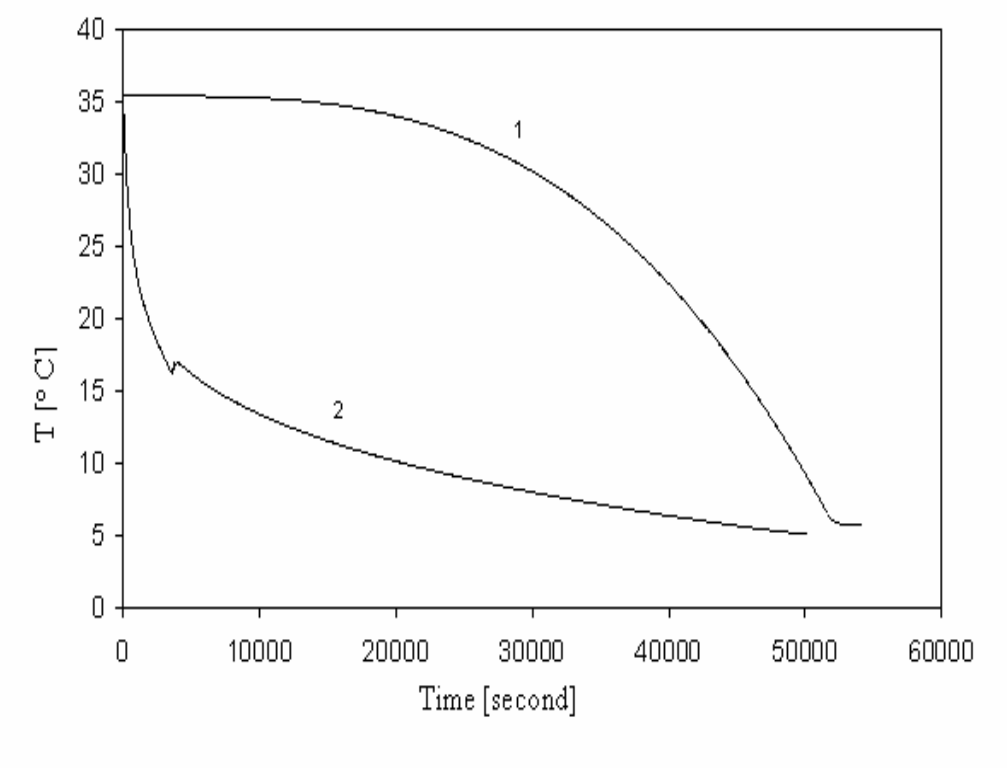

Figure 7.10 The recorded cooling profile. 1-optimal cooling, 2-forced cooling

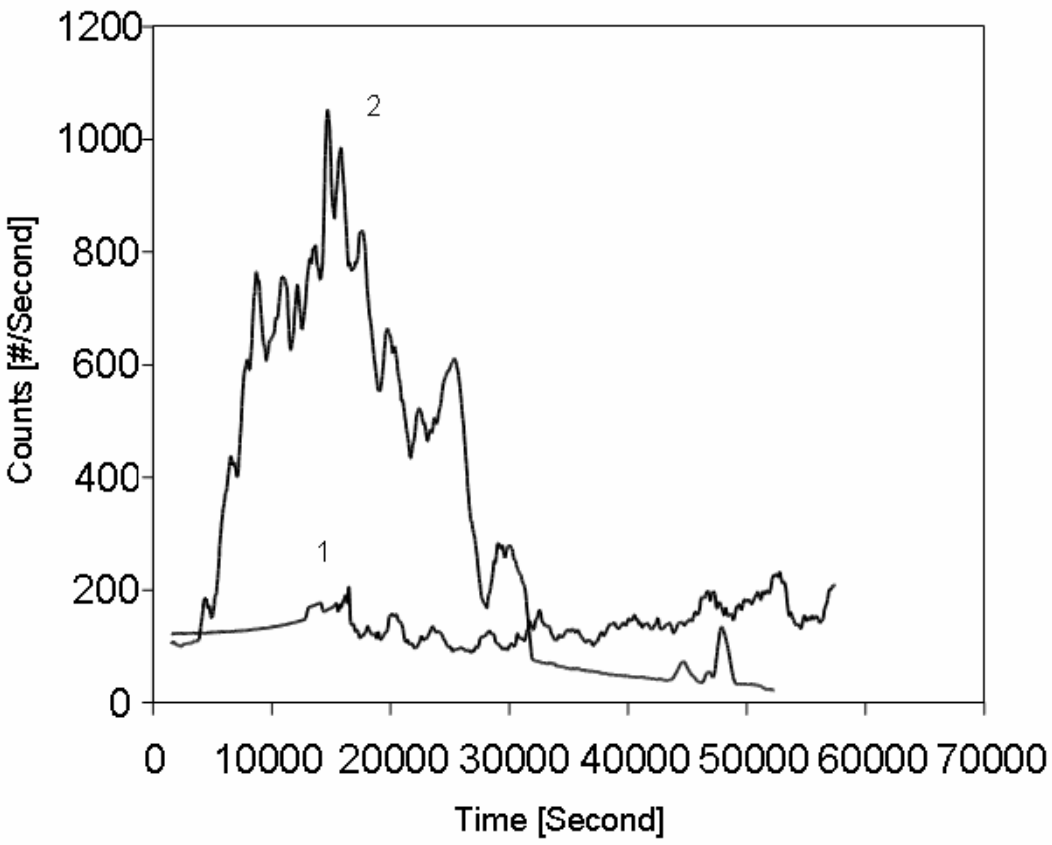

Figure 7.11 FBRM data of the number of fine counts with two different temperature profiles (1μm <chord length<5μm): 1-optimal cooling, 2-Forced cooling

7.6.2 Progression of preferential crystallization

From the recorded forced cooling temperature profile in Figure 7.10, an obvious increasing peak was observed at the point (3890 s, 16.2 ^{o}C). This indicates that a sudden exothermic phenomenon - nucleation might occur in the solution at this point. This phenomenon was also confirmed in the corresponding FBRM measurement as shown in Figure 7.11. There was a steep increase of fine counts at the same moment. In contrast, for the optimal cooling temperature profile, there was no any evident change recorded. The

subsequent effects of different cooling profiles were reflected in the following product properties.

7.6.3 Optical purity of final products

Prior to determining the optical purity of crystallization products by means of DSC, a calibration curve of melting temperature with enantiomeric excess (ee%) was constructed in Figure 7.12. The examination for each sample was conducted under three different heating rates - 2, 5, and 10 ^{o}C/min. The reproducible results indicate the melting temperature is independent of the heating rates within 2 – 10 ^{o}C/min. The DSC thermograms of final crystal products obtained from the experiments under optimal cooling and forced cooling profiles as well as the pure R-enantiomer were shown in Figure 7.13.

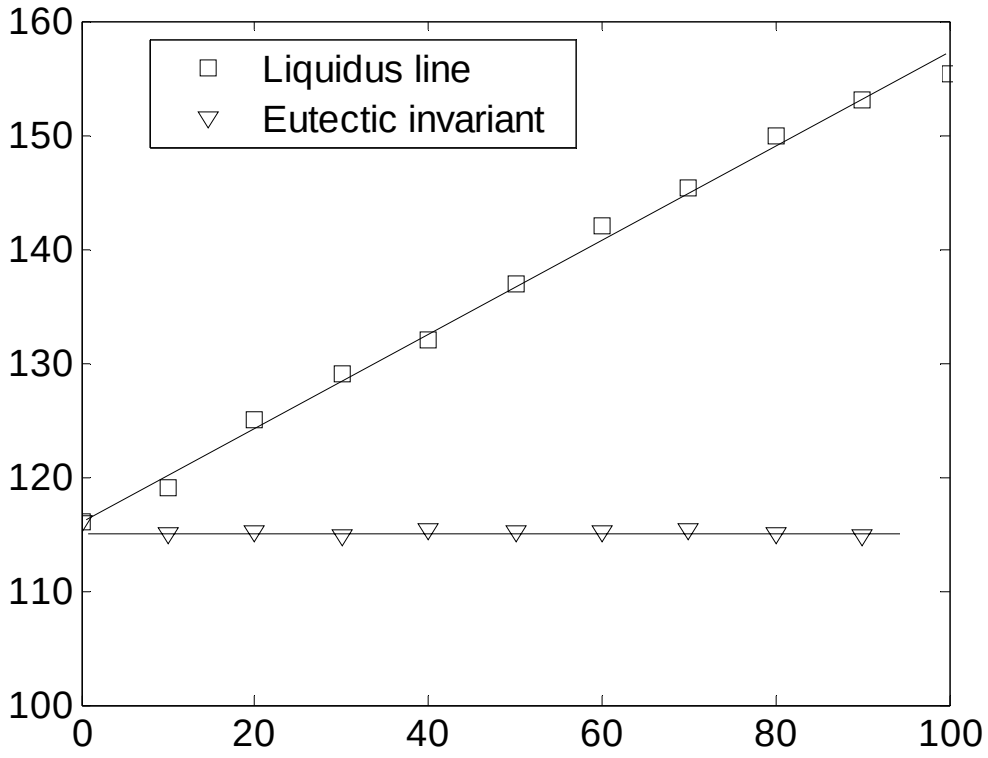

Figure 7.12 Calibration curve of melting temperature with enantiomeric excess

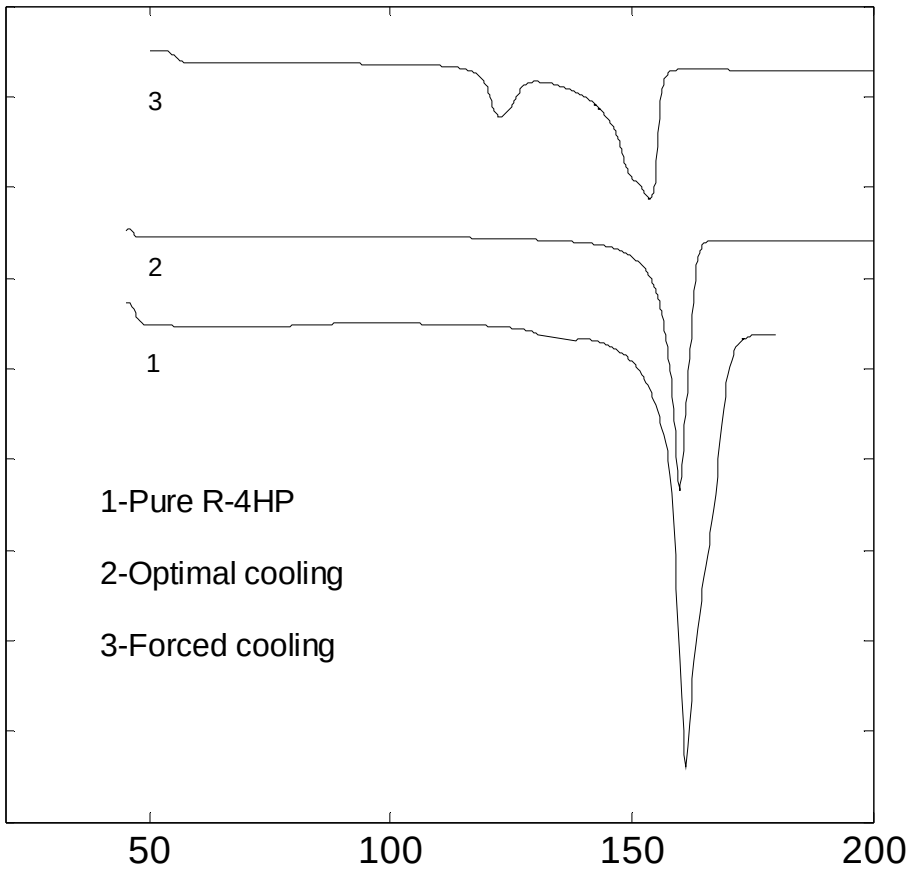

Figure 7.13 DSC thermograms for final crystallization products and pure R-enantiomer

The optical purity of the final crystal products were also verified by means of polarimetry methods. Similarly, a calibration curve of optical rotation with concentration for pure R-enantiomer was constructed in Figure 7.14. The relationship of concentration of pure R-enantiomer C with optical rotation α is expressed as Equation 7.38.

$$C = 6.91\ \alpha \tag{7.38}$$

The optical purities of the final crystal products from the crystallization experiments, which were analyzed using the above-mentioned methods, were listed in Table 7.1.

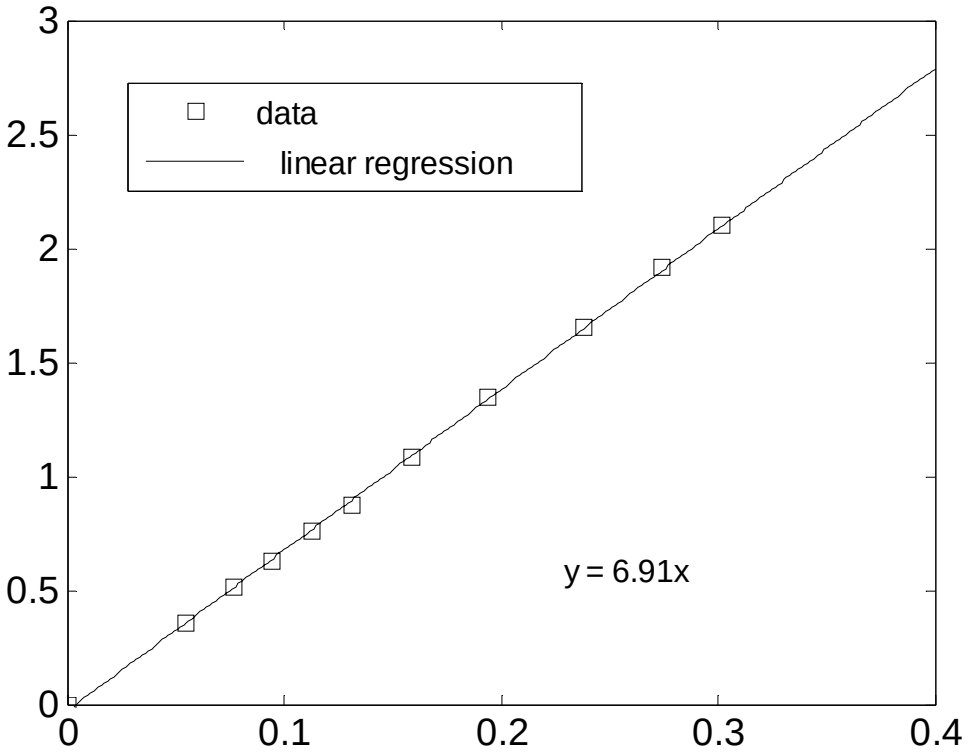

Figure 7.14 Calibration curve (linear) of optical rotation with concentration for pure R-enantiomer

Table 7.1. Final crystal products properties

Experiment	DSC sample, [mg]	Temperature, [^{o}C]	Polarimeter sample, [mg/10g IPA]	α	Optical purity, ee%
Controlled cooling, [(35-5) ^{o}C, 14 hrs]	9.05	155	180	0.2602	100
Forced cooling [(35-5) ^{o}C, 14 hrs]	6.61	148	180	0.2047	78.5

Figure 7.13 and Table 7.1 show that pure R-enantiomer crystal product was obtained from the controlled crystallization experiment. This indicates the optimal operation strategy was successful. The induced nucleation of S-enantiomer was effectively inhibited by controlling the supersaturation of R-enantiomer within the critical value. Based on the added R-enantiomer, circa 52% yield was obtained. This is comparable to the theoretical value 68% when the filtration lost and extra unconsumed supersaturation are considered.

On the contrary, only 78.5%ee crystal product was produced from the forced cooling crystallization experiment (Table 7.1), and two peaks were obviously observed in the DSC thermograms shown as Figure 7.13. The crystal nucleation and growth of S-enantiomer must occur in this operation. Indeed, both Figure 7.10 and Figure 7.11 show that a significant nucleation happened at 16.2 ^{o}C, which should contribute to the poor optical purity. But at this temperature, the S-enantiomer was still far away from its metastable zone. This indicates that the nucleation of S-enantiomer could be induced by R-enantiomer nucleation. The R-enantiomer induced nucleation could be due to either or

both, (i) the spontaneous nucleation of both R and S enantiomers when the supersaturation of R-enantiomer surpassed its metastable zone; (ii) the supersaturation of R-enantiomer was still within its metastable zone, but surpassed a critical limit that its secondary nucleation would breed the nucleation of S-enantiomer (Qian and Botsaris, 1998). It was also argued that if high supersaturations within the metastable zone are used, some conglomerates will form crystals that contain domains of both lattices in a single crystal, which means that the enantiomerically pure seed could nucleate the other enantiomer at its surface (Black et al., 1989; Collins et al., 1997).

The present results support the findings in the metastable zone measurements (Chapter 5) where some extent of nucleation of S could initiate itself or could be induced by spontaneous nucleation of R when the supersaturation surpassed a critical level. This is also consistent with the observations of, (i) very low supersaturation required for high optical purity (Furberg and Hassel, 1950; Black et al., 1989; Collins et al., 1997), (ii) a relatively lower second metastable region (Hongo et al., 1981), (iii) and the importance of controlled cooling program highlighted by Coquerel's group (Ndzié et al., 1997; Beilles et al., 2001; Dufour et al. 2001; Courvoisier et al., 2003).

7.6.4 Crystal size distribution

The crystal size distribution (CSD, volume basis) and the population density of the prepared seeds as well as the product crystals obtained from the crystallization experiments under controlled cooling profile and forced cooling profile are shown in Figure 7.15. It should be noted that the measured CSD and population density do not match the simulated results (Figure 7.5) so well although the main shapes and the newly formed crystals are consistent with each other. This difficulty in recovering CSD and n

from moment transformations has been well discussed by Rawlings et al. (1993). Other factors such as crystallization kinetics could also contribute to the deviation. Figure 7.15 shows that the optimal cooling profile produced larger particles with narrower distribution and much less fine crystals compared to forced cooling. The crystal weighted mean size of optimal operation is 247 μm (this is comparable to the targeted 230 μm) with 59% coefficient of variation (CV), while the forced cooling gave crystals with 193 μm weighted mean size and 78% coefficient of variation. Figure 7.16shows typical SEM images of final product crystals obtained from the experiments under optimal cooling and forced cooling profiles. It is apparent that the crystals from controlled cooling profile are of bigger size and smoother surface than those obtained from forced cooling profile. A good crystal habit would be very helpful to the downstream filtration/washing operation to improve the product purity (Courvoisier et al., 2003; Matthews and Rawlings, 1998).

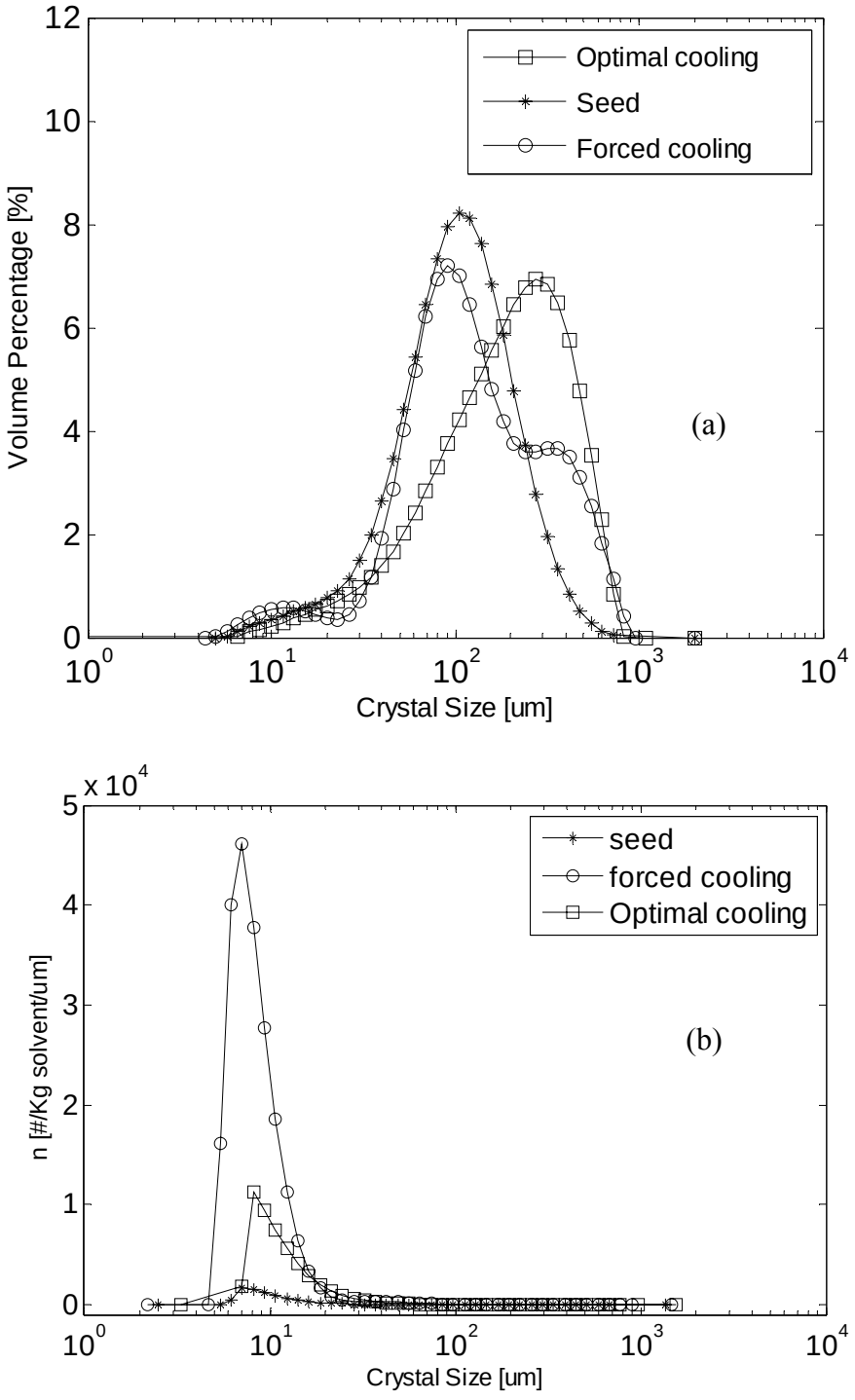

Figure 7.15 Crystal size distribution of pure R-enantiomer seeds and crystal products from different cooling profiles (a) volume basis (b) population density

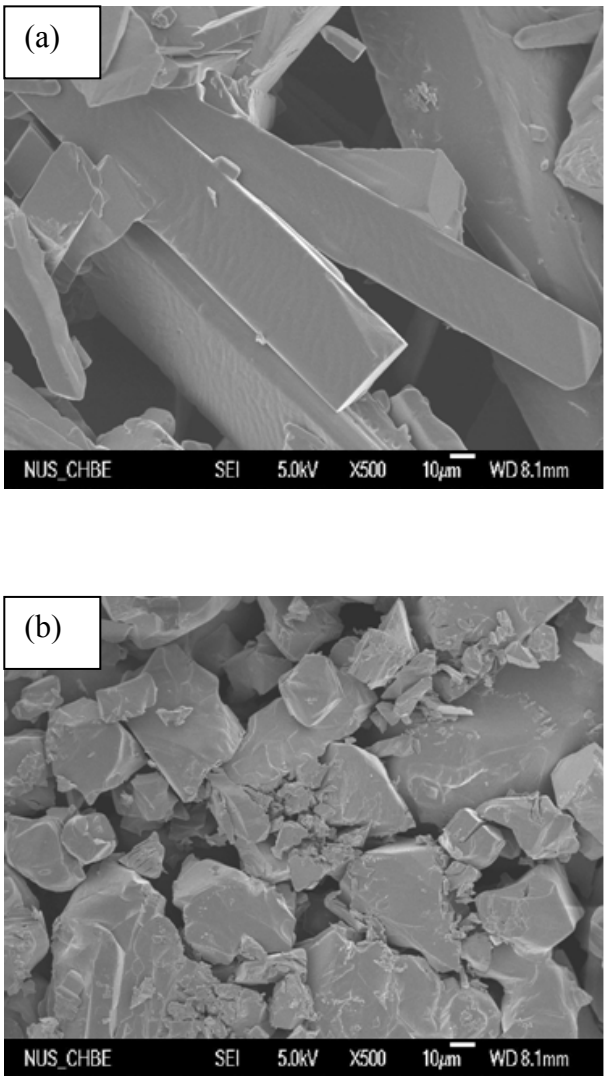

Figure 7.16 SEM images of final crystal products from different cooling profiles:

(a) Controlled cooling, (b) Forced cooling

The above in-situ monitoring observations, final product purity and crystal habit all indicate that it is essential to control the supersaturation of R-enantiomer within a

critical range to prevent the nucleation of S-enantiomer in preferential crystallization. The proposed optimal cooling profile was successful in 4-hydroxy-2-pyrrolidone resolution.

7.6.5 Critical supersaturation range

In Section 7.6.1-7.6.5, the used critical supersaturation was safely chosen as 2-3 ^{o}C (corresponding Δc= 0.001-0.0015 kg/kg solvent) as various factors were considered. According to the metastable zone data, the applicable supersaturation is more than 7 ^{o}C. Therefore, it is interesting to investigate that if the operation supersaturation can be further increased. This is especially important when operation time is key factor in the industrial application.

The mathematical model and the methodology developed in Section 7.4.1 were again employed here to predict the cooling profiles at different supersaturations. As the critical supersaturation can not be predicted with current theory development ((Mersmann and Bartosch, 1997; Kim and Mersmann, 2001), three supersaturations, namely Δc= 0.0018; 0.0020 and 0.0022 kg/kg solvent, were used to simulate the batch crystallization process. The calculated temperature via time curves are shown in Figures 7.17-7.19 respectively. The three cooling curves are pretty similar to that of Δc= 0.0015 kg/kg solvent, but the operation periods are shorter with higher supersatuartion. The corresponding operation time is circa 630, 500 and 400 minutes, respectively.

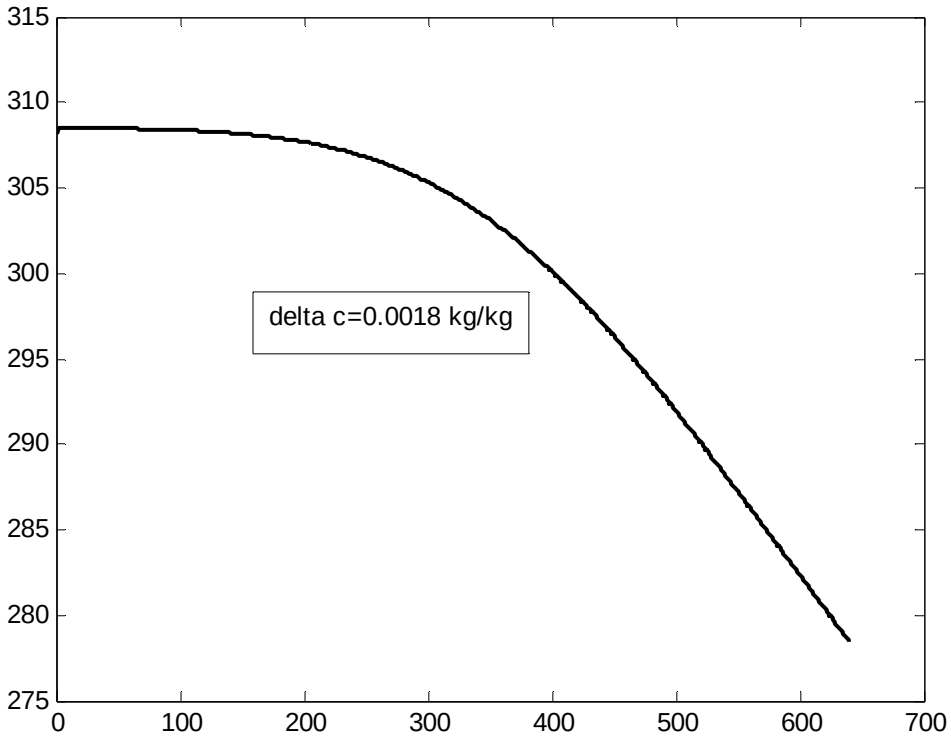

Figure 7.17 Cooling profile, Δc= 0018 kg/kg solvent

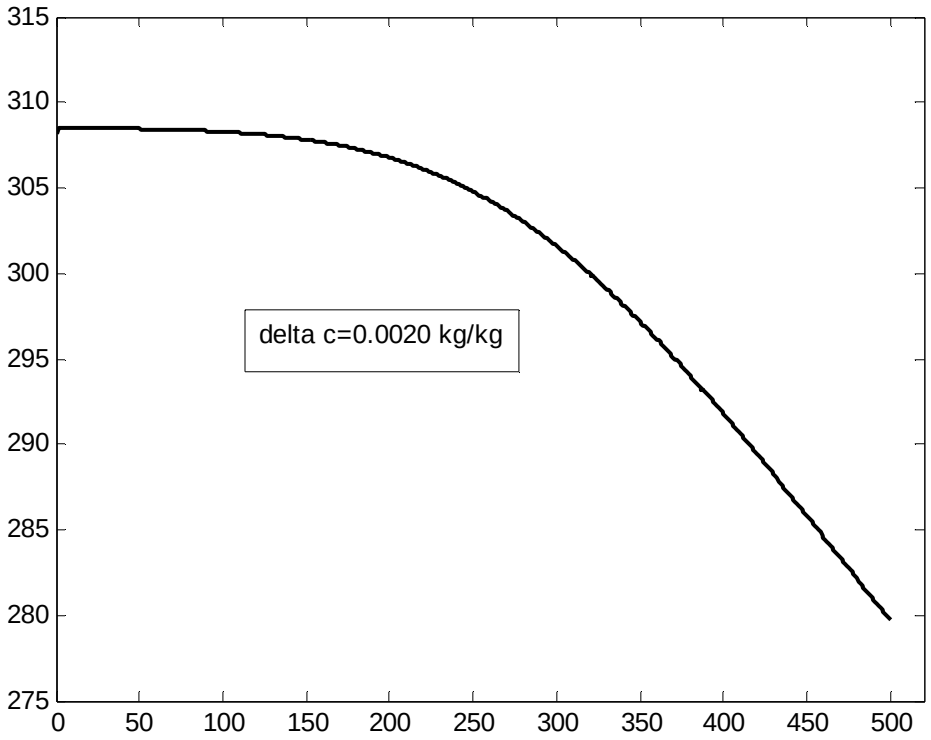

Figure 7.18 Cooling profile, Δc=0020 kg/kg solvent

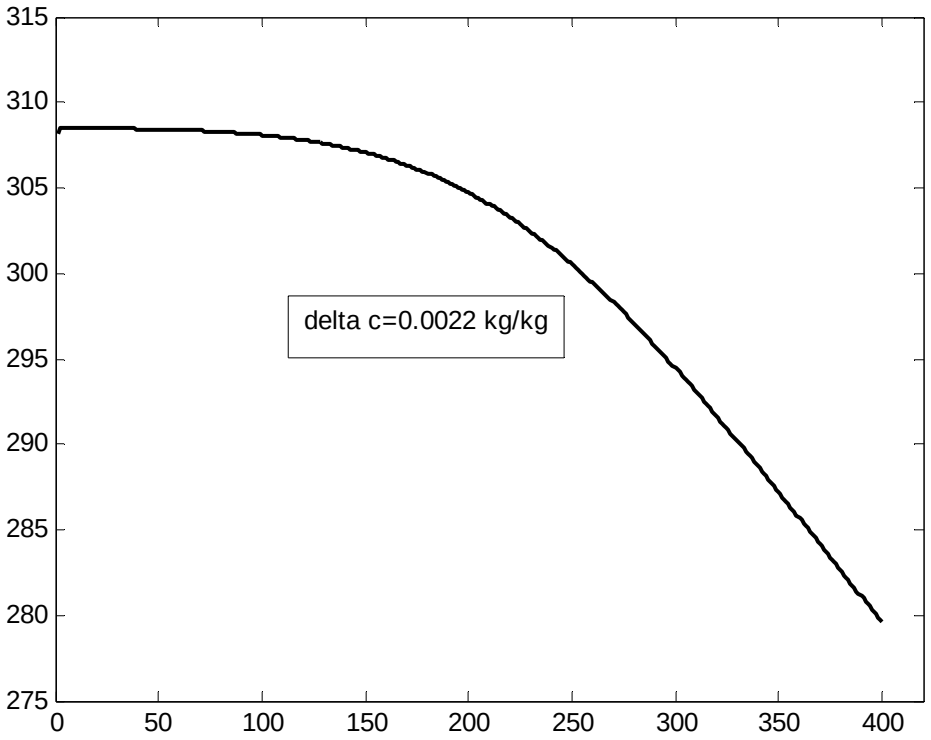

Figure 7.19 Cooling profile, Δc=0022 kg/kg

The temperature of the solutions inside the crystallizer was well controlled according to the proposed curves (Figures 7.17-7.19) by the LabMax system. The chord length distributions over the whole crystallization process were recorded using FBRM as shown in Figures 7.20-7.21 respectively. A deep increase of fine counts (1-5 μm) was observed when Δc=0022 kg/kg solvent was used, which implies that a sudden nucleation could happen at this time. There was no any evident change in the fine counts (1-5 μm) recorded for the other two cases.

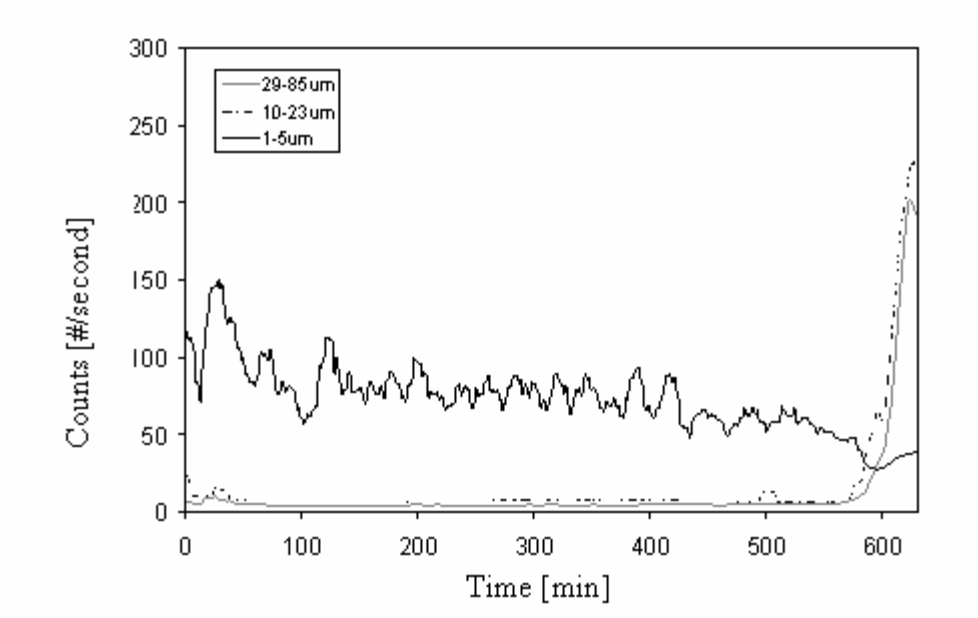

Figure 7.20 FBRM record of the number of fine counts, Δc=0018 kg/kg solvent

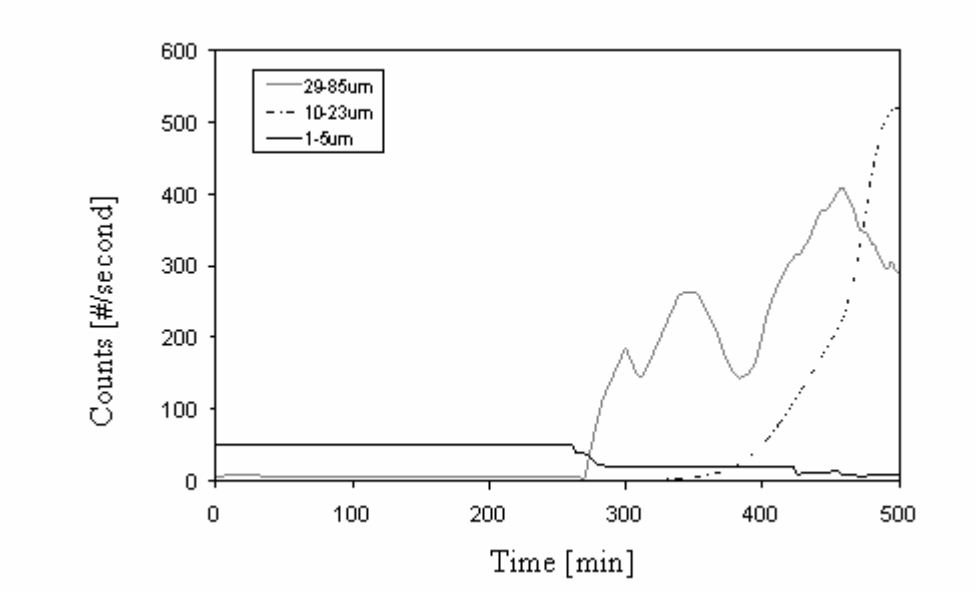

Figure 7.21 FBRM record of the number of fine counts, Δc=0020 kg/kg solvent

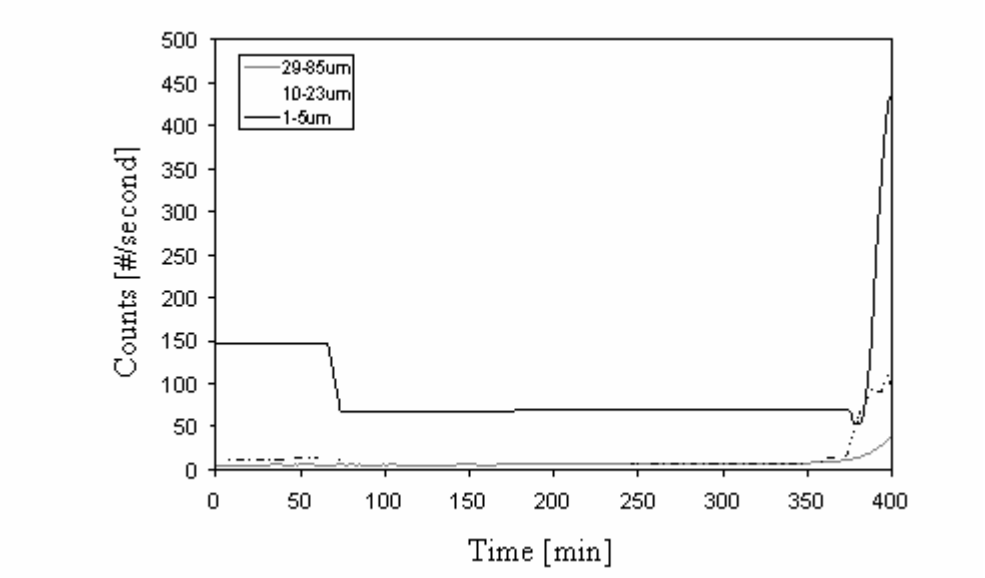

Figure 7.22 FBRM record of the number of fine counts, Δc=0022 kg/kg solvent

The DSC thermograms of final crystal products obtained from the three experiments as well as the pure R-enantiomer and RS racemate are shown in Figure 7.23. The optical purity of the final crystal products were also verified by means of polarimetry. Table 7.2. lists the optical purities. When the supersaturation is Δc= 0.0018 and 0.0020 kg/kg solvent, the final crystals still show very pure optical purity. This again indicates that the induced nucleation of S-enantiomer was effectively inhibited by controlling the supersaturation of R-enantiomer within the current critical value (0.0020 kg/kg). This is also shown in the FBRM observations (Figures 7. 20 and 7.21). Therefore, under current experimental conditions, the optimal operation time could be further reduced to circa 8.5 hours. From the economic viewpoint in industrial applications, cutting operation time means low investment cost and/or efficient usage of equipment and so on.

However, when the supersaturation exceeds this critical point, i.e. 0.0022 kg/kg solvent, the product optical purity begins to decrease to circa 85%. As discussed

previously, this purity drop could again come from the induced S-enatiomer nucleation (Furberg and Hassel, 1950; Hongo et al., 1981; Black et al., 1989; Collins et al., 1997; Qian and Botsaris, 1998) when the supersaturation surpasses a certain level. Indeed, as shown in Figure 7.22, a sudden nucleation was observed from the in-situ chord length distribution using FBRM.

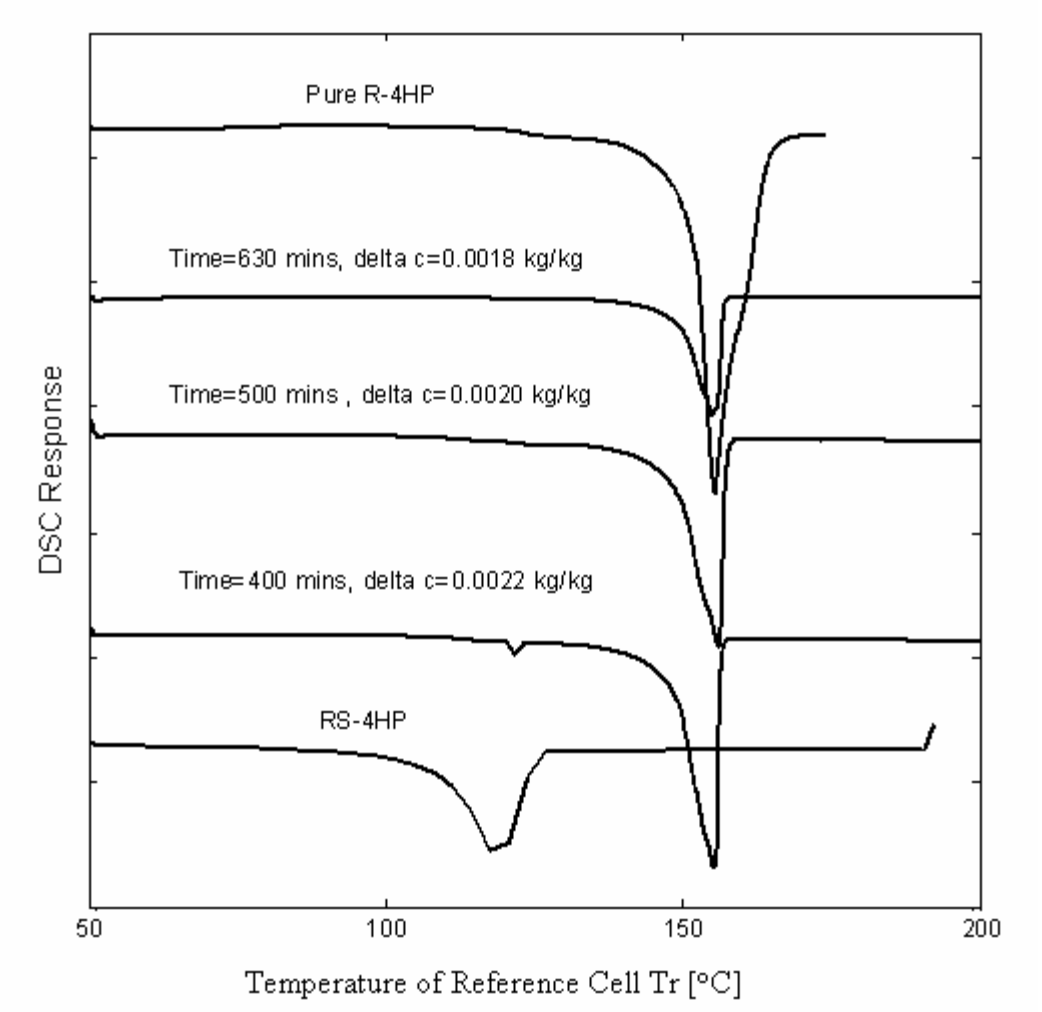

Figure 7.23. Product purities with different operating supersaturations

Table 7.2 Final crystal products properties with different operating supersaturations

Experiment	DSC sample, mg	Temperature, ^{o}C	Polarimeter sample, mg/10g IPA	α	Optical purity, ee%
Δc=0.0018 kg/kg	3.54	155	180	0.2602	100
Δc=0.0020 kg/kg	3.31	155	180	0.2601	100
Δc=0.0022 kg/kg	5.24	153	180	0.2217	85.2

In the aspect of crystal size distribution and crystal habits, it is interesting to find that there is no significant difference for the three operations at different supersaturations. Figure 7.24 presents the crystal distribution for the final crystal products. The SEM imagines are shown in Figure 7.25. All the crystal products show good crystal habits although more small crystals can be seen from the SEM imagines when Δc= 0.0022 kg/kg was used, which could be due to the observed nucleation from FBRM observations (Figure 7.22). As mentioned before, many efforts have been tried to optimize batch crystallization using various objectives, such as mean crystal size and coefficient of variation (Chianese et al., 1984; Choong and Smith, 2004; Costa and Maciel Filho, 2005), seed ratio (Bohlin and Rasmuson, 1992; Matthews and Rawlings, 1998; Chung et al., 1999) and even shape (Ma et al., 2002). But for preferential crystallization process, current results show that the supersaturation is the most important factor to get high optical purity.

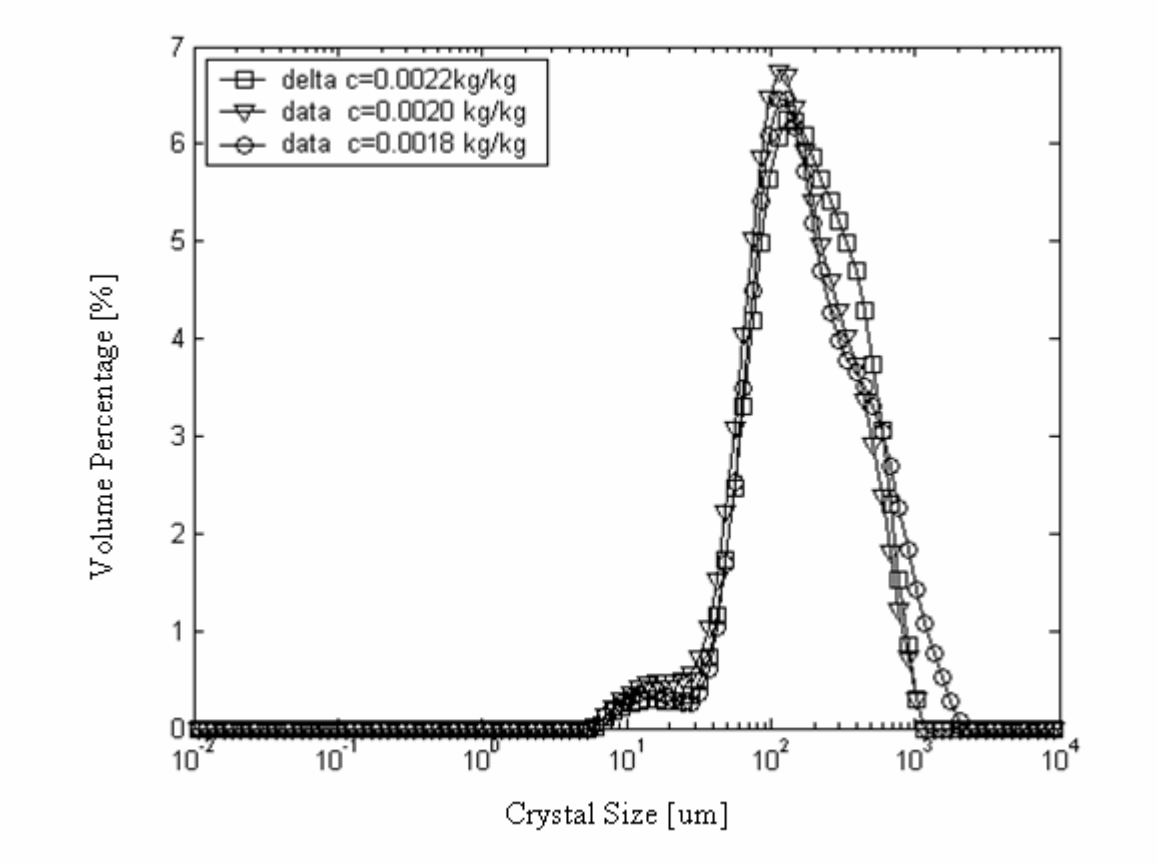

Figure 7.24 Crystal size distributions from optimal operation at different supersaturations

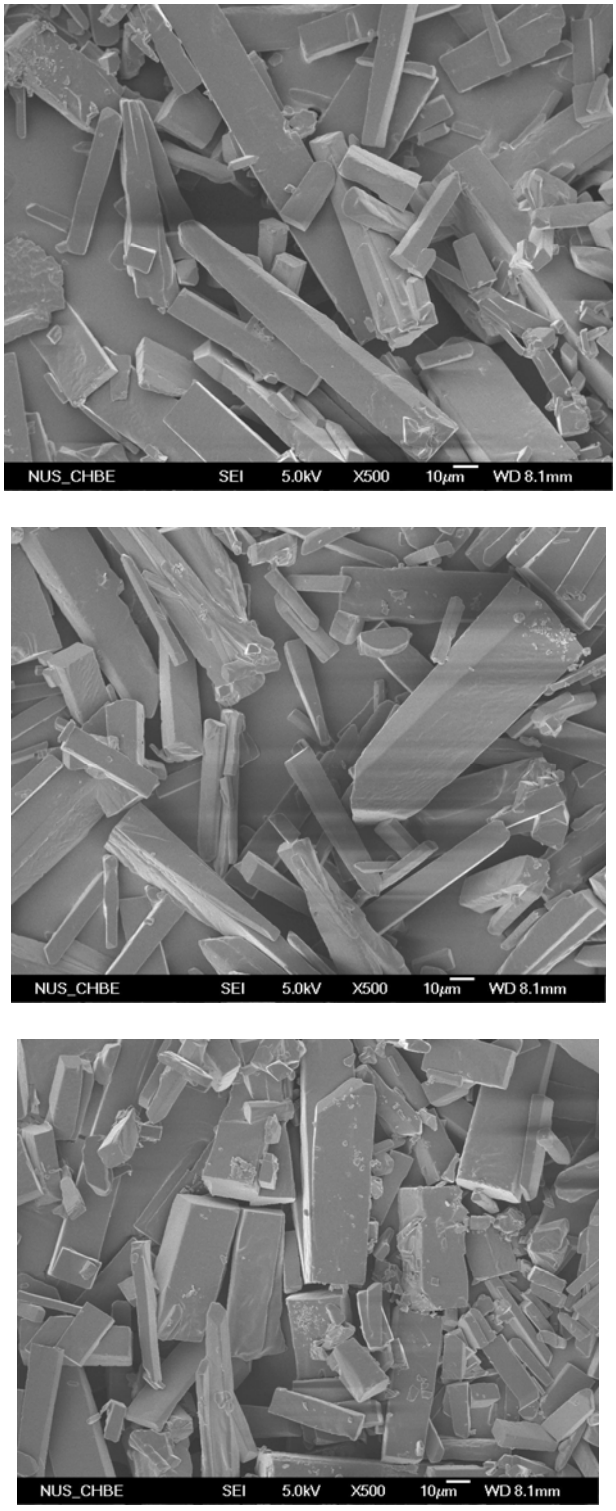

Figure 7.25 SEM images of final crystal products from different cooling profiles.

From top to bottom: Δc=0.0018; kg/kg; Δc=0.0020 kg/kg; Δc=0.0022 kg/kg

7.7 Summary

The critical supersaturation control in preferential crystallization was proposed. Mathematical model and solution were developed for batch cooling preferential crystallization process. The orthogonal collocation method and the second momentum were combined to solve the population balance and mass balance equations. The methodology was successfully used in establishing the cooling profiles for the preferential crystallization of 4-hydroxy-2-pyrrolidone in isopropanol. A series of batch operations of 4-hydroxy-2-pyrrolidone were experimentally studied under various supersaturatiuons.

In-situ monitoring showed that relatively high supersaturation of the target enantiomer induced spontaneous nucleation of the undesired enantiomer, which accordingly resulted in low optical purity and poor crystal size distribution. The proposed optimal temperature trajectory to control the critical supersaturation successfully inhibited the induced nucleation of the undesired enantiomer, and hence produced almost pure crystals with good habits. Further investigations presented the optional operating strategy without sacrifice of product optical purity. The critical supersaturation control used here is expected to be applicable widely for preferential resolution. The integration of thermodynamics, crystallization kinetics and population balance modeling was proved essential and helpful to establish this control strategy.

Part of results in this chapter has been reported on Chemical Engineering Science (Vol 61, pp.2406-2417. 2006)

CHAPTER 8 APPLICATION OF DIRECT CRYSTALLIZATION FOR RACEMIC COMPOUND PROPRANOLOL HYDROCHLORIDE

8.1 Introduction

Direct crystallization plays an important role in the resolution of a racemic conglomerate (preferential crystallization) or purification of a partially resolved racemic compound (direct crystallization) whenever it is applicable. As illustrated in Chapter 7, direct crystallization is feasible for the resolution of a conglomerate, which has been also highlighted by many authors (Collet et al., 1980; Sheldon, 1993; Jacqueas et al., 1994; Beilles et al., 2001; Elsner et al., 2005). With the big progress made in the field of asymmetric synthesis and SMB chromatography etc, the partially resolved chiral samples are easily available. However, these samples are often highly diluted and the enantiomeric purity is insufficient. It would require much more extra efforts to acquire an optically pure product rather than a partially resolved sample using asymmetric synthesis or SMB alone. Instead, direct crystallization can be applied to further purify these partially resolved samples. In the aspects of low cost and advantages of solid product, direct crystallization also shows big advantages for the enrichment of chiral compounds (Lorenz, et al, 2001; Schroer et al, 2001). This Chapter will explore the application of direct crystallization to racemic compound coupling with chromatography.

As we learned from Chapter 5, the feasibility and yield of pure enantiomer obtainable by direct crystallization is determined by the shape of the phase diagrams (binary or ternary phase diagram) of the system and the initial enantiomeric composition of the feed to the crystallizer. For a racemic compound, three possible situations are illustrated in Figure 8.1. We can see that the knowledge of the phase equilibria is even more important for a racemic compound because the existence region of the pure enantiomers in the phase diagram, which is defined by the position of the ternary eutectic point, in most cases, is much smaller than a racemic conglomerate. A pure enantiomer can only be produced by direct crystallization when the initial solution composition is located inside the existence region of the pure enantiomers covered by AED or A'E'L. In the most favorable case, as shown in Figure 8.1 (c), the racemic compound exhibits an ideal phase diagram with the maximum operating region to obtain pure enantiomers by crystallization. In the case of a combined process of chromatography and crystallization, the previous chromatographic step must deliver a minimum enantiomeric enrichment which exceeds that of the eutectic point in the ternary phase diagram. Subsequently, the resulting highly diluted and undersaturated solution has to be evaporated to reach a composition in the pure enantiomer existence region to gain a pure enantiomer by following crystallization step.

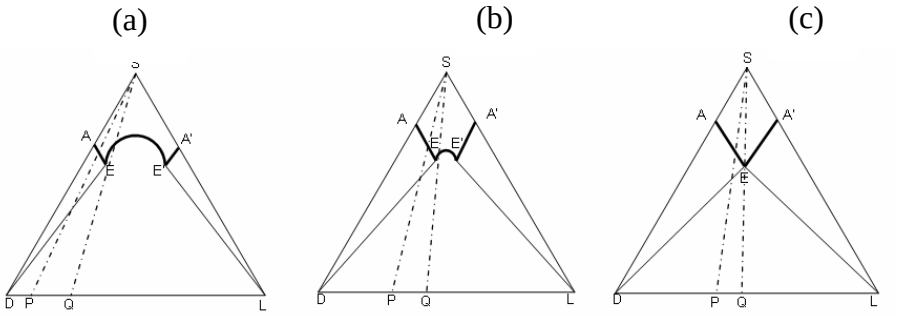

Figure 8.1 Ternary phase diagrams for a racemic compound: (a) unfavorable; (b) more favorable; (c) most favorable

Propranolol hydrochloride, as shown in Figure 8.2, is a synthetic beta-adrenergic receptor blocking agent widely used in the treatment of hypertension. Although it is administrated as the racemate form, only (S)-enantiomer has the desired beta-adrenergic blocking effect. In Chapter 4, it was identified as a racemic compound forming system. The ternary phase diagram of propranolol hydrochloride dissolved in the mixture of methanol and isopropanol (Figure 5.17) has the most favorable shape as shown in Figure 8.1 (c) for obtaining the pure enantiomer by direct crystallization. The mixture having the eutectic composition is the racemate. The racemate can be readily separated by chromatography. Furthermore, the two pure enantiomers are commercially available at a reasonable price. Therefore, propranolol hydrochloride dissolved in the mixture of methanol and isopropanol was chosen as a suitable model system to explore the combination of chromatographic and crystallization separation techniques.

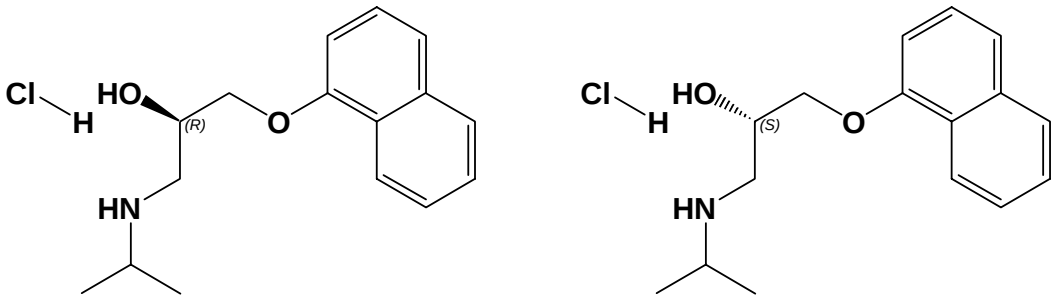

R-propranolol hydrochloride **S-propranolol hydrochloride**

Figure 8.2 Chemical structure of (R)- and (S)-propranolol hydrochloride

The resolution of propranolol hydrochloride via chromatography has been reported by Ching et al. (2000) and Gritti & Guiochon (2004). However, the mechanism of crystallization process for propranolol hydrochloride, which is a racemic compound, has

been rarely investigated. This Chapter presents such an effort to obtain a certain enantiomerically enriched propranolol hydrochloride starting from a racemic composition using a HPLC with a semi-preparative chiral column. A subsequent systematical study of direct crystallization process starting from the same enantiomeric composition with the partially resolved propranolol hydrochloride from the HPLC was conducted. The critical supersaturation control strategy and the scheme to obtain pure enantiomer via direct crystallization for the partially resolved racemic compound propranolol hydrochloride were investigated. The crystallization progression was illustrated in terms of the diagram of solubilities and metastable zone widths with different compositions.

8.2 Experimental setup and procedure

Semi-preparative HPLC separation of propranolol hydrochloride was performed using an Agilent 1100 series HPLC system with Chiralcel OD-H semi-preparative column (10mm ID x 250mm L). The mobile phase was 100% isopropanol. The flow rate was 1.0 ml/min. Isopropanol was chosen as the main eluant for HPLC separation due to the solubility of propranolol hydrochloride in pure alcohols such as 100% isopropanol or methanol are much higher than hexane/isopropanol solvent mixtures.

The batch direct crystallization experiments with and without seeding were carried out using the experimental set-up shown in Figure 3.9. The 36.7%ee (consistent with the above HPLC partial separation composition) R-enantiomer saturated solutions were prepared at 35 ^{o}C. For seeding experiments, after slightly supersaturated, that is to say, at 34 ^{o}C, pure R-enantiomer seeds were added into the solutions and cooled down from 35 ^{o}C to 23 ^{o}C, 20.5 ^{o}C, and 17 ^{o}C, respectively. The seeds were prepared by fast cooling the

solution of certain amount of pure R-enantiomer in isopropanol. Typical load of crystallizer was a solute mixture of 3.602 g of (RS)-propranolol hydrochloride and 2.091 g (R)-propranolol hydrochloride dissolved in 471 ml of solvent mixture of methanol and isopropanol (V:V = 1:5).

The optical purity was measured using an Agilent 1100 series HPLC system with Chiralcel OD-H analytical column. The mobile phase was a mixture of hexane/isopropanol (v/v = 80/20). The flow rate was 1.0 ml/min. The detection wavelength was 254 nm.

The optical purity of crystal products were also verified using a Mettler Toledo DSC 822^e Module (heat flux DSC), together with the STAR^e software. Samples of 2-4 mg were prepared in standard 40 µl aluminum crucibles. The crucibles were sealed with a perforated cover. Preceding investigation of samples, a calibration curve of standard samples with different enantiomerical excess was recorded. The examination for each sample was conducted under three different heating rates - 2, 5, and 10 ^oC/min. The reproducible results indicate the melting temperature is independent of the heating rates within 2 – 10 ^oC/min.

The crystal size distribution was measured using a Malvern Mastersizer 2000 with a Hydro 2000µP dispersion cell unit. Analytical hexane, in which propranolol hydrochloride is almost insoluble, was used as the liquid dispersion medium. The crystal morphology was investigated using a Jeol JSM-6700F Field Emission SEM. A small amount of samples were scattered on double-sided adhesive carbon tabs mounted on SEM stubs, and were coated with Au/Pd in a Cressington 208 sputter coater.

8.3 Results and discussion

8.3.1 Semi-preparative HPLC separation of propranolol hydrochloride using Chiralcel OD-H column

The loading capacity of propranolol hydrochloride on Chiralcel OD-H column (10mm ID x 250mm L) was determined by injecting different amount of sample onto the column. Propranolol hydrochloride shows almost baseline separation on Chiralcel OD-H at 8.95mg loading. As sample loading increased to up to 14.56mg, partial separation of propranolol hydrochloride was obtained as shown in Figure 8.3. Through semi-preparative chiral HPLC separation (14.56mg per analysis), we had isolated the R and S enantiomer from its racemate, by collecting at two different fractions at retention time, t =15-25 mins (fraction a) and at t =25-30 mins (fraction b) as shown in Figure 8.4. The enantiopurities of these two fractions were analysed on analytical column (Chiralcel OD-H, 4.6mm ID x 250mm L) using hexane/isopropanol (80/20 v/v) as the mobile phase and flow rate of 1.0ml/min (shown in Figure 8.5). From the obtained chromatographic data, fraction (a) consisted of R enantiomer with 36.7 % ee and fraction (b) consisted of S enantiomer with 100% ee. Upon continuous HPLC separation using an autosampler and automated fraction collector, these two fractions could be accumulated until a certain volume (e.g. 1000ml) and transferred into separate jacketed crystallizers for direct crystallization of respective enantiomers.

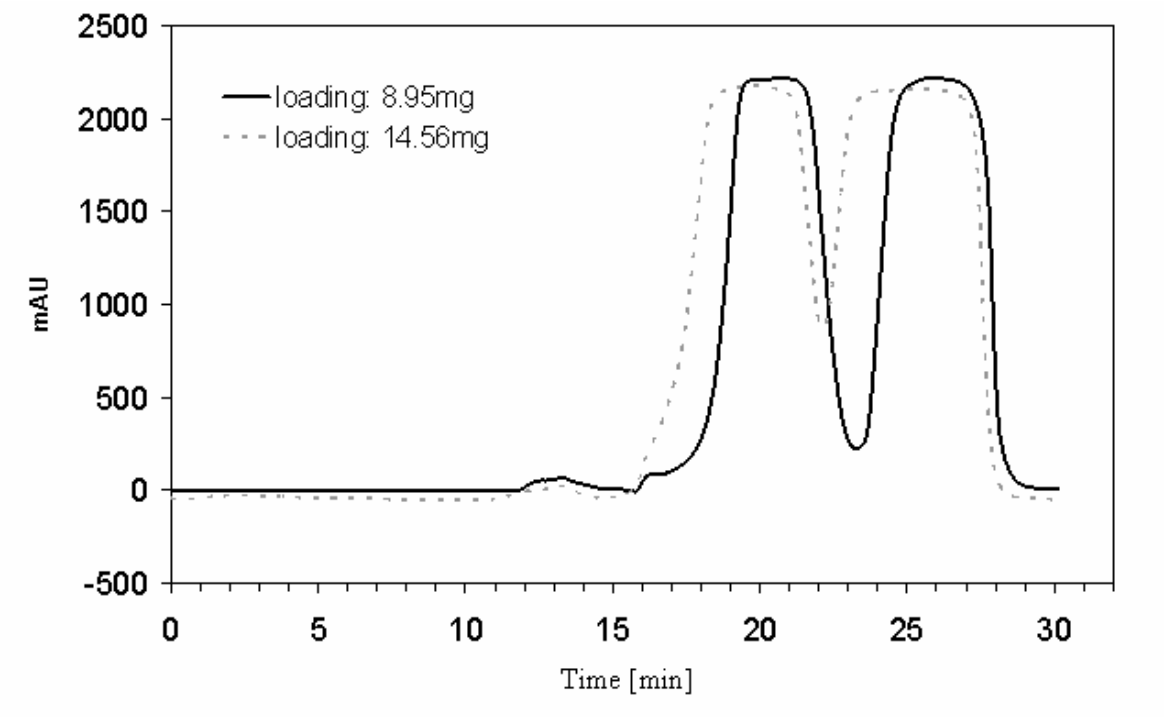

Figure 8.3 Partial separation of propranolol on Chiralcel OD-H semi-preparative HPLC column (dimension 250mm L x 10mm I.D) at different loadings (8.95mg and 14.56mg per injection) using 100% IPA as mobile phase, at 25^{o}C column temperature, flow rate of 1ml/min and UV-Vis detection at 254nm.

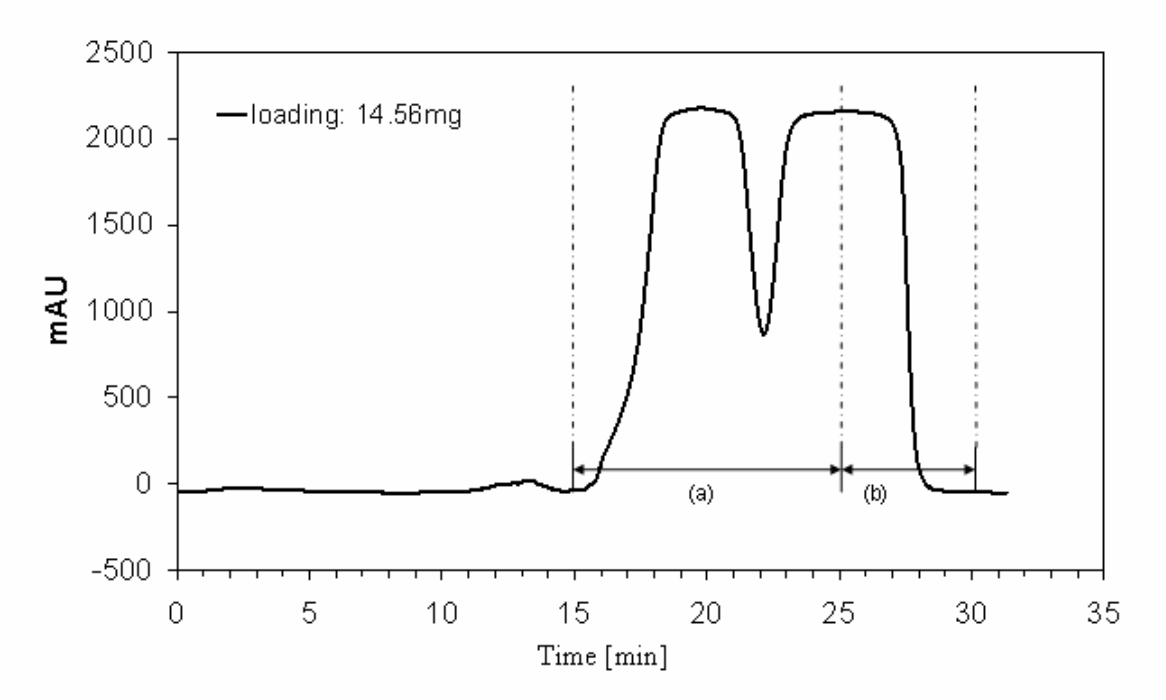

Figure 8.4 Fraction collection under semi-preparative HPLC separation of propranolol on Chiralcel OD-H column (dimension 250mm L x 10.00 mm I.D.) under separation conditions: IPA (100%) at 25^{o}C column temperature, flow rate of 1.0ml/min and UV-Vis detection at 254nm. Fraction (a) collected at retention time 15-25 minutes and fraction (b) is collected at 25-30 minutes.

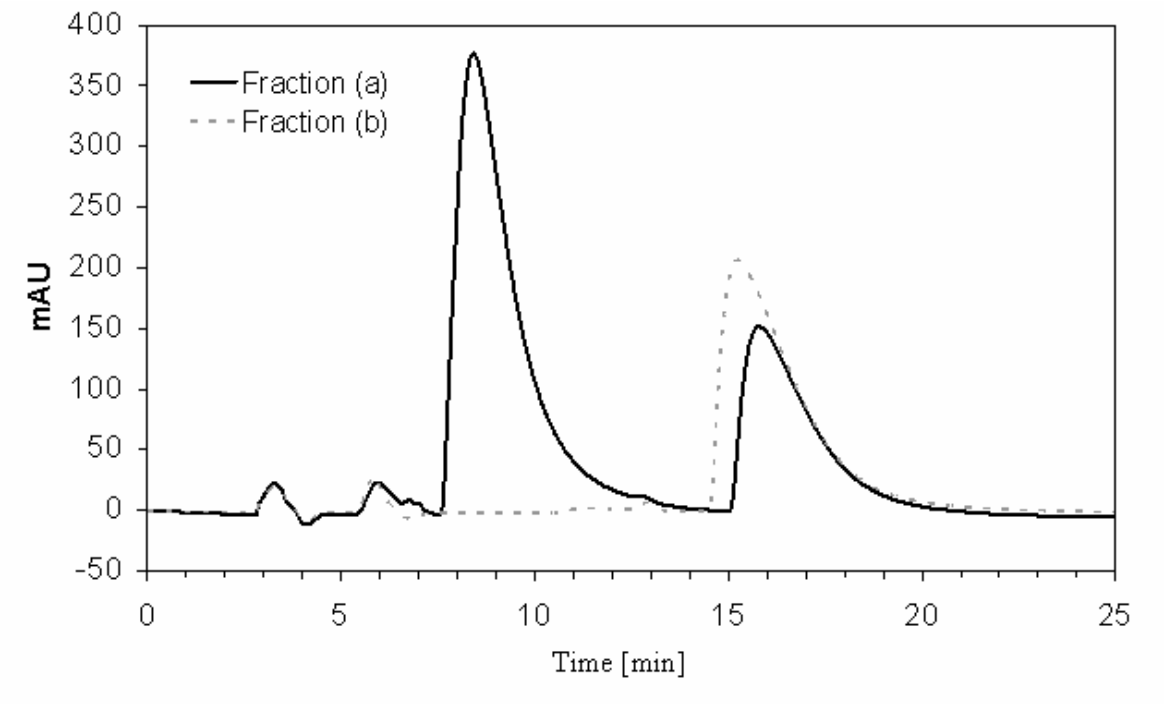

Figure 8.5 Chromatogram of two fractions (a) and (b) obtained through semi-preparative HPLC separation of propranolol on Chiralcel OD-H analytical column (dimension 250mm L x 4.6 mm I.D.) under separation conditions: Hexane/IPA (80/20 v/v) at 25^{o}C column temperature, flow rate of 1.0ml/min and UV-Vis detection at 254nm.

8.3.2 Solubility and metastable zone width

As described in Chapter 5, the selection of a suitable solvent for an effective crystallization operation is crucial. A mixture of two or more solvents is sometimes found to possess the best properties for a particular crystallization purpose. It was found that the solubility of propranolol hydrochloride in methanol or water was too high. Thus the mixture of solvents was considered. The solubility of propranolol hydrochloride with different composition in the mixture of methanol and acetone was measured in my previous study (Wang et al, 2002). However, it was found that propranolol hydrochloride was easily decomposed in the presence of acetone at ambient temperature. In this study, the mixture of methanol and isopropanol was employed.

The solubilities and metastable zone widths of propranolol hydrochloride in the mixture of methanol and isopropanol were determined in Chapter 5. From the ternary phase diagram Figure 5.18, it can be seen that the eutectic composition is the one of the racemate, which is the most favorable situation for a racemic compound. The solubility of propranolol hydrochloride with different composition in the mixture of methanol and isopropanol (V:V =1:5) properly increases with temperature over the range of 12 – 35 ^{o}C. This suggests that the cooling crystallization for the chosen system is more favorable as temperature decreases. As illustrated by Wood (Collins et al., 1997), the difference of the saturation temperatures of (RS)- and (R)-propranolol hydrochloride at their respective concentrations is suitable for the cooling crystallization process.

The solubilities and supersolubilities of (R)- and (RS)-propranolol hydrochloride at cooling rate of 5 ^{o}C/h are shown in Figures 8.6. It was found that the MSZWs did not change obviously with the cooling rate at the range of 1 - 10 ^{o}C/h. These results show that

the characteristic of solubility and the widths of metastable zone over the experimental temperature range are favorable for direct crystallization process.

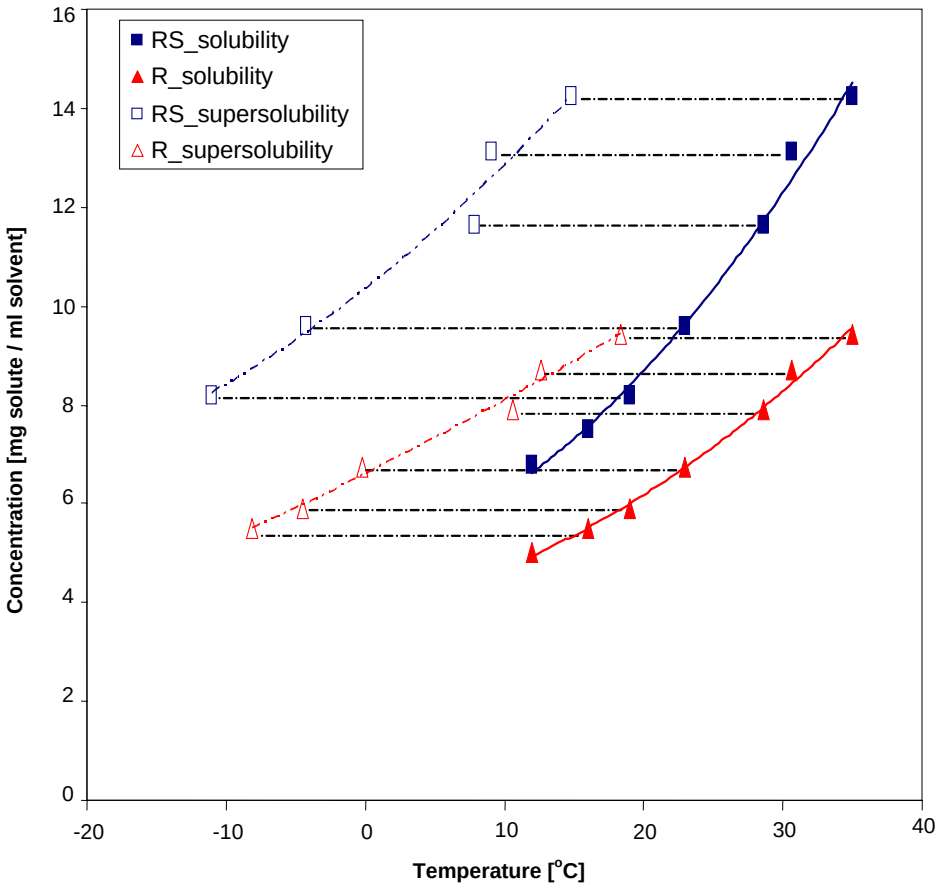

Figure 8.6 Solubility and supersolubility of (R)- and (RS)-propranolol hydrochloride

8.3.3 Progression of direct crystallization

Four batches of direct crystallization of propranolol hydrochloride in mixture of methanol and isopropanol were carried out starting from the same solution containing 36.7% ee (R)-enantiomer with four different modes, which are (a) Exp01: with seeding and final temperature at 23 ^{o}C; (b) Exp02: with seeding and final temperature at 20.5 ^{o}C;

(c) Exp03: with seeding and final temperature at 18 ^{o}C; (d) Exp04: without seeding until nucleation occurred.

As described in Figure 8.7, a saturated solution at 35 ^{o}C containing 36.7% ee (R)-enantiomer is represented by point A. From the diagram of solubility and metastable zone widths of (R)- and (RS)-propranolol hydrochloride in Figure 8.6, the solution was saturated in the (R)-enantiomer at 30 ^{o}C represented by point B, and in the (RS)-propranolol hydrochloride at 18 ^{o}C represented by point C. The solution was then seeded with (R)-enantiomer crystals and cooled to 23 ^{o}C, 20.5 ^{o}C and 18 ^{o}C, respectively. It was found that at temperature greater than 18 ^{o}C, the product crystals were in the form of pure (R)-enantiomer, but at temperature lower than 18 ^{o}C, the product crystals were in the form of mixture of (R)- and (RS)-propranolol hydrochloride. This might imply that there is no selectivity of crystal growth of the pure enantiomer and racemate for a racemic compound when both (R) and (RS) reach supersaturation. It suggests that only the excess enantiomer can be crystallized out and no further resolution is attainable for a racemic compound. This is unlike preferential crystallization of a conglomerate, where the crystallization rates of two opposite enantiomers can be controlled to some extent and certain resolution can be achieved by carefully designed and controlled entrainment procedure. However, as mentioned before, as partially resolved solutions are readily obtained by other purification processes, when it is well designed and controlled, direct crystallization is a good way to get pure enantiomer.

When the solution was cooled to 17 ^{o}C without seeding, the primary nucleation occurred after it exceeded the metastable zone of propranolol hydrochloride with initial composition of 36.7% ee, and the mixture crystals of (R)- and (RS)-propranolol

hydrochloride were always obtained. This again might be due to the crucial characteristic of a racemic compound – no selectivity of nucleation between the pure enantiomer and racemate for a racemic compound. The corresponding consequences of different cooling extent were reflected in the following product properties.

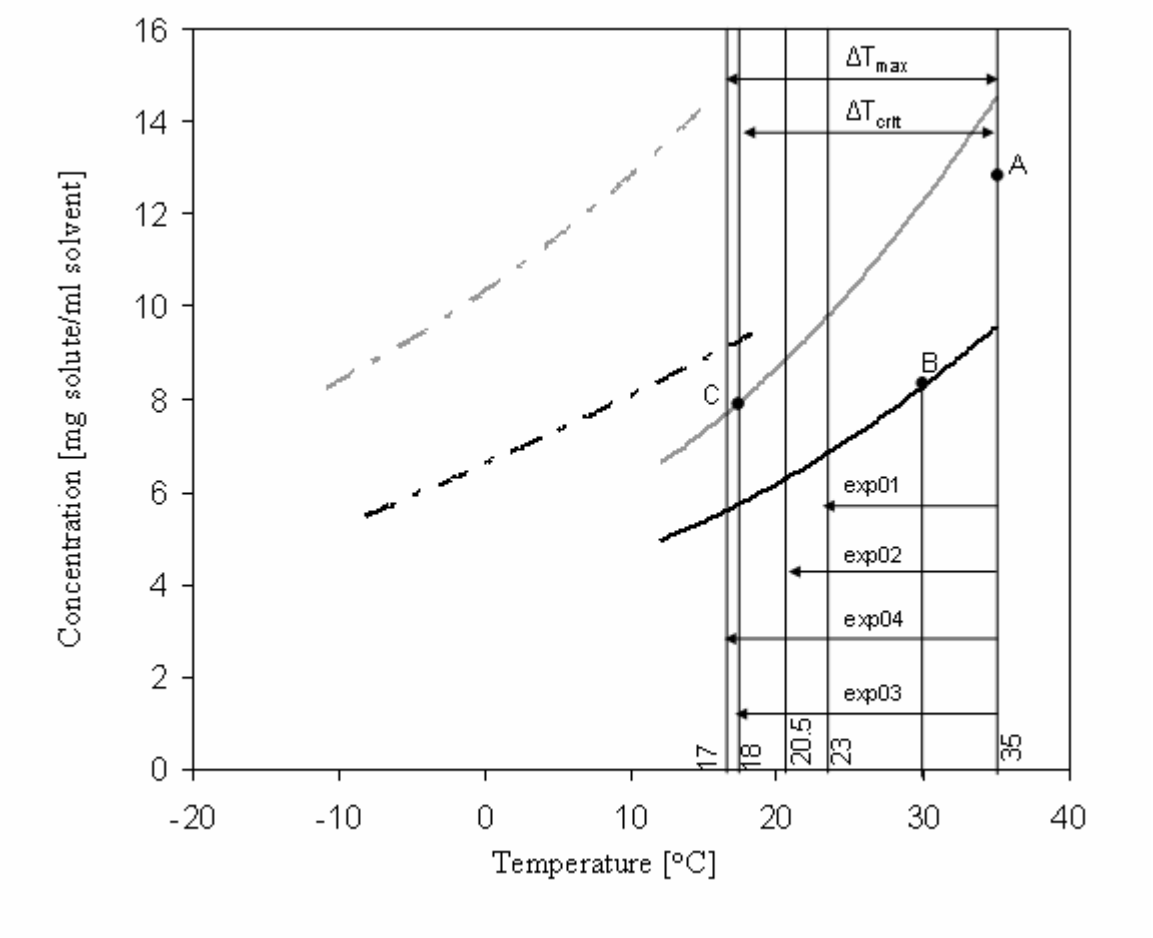

Figure 8.7. Progression of direct crystallization

8.3.4 Optical purity of final products

The optical purity of the final crystal products were analyzed by means of HPLC method which was mentioned in Section 8.2. The chromatograms of the final crystal products are shown in Figures 8.8- 8.11.

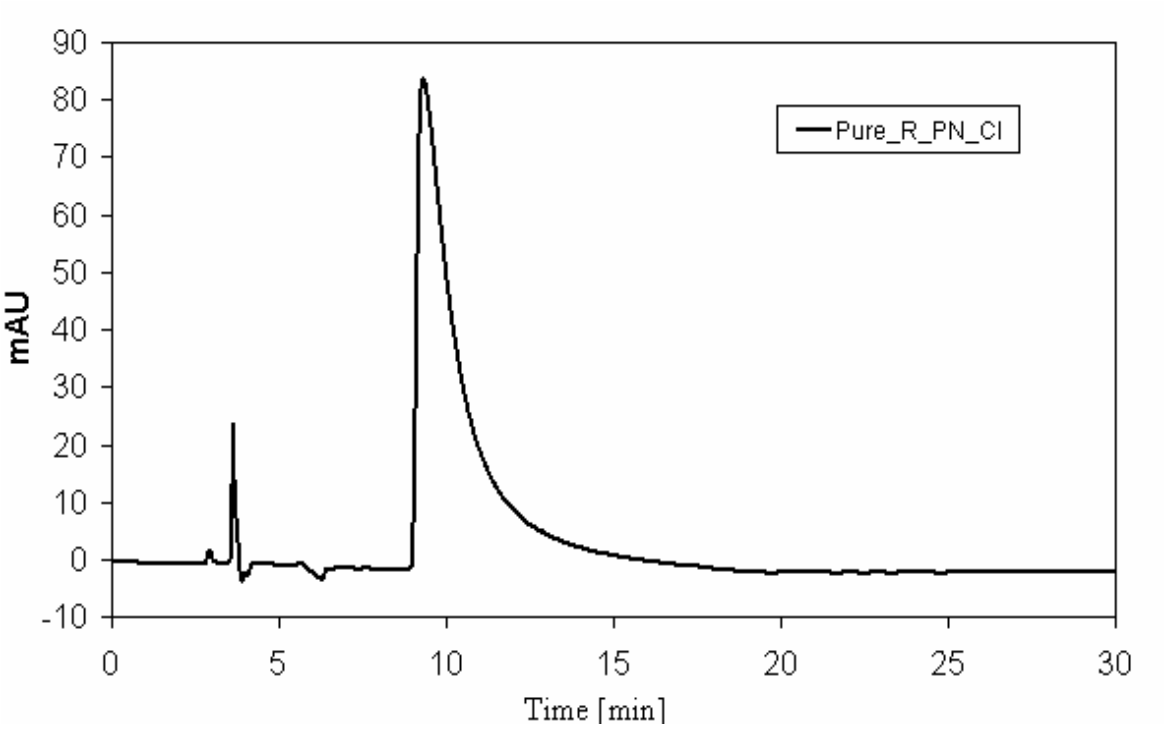

Figure 8.8 Chromatogram of final crystal product obtained from exp01 on Chiralcel OD-H analytical column (dimension 250mm L x 4.6 mm I.D.) under separation conditions: Hexane/IPA (80/20 v/v) at 25^{o}C column temperature, flow rate of 1.0ml/min and UV-Vis detection at 254nm.

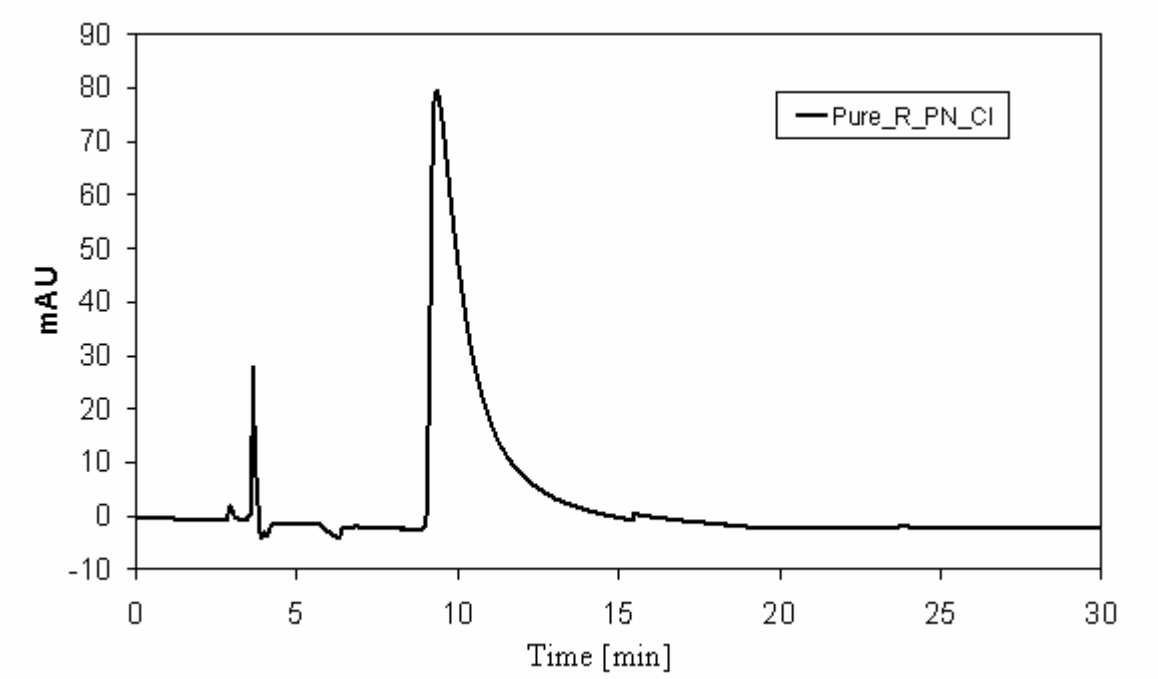

Figure 8.9 Chromatogram of final crystal product obtained from exp02 on Chiralcel OD-H analytical column (dimension 250mm L x 4.6 mm I.D.) under separation conditions: Hexane/IPA (80/20 v/v) at 25 ^{o}C column temperature, flow rate of 1.0ml/min and UV-Vis detection at 254nm.

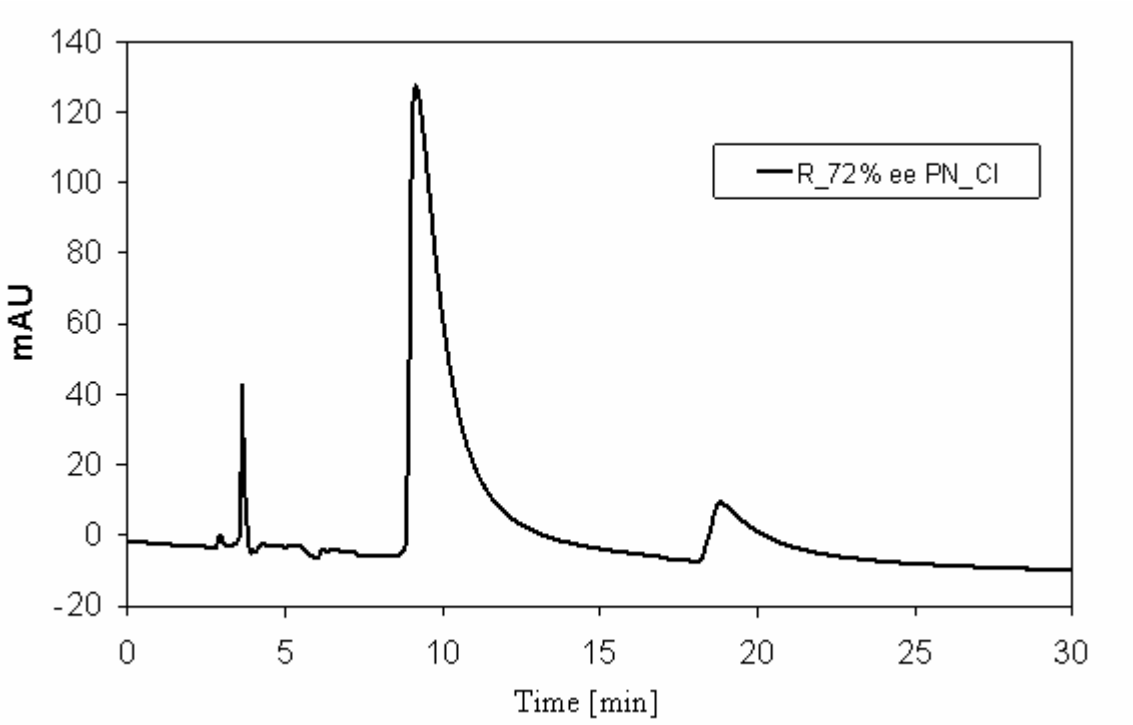

Figure 8.10 Chromatogram of final crystal product obtained from exp03 on Chiralcel OD-H analytical column (dimension 250mm L x 4.6 mm I.D.) under separation conditions: Hexane/IPA (80/20 v/v) at 25^{o}C column temperature, flow rate of 1.0ml/min and UV-Vis detection at 254nm.

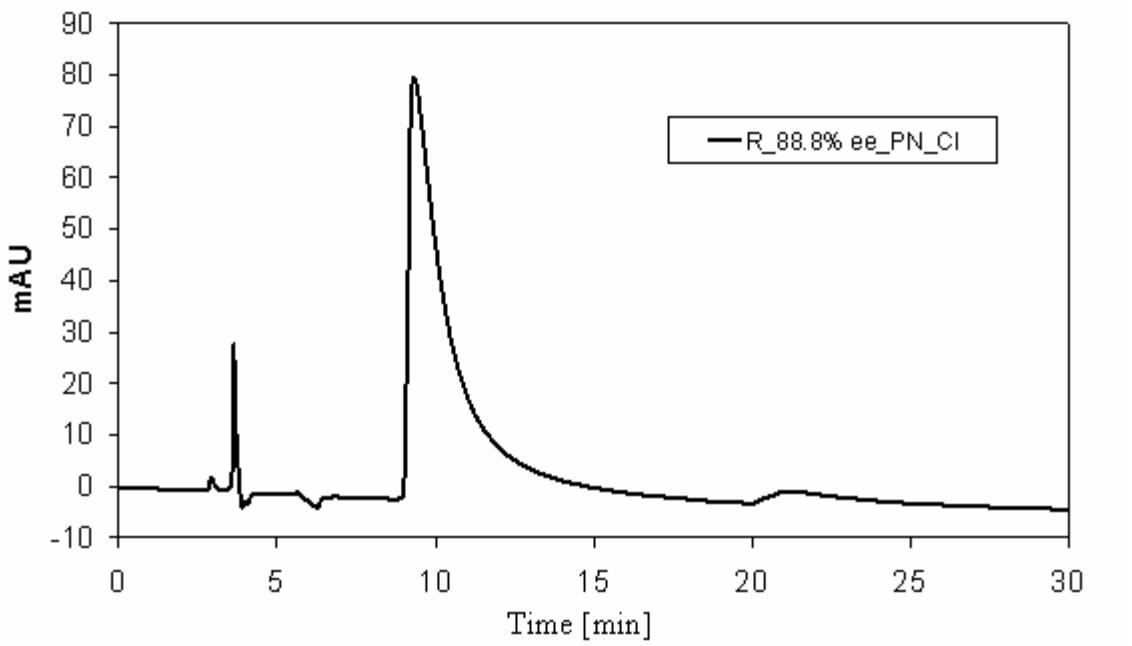

Figure 8.11 Chromatogram of final crystal product obtained from exp04 on Chiralcel OD-H analytical column (dimension 250mm L x 4.6 mm I.D.) under separation conditions: Hexane/IPA (80/20 v/v) at 25^{o}C column temperature, flow rate of 1.0ml/min and UV-Vis detection at 254nm

The optical purity of the final crystal products was also verified by means of DSC measurement. Prior to determining the optical purity of crystallization products by means of DSC, a calibration curve of melting temperature with enantiomeric excess (ee%) was constructed in Figure 8.12. The DSC thermograms of final crystal products obtained from the experiments at different temperature as well as the pure (R)- and (RS)-propranolol hydrochloride are shown in Figure 8.13.

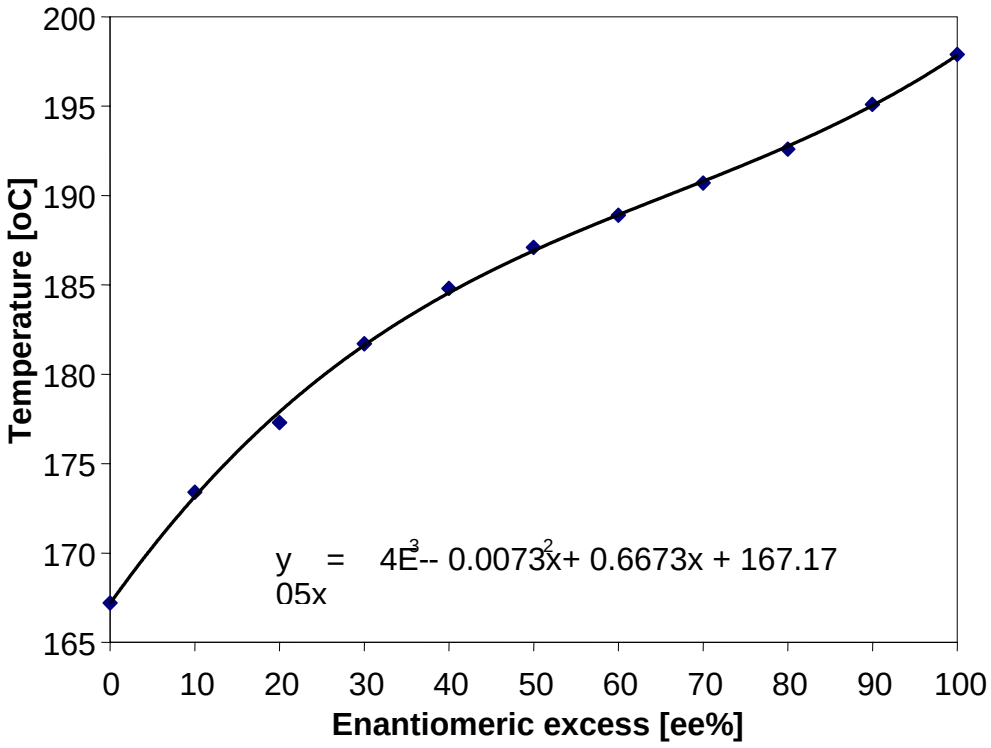

Figure 8.12 Calibration curve of melting temperature with enantiomeric excess

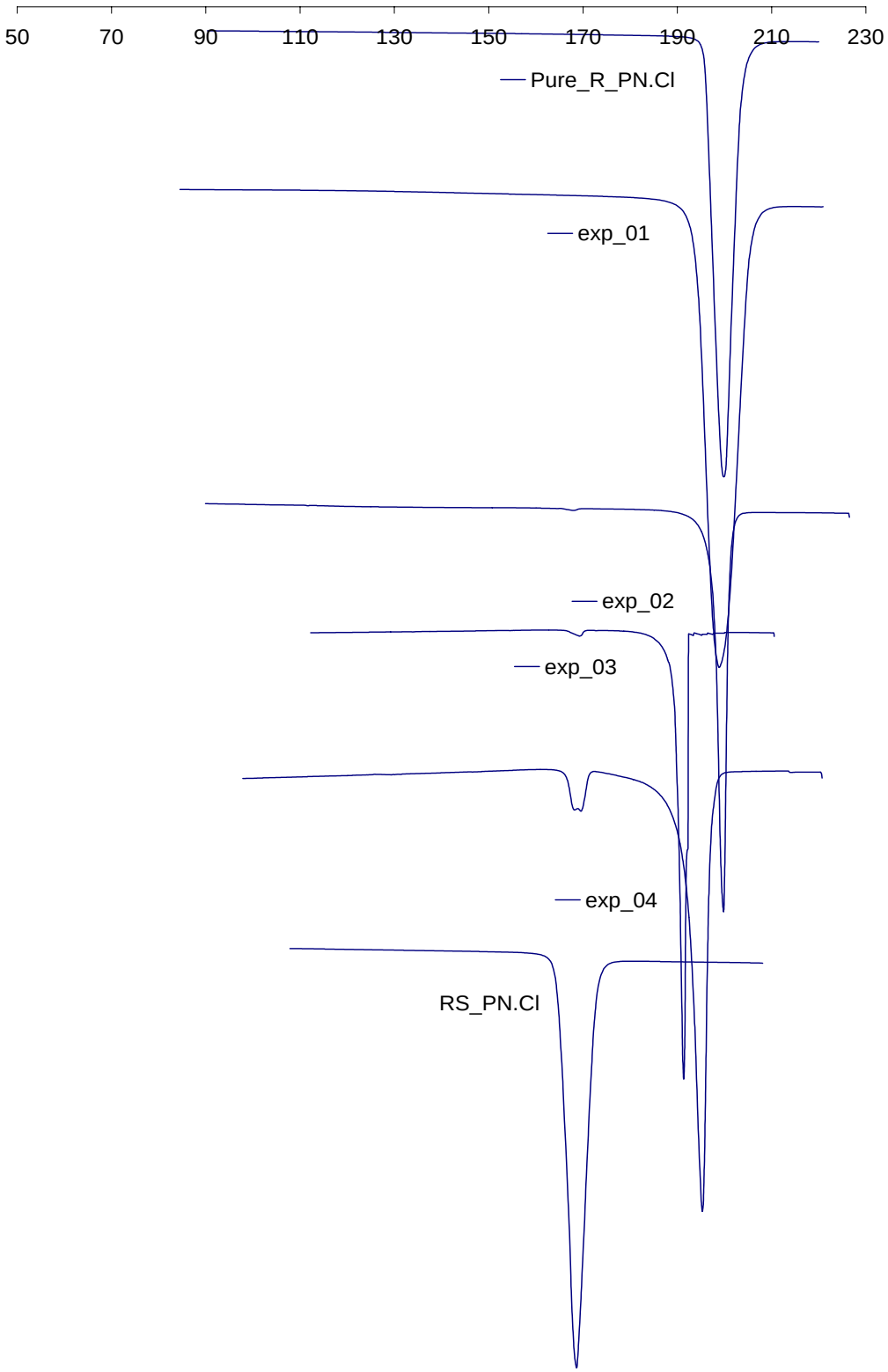

Figure 8.13 DSC thermograms for final crystallization products and pure R- and RS-propranolol hydrochloride

The optical purities of the final crystal products from the crystallization experiments, which were analyzed using the above-mentioned methods, are listed in Table 8.1.

Table 8.1. Final crystal products properties

	Experiment	DSC sample, mg	Temperature, °C	Optical purity, ee%	Cooling Degree
With seeds	Exp_01	3.95	197.9	100	Within ΔT_{crit}
	Exp_02	3.01	197.9	100	
	Exp_03	2.53	191.5	72	Outside ΔT_{crit}
Without seeds	Exp_04	2.93	194.6	88.8	Primary nucleation occurred

Figure 8.13 and Table 8.1 show that pure (R)-enantiomer crystal product was obtained from the seeding cooling crystallization experiments within certain safe limit. The crystallization of (RS)-propranolol was effectively inhibited by controlling the supersaturation of (R)- and (RS)-propranolol hydrochloride within the critical value.

On the contrary, no optically pure crystal product was obtained from the non-seeding crystallization experiment, and two peaks were obviously observed in the DSC thermograms shown as Figure 8.13. The crystal nucleation and growth of both pure

enantiomer and racemate must occur in this operation. That indicates primary nucleation of pure-enantiomer could induce nucleation of racemate (RS)-propranolol hydrochloride.

8.3.5 Crystal morphology and size distribution

The measurement of crystal size distribution (CSD) was described in Chapter 3. The CSDs of the product crystals obtained from the different cooling degree experiments are shown in Figure 8.14. The volume fraction of crystals was plotted versus their size (equivalent sphere diameter) in a semi-logarithmic diagram. From the distribution of exp_01, exp_02 and exp_03, it is observed, for the seeding crystallization experiments, the distribution of the product crystals was shifted to bigger size with the lower cooling degree. This indicates that crystal growth attained during the seeding cooling crystallization. For the non-seeding crystallization experiment exp_04, primary nucleation occurred, hence, the crystal size is obviously smaller. The properties of crystal shape and size were also reflected in the SEM images, shown in Figure 8.15.

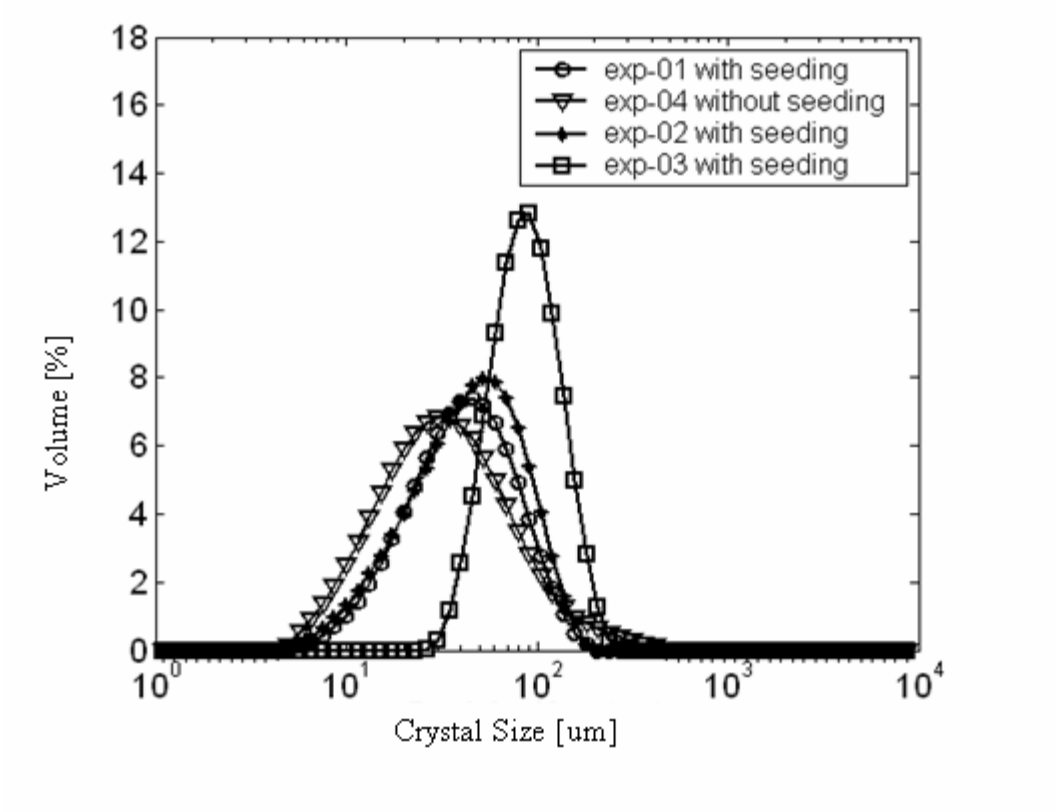

Figure 8.14 Crystal size distribution of crystal products from different experiments

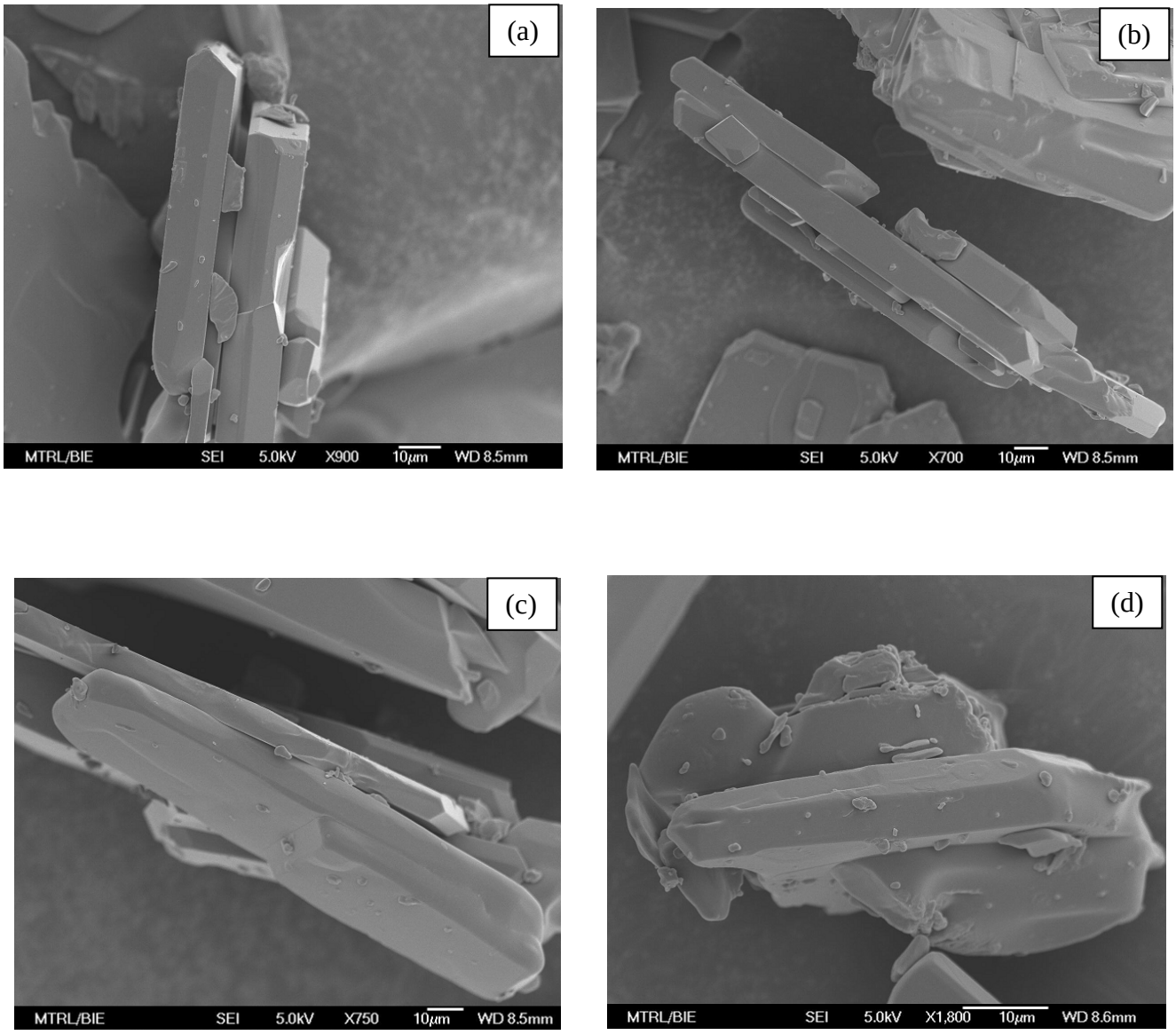

Figure 8.15 SEM images of crystals produced from different conditions: (a) exp_01_with seeds; (b) exp_02_with seeds; (c) exp_03_with seeds; (d) exp_04_without seeds

8.4 Summary

This Chapter performed an exploratory investigation to extend the application of direct crystallization to racemic compound coupling with chromatography. The partially resolved propranolol hydrochloride with 36.7% ee was obtained from HPLC with semi-preparative column. Subsequently, the direct crystallization of propranolol hydrochloride with initial composition 36.7% ee was systematically studied in an automated reactor system. Based on the solubilities and MSZWs of (R)- and (RS)-propranolol hydrochloride, the direct crystallization progression was clearly illustrated under seeding and non-seeding processes. The optical purity of product crystals was accurately determined using HPLC and DSC methods. It was found that the direct crystallization was successfully applied to the enrichment of its partially resolved sample and optically pure crystal product could be obtained within certain safe supersaturation limit. There was no selectivity of crystal growth or nucleation between the pure enantiomer and its racemate when the solution reaches the temperature lower than the temperature of the supersaturated limit of the pure-enantiomer. The relative solubility and critical supersaturation control of the solution with respect to the pure enantiomer and racemate were found essential to obtain the pure enantiomer.

CHAPTER 9 CONCLUSIONS AND FUTURE WORK

9.1 Conclusions

The present work systematically studied the application of preferential crystallization in the optical resolution of chiral pharmaceutical intermediates from the system engineering perspective. In particular, the preferential crystallization of 4-hydroxy-2-pyrrolidone in isopropanol, and the direct crystallization of propranolol hydrochloride in the mixture of methanol and isopropanol (Vol 1:5) were investigated from characterization, thermodynamics measurement and analysis, metastable zone width measurement and interpretation, crystal growth and nucleation kinetics estimation and process optimization and online monitoring. The results provided a systematic engineering approach to study preferential crystallization. Especially, the importance of critical supersaturation control and the integration of thermodynamics, crystallization kinetics and process modeling were proved essential to obtain pure enantiomer crystal products.

In Chapter 4, three types of racemic crystals, namely racemic conglomerates, racemic compounds and pseudoracemates were identified with thermal analysis and structural characterizations. 4-hydroxy-2pyrrolidone and N-methylephedrine were classified as racemic conglomerate forming systems with a eutectic composition of a racemic mixture (R:S=50%:50%) using binary melting phase diagrams. Thermodynamic analysis showed positive values of the difference in the enthalpies of fusion (1600 and 5100 J mol^{-1}) of pure-enantiomer and racemic mixture and a typical values (close to ideal

Rln2) of entropies of mixing of the enantiomers in the liquid states. On the other hand, although propranolol hydrochloride showed similar characteristic of melting point phase diagram to that of a conglomerate forming system, the obviously negative value of the difference in the enthalpies of fusion of (S)- and (RS)-propranolol hydrochloride indicates it is a racemic compound favoring system. The close match of the FTIR, Raman spectra and the PXRD patterns of pure-enantiomer and of its corresponding racemic mixture for 4-hydroxy-2-pyrrolidone and N-methylephedrine and the significant difference of the FT-IR, Raman spectra, PXRD patterns and NMR spectra for propranolol hydrochloride confirmed the above claims. Thermal analysis indicates that atenolol is an ideal pseudoracemate forming system.

In Chapter 5, the thermodynamic properties in solution were investigated using Lasentec FBRM and PVM for the above-mentioned four systems. Suitable solvents were firstly chosen and the solubilities, metastable zone widths and ternary phase diagrams at different enantiomer excess (ee) were subsequently measured. In the aspect of solubility, 4-hydroxy-2-pyrrolidone in isoprapanol and N-methylephedrine in the mixture of isopropanol and water (Vol 1:3) showed similar characteristics of higher solubility with lower ee. The racemic compound propranolol hydrochloride in the mixture of methanol and isopropanol (Vol = 1:5) also showed the similar solubility characteristics. However, their MSZW properties were found quite different. The metastable zone widths of both studied conglomerates 4-hydroxy-2-pyrrolidone and N-methylephedrine were independent of enantiomer excess, which is consistent with the characteristic of two enantiomers forming separate crystals in solution. On the other hand, for the racemic compound propranolol hydrochloride, the metastable zone widths of racemate and pure enatiomer were different. The properties of the evenly distributed molecules in the crystal lattice of a

racemic compound were contributed to this difference with nucleation theory. Three MSZW possibilities were raised for different solubility ratio of racemate to pure enantiomer for a racemic compound, where a cut value of 2 was highlighted. Furthermore, for the conglomerate 4-hydroxy-2-pyrrolidone, different orders of primary nucleation rate at different enantiomeric excess were found, which indicate there may be a critical supersaturation beyond which the nucleation of opposite isomer could occur. This appears to be the first detailed experimental investigation of metastable zone widths of different types of racemates in solution.

In Chapter 6, the dynamic method was used to measure the crystal nucleation and growth kinetics of (R)-4-hydroxy-2-pyrrolidone and (S)-4-hydroxy-2-pyrrolidone in isopropanol. S-plane analysis was developed and applied to the crystallization kinetics parameters estimation and a more suitable transform s was found for the studied system. The regressed crystal nucleation and growth kinetics for both (R)- and (S)-enatiomers from each four batch measurements were pretty similar. No size dependent crystal growth was found and the crystal nucleation rate could be thought as temperature independent under the studied experimental conditions.

In Chapter 7, the concept of critical supersaturation control was proposed for preferential crystallization. With combination of the thermodynamics properties and crystallization kinetics, a detailed mathematical modelling for batch crystallization was established and the orthogonal collocation method was employed to solve the population balance equation to predict the cooling profiles for the preferential crystallization of 4-hydroxy-2-pyrrolidone in isopropanol. A simplified population balance model was found to be suitable for control the critical supersaturation for this system. A series of forced cooling and optimal operations of 4-hydroxy-2-pyrrolidone were experimentally studied

in the automated LabMax with online monitoring with FBRM and PVM. The in-situ monitoring shows that relatively high supersaturation of the target enantiomer induced spontaneous nucleation of the undesired enantiomer, which accordingly resulted in low optical purity and poor crystal size distribution. The proposed optimal temperature trajectory to control the critical supersaturation successfully inhibited the induced nucleation of the undesired enantiomer, and hence produced almost pure crystals with good habits. Further investigations under various supersaturations indicate that there could be an optimal supersaturation which would not lose optical purity. The importance and efficiency of critical supersaturation control was theoretically and experimentally proven. The integration of thermodynamics, crystallization kinetics and population balance modelling was proved essential and helpful to establish this control strategy.

In Chapter 8, an exploratory investigation was carried out to extend the supersaturation control to the direct crystallization of racemic compound propranolol hydrochloride coupling with chromatography. The direct crystallization started with an initial composition of 36.7% ee which can be obtained from semi-preparative HPLC. The progression of direct crystallization with and without seeding was illustrated on the solubility and MSZW diagram. Optically pure crystal product could be obtained within certain carefully controlled supersaturation limit using partially chromatography resolved sample. No selective crystal nucleation and growth was found with respect to the pure enantiomer and its racemate when the solution passed the pure-enantiomer supersaturation limit.

9.2 Suggestions for Future Work

The current optimal crystallization time might be relatively longer for industrial application, although it may be still worth have such an optimal operation to obtain the value-added optically pure pharmaceuticals. As crystallization time is determined by system thermodynamics and crystallization kinetics, for other systems, the crystallization time could be as short as 1-2 hours. It would be attractive for industrial application to find such kind of systems. Furthermore, for the process scale-up, there could be more factors to investigate to determine the value of critical supersaturation.

The development of process analytical technology (PAT) is very fast recently. This technique could be implemented with the current model-based critical supersaturation control from laboratory to large scale on chiral crystallization process.

Although the systematic characterization of different racemic species has been studied, substantial investigation on the melting mechanism of N-methylephedrine during DSC measurement is needed.

Although some exploratory work has been done for the characteristic of MSZWs for three different types of racemic species, in order to further confirm the general relationship of MSZWs with different racemic species, more detailed experimental measurements for many other chiral systems are needed.

To obtain the optimal operating strategy for preferential crystallization, further research can be focused on the seeding programs, e.g. different seed size, seeding temperature.

Further studies on mechanism of crystal nucleation and growth of pure enantiomer, racemate and eutectic mixture are necessary for the purification of racemic compound by direct crystallization.

REFERENCES

Abegg, C. F.; J. D. Stevens and M. A. Larson. Crystal Size Distributions in Continuous Crystallizers When Growth Rate Is Size Dependent. AIChE Journal *14(1)*, pp. 118-122. 1968.

Agranat, I. and H. Caner. Intellectual Property and Chirality of Drugs. Drug Discovery Today, *4,* pp.313-321. 1999.

Allen, T. Particle Size Measurement, Volume 1. London: Chapman & Hall. 1997.

Amiard, G. Direct Resolution of Threonine By Entrainment. Bulletin de la Societe Chimique de France, 447. 1956.

Amiard, G. Resolution by entrainment. The Idea of "Residual" Supersaturation. Experientia. *15*, pp. 38-40. 1959.

Ammon, H. L., D. B. Howe, W. D. Erhardt, A. Balsamo, B. Macchia, F. Macchia and W. E. Keefe. The Crystal Structures of Dichloroisoproterenol, Propranolol and Propranolol Hydrochloride. Acta Crystallographica Section B: Structural Science, *33*, pp.21-29. 1977.

Angelov, I., J. Raisch, M. P. Elsner and A. Seidel-Morgenstern. Optimization of Initial Conditions for Preferential Crystallization.

Industrial and Engineering Chemistry Research, *45*, pp.759-766. 2006.

Anon. FDA's Policy Statement for the Development of New Stereoisomeric Drugs. US Food and Drug Administration Guidance. Washington, DC. 1992.

Anon. Market Trends in Chiral Separations. Universal Pharma Technologies LLC Report. North Andover, MA. 1993.

Aubé, J., Y. Wang, S. Ghosh and K. L. Lnghans. Oxaziridine-Mediated Ring Expansions Of Substituted Cyclobutanones: Synthesis of (-)-γ-Amino-β-Hydroxybutyric Acid (GABOB). Synthetic Communications, *21*, pp.693-701. 1991.

Barrans, P. Y. and M., Cotrait. Conformations Cristallines d'Adrenolytiques β-Bloquants: Propranolol et Alprenolol. Acta Crystallographica Section B: Structural Science, *29*, pp.1264-1272. 1973.

Barrett, P. and B. Glennon. In-Line FBRM Monitoring of Particle Size in Dilute Agitated Suspensions. Particle and Particle Systems Characterization, *16*, pp.207-211. 1999.

Barrett, P. and B. Glennon. Characterizing the Metastable Zone Width and Solibility Curve Using Lasentec FBRM and PVM. Chemical Engineering Research and Design, *80*, pp.799–805. 2002.

Barrett, P., B. Smith, J. Worlitschek, V. Bracken, B. O. Sullivan and D. O. Grady. A Review of the Use of Process Analytical Technology for the Understanding and Optimization of Production Batch Crystallization Processes. Organic Process Research & Development, *9*, pp.348-355. 2005.

Barthe, S. and R. W. Rousseau. Utilization of Focused Beam Reflectance Measurement in The Control of Crystal Size Distribution in A Batch Cooled Crystallizer. Chemical Engineering & Technology, *29(2*), pp. 206-211. 2006.

Beilles, S., P. Cardinael, E. Ndzié, S. Petit and G. Coquerel. Preferential Crystallisation and Comparative Crystal Growth Study Between Pure Enantiomer and Racemic Mixture of A Chiral Molecule: 5-Ethyl-5-Methylhydantoin. Chemical Engineering Science, *56*, pp. 2281-2294. 2001.

Berglund, K. A. and M.A. Larson. Growth of Contact Nuclei of Citric Acid Monohydrate. AIChE Symposium Series. *78*(215), pp. 9-13. 1982.

Berry, D. A. and K. M. Ng. Synthesis of Reactive Crystallization Processes. AIChE Journal *43*(7), pp.1737-1750. 1997.

Berry, D. A. and K. M. Ng. Synthesis of Crystallization-Distillation Hybrid Separation Processes. AIChE Journal, *43*(7), pp.1751-1762. 1997.

Bettinetti, G., F. Giordano, G. Fronza, A. Italia, R. Pellegata, M. Villa and P. Ventura. Sobrerol Enantiomers and Racemates-Solid-State Spectroscopy. Thermal-Behavior, and Phase Diagrams. Journal of Pharmaceutical Sciences, *79*, pp.470-475. 1990.

Black, S. N., L. J. Williams, R. J. Davey, F. Moffatt, R. V. H. Jones, D. M. McEwan and D. E. Sadler. The Preparation of Enantiomers of Paclobutrazol: A Crystal Chemistry Approach. Tetrahedron, *45*(9), pp.2677-2682. 1989.

Bohlin, M. and A. C. Rasmuson. Application of Controlled Cooling and Seeding in Batch Crystallization. The Canadian Journal of Chemical Engineering, *70*, pp.120-126. 1992.

Botsaris, G. D., R. Y. Qian and A. Barrett. New Insights into Nucleation through Chiral Crystallization. AIChE Journal, *45*, pp.201-203. 1999.

Botting, J. The History of Thalidomide. Drug News & Perspective, *15*(9), pp. 604-611. 2002.

Bredikhin, A. A., D. V. Savelev, Z. A. Bredikhina, A. T. Gubaidullin and I. A. Litvinov. Crystallization of Chiral Compounds. 2. Propranolol: Free Base and Hydrochloride. Russian Chemical Bulletin, *52*, pp.853-861. 2003.

Bredikhin, A. A., Z. A. Bredikhina, A. T. Gubaidullin, D. B. Krivolapov and I. A. Litvinov. Rational Approach to A Conglomerate-Forming Propranolol Derivative:

Pointed Modifications of the Crystal Structure. Mendeleev Communications, *14*, pp.268-270. 2004.

Brock, C. P., W. B. Schweizer and J. D. Dunitz. On the Validity of Wallach's Rule: On the Density and Stability of Racemic Crystals Compared with Their Chiral Counterparts. Journal of the American Chemical Society, *113*, pp.9811-9820. 1991.

Brugidou, J., H. Christol and R. Sales. Apparatus for The Resolution of Conglomerates. Bulletin de la Societe Chimique de France, *9-10*, Pt. 2, pp.2033-2034. 1974.

Buser, HR., P. Thomas and M. Markus D. Changed Enantiomer Composition of Metolachlor in Surface Water Following the Introduction of the Enantiomerically Enriched Product to the Market. Environmental Science and Technology, *34*(13), pp.2690-2696. 2000

Burger, A., J. M. Rollinger and W. Lindner. Fundamentals and Predictions of Resolution of Enantiomer Mixtures by Crystallization in the Example of Phase Diagrams of Atenolol and Atenolol Hydrochloride Salt. Pharmazie, *54*, pp.47-51. 1999.

Caldwell, J. and B. E. Leonard. An Introduction to the 'Enantiomer Debate'. Human Psychopharmacology Clin Exp, *16*, pp.65. 2001.

Caldwell, J. Do Single Enantiomers Have Something Special to Offer?. Human Psychopharmacology Clin Exp, *16*, pp.67-71. 2001.

Challener, C.A. (ed). Chiral Intermediates. pp. 3-109, New York: John Wiley & Sons Limited.2001.

Chianese, A., S. Di Cave and B. Mazzarotta. Investigation on Some Operating Factors Influencing Batch Cooling Crystallization, Industrial Crystallization: Proceedings of the Symposium, *84*, pp.443-446. 1984. Amsterdam.

Ching, C. B., P. Fu, S. C. Ng and Y. K. Xu. Effect of Mobile Phase Composition on the Separation of Propranolol Enantiomers Using A Perphenylcarbamate Beta-Cyclodextrin Bonded Chiral Stationary Phase. Journal of Chromatography A, *898*, pp.53-61. 2000.

Choong, K. L. and R. Smith. Optimization of Batch Cooling Crystallization. Chemical Engineering Science, *59*, pp.313–327. 2004.

Chung, S.H., D. L. Ma and R. D. Braatz. Optimal Seeding in Batch Crystallization. The Canadian Journal of Chemical Engineering, *77*, pp.590–596. 1999.

Clontz, N. A., and W. L. McCabe. Contact Nucleation of Magnesium Sulfate Heptahydrate. Chemical Engineering Progress Symposium, Series *67* (110), pp. 6–17. 1971.

Collet, A., M. J. Brienne and J. Jacques. Optical Resolution by Direct Crystallization of Enantiomer Mixtures. Chemical Reviews, *80*, pp.215-230. 1980.

Collet, A. Resolution of Racemates: Did You Say "Classical"? Angewandte Chemie International Edition, *37*, pp.3239-3241. 1998.

Collet, A. Separation and Purification of Enantiomers by Crystallization Methods. Enantiomer, *4*, pp.157 – 172. 1999.

Collins, A. N., G. N. Sheldrake and J. Crosby. (ed). Chirality in Industry II. pp. 119-155, Chichester: John Wiley and Sons. 1997.

Coquerel, G., R. Bouaziz and M. J. Brienne. Optical Resolution of (+/-)-Fenfluramine and (+/-)-Nonfenfluramine by Preferential Crystallization, Chemistry Letters, *7*, pp.1081-1084. 1988.

Coquerel, G., R. Bouaziz and M. J. Brienne. Optical Resolution of (±)-N-Acylnorfenfluramine Derivatives by Preferential Crystallization. Tetrahedron Letters, *31*, pp.2143-2144. 1990.

Coquerel, G. and S. Petit. Recognition of Enantiomers through Morphology of Single Crystals; Application to Some 5-Alkyl-5-Aryl-Hydantoin Derivatives. Journal of Crystal Growth, *130*(1-2), pp. 173-80. 1993.

Coquerel, G., M. N. Petit and R. Bouaziz. Method of Optical Resolution by Crystallization. PCT Int. Appl. pp. 77. 1995.

Coquerel, G. Review on the Heterogeneous Equilibria Between Condensed Phases in Binary Systems of Enantiomers. Enantiomer, *5*, pp.481-498. 2000.

Coquerel, G. Chirality and Crystallisation. Present and Prospects. Chimica Oggi, *21*(3/4), pp. 56-57. 2003.

Costa., C. B. B. and R. Maciel Filho. Evaluation of Optimisation Techniques and Control Variable Formulations for a Batch Cooling Crystallization Process. Chemical Engineering Science, *60*, pp.5312 – 5322. 2005.

Courvoisier, L., E. Ndzié, M. N. Petit, U. Hedtmann, U. Sprengard and G. Coquerel. Influence of the Process on the Mechanisms and the Performances of the Preferential Crystallization: Example with (+/-)-5-(4-Bromophenyl)-5-Methylhydantoin. Chemistry Letters, *4*, pp.364-365. 2001.

Courvoisier, L., L. Mignot, M. N. Petit, U. Sprendgard, U. Hedtman and G. Coquerel. Preferential Crystallization of (F)-5(4V-Bromophenyl)-5-Methylhydantoin. Comparison between SIPC and AS3PC Processes at 2L and 10L Scales. Proceedings of the 9th International Workshop on Industrial Crystallization (BIWIC). 2002. Germany.

Courvoisier, L., L. Mignot, M. N. Petit and G. Coquerel. Combined Effect of Polymorphism and Process on Preferential Crystallization: Example with (±)-5(4′-Methylphenyl)-5-Methylhydantoin. Organic Process Research and Development, *7*, pp. 1007-1016. 2003.

Crosby, J. Synthesis of Optically Active Compounds: A Large Scale Perspective. Tetrahedron, *47*, pp.4789-4846. 1991.

Davey, R. J., S. N. Black, L. J. Williams, D. McEwan and D. E. Sadler. The Chiral Purity of a Triazolylketone Crystallized from Racemic Solutions. Journal of Crystal Growth, *102*, pp.97–102. 1990.

Denk, E. G. and G. D., Botsaris. Mechanism of Contact Nucleation. Journal of Crystal Growth, *13*(1), pp. 57-60. 1972.

Denk, E. G. and G. D. Botsaris. Fundamental Studies in Secondary Nucleation, Journal of Crystal Growth, *13-14*, pp.493–499. 1972.

DIN 51004, 1994, Normenausschuß für Materialprüfung (NMP) im DIN, DIN 51004, Thermische Analyse (TA), Bestimmung der Schmelztemperaturen Kristalliner Stoffe mit der Differenzialthermoanalyse (DTA) (engl.: Thermal Analysis, Determinition of Melting Temperatures of Crystalline Materials by Differential Thermal Analysis), Deutsches Institut für Normung e.V., 1994, (German Standards, 1994).

Di Silvestro, G., G. Palmisano and R. Pellegata. Phase Diagram of (R)- and (S)-4 Hydroxy-2-Pyrrolidone; Mixtures: A New Case of a Conglomerate-Forming System. Journal of Pharmaceutical Sciences, *82*, pp.758-760. 1993.

Doki, N., M. Yokota, S. Sasaki and N. Kubota. Simultaneous Crystallization of D- and L-Asparagines in the Presence of a Tailor-Made Additive by Natural Cooling Combined with Pulse Heating. Crystal Growth & Design, *4*, pp.1359-1363. 2004.

Dolling, U. H., A. W. Douglas, E. J. J. Grabowski, E. F. Schoenewaldt, P. Sohar, and M. Sletzinger. Synthesis and Resolution of 3-Fluoro-D,L-Alanine-2-d: A Selective Deuteration via Reductive Amination With Sodium Borodeuteride. Journal of Organic Chemistry, *43*(9), pp.1634-1640. 1978.

Dowling, B. B. Resolution of Racemic Glutamic Acid. US 2898358. 1959.

Druot, S., M. N. Petit, S. Petit, G. Coquerel and N. B. Chanh . Experimental Data and Modelling of The Interactions in Solid State and in Solution Between (R)-and (S)-N-

Acetyl-Alpha-Methylbenzylamine. Influence on Resolution by Preferential Crystallization. Molecular Crystals and Liquid Crystals Science and Technology, Section A-Molecular Crystals and Liquid Crystals, *275*: pp.271-291. 1996.

Dufour, F., C. Gervais, M. N. Petit, G. Perez and G. Coquerel. Investigations on the Reciprocal Ternary System (±)-2-Phenylpropionic Acid-(±)-α-Methylbenzylamine. Impact of an Unstable Racemic Compound on the Simultaneous Resolution of Chiral Acids and Bases by Preferential Crystallisation. Journal of the Chemical Society, Perkin Transactions *2*, pp. 2022-2036. 2001.

Dufour, F., G. Perez and G. Coquerel. A Priori Assessment of the Maximum Possible Entrainment Effect Attainable during Preferential Crystallization. The Case of the Simultaneous Resolution of (±)-Ephedrine and (±)-Mandelic Acid. Bulletin of the Chemical Society of Japan, *77*, pp.79-86. 2004.

Duschinsky, R. Spontaneous Resolution of A Racemic Compound (Histidine Monohydrochloride). Chemistry & Industry (London, United Kingdom), 10. 1934.

Dwivedi, S. K., S. Sattari, F. Jamali and A. G. Mitchell. Ibuprofen Racemate and Enantiomers: Phase Diagram, Solubility and Thermodynamic Studies.
International Journal of Pharmaceutics, *87*, pp.95-104. 1992.

Elsner, M. P, H. Lorenz and A. Seidel-Morgenstern. Preferential Crystallization for Enantioseparation - New Experimental Insights Indispensable for a Theoretical Approach and an Industrial Application. Coquerel, G. (ed). Proceedings of the 10th International Workshop on Industrial Crystallization (BIWIC), pp. 18 – 25. 2003. Rouen.

Elsner, M. P., D. F. Menendez, E. A. Muslera and A. Seidel-Morgenstern. Experimental Study and Simplified Mathematical Description of Preferential Crystallization. Chirality, *17*, pp. S183-S195. 2005.

Evans, T.W., G. Margolis and A. F. Sarom. Mechanisms of Secondary Nucleation in Agitated Crystallizers. AIChE Journal. *20*, pp. 950–958. 1974

Ewing, G.W. Instrumental Methods of Chemical Analysis. New York: McGraw-Hill. 1985.

Farrell R. J. and Y. C. Tsai. Modeling, Simulation and Kinetic Estimation in Batch Crystallization Parameter Processes. AIChE J, *40*, pp.586-593. 1994.

Fung, K. Y., K. M. Ng and C. Wibowo. Synthesis of Chromatography-Crystallization Hybrid Separation Processes. Industrial & Engineering Chemistry Research, *44*, pp.910-921. 2005.

Furberg, S. and O. Hassel. Phenylglyceric Acids. Acta Chemica Scandinavica, *4* pp. 1020-1023. 1950.

Garside, J., A. Mersmann and J. Nývlt. Measurement of Crystal Growth and Nucleation Rates. Institution of Chemical Engineers (IChemE). 2002.

Garside, J., L. G. Gibilaro and N. S. Tavare. Evaluation of Crystal Growth Kinetics from A Desupersaturation Curve Using Initial Derivatives. Chemical Engineering Science, *37*, pp.1625-1628. 1982.

Garside, J. and S. J. Jancic. Growth and Dissolution of Potash Alum Crystals in the Subsieve Size Range. AIChE J, *22*, pp.887-894. 1976.

Gerson, A. R., K. J. Roberts and J. N. Sherwood. An Instrument for the Examination of Nucleation from Solution and Its Application to the Study of Precipitation from Diesel Fuels and Solutions of N-Alkanes, Powder Technology, *65*, pp.243-249. 1991.

Gervais, C., S. Beilles, P. Cardinael, S. Petit and G. Coquerel. Oscillating Crystallization in Solution between (+)- and (-)-5-Ethyl-5-Methylhydantoin under the Influence of Stirring. Journal of Physical Chemistry B, *106*, pp.646-652. 2002.

Gervais, C. and G., Coquerel. Simple Model Designed to Generate New Crystal Structures Derived From a Mother Phase. Acta Cryst. B*58*, pp. 662-672. 2002.

M. W. Girolami and R. W. Rousseau. Initial Breeding in Seeded Batch Crystallizers. Industrial & Engineering Chemistry Process Design and Development, *25*(1), pp.66-70. 1986.

Gritti, F. and G. Guiochon. Effect of the Ionic Strength of Salts on Retention and Overloading Behavior of Ionizable Compounds in Reversed-Phase Liquid Chromatography: II. Symmetry-C18. Journal of Chromatography A, *1033*, pp.57-69. 2004.

Halfon, A. and S. Kaliaguine. Alumina Trihydrate Crystallization. Canadian Journal of Chemical Engineering, *54*, pp.160-172. 1976.

Harada, K., H. Mizumoto, M. Nomoto and S. Wakita. Optical Resolution of Monoammonium DL-Malate by Preferential Crystallization. Chemistry and Industry, *20*, pp.68-69. 1986.

Heath, A. R., P. D. Fawell, P. A. Bahri and J. D. Swift. Estimating Average Particle Size by Focused Beam Reflectance Measurement (FBRM). Particle and Particle Systems Characterization, *19*, pp.84–95. 2002.

Herráez-Hernández, R. and P. Campíns-Falcó. Chiral Separation of Ephedrines by Liquid Chromatography Using β-Cyclodextrines. Analytica Chimica Acta, *434*, pp.315-324. 2001.

Hongo,C., M. Shibazaki, S. Yamada and I. Chibata. Preparation of Optically Active Proline. Optical Resolution of N-Acyl-DL-Proline by Preferential Crystallization Procedure. Journal of Agricultural and Food Chemistry, *24*, pp.903-906. 1976.

Hongo,C., S. Yamada and I. Chibata. The Stability of Supersaturation State in Optical Resolution by the Preferential Crystallization Procedure. Bulletin of the Chemical Society of Japan, *54*, pp.1905-1910. 1981.

Hongo, Chikara; S., Yamada and I., Chibata. The Prediction of The Optical Resolution Process By The Use of The Preferential Crystallization Procedure Res. Lab. Appl. Biochem.. Bulletin of the Chemical Society of Japan , *54*(7), pp.1911-13. 1981.

Hongo, C., R. Yoshioka, M. Tohyama, S. Yamada and I. Chibata. Racemization of Optically Active Amino Acid Salts and an Approach to Asymmetric Transformation of DL-Amino Acids. Bulletin of the Chemical Society of Japan, *56*, pp.3744-3747. 1983.

Houllemare-Druot, S. and G. Coquerel. How Far Can an Unstable Racemic Compound Affect the Performances of Preferential Crystallization? Example with (R) and (S)-α-Methylbenzylamine Chloroacetate. Journal of the Chemical Society. Perkin Transactions,

2, pp. 2211-2220. 1998.

Hu, Q., S. Rohani, D. X. Wang and A. Jutan. Nonlinear Kinetic Parameter Estimation for Batch Cooling Seeded Crystallization. AIChE J, *50*, pp.1786-1794. 2004.

Huang, P. Q., X. Zheng, S. L. Wang, J. L. Ye, L. R. Jin, and Z. Chen. A New Approach to (S)-4-Hdroxy-2-Pyrrolidone and Its 3-Substituted Analogues. Tetrahedron: Asymmetry, *10*, pp.3309-3317. 1999.

Hulburt, H. M. and S. Katz. Some Problems in Particle Technology: A Statistical Mechanical Formulation. Chemical Engineering Science, *19*, pp.555-574,1964.

Inoue, T. and S. Suzuki. The Metabolism of (±)-Methylephedrine in Rat and Man. Xenobiotica, *20*, pp.99-106. 1990.

Ishigooka, J., Y. Yoshida and M. Murasaki. Abuse of BORN – A Japanese OTC Cough Suppressant Solution Containing Methylephedrine, Codeine, Caffeine and Chlorpheniramine, Progress in Neuro-Psychopharmacology&Biological Psychiatry, *15*, 513ff. 1991.

Jacobsen, C., J. Garside and M. Hoare. Nucleation and Growth of Microbial Lipase Crystals from Clarified Concentrated Fermentation Broths. Biotechnology and Bioengineering, *57*, pp. 666-675, 1998.

Jacques, J., A. Collet and S. H. Wilen. Enantiomers, Racemates and Resolution Malabar, Florida: Krieger Publishing Company. 1994.

Jones, A. G. and J. W. Mullin. Programmed Cooling Crystallization of Potassium Sulphate Solutions. Chemical Engineering Science, *29*, pp.105–118. 1974.

Jones, A. G. Optimal Operation of A Batch Cooling Crystallizer. Chemical Engineering Science, *29*, pp.1075–1087. 1974.

Juza, M., M. Mazzotti and M. Morbidelli. Simulated Moving-Bed Chromatography and its Application to Chirotechnology. Tibtech, *18*, pp.108-118. 2000.

Kawasuji, T., K. Koike and H. Saito. Chronotropic Effects of Optical Isomers of Ephedrine and Methylephedrine in the Isolated Rat Right Atria and in Vitro Assessment of Direct and Indirect Actions on β_1-Adrenoceptors. Biological & Pharmaceutical Bulletin, *19*, pp.1423-1428. 1996.

Kauffman, G. B. and R. D. Myers. The Resolution of Racemic Acid. A Classic Stereochemical Experiment for The Undergraduate Laboratory. Journal of Chemical Education, *52*(12), pp. 777-781. 1975.

Kim, K. J. and S. K. Ryu. Nucleation of Thiourea Adduct Crystal with Cyclohexane}Methylcyclopentane. Chemical Engineering Communications, *159*(1), pp. 51. 1997.

Kim, K. J. and A. Mersmann. Estimation of Metastable Zone Width in Different Nucleation Processes. Chemical Engineering Science, *56*, pp.2315-2324. 2001.

Kommuru, T. R., M. A. Khan and I. K. Reddy. Racemate and Enantiomers of Ketoprofen: Phase Diagram, Thermodynamic Studies, Skin Permeability, and Use of Chiral Permeation Enhancers. Journal of Pharmaceutical Sciences, *87*, pp.833-840. 1998.

Kondepudi, D. K., R. J. Kaufman and N. Singh. Chiral Symmetry Breaking in Soldium Chlorate Crystallization, Science, *250*, pp.975-977. 1990.

Kondepudi, D. K., K. L. Bullock, J. A. Digits, J. K. Hall and J. M. Miller. Kinetics of Chiral Symmetry Breaking in Crystallization. Journal of the American Chemical Society, *115*, pp.211-216. 1993.

Kondepudi, D. K., K. L. Bullock, J. A. Digits and P. D. Yarborough. Stirring Rate as a Critical Parameter in Chiral Symmetry Breaking Crystallization.
Journal of the American Chemical Society. *117*, pp.401-404. 1995.

Kondepudi D. K. and Culha M. Chiral Interaction and stochastic kinetics in stirred crystallization of amino acids. Chirality. 10, pp.238–245,1998.

Kougoulos, E., A. G. Jones and M. W. Wood-Kaczmar. Estimation of Crystallization Kinetics for an Organic Fine Chemical Using a Modified Continuous Cooling Mixed Suspension Mixed Product Removal (MSMPR) Crystallizer. Journal of Crystal Growth. *273*, pp.520–528. 2005.

Kougoulos, E., A. G. Jones, K. H. Jennings and M. W. Wood-Kaczmar. Use of Focused Beam Reflectance Measurement (FBRM) and Process Video Imaging (PVI) in a Modified Mixed Suspension Mixed Product Removal (MSMPR) Cooling Crystallizer. Journal of Crystal Growth, *273*, pp.529–534. 2005.

Kunsman, G. W., R. Jones, B. Levine and M. L. Smith. Methylephedrine Concentrations in Blood and Urine Specimens. Journal of Analytical Toxicology, *22*, pp.310-313. 1998.

Leusen, F. J. J., J. H. Noordik and H. R. Karfunkel. Racemate Resolution via Crystallization of Diastereomeric Salts: Thermodynamic Considerations and Molecular Mechanics Calculations. Tetrahedron, *49*, pp.5377-5396. 1993.

Leusen, F. J. J. Crystal Structure Prediction of Diastereomeric Salts: A Step Toward Rationalization of Racemate Resolution. Crystal Growth and Design, *3*, pp. 189-192. 2003.

Levkin, P. A., Y. A. Strelenko, K. A. Lyssenko, V. Schurig and R. G. Kostyanovsky. Temperature-Dependent Racemic Compound-Conglomerate Crystallization of 2,3:6,7-Dibenzobicyclo[3.3.1]Nona-2,6-Diene-4,8-Dione. Tetrahedron-Asymmetry, *14*, pp.2059-2066. 2003.

Li, Z. J. and J. W. Grant. Relationship Between Physical Properties and Crystal Structures of Chiral Drugs. Journal of Pharmaceutical Science, *86*, pp.1073-1078. 1997.

Li, Z. J., M. T. Zell, E. J. Munson and J. W. Grant. Characterization of Racemic Species of Chiral Drugs Using Thermal Analysis, Thermodynamic Calculation, and Structural Studies. Journal of Pharmaceutical Science, *88*, pp.337-346. 1999.

Li, Z. J., W. H. Ojala and D. J. W. Grant. Molecular Modeling Study of Chiral Drug Crystals: Lattice Energy Calculations. Journal of Pharmaceutical Science, *90*, pp.1523-1539. 2001.

Lim, B.G., C. B. Ching, R. B. H. Tan and S. C. Ng. Recovery of (–)-Praziquantel from Racemic Mixtures by Continuous Chromatography and Crystallisation. Chemical Engineering Science, *50*, pp.2289-2298. 1995.

Lin, G.Q., Y. M. Li and A. S. C. Chan. Principles and Applications of Asymmetric Synthesis. New York: John Wiley and Sons. 2001.

Lorenz, H., P. Sheehan and A. Seidel-Morgenstern. Coupling of Simulated Moving Bed Chromatography and Fractional Crystallisation for Efficient Enantioseparation, Journal of Chromatography A, *908*, pp.201-214. 2001.

Lorenz, H., D. Sapoundjiev and A. Seidel-Morgenstern. Study of Solubility Equilibria in Chiral Systems. Chianese, A. (ed). Proceedings of 15th International Symposium on Industrial Crystallization. Italy, pp.167-172, 2002.

Lorenz, H. and A. Seidel-Morgenstern. Binary and Ternary Phase Diagrams of Two Enantiomers in Solvent Systems. Thermochimica Acta, *382*, pp.129-142. 2002.

Lorenz H, D. Sapoundjiev and A. Seidel-Morgenstern. Enantiomeric Mandelic Acid System-Melting Point Phase Diagram and Solubility in Water. Journal of Chemical Engineering Data, *47*, pp.1280-1284. 2002.

Lu, Y. H. and C. B. Ching. Study on the Metastable Zone Width of Ketoprofen. Chirality, *18*, pp.239-244. 2006.

Maciel, G. E., N. R. Jagannathan and J. S. Frye. Solid-state NMR: Opportunities and Challenges. In NMR and X-ray Crystallography: Interfaces and Challenges; Etter, M. C., Ed.; Trans. Am. Crystallogr. Assoc. *24*, pp. 1-23, 1988.

Ma, D. L., D. K. and R. D. Braatz. Optimal Control and Simulation of Multidimensional Crystallization Processes, Computers and Chemical Engineering, *26*, pp.1103–1116. 2002.

Maier, N. M., P. Franco and W. Lindner. Separation of Enantiomers: Needs, Challenges, Perspectives. Journal of Chromatography A, *906*, pp.3-33. 2001.

Matsumoto, T., W. Trueb, R. Gwinner and C. H. Eugster. Isolierung von (-)-R-4-Hydroxy-2-Pyrrolidon-(2) und Einigen Weiteren Verbindungen aus Amanita Muscaria. Helvetica Chemica Acta, *52*, pp.716-720. 1969.

Matsuoka, M., H. Hasegawa and K. Ohori. Purity Decrease of L-Threonine Crystals in Optical Resolution by Batch Preferential Crystallization. In Myerson, A. S. and K. Toyokura. (ed). Crystallization as a Separations Process. pp. 251-260, Washington, DC: American Chemical Society. 1990.

Matsuoka, M. Purity Drop in Optical Resolution of Racemic Mixtures. In: Botsaris, G. D. and K. Toyokura. (ed). Separation and Purification by Crystallization. pp. 59-72, Washington, DC: American Chemical Society. 1997.

Matthews H. B. and J. B. Rawlings. Batch Crystallization of a Photochemical: Modeling, Control, and Filtration. AIChE J, *44*, pp.1119-1127. 1998.

Mayrhofer B. and J. Nyvlt. Programmed Cooling of Batch Crystallizers. Chemical Engineering Process, *24*, pp.217-220. 1988.

Meyerhoffer, W. The Breaks in The Solubility Curves. Journal of Physical Chemistry, *8*(8), pp.571-575. 1904.

McBride, J. M. and R. L. Carter. Spontaneous Resolution by Stirred Crystallization. Angewandte Chemie-International Edition, *30*, pp.293-295. 1991.

McCague, R. Crystallisation and Industrial Chiral Synthesis. Manufacturing Chemist, *69*, pp.13-15,17. 1998.

McCague, R. Enantiomeric Purity with Conglomerates. Manufacturing Chemist, *69*, pp. 22-23. 1998.

Merck Company, MERCK Achievement – First Commercial, Continuous Process to Use Selective Crystallization Separates Optically Active Isomers, Chemical Engineering, *8*, pp.247-248. 1965.

Mersmann A. Crystallization Technology Handbook. New York: Marcel Dekker. 1995.

Mersmann, A. Supersaturation and Nucleation. Chemical Engineering Research and Design, *74*(1), pp. 812. 1996.

Mersmann, A. and K., Bartosch. How to Predict the Metastable Zone Width. Journal of Crystal Growth*, 183*, pp.240., 1997.

Miller, S. M. Modelling and Quality Control Strategies for Batch Cooling Crystallizers. PhD Thesis, University of Texas at Austin, 1993.

Miyazaki, H., H. Morita, T. Shiraiwa and H. Kurokawa. Optical Resolution by Preferential Crystallization and Replacing Crystallization of DL-Allothreonine. Bulletin of the Chemical Society of Japan, *67*, pp.1899-1903. 1994.

Mullin, J. W. and J. Nyvlt. Programmed Cooling of Batch Crystallizers. Chemical Engineering Science, *26*, pp.369–377. 1971.

Mullin, J. W. and S. J. Jancic. Interpretation of the Metastable Zone Width. Trans IChemE, *57*, pp.188-193. 1979.

Mullin, J. W. Crystallization. Oxford: Butterworth-Heinemann. 2001.

Murakami, K., M. Ohashi, A. Matsunaga, Y. Yamamoto, A. Tomiguchi and H. Nohira. Optical Resolution by Preferential Crystallization of 2-(3,4-Carbonyldioxyphenyl)-2-(Phthalimidooxy)Acetic Acid, a Key Intermediate of Cephalosporin Antibiotic M-14659. Bulletin of the Chemical Society of Japan, *65*, pp. 3288-3293. 1992.

Murakami, K., M. Ohashi, A. Matsunaga, I. Yamamoto and H. Nohira. Asymmetric Transformation of a Racemic α-(Phthalimidooxy)Arylacetic Ester by a Combination of Preferential Crystallization and Simultaneous Racemization. Chirality, *5*, pp.41-48. 1993.

Myerson, A. S. and R. Ginde. Crystals, Crystal Growth, and Nucleation. Handbook of Industrial Crystallization. Oxford: Butterworth-Heinemann. pp. 33-65. 2002.

Nass, K. K. Rational Solvent Selection for Cooling Crystallizations. Industrial and Engineering Chemistry Research, *33*, pp.1580-1584. 1994

Ndzié, E., P. Cardinael, A. R. Schoofs and G. Coquerel. An Efficient Access to the Enantiomers of α-Methyl-4-Carboxyphenylglycine via a Hydantoin Route Using a Practical Variant of Preferential Crystallization. AS3PC (Auto Seeded Programmed Polythermic Preferential Crystallization). Tetrahedron Asymmetry, *8*, pp. 2913-2920. 1997.

Ndzié, E., P. Cardinael, M. N. petit and G. Coquerel. Enantiomeric Resolution of (+/-)-5-Ethyl-5-Methylhydantoin by Means of Preferential Nucleation. Enantiomer, *4*, pp.97-101. 1999.

Neau, S. H., M. K. Shinwari and E. W. Hellmuth. Melting Point Phase Diagrams of Free Base and Hydrochloride Salts of Bevantolol, Pindolol and Propranolol. International Journal of Pharmaceuticals, *99*, pp.303-310. 1993.

Nelson, H. S., G. Bensch, W. W. Pleskow., R. DiSantostefano, S. DeGraw, D. S. Reasner, T. E. Rollins and P. D. Rubin. Improved Bronchodilation with Levalbuterol Compared with Racemic Albuterol in Patients with Asthma. Journal of Allergy and Clinical Immunology, 102(6, Pt. 1), pp.943-952. 1998.

Noyori, R., M. Tokunaga and M. Kitamura. Stereoselective Organic Synthesis via Dynamic Kinetic Resolution. Bulletin of the Chemical Society of Japan, *68*(1), pp.36-56. 1995.

Nyvlt, J. and V. Vaclavu. Cooling Rate in A Batch Crystallizer. Chemicky Prumysl. 14(2), pp.79-81, 1964.

Nyvlt, J. Kinetics of Nucleation in Solutions. Journal of Crystal Growth, *3,4*, pp.377-383. 1968.

Nyvlt, J., R. Rychly, J. Gottfried and J. Wurzelova. Metastable Zone-Width of Some Aqueous Solutions. Journal of Crystal Growth, *6*, pp.151-162. 1970.

Nyvlt, J., F. Moudry and V. Veverka. Mathematical Models of a Cascade of Ideally Agitated Crystallizers. Collection of Czechoslovak Chemical Communications. *38*(7), pp.1815-1839,1973.

Nyvlt, J. Optimal Crystallization Temperature. Chemicky Prumysl. *33*(9), pp. 463-6, 1983.

Nyvlt, J., O. Sohnel, M. Matuchova and M. Broul. The Kinetics of Industrial Crystallization. pp. 47-65, Amsterdam: Elsevier. 1985.

Nyvlt, J. Calculation of the Kinetics of Crystallization Based on a Single Batch Experiment. Collection of Czechoslovak Chemical Communications, *54*, pp.3187. 1989.

O'Dell, F. P. and R.W. Rousseau. Magma Density and Dominant Size for Size Dependent Crystal Growth. AIChE Journal, *24*(4), pp. 738-741.1978.

O'Dell, F. P.; R.W. Rousseau and W.L. McCabe. Selective Nucleation of Mutually Soluble Substances. Institution of Chemical Engineers Symposium Series, *54*(Alternatives Distill.), pp.13-20. 1978.

Omran, A. M. and C. J. King. Kinetics of Ice Crystallization in Sugar Solutions and Fruit Juices. AIChE. Journal, *20*, pp.795-803. 1974.

Ostwald, W. Studies on the Formation and Inversion of Solids. First paper: Supersaturation and Supercooling. Zeitschrift fuer Physikalische Chemie, Stoechiometrie und Verwandtschaftslehre, 22 pp.289. 1897.

Pallavicini, M., C. Bolchi, R. DiPumpo, L. Fumagalli, B. Moroni, E. Valoti and F. Demartin. Resolution of 5-Hydroxymethyl-2-Oxazolidinone by Preferential Crystallization and Investigations on the Nature of the Racemates of Some 2-Oxazolidinone Derivatives. Tetrahedron-Asymmetry, *15*, pp.1659-1665. 2004.

Pasteur, L. Mémoire sur la relation qui peut exister entre la forme cristalline et la composition chimique, et sur la cause de la polarisation rotatoire. Compt. Rend. Acd Sci.,*26*(21), pp. 535-538.1848.

Pena, R., A. Chauvet, J. Masse, J. P. Ribet and J. L. Maurel. Phase Diagram of R(+)-S(-) Efaroxan Hydrochloride. Journal of Thermal Analysis and Calorimetry, *53*, pp. 697-709. 1998.

Perez-Garcia, L. and D. B. Amabilino. Spontaneous Resolution under Supramolecular Control. Chemical Society Reviews, *31*, pp.342-356. 2002.

Perlberg, A., H. Lorenz and A. Seidel-Morgenstern. Determination of Crystallization Relevant Data for Enantioseparation Purposes. Chianese, A. (ed). Proceedings of 15th International Symposium on Industrial Crystallization. pp.173-178. 2002.

Perlberg, A., H. Lorenz and A. Seidel-Morgenstern. Determination of Crystallization Kinetics in Chiral Systems. Coquerel, G. (ed). Proceedings of 10th International Workshop on Industrial Crystallization (BIWIC). pp.180-187. 2003.

Perlberg, A., H. Lorenz and A. Seidel-Morgenstern. Aspects of Crystal Growth in Chiral Systems on the Example of Mandelic Acid in Water, VDI-Berichte 1901 II, pp. 689-694. 2005.

Perlberg A., H. Lorenz and A. Seidel-Morgenstern. Crystal Growth Kinetics via Isothermal Seeded Batch Crystallization: Evaluation of Measurement Techniques and Application to Mandelic Acid in Water. Industrial & Engineering Chemistry Research. *44* (4), pp. 1012-1020, 2005.

Petit, M. N. and G. Coquerel. Resolution of Pasteur Salts by Auto-Seeded Preferential Crystallization. Mendeleev Communications, *3*, pp. 95-96. 2003.

Pons, MN, K. Milferstedt and E. Morgenroth. Modeling of Chord Length Distributions. Chemical Engineering Science. *61*, pp. 3962-3973, 2006.

Prankerd, R. J. and M. Z. Elsabee. Thermal Analysis of Chiral Drug Mixtures: the DSC Behaviour of Mixtures of Ephedrine HCl and Pseudoephedrine HCl Enantiomers. Thermochimica Acta, *248*, pp.147-160. 1995.

Prigogine and R. Defay. Thermodynamique Chimique conformément aux méthodes de Gibbs et De Donder (2 Tomes), Liège, Desoer, 1944-1946. Or the translation in English: Chemical Thermodynamics, translated by D.H. Everett, Langmans 1954, 1962.

Profir, V. M. and M. Matsuoka. Processes and Phenomena of Purity Decrease during the Optical Resolution of DL-Threonine by Preferential Crystallization. Colloids and Surfaces A: Physicochemical and Engineering Aspects, *164*, pp.315-324. 2000.

Profir V. M. and A. C. Rasmuson. Influence of Solvent and the Operating Conditions on the Crystallization of Racemic Mandelic Acid. Crystal Growth & Design, *4*, pp.315-323. 2004.

Qian, R.Y., Z. D. Chen, H. G. Ni, Z. Z. Fan and F. D. Cai. Crystallization Kinetics of Potassium Chloride from Brine and Scale-up Criterion. AIChE Journal *33*, 1690–1697. 1987.

Qian, R.Y., X. S. Fang and Z. K. Wang. Supersaturation and Crystallization Kinetics of Potassium Chloride. Industrial and Engineering Chemistry Research. *28*, pp.844–850, 1989.

Qian, R.Y. and G. D. Botsaris. Laboratory Simulation of Industrial Crystallizer Cycling. Industrial and Engineering Chemistry Research. *35*, pp.1163–1172, 1996.

Qian, R. Y. and G. D. Botsaris. A New Mechanism for Nuclei Formation in Suspension Crystallizers: the Role of Interparticle Forces. Chemical Engineering Science, *52*, pp.3429–3440. 1997.

Qian, R. Y. and G. D. Botsaris. Nuclei Breeding from a Chiral Crystal Seed of NaClO3. Chemical Engineering Science, *53*, pp.1745–1756. 1998.

Qian, R. Y. and G. D. Botsaris. The Effect of Seed Preparation on the Chirality of the Secondary Nuclei. Chemical Engineering Science, *59*, pp.2841–2852. 2004.

Qiu, Y. and A. C. Rasmuson. Crystal Growth Rate Parameters from Isothermal Desupersaturation Experiments. Chemical Engineering Science, *46*, pp.1659-1667. 1991.

Qiu, Y. and A. C. Rasmuson, A. Estimation of Crystallization Kinetics from Batch Cooling Experiments. AIChE Journal, *40*, pp.799-812. 1994.

Randolph, A. D. and M. A. Larson. Transient and Steady State Size Distributions in Continious Mixed Suspension Crystallizers. AIChE Journal, *8*, pp.639-645. 1962.

Randolph, A. D. and M. A. Larson. Theory of Particulate Processes: Analysis and Techniques of Continuous Crystallization. San Diego California: Academic Press. 1988.

Rawle, A. The Basic Principles of Particle Size Analysis. Malvern Instruments Ltd. available at: http://www.malvern.co.uk

Rawlings, J. B., S. M. Miller and W. R. Witkowskit. Model Identification and Control of Solution Crystallization Processes: A Review, Industrial and Engineering Chemistry Research, *32*, pp.1275-1296. 1993.

Reinhold, D. F., R. A. Firestone, W. A. Gaines, J. M. Chemerda and M. Sletzinger. Synthesis of L-α-Methyldopa from Asymmetric Intermediates. The Journal of Organic Chemistry, *33*, pp.1209-1213. 1968.

Rekoske, J. E. Chiral Separations. AIChE Journal, *47*, pp.2-5. 2001.

Roberts, R. J. and R. C. Rowe. The Unit Cell Dimensions of (R, S)-Propranolol Hydrochloride-A Confirmatory Study using Data from Powder X-ray Diffraction. International Journal of Pharmaceutics, *109*, pp.83-87. 1994.

Rodrigo, A. A., H. Lorenz and A. Seidel-Morgenstern. Online Monitoring of Preferential Crystallization of Enantiomers. Chirality, *16*, pp.499-508. 2004.

Rodriguez-Hornedo, N. and D. Murphy. Significance of Controlling Crystallization Mechanisms and Kinetics in Pharmaceutical Systems. Journal of Pharmaceutical Sciences, *88*, pp.651-660. 1999.

Rohani, S. and J. R. Bourne. A Simplified Approach to the Operation of a Batch Crystallizer. The Canadian Journal of Chemical Engineering, *68*, pp.799–806. 1990.

Roozeboom, H.W.B. Löslichkeit und Schmelzpunkt als Kriterien für Racemische Verbindungen, Pseudoracemische Mischkristalle und Inaktive Konglomerate, Zeitschrift für Physikalische Chemie, *XXVIII*, pp.494-517. 1899.

Rosanoff, M. A. On Fischer's Classification of Stereo-Isomers. Journal of the American Chemical Society, *28*(1), pp.114-21.1906.

Rousseau, R. W., W. L. McCabe and C. Y. Tai. Stability of Nuclei Generated by Contact Nucleation. AIChE Journal. *21*(5), pp.1017-19, 1975.

Rousseau, R. W., K. K. Li and W. L. McCabe. The Influence of Seed Crystal Size on Nucleation Rates. AIChE Symposium Series, *72*(153), pp. 48-52. 1976.

Rousseau, R. W. Handbook of Separation Process Technology. New York: John Wiley & Sons. 1987.

Rouhi, A.M. Chiral Roundup. Chemical & Engineering News, *80*, pp.43-50. 2002.

Routhven, D. M. and C. B. Ching. Counter-Current and Simulated Counter-Current Adsorption Separation Processes. Chemical Engineering Science, *44*, pp.1011-1038. 1989.

Ruf, A., J. Worlitschek and M. Mazzotti**.** Modeling and Experimental Analysis of PSD Measurements through FBRM. Particle and Particle Systems Characterization, *17*, pp.167-179. 2000.

Sato, N., T. Uzuki, K. Toi and T. Akashi. Direct Resolution of DL-lysine-3,5-Dinitrobenzoate. Agricultural and Biological Chemistry, *33*(7), pp. 1107, 1969.

Schröder, I. Über die Abhängigkeit der Löslichkeit eines festen Körpers von seiner Schmelztemperatur, Zeitschrift für Physikalische Chemie, *XI*, pp.29-30. 1893.

Schroer, J. W., C. Wibowo and K. M. Ng. Synthesis of Chiral Crystallization Processes. AIChE Journal, *47*, pp.369-387. 2001.

Schroer, J. W. and K. M. Ng. Process Paths of Kinetically Controlled Crystallization: Enantiomers and Polymorphs. Industrial & Engineering Chemistry Research, *42*, pp.2230-2244. 2003.

Secor, R. M. Resolution of Optical Isomers by Crystallization Procedures. Chemical Reviews, 63, pp.297-309. 1963.

Shankland, K. and K. S. Knight. Some Observations on the Crystal Structure of (R, S)-Propranolol Hydrochloride. International Journal of Pharmaceutics, *137*, pp.255-259. 1996.

Sheldon, R.A. Chirotechnology - Industrial Synthesis of Optically Active Compounds. New York: Marcel Dekker, Inc. 1993.

Sheldon, R. A. Chirotechnology : Designing Economic Chiral Syntheses. Journal of Chemical Technology & Biotechnology, *67*(1), pp.1-14. 1996.

Shiraiwa, T., S. Sakata, H. Natsuyama, K. Fujishima, H. Miyazaki, S. Kubo, T. Nitta and H. Kurokawa. Racemization of Optically-Active Aromatic N-Acetylamino Acids and Asymmetric Transformation of N-Acetyl-2-(4-Hydroxyphenyl)Glycine via Salt Formation with Optically-Active Alpha-Methylbenzylamine. Bulletin of the Chemical Society of Japan, *65*, pp.965-970. 1992.

Shiraiwa, T., Y. Ohki, Y. Sado, H. Miyazaki and H. Kurokawa. Optical Resolution by Preferential Crystallization of 4-Methylpiperidinium Hydrogen (RS)-Phenylsuccinate. Chirality *6*, pp.202-206. 1994.

Shiraiwa, T., H. Miyazaki and H. Kurokawa. Successive Optical Resolution by Replacing Crystallization of DL-Threonine. Chirality, *6*, pp.654-657.1994.

Shiraiwa, T., H. Miyazaki, M. Ohkubo, A. Ohta, A. Yoshioka, T. Yamane and H. Kurokawa. Optical Resolution by Preferential Crystallization of (RS)-2-Amino-3-Chloropropanoic Acid Hydrochloride. Chirality, *8*, pp.197-200.1996.

Shiraiwa, T., H. Miyazaki, A. Ohta, Y. Waki, M. Yasuda, T. Morishita and H. Kurokawa. Optical Resolution by Preferential Crystallization of (RS)-α-Amino-γ-Butyrolactone Hydrochloride. Chemical and Pharmaceutical Bulletin, *44*, pp.2322-2325. 1996.

Shiraiwa, T., H. Miyazaki, T. Watanabe and H. Kurokawa. Optical Resolution by Preferential Crystallization of DL-Methionine Hydrochloride. Chirality, *9*, pp.48-51. 1997.

Shiraiwa, T., H. Miyazaki, A. Ohta, K. Motonaka, E. Kobayashi, M. Kubo and H. Kurokawa. Optical Resolution by Preferential Crystallization of (2RS,3SR)-2-Amino-3-Chlorobutanoic Acid Hydrochloride. Chirality, *9*, pp.656-660. 1997.

Shiraiwa, T., M. Ohkubo, H. Miyazaki and M. Kubo. Optical Resolution by Preferential Crystallization of (RS)-Bromosuccinic Acid. Bulletin of the Chemical Society of Japan *71*, pp. 735-739. 1998.

Shirawai, T., K. Tadokoro, H. Tanaka, K. Nanba, N. Yokono, K. Shibazaki and M. Kubo. Synthesis of Optically Active 1,4-Thiazane-3-Carboxylic Acid *via* Optical Resolution by Preferential Crystallization of (*RS*)-2-Amino-3-[(2-Chloroethyl)Sulfanyl]Propanoic Acid Hydrochloride. Bioscience Biotechnology and Biochemistry, 62, pp.2382-2387. 1998.

Shiraiwa, T., M. Ohkubo, M. Kubo, H. Miyazaki, M. Takehata, H. Izawa, K. Nakagawa and H. Kurokawa. Optical Resolution of (RS)-Mercaptosuccinic Acid and Syntheses of Four Stereoisomers of 2-Amino-3-[(1,2-Dicarboxyethyl)Sulfanyl]propanoic Acid. Chemical and Pharmaceutical Bulletin, *46*, pp.1364-1369. 1998.

Shiraiwa, T., M. Kubo, M. Watanabe, H. Nakatani, M. Ohkubo and H. Kurokawa. Optical Resolution by Preferential Crystallization of (RS)-2-Amino-3-(2-Carboxyethylthio)Propanoic Acid. Bioscience Biotechnology and Biochemistry, 62, pp.818-820. 1998

Shiraiwa, T., M. Suzuki, Y. Sakai, H. Nagasawa, K. Takatani, D. Noshi and K. Yamanashi. Optical Resolution by Preferential Crystallization of (*RS*)-2-Benzoylamino-2-Benzyl-3-Hydroxypropanoic Acid and Its Use in Synthesizing Optically Active 2-Amino-2-Methyl-3-Phenylpropanoic Acid. Chemical and Pharmaceutical Bulletin, *50*, pp.1362-1366. 2002.

Shiraiwa, T., K. Fukuda and M. Kubo. Preparation of Optically Active Allothreonine *via* Optical Resolution by Replacing Crystallization. Chemical and Pharmaceutical Bulletin, *50*, pp.287-291. 2002.

Shiraiwa, T., R. Saijoh, M. Suzuki, K. Yoshida, S. Nishimura and H. Nagasawa. Preparation of Optically Active Threo-2-Amino-3-Hydroxy-3-Phenylpropanoic Acid (Threo-β-Phenylserine) via Optical Resolution. Chemical and Pharmaceutical Bulletin,

51, pp. 1363-1367. 2003.

Shiraiwa, T. and R. Kiyoe. Optical Resolution by Preferential Crystallization of (1RS,3RS)-1,2,3,4-Tetrahydro-6,7-Dihydroxy-1-Methyl-3-Isoquinolinecarboxylic Acid. Chemical and Pharmaceutical Bulletin, *53*, pp.1197-1199. 2005.

Sohnel, O. and J. Nyvlt. Evaluation of Experimental Data on Width of Metastable Region in Aqueous Solutions. Collection of Czechoslavak Chemical Communications, *40*, pp. 511. 1975.

Soichiro, A. Various Procedures for Preferential Crystallization of Ionizable Racemic Mixtures. Resolution of (±) 3, 4-Dihydroxy-Beta-Phenylalanine. Industrial & Engineering Chemistry Process Design and Development, *22*, pp.429-432. 1983.

Sparks, R. G. and C. L. Dobbs. The Use of Laser Backscatter Instrumentation for the On-Line Measurement of Particle Size Distribution for Emulsions. Particle and Particle Systems Characterization, *10*, pp.279-289. 1993.

Stinson, S.C. Chiral Pharmaceuticals. Chemical & Engineering News, *79*, pp.79-97. 2001.

Tadayyon, A. and S. Rohani. Determination of Particle Size Distribution by Partec 100: Modeling and Experimental Results. Particle and Particle Systems Characterization, *15*,

pp.127-135. 1998.

Tadayon, A., S. Rohani and M. K. Bennett. Estimation of Nucleation and Growth Kinetics of Ammonium Sulfate from Transients of a Cooling Batch Seeded Crystallizer. Industrial & Engineering Chemistry Research, *41*(24), pp.6181-6193. 2002.

Tamura, R., D. Fujimoto, Z. Lepp, K. Misaki, H. Miura, H. Takahashi, T. Ushio and K. Hirotsu. Mechanism of Preferential Enrichment, an Unusual Enantiomeric Resolution Phenomenon Caused by Polymorphic Transition During Crystallization of Mixed Crystals Composed of Two Enantiomers. Journal of the American Chemical Society, *124*, pp. 13139-13153. 2002.

Tavare, N. S. and J. Garside. Simultaneous Estimation of Crystal Nucleation and Growth Kinetics from Batch Experiments. Chemical Engineering Research Design, *64*, pp.109-118. 1986.

Tavare, N. S. Industrial Crystallization: Process Simulation, Analysis and Design. New York: Plenum. 1995.

Teja, A. S. and R. W. Rousseau. Thermodynamics of Crystallization. Chemical Thermodynamics for Industry, pp. 230-242. Publisher: Royal Society of Chemistry, Cambridge, 2004.

Ting, H. H. and W. L. McCabe. Supersaturation and Crystal Formation in Seeded Solutions. Journal of Industrial and Engineering Chemistry (Washington, D. C.), *11* pp.1201-1207. 1934.

van Annum, P. Single Enantiomer Drugs Keep Pace. Chemical Market Reporter, Jan. *18*. 1999.

Velluz, L., G. Amiard and R. Joly. Resolution of DL-threo-1-p-nitrophenyl-2-aminopropane-1,3-diol. Bulletin de la Societe Chimique de France, pp. 342-344. 1953.

Velluz, L and G., Amiard. Direct Resolution of DL-threonine. Bulletin de la Societe Chimique de France, pp. 903-904. 1953.

Villadsen, J. and M. L. Michelsen. Solution of Differential Equation Models by Polynomial Approximation, Prentice-Hall, Englewood Cliffs, NJ, 1978.

Wang, X. and C. B. Ching. Chiral Separation of ß-Blocker Drug (Nadolol) by Five-Zone Simulated Moving Bed Chromatography. Chemical Engineering Science, *60*, pp.1337-1347. 2005.

Wang, X., X. J. Wang and C. B. Ching. Solubility, Metastable Zone Width, and Racemic Characterization of Propranolol Hydrochloride. Chirality, *14*, pp.318-324. 2002.

Wang X. J., J. Lu and C. B. Ching. Aspects of Enantioselective Crystallization for Chiral Drugs and Intermediates. Chianese, A. (ed). Proceedings of 15th International Symposium on Industrial Crystallization. pp.1059-1064. 2002.

Wang, X. J., H. Wiehler and C. B. Ching. Physicochemical Properties and the Crystallization Thermodynamics of the Pure Enantiomer and the Racemate for N-Methylephedrine. Journal of Chemical and Engineering Data, *48*, pp.1092-1098. 2003.

Wang, X. J., H. Wiehler and C. B. Ching. Study of the Characterization and Crystallization of 4-Hydroxy-2-Pyrrolidone. Chirality, *16*, pp.220-227. 2004.

Wang, X. J. and C. B. Ching. A Systematic Approach for Preferential Crystallization of 4-Hydroxy-2-Pyrrolidone: Thermodynamics, Kinetics, Optimal Operation and In-Situ Monitoring Aspects. Chemical Engineering Science, *61*, pp.2406-2417. 2006.

Watanabe, T. and G. Noyori. Optical Resolution of Racemic Glutamic Acid. VII. Reasonable Selection of Resolution Procedures for Optical Resolution by Fractional Crystallization. Kogyo Kagaku Zasshi, *72*(5), pp. 1083-6. 1969.

Way, J. S. Analysis of Batch Crystallization Process, Chemical Engineering Communication, *35*, pp.231-252. 1985.

Weissbuch, I., M. Lahav and L. Leiserowitz. Toward Stereochentical Control,

Monitoring, and Understanding of Crystal Nucleation. Crystal Growth & Design, *3*, pp.125-150. 2003.

Werner, A. The Asymmetric Cobalt Atom. XI. Oxalodiethylenediaminocobalti Salts and a New Method for Splitting Racemic Inorganic Compounds. Ber. *47* pp.2171-2182. 1914.

Wermester, N., E. Aubin, S. Coste and G. Coquerel**,** Preferential Crystallization of the Ethanolamine Salt of (±) Mandelic Acid: The Unusual Case of Conglomerate with Partial Solid Solutions. VDI-Berichte 1901 I, Dresden, pp. 223-228. 2005.

Wibowo, C. and K. M. Ng. Unified Approach for Synthesizing Crystallization-Based Separation Processes. AIChE Journal, *46*, pp.1400-1421. 2000.

Wibowo, C. and L. O'Young. Chromatographic Resolution Coupled with Crystallization Can Be Your Best Option for Manufacturing Chirally Pure Products. Chemical Engineering Progress, *101*(11), pp. 22-27. 2005.

Wilen, S. H., A. Collet and J. Jacques. Strategies in Optical Resolutions. Tetrahedron, *33*, pp.2725-2736. 1977.

Witkowski, W. R., S. M. Miller and J. B. Rawlings. Light-Scattering Measurements to Estimate Kinetic Parameters of Crystallization. ACS Symposium Series, *438*, pp.102-114. 1990.

Worlitschek, J. and M. Mazzotti. Choice of the Focal Point Position using Lasentec FBRM. Particle and Particle Systems Characterization, *20*, pp.12-17. 2003.

Worlitschek, J., T. Hocker and M. Mazzotti. Restoration of PSD from Chord Length Distribution Data Using the Method of Projections onto Convex Sets. Particle & Particle Systems Characterization. *22*, pp. 81-98, 2005.

Yamada, S., M. Yamamoto and I. Chibata. Optical Resolution of DL-amino Acids by Preferential Crystallization Procedure. Journal of Organic Chemistry, *38*(26), pp.4408. 1973.

Yamada, S., M. Yamamoto and I. Chibata. Optical Resolution of N Acyl DL Amino Acids by Preferential Crystallization Procedure. Preparation of L DOPA and L α Methyl DOPA. Journal of Organic Chemistry, *40*, pp.3360-3362. 1975.

Yokota, M. and K. Toyokura. Heterogeneous Nucleation of D-SCMC on the Surface of L-SCMC Crystal. AIChE Annual Meeting, Florida. 1992.

Yokota, M., A. Sato and N. Kubota. A Simple Method for Evaluating Kinetic Parameters in Non-Isothermal Batch Crystallization. Chemical Engineering Science, *55*, pp.717-722. 2000.

Young, S. W. and W. J. Van Sicklen. "The Mechanical Stimulus to Crystallisation". Journal of American Chemical Society, *35*, pp. 1067-1078, 1913.

Zaugg, H. E. A Mechanical Resolution of DL-Methadone Base. Journal of the American Chemical Society, *77*, pp.2910. 1955.

Zhang, G. P. and S. Rohani. On-line Optimal Control of a Seeded Batch Cooling Crystallizer. Chemical Engineering Science, *58*, pp.1887–1896. 2003.

Zumstein, R. C. and R.W. Rousseau. Growth Rate Dispersion in Batch Crystallization with Transient Conditions. AIChE Journal, *33*(11), pp.1921-1925, 1987.

Zumstein, R. C. and R. W. Rousseau. Growth Rate Dispersion by Initial Growth Rate Distributions and Growth Rate Fluctuations. AIChE Journal, *33*(1), pp.121-129. 1987.

Zumstein, R. C. and R. W. Rousseau. Experimental and Theoretical Analyses of Growth Rate Dispersion Technology. Proceedings, *6*(Ind. Cryst. 87), pp.211-214. 1989.

LIST OF PUBLICATIONS

Wang, X., X. J. Wang and C. B. Ching. Solubility, Metastable Zone Width, and Racemic Characterization of Propranolol Hydrochloride. Chirality, *14*, pp.318-324. 2002.

Wang X. J., J. Lu and C. B. Ching. Aspects of Enantioselective Crystallization for Chiral Drugs and Intermediates. Chianese, A. (ed). Proceedings of 15th International Symposium on Industrial Crystallization. pp.1059-1064. 2002.

Wang, X. J., H. Wiehler and C. B. Ching. Physicochemical Properties and the Crystallization Thermodynamics of the Pure Enantiomer and the Racemate for N-Methylephedrine. Journal of Chemical and Engineering Data, *48*, pp.1092-1098. 2003.

Wang, X. J., H. Wiehler and C. B. Ching. Study of the Characterization and Crystallization of 4-Hydroxy-2-Pyrrolidone. Chirality, *16*, pp.220-227. 2004.

Wang, X. J. and C. B. Ching. Determination of Thermodynamic Data and Kinetics for Chiral Crystallization. Proceedings of 16th International Symposium on Industrial Crystallization. pp.47-53. 2005.

Wang, X. J. and C. B. Ching. A Systematic Approach for Preferential Crystallization of 4-Hydroxy-2-Pyrrolidone: Thermodynamics, Kinetics, Optimal Operation and In-Situ Monitoring Aspects. Chemical Engineering Science, *61*, pp.2406-2417. 2006.

Wang, X. J. and C. B. Ching. Implications of MSZW and Nucleation Mechanism for Different Chiral Racemic Species. *In preparation*.

Wang, X. J. and C. B. Ching. Application of Direct Crystallization for Racemic Compound: Propranolol Hydrochloride. Journal of Pharmaceutical Sciences. *In press,2007.*